

ResearchOnline@JCU

This file is part of the following reference:

Kockler, Jutta (2014) *Sunscreens: photostability, formulation and skin penetration*. PhD thesis, James Cook University.

Access to this file is available from:

<http://researchonline.jcu.edu.au/40698/>

The author has certified to JCU that they have made a reasonable effort to gain permission and acknowledge the owner of any third party copyright material included in this document. If you believe that this is not the case, please contact

*ResearchOnline@jcu.edu.au and quote
<http://researchonline.jcu.edu.au/40698/>*

Sunscreens

Photostability, Formulation and Skin Penetration

Jutta Kockler, Approbierte Apothekerin
(Germany) - Certified Pharmacist

This thesis is submitted for the degree of
Doctor of Philosophy

at

James Cook University

School of Pharmacy and Molecular Sciences

Discipline of Pharmacy

February 2014



Statement of Access

I, Jutta Kockler, the author of this thesis, understand that this thesis will be made available for use to others. All users consulting this thesis will have to sign the following statement:

In consulting this thesis I agree not to copy or closely paraphrase it in whole or part without the written consent of the author; and to make proper public written acknowledgement for any assistance which I have obtained from it.

Beyond this, I do not wish to place any restriction on access to this thesis.

(Author's signature)

18 February 2014

.....
(Date)

Declaration

I declare that this thesis is my own work and has not been submitted in any form for another degree or diploma at any university or institution of tertiary education. Information derived from the published or unpublished work of others has been acknowledged in the text and a list of references is given.

(Author's signature)

18 February 2014

.....
(Date)

Acknowledgements

I gratefully acknowledge my principal supervisor Prof Beverley Glass for her invaluable guidance and encouragement during this project and her critical reviews of my written work. Without her great support I could not have completed this degree.

I am also very grateful to my co-supervisors Assoc Prof Michael Oelgemöller and Dr Sherryl Robertson for their assistance. Michael Oelgemöller for great discussions about study results, due to his incredible knowledge in photochemistry. Dr Sherryl Robertson for her help with laboratory equipment and experimental set ups, in particular during skin penetration studies.

I wish to thank Dr Cherie Motti from the Australian Institute of Marine Science (AIMS) for providing training on the LC-MS and FTMS and helpful guidance during the interpretation of results. During the conduction of kinetic studies, the help and guidance from Prof Anthony Beezer from the University College London was absolutely essential and I am very grateful for his assistance. I also wish to thank Assoc Prof Bruce Bowden and Dr Murray Davies from the Discipline of Chemistry for their help with NMR and IR analysis.

I am very grateful to all Staff members of the Discipline of Pharmacy for their invaluable support throughout the three years of my PhD candidature, which made this difficult time much easier. I also want to thank the School of Pharmacy and Molecular Science, who financially supported me with a scholarship.

Abstract

Introduction: Sunscreen products, containing UV-filters, are used worldwide to protect from the deleterious effects of sunlight. However, in order to provide this photoprotective function, they should be photostable and remain on the surface of the skin. The photostability of UV-filters, individually and in combination, using different light sources, light intensities, UV-filter concentrations, solvents and formulations has been extensively investigated. Regulations for sunscreen products in Australia, the USA and Europe do not require photostability testing, as per the International Conference on Harmonisation (ICH) Guideline Q1B for new drug substances and drug products. During UV-irradiation on exposure to sunlight, there is potential for chemical UV-filters to degrade by direct photolysis. Chemical UV-filters are also often used in combination with the physical UV-filter, titanium dioxide (TiO₂), increasing the complexity of the system, due to the ability of TiO₂ to cause photocatalytic reactions. In recent years issues have been raised that TiO₂ nano-particles may penetrate through the skin, but no evidence has been found and the Therapeutic Goods Administration (TGA) regards them as safe. However, whether these TiO₂ nano-particles may have an effect on the photostability of chemical UV-filters has not been investigated. The aim of the study was therefore to determine the photostability and skin penetration of a combination of chemical UV-filters with TiO₂, investigating the effect of particle size on photostability.

Methods: Chemical UV-filters, Butyl methoxy dibenzoylmethane (**BMDM**), Octocrylene (**OC**) and Benzophenone-3 (**B3**) were verified for purity by melting point determinations, differential scanning calorimetry (DSC) and high performance liquid chromatography (HPLC). UV-filter identity was confirmed by nuclear magnetic resonance (NMR)-, infrared (IR)- and ultraviolet (UV)-spectroscopy. A reverse-phase HPLC method was developed and validated for the simultaneous determination of **BMDM** and **OC** in the presence of their photodegradants. Validation parameters included linearity, accuracy, precision, specificity, sensitivity and robustness. This HPLC method was also employed for the determination of UV-filter **B3** during skin penetration studies and to identify photodegradants by liquid chromatography - mass spectroscopy (LC-MS).

Photostability studies of **BMDM** and **OC** individually and in combination were undertaken in methanol and a microemulsion. The microemulsion was adapted from a formula in the literature, with xanthan gum added to optimise the viscosity for topical application. Photodegradation profiles of chemical UV-filters in methanol were determined in a photoreactor using a medium pressure mercury lamp as light source and a pyrex glass vessel ($\lambda \geq 300$ nm). Incorporated in a microemulsion, UV-filter photostability was determined in a solar simulator ($\lambda \geq 290$ nm), according to ICH Guideline Q1B. The influence of silica coated TiO₂

(~ 119 nm), uncoated micro- (~ 0.6 μm) and nano-TiO₂ (< 25 nm) on the photostability of both chemical UV-filters was investigated. Degradation kinetics of **BMDM** and **OC** separately and in combination were studied in methanol in the photoreactor, using a quartz glass vessel ($\lambda \geq 200$ nm).

Skin penetration of **BMDM** and **OC**, incorporated in the microemulsion, was then studied *in vitro* using porcine ear skin in Franz diffusion cells. Results were compared to the skin penetration of UV-filter **B3**, which is known to penetrate the skin and cause photoallergic skin reactions. UV-filter concentrations were determined in the receptor fluid, the skin (stratum corneum and viable epidermis/dermis) and the remaining microemulsion on the skin surface using the validated HPLC method. The stratum corneum was separated from the viable epidermis/dermis using the tape stripping method.

Results and Discussion: In methanol, photodegradation of **BMDM** in the presence of silica coated, micro- and nano-TiO₂ was higher than without TiO₂. In general, **OC** showed less photodegradation than **BMDM**. Both, **BMDM** and **OC**, followed mixed zero- and first-order degradation kinetics. Photodegradants of both UV-filters were identified by LC-MS and molecular weights were confirmed by Fourier transform - mass spectroscopy (FTMS). Two major photodegradants were found for **BMDM**. Although in the presence of nano-TiO₂ (pyrex glass), **OC** recovery was reduced by 38 %, after irradiation through quartz glass, one major photodegradant was identified for **OC**. The major findings from methanol studies, that nano-TiO₂ causes higher photodegradation than micro-TiO₂ and that **BMDM** is less photostable than **OC**, were confirmed in the microemulsion and a reference cream. **OC** did not degrade in the absence or presence of coated TiO₂ and the lowest **OC** recovery was determined in the presence of nano-TiO₂ (88 %), while **BMDM** recovery varied from 0 to 16 %. Irradiated in combination with **OC** UV-filter **BMDM** showed a higher recovery (16 %) than irradiated alone (4 %), due to the stabilising effect of UV-filter **OC** on **BMDM** *via* triplet-triplet energy transfer.

Although the combination of **BMDM** and **OC** influenced their photostability, skin penetration was not affected by their presence in combination. Generally, **BMDM**, **OC** and **B3** showed low skin penetration. **BMDM** and **OC** were not detected in the receptor fluid after 24 hours and only 0.03 % of **B3** was detected. To maintain its photoprotective character, a UV-filter should remain on the surface of the skin or in the stratum corneum. Therefore, the presence of these UV-filters in the viable epidermis/dermis is of interest. As expected **B3** showed the highest concentration in this skin compartment (1.09 %), followed by **BMDM** (0.14 %) and **OC** with the lowest concentration (0.02 %). Percentages were related to the complete UV-filter content in the microemulsion. This penetration is explained in terms of lipophilicity and molecular

weight of the UV-filters, with **B3** being the least lipophilic molecule with the smallest molecular weight, while **OC** is the most lipophilic molecule with the largest molecular weight.

Conclusions: Photostability of **BMDM** and **OC**, including TiO_2 , has been extensively investigated. UV-filters are often used in combinations in sunscreen products to increase their photoprotective effect and to reduce their individual components to minimise toxicity. Although the inclusion of nano- TiO_2 in sunscreen products is regarded as safe in terms of skin penetration, the effect of this physical UV-filter on the photostability of chemical UV-filters is noteworthy. This research presents the first findings on the effect of particle size of TiO_2 on the photostability of chemical UV-filters and is significant because of the potential for the photoprotection of sunscreen products containing these UV-filters, to be compromised.

List of Publications

Kockler J, Oelgemöller M, Robertson S, Glass BD 2012 **Photostability of Sunscreens**. *J Photochem Photobiol C Photochem Rev* 13(1):91-110.

Kockler J, Robertson S, Oelgemöller M, Davies M, Bowden B, Brittain HG, Glass BD 2013 **Chapter three: Butyl methoxy dibenzoylmethane**. In Brittain HG, editor. *Profiles of Drug Substances, Excipients and related Methodology Vol. 38*, San Diego, USA: Academic Press. p 87-111.

Kockler J, Motti CA, Robertson S, Oelgemöller M, Glass BD 2013 **HPLC Method for the Simultaneous Determination of the UV-Filters Butyl Methoxy Dibenzoylmethane and Octocrylene in the Presence of Their Photodegradants**. *Chromatographia* 76(23):1721-1727.

Kockler J, Oelgemöller M, Robertson S, Glass BD 2014 **Influence of Titanium Dioxide Particle Size on the Photostability of the Chemical UV-Filters Butyl Methoxy Dibenzoylmethane and Octocrylene in a Microemulsion**. *Cosmetics* 1(2):128-139

Table of Contents

Statement of Access.....	i
Declaration.....	ii
Acknowledgements	iii
Abstract.....	iv
List of Publications.....	vii
List of Tables	xiii
List of Figures	xvi
List of Schemes	xix
List of Abbreviations	xxi

Chapter 1 Introduction

1.1. Solar UV-radiation.....	1
1.2. Health Effects Caused by UV-radiation.....	2
1.3. Sunscreen Products	2
1.4. Overall Aim, Hypothesis and Objectives	3
1.5. Thesis Outline.....	5

Chapter 2 Photostability and Skin Penetration – A Review

2.1. Introduction	7
2.2. Regulations.....	7
2.2.1. Australia - Therapeutic Goods Administration (TGA).....	7
2.2.2. USA - Federal Drug Administration (FDA)	9
2.2.3. Europe - European Cosmetic, Toiletry and Perfumery Association (Colipa).....	10
2.3. Chemical UV-filters.....	12
2.4. Photostability of Chemical UV-filters	18
2.4.1. Photostability of Individual Chemical UV-filters	19
2.4.2. Photostability of Chemical UV-filters in Combinations	21
2.4.3. Possible Photodegradants of Chemical UV-filters.....	27
2.4.3.1. Identification of Photodegradants.....	27
2.4.3.2. Toxicity of Photodegradants	35

2.5. Effects of UV-filter Photostability by the Addition of other Active Ingredients.....	39
2.5.1. Addition of Physical UV-filters (Metal Oxides).....	39
2.5.1.1. Coated Metal Oxides	40
2.5.1.2. Doped Metal Oxides.....	44
2.5.2. Addition of Antioxidants.....	46
2.6. Change of UV-protective Performance by Formulation Components.....	50
2.6.1. Different Solvents and Formulations	50
2.6.2. New Formulation Additives to Reduce Photodegradation of UV-filters	54
2.7. Skin Penetration of Chemical UV-filters and Sunscreen Formulations.....	55
2.7.1. Skin Penetration of Chemical UV-filters in vitro.....	56
2.7.2. Microemulsions as Sunscreen Formulation.....	57
2.7.3. Photoallergic and Phototoxic Skin Reactions	61
2.8. Summary	64

Chapter 3 Characterisation of Chemical UV-filters

3.1. Introduction	65
3.2. Materials and Methods.....	67
3.2.1. Solvents and Reagents.....	67
3.2.2. Instrumentation	67
3.2.3. Methodology.....	67
3.2.3.1. Solubility.....	67
3.2.3.2. Ultraviolet (UV)-spectroscopy.....	68
3.2.3.3. High Performance Liquid Chromatography (HPLC)	68
3.2.3.4. Melting Point Measurement.....	69
3.2.3.5. Differential Scanning Calorimetry (DSC)	69
3.2.3.6. Nuclear Magnetic Resonance (NMR)-spectroscopy	69
3.2.3.7. Infrared (IR)-spectroscopy.....	70
3.3. Results and Discussion.....	70
3.3.1. Butyl methoxy dibenzoylmethane (BMDM) [70356-09-1]	70
3.3.1.1. Solubility.....	71
3.3.1.2. Ultraviolet (UV)-spectroscopy.....	71
3.3.1.3. High Performance Liquid Chromatography (HPLC)	71
3.3.1.4. Melting Point Measurement.....	72
3.3.1.5. Differential Scanning Calorimetry (DSC)	73

3.3.1.6. Nuclear Magnetic Resonance (NMR)-spectroscopy	73
3.3.1.6.1. Determination of the Diketo-enol Ratio.....	74
3.3.1.7. Infrared (IR)-spectroscopy.....	76
3.3.2. Octocrylene (OC) [6197-30-4]	77
3.3.2.1. Solubility.....	77
3.3.2.2. Ultraviolet (UV)-spectroscopy	77
3.3.2.3. High Performance Liquid Chromatography (HPLC)	78
3.3.2.4. Nuclear Magnetic Resonance (NMR)-spectroscopy	78
3.3.2.5. Infrared (IR)-spectroscopy.....	79
3.3.3. Benzophenone-3 (B3) [131-57-7]	81
3.3.3.1. Solubility.....	81
3.3.3.2. Ultraviolet (UV)-spectroscopy	81
3.3.3.3. High Performance Liquid Chromatography (HPLC)	82
3.3.3.4. Melting Point Measurement	82
3.3.3.5. Differential Scanning Calorimetry (DSC)	83
3.3.3.6. Nuclear Magnetic Resonance (NMR)-spectroscopy	83
3.3.3.7. Infrared (IR)-spectroscopy.....	84
3.4. Summary	86

Chapter 4 High Performance Liquid Chromatography (HPLC) – Method Development and Validation

4.1. Introduction	87
4.2. Materials and Instrumentation	90
4.2.1. Solvents and Reagents.....	90
4.2.2. Instrumentation	90
4.3. HPLC Method Development.....	90
4.3.1. Choice of Analytical Column	90
4.3.2. Choice of Mobile Phase.....	91
4.3.3. Chromatographic Conditions	95
4.4. HPLC Method Validation	95
4.4.1. Filter Evaluation.....	95
4.4.2. Linearity	96
4.4.3. Accuracy and Precision	96
4.4.4. Specificity	96
4.4.5. Sensitivity	97

4.4.6. Robustness	97
4.5. Results and Discussion.....	98
4.5.1. Butyl methoxy dibenzoylmethane (BMDM) and Octocrylene (OC)	98
4.5.1.1. Filter Evaluation	98
4.5.1.2. Linearity.....	99
4.5.1.3. Accuracy and Precision	101
4.5.1.4. Specificity	102
4.5.1.5. Sensitivity	104
4.5.1.6. Robustness	105
4.5.2. Benzophenone-3 (B3)	106
4.5.2.1. Filter Evaluation.....	106
4.5.2.2. Linearity.....	106
4.5.2.3. Accuracy and Precision	107
4.5.2.4. Specificity	108
4.5.2.5. Sensitivity	109
4.5.2.6. Robustness	109
4.6. Summary	110

Chapter 5 Photostability of Chemical UV-filters

5.1. Introduction	111
5.2. Materials and Methods.....	113
5.2.1. Solvents and Reagents.....	113
5.2.2. Instrumentation	114
5.2.3. Preparation of Standards.....	114
5.2.4. Photostability Studies	115
5.2.4.1. Photostability Studies in the Presence of Different TiO ₂ Particle Sizes	115
5.2.4.2. Photostability Studies in the Presence of Coated TiO ₂ and Vitamin E.....	115
5.2.4.3. Adsorption Studies	116
5.2.5. Kinetic Studies	116
5.2.6. Data Analysis.....	116
5.2.7. Identification of Major Photodegradants using LC-MS and FTMS.....	117
5.3. Results and Discussion.....	117
5.3.1. Influence of TiO ₂ Particle Size on Photodegradation.....	117
5.3.1.1. Butyl methoxy dibenzoylmethane (BMDM).....	118
5.3.1.2. Octocrylene (OC).....	121

5.3.2. Influence of Coated TiO ₂ and Vitamin E on Photodegradation.....	127
5.3.2.1. Butyl methoxy dibenzoylmethane (BMDM).....	128
5.3.2.2. Octocrylene (OC).....	132
5.3.3. Kinetic Studies.....	134
5.3.3.1. Butyl methoxy dibenzoylmethane (BMDM).....	135
5.3.3.2. Octocrylene (OC).....	136
5.3.4. Identification of Major Photodegradants using LC-MS and FTMS.....	138
5.4. Summary.....	145

Chapter 6 Microemulsion – Photostability and Skin Penetration of Chemical UV-filters

6.1. Introduction.....	146
6.2. Materials and Methods.....	150
6.2.1. Solvents and Reagents.....	150
6.2.2. Instrumentation.....	150
6.2.3. Preparation of Standards.....	151
6.2.4. Preparation of Microemulsion.....	151
6.2.5. Preparation of Cream.....	153
6.2.6. Preliminary Stability Studies.....	155
6.2.7. Photostability Studies.....	155
6.2.8. Skin Penetration Studies.....	156
6.3. Results and Discussion.....	157
6.3.1. Microemulsion Development.....	157
6.3.2. Preliminary Stability Studies.....	158
6.3.3. Photostability Studies.....	161
6.3.4. Skin Penetration Studies.....	165
6.4. Summary.....	168

Chapter 7 Conclusions and Recommendations

7.1. Conclusions.....	169
7.2. Recommendations.....	172

8. References.....	173
--------------------	-----

APPENDIX A: International Biosafety Committee (IBC) Approval.....	185
--	------------

List of Tables

Table 1.1.	Relationship between UV-Index and UV-exposure category.....	1
Table 1.2.	UV-classifications and their wavelengths.	1
Table 2.1.	Labelled category description according to the SPF value.....	8
Table 2.2.	Maximum water resistance on product according to SPF value.	9
Table 2.3.	Labelled SPF and category description according to measured SPF.	11
Table 2.4.	Chemical UV-filters with CAS-numbers, INCI-names, chemical names, UV-absorbance (UVA/UVB), UV-absorbance maxima (λ_{\max}) with solvent and references for λ_{\max}	16
Table 2.5.	SPF ₀ and t _{90%} of the 18 tested UV-filters.....	20
Table 2.6.	Photostability of UV-filters after irradiation.	21
Table 2.7.	UV-filters 1, 3, 10, 14, 16 and 23 and their approximate recovery in % in the formulations F1, F2, F3 and F4.....	23
Table 2.8.	Combination of chemical UV-filters and TiO ₂ . ⁸⁵	42
Table 2.9.	Combination of chemical UV-filters and ZnO. ⁸⁵	43
Table 2.10.	Doped and undoped ZnO: Crystal size, the time it takes to reduce the DPPH radical and PI.	45
Table 2.11.	TiO ₂ samples, commercial name, composition and crystal phase in %.	49
Table 2.12.	Comparative photostability of UV-filter 3 in different solvents. ^{37,63,64}	52
Table 2.13.	Absorbance of seven commercial sunscreen products before UV-exposure and photoinactivation after increasing UV-exposure in the UVA-range.	54
Table 2.14.	Surfactant and lipid compositions of microemulsions 1-5 with the corresponding cumulative amount released after 22 hours (Q ₂₂). ¹¹⁶	59
Table 2.15.	Surfactant, co-surfactant and lipid compositions of microemulsions 1 - 13 with the corresponding cumulative amount released after 24 hours (Q _{24r}) and penetrated through the skin after 24 hours (Q _{24p}). ¹¹⁷	61
Table 3.1.	Concentration and solvent of UV-filters used in UV-spectroscopy.....	68
Table 3.2.	UV-filters with weight and DSC-heating range.....	69
Table 3.3.	Solubilities of BMDM	71
Table 3.4.	¹ H spectral assignment and chemical shifts of BMDM	74
Table 3.5.	Infrared absorption bands of BMDM	76
Table 3.6.	Solubilities of OC	77
Table 3.7.	¹ H spectral assignment and chemical shifts of OC	79
Table 3.8.	Infrared absorption bands of OC	80
Table 3.9.	Solubilities of B3	81
Table 3.10.	¹ H spectral assignment and chemical shifts of B3	84

Table 3.11.	Infrared absorption bands of B3 .	85
Table 4.1.	Relevant HPLC method components for UV-filters.	89
Table 4.2.	Filter Evaluation data for BMDM .	98
Table 4.3.	Filter Evaluation data for OC .	99
Table 4.4.	Linearity data for BMDM .	100
Table 4.5.	Linearity data for OC .	101
Table 4.6.	Accuracy and Precision data for BMDM .	102
Table 4.7.	Accuracy and Precision data for OC .	102
Table 4.8.	LOD and LOQ data for OC and BMDM .	105
Table 4.9.	Rs for BMDM and OC .	105
Table 4.10.	Filter Evaluation data for B3 .	106
Table 4.11.	Linearity data for B3 .	107
Table 4.12.	Accuracy and Precision data for B3 .	108
Table 4.13.	LOD and LOQ data for B3 .	109
Table 4.14.	Rs for B3 .	109
Table 5.1.	% Recovery \pm SD of BMDM in the presence and absence of TiO ₂ .	119
Table 5.2.	% Recovery \pm SD of BMDM in combination with OC in the presence and absence of TiO ₂ .	120
Table 5.3.	% Recovery \pm SD of OC in the presence and absence of TiO ₂ .	122
Table 5.4.	% Recovery \pm SD of OC in combination with BMDM in the presence and absence of TiO ₂ .	123
Table 5.5.	% Recovery \pm SD of BMDM in the presence and absence of coated TiO ₂ and vitamin E (Vit E).	129
Table 5.6.	% Recovery \pm SD of BMDM in a combination with OC in the presence and absence of coated TiO ₂ and vitamin E (Vit E).	130
Table 5.7.	% Recovery \pm SD of OC in the presence and absence of coated TiO ₂ and vitamin E.	133
Table 5.8.	% Recovery \pm SD of OC in a combination with BMDM in the presence and absence of coated TiO ₂ and vitamin E (Vit E).	134
Table 5.9.	First-order kinetic data for BMDM and OC .	138
Table 5.10.	Major photodegradants of BMDM .	140
Table 5.11.	Photodegradant of OC .	143
Table 6.1.	Comparison of micro- and macroemulsions.	146
Table 6.2.	Microemulsion formulae containing UV-filters.	152
Table 6.3.	Cream formulae containing UV-filters.	154
Table 6.4.	Microemulsions (ME) reported on in the literature.	157
Table 6.5.	Physical stability of microemulsions, stored at 25 °C.	159

Table 6.6.	Physical stability results of microemulsions, stored at 40 °C/75 % RH.....	160
Table 6.7.	Chemical stability of BMDM and OC in microemulsions, stored at 25 °C...	160
Table 6.8.	Chemical stability of BMDM and OC in microemulsions, stored at 40 °C/75 % RH.	161
Table 6.9.	% Recovery of BMDM and OC ($n \geq 3$) \pm SD in both formulations in the presence and absence of TiO ₂	163
Table 6.10.	UV-filter recovery in % after skin penetration studies.....	167

List of Figures

Figure 2.1.	Chemical structures of chemical UV-filters.	15
Figure 2.2.	Recovery of the UV-filters 1, 3, 8, 9, 12, 20 and 23 after four hours of irradiation in a solar simulator at 765 Wh/m ² . A: UV-filters irradiated separately and B: the UV-filters 1, 8, 9, 12, 20 and 23 in combination with UV-filter 3 . Adapted from. ⁴⁵	22
Figure 2.3.	UVA/UVB ratio for the formulations F1, F2, F3 and F4, after 0, 30, 60 and 120 minutes irradiation in a solar simulator. Adapted from. ⁴⁶	24
Figure 2.4.	TBARS concentration in PC multilamellar liposomes after UVA-irradiation. □= no UVA-exposure, ■ = UVA-exposure, ▣ = UVA -exposure in the presence of A: individual UV-filters or B and C: in combinations. Adapted from. ⁴⁹	25
Figure 2.5.	Algal toxicity of the mixture of UV-filters and their photodegradants: A: 1, B: 2, and C: 6 . Reproduction inhibition of the algae <i>S. vacuolatus</i> in % plotted against the remaining UV-filter concentration after UV-exposure. Adapted from. ⁵⁴	38
Figure 2.6.	Relative photoreactivity of ZnO and TiO ₂ , coated and uncoated, measured by the photocatalytic oxidation of isopropanol to propanone. Adapted from. ⁸⁴	41
Figure 2.7.	Presence of UV-filter 3 in combination with TiO ₂ after exposure of 10 mW/cm ² for 120 minutes in a solar simulator. Adapted from. ⁸⁷	44
Figure 2.8.	ROS generation, measured <i>via</i> TBARS concentration. □: no UVA-exposure, ■: UVA-exposure, ▣: UVA-exposure in the presence of UV-filters 1, 3, 23 , vitamin E (Vit E), vitamin E acetate (Vit E Ac) and their combinations (▣). Adapted from. ⁹⁴	47
Figure 2.9.	MDA concentration in the absence and presence of TiO ₂ (PW Covasil S-1 and Tego Sun TS plus), with or without the antioxidants phenylalanine (Phe), sodium ascorbyl phosphate (SAPh) and ascorbyl palmitate (AP). Adapted from. ⁹⁶	50
Figure 3.1.	Chemical structure of BMDM showing the diketo- and the two enol-forms... 70	
Figure 3.2.	UV-absorption spectrum of BMDM	71
Figure 3.3.	HPLC-chromatogram of BMDM measured at 358 nm. A: after recrystallisation, B: before recrystallisation.	72
Figure 3.4.	DSC-thermogram of BMDM	73
Figure 3.5.	¹ H NMR spectrum sections of BMDM showing integration of proton signals of the enol- and diketo-form; A: proton signals of the <i>t</i> -butyl-group and B: proton signals of the aromatic ring protons on C ₁ /C ₃ and C ₄ /C ₆	75

Figure 3.6.	IR-spectrum of BMDM	76
Figure 3.7.	Chemical structure of OC	77
Figure 3.8.	UV-absorption spectrum of OC	78
Figure 3.9.	HPLC-chromatogram of OC	78
Figure 3.10.	IR-spectrum of OC	80
Figure 3.11.	Chemical structure of B3	81
Figure 3.12.	UV-absorption spectrum of B3	82
Figure 3.13.	HPLC-chromatogram of B3	82
Figure 3.14.	DSC-thermogram of B3	83
Figure 3.15.	IR-spectrum of B3	85
Figure 4.1.	HPLC chromatogram of BMDM and OC in combination, using the mobile phase A methanol/water (95/5 % v/v): OC at 5.65 min, BMDM at 7.67 min and B methanol/water (90/10 % v/v): OC at 8.64 min, BMDM at 12.27 min. 92	
Figure 4.2.	HPLC chromatogram of BMDM and OC in combination, detected at 358 nm; A mobile phase: methanol/water (90/10 % v/v): BMDM elution at 12.27 min, tailing factor: 1.99 and peak width $\frac{1}{2}$: 17.9 sec; B mobile phase: methanol/water/acetic acid (90/9.99/0.01 % v/v): BMDM elution at 12.30 min, tailing factor: 0.93 and peak width $\frac{1}{2}$: 19.8 sec; C mobile phase: methanol/water/acetic acid (89/10/1 % v/v): BMDM elution at 12.25 min, tailing factor: 1.22 and peak width $\frac{1}{2}$: 10.4 sec.	93
Figure 4.3.	HPLC chromatogram of the UV-filters BMDM and OC in the presence of photodegradants, detected at A 358 nm and B 303 nm.	94
Figure 4.4.	HPLC chromatogram of UV-filter B3 (retention time: 5.24), using the mobile phase: methanol/water/acetic acid (89/10/1), detected at 324 nm.	94
Figure 4.5.	Three samples analysed A unfiltered sample, B first 5 mL of filtrate and C second 5 mL of filtrate.	96
Figure 4.6.	Calibration curve for BMDM	100
Figure 4.7.	Calibration curve for OC	101
Figure 4.8.	UV-spectra at selected points of BMDM peak in the chromatogram after normalisation.	103
Figure 4.9.	UV-spectra at selected points of OC peak in the chromatogram after normalisation.	104
Figure 4.10.	Calibration curve for B3	107
Figure 4.11.	UV-spectra of selected points of B3 chromatogram after normalisation.	108
Figure 5.1.	Chemical structures of BMDM and OC	112
Figure 5.2.	Photodegradation profile of BMDM in the presence and absence of TiO_2	118

Figure 5.3.	Photodegradation profile of BMDM in combination with OC in the presence and absence of TiO_2	120
Figure 5.4.	Photodegradation profile of OC in the presence and absence of TiO_2	121
Figure 5.5.	Photodegradation profile of OC in combination with BMDM in the presence and absence of TiO_2	122
Figure 5.6.	Simplified Jablonski Diagram. ¹⁶⁶	124
Figure 5.7.	Molar absorption coefficients (ϵ) of BMDM and OC , main emission lines of TQ 150 mercury lamp (radiation flux) and % transmittance of pyrex glass vessel.	125
Figure 5.8.	Formation of electron-hole pair on surface of TiO_2 particle.....	126
Figure 5.9.	Photodegradation profile of BMDM in the presence and absence of coated TiO_2 and vitamin E (Vit E).....	128
Figure 5.10.	Photodegradation profile of BMDM in a combination with OC in the presence and absence of coated TiO_2 and vitamin E (Vit E).....	130
Figure 5.11.	UV-absorption spectrum of vitamin E.	131
Figure 5.12.	Photodegradation profile of OC in the presence and absence of coated TiO_2 and vitamin E (Vit E).....	132
Figure 5.13.	Photodegradation profile of OC in a combination with BMDM in the presence and absence of coated TiO_2 and vitamin E (Vit E).....	133
Figure 5.14.	BMDM recovery in % \pm SD, alone and in combination with OC	136
Figure 5.15.	OC recovery in % \pm SD, alone and in combination with BMDM	137
Figure 5.16.	First order kinetic plots of A: OC alone; B: OC in combination; C: BMDM alone; D: BMDM in combination, plotted as $\ln (P_A/P_{A_0}) \pm$ SD against time.....	138
Figure 5.17.	HPLC chromatogram of BMDM after four hours irradiation, detected at 253 nm.	139
Figure 5.18.	Mass spectrum with the observed ion for BMDM-1 (m/z 150.9).....	141
Figure 5.19.	Mass spectrum with the observed ion for BMDM-2 (m/z 177.0).....	141
Figure 5.20.	HPLC chromatogram of OC after 24 minutes irradiation, detected at 303 nm.....	143
Figure 5.21.	Mass spectrum with the observed ion for OC-1 (m/z 286.3) and other detected molecular weights, which are part of a pattern (m/z 261.3, 305.4, 349.5, 393.5).....	144
Figure 6.1.	Franz diffusion cell.	148
Figure 6.2.	Chemical structure of B3	150

List of Schemes

- Scheme 2.1.** Trans- to cis-transformation of UV-filter **1**. 18
- Scheme 2.2.** Diketo-enol-tautomerism of UV-filter **3**. 18
- Scheme 2.3.** Fragmentation of UV-filter **3** into a phenacyl radical (**3a**) and a benzoyl radical (**3b**) with $R_1 = -OCH_3$ and $R_2 = -C(CH_3)_3$ or *vice versa*; Norris-cleavage Type I reaction at either i) or ii). 19
- Scheme 2.4.** Proposed photodegradants of UV-filter **6** after 140 hours of irradiation in cyclohexane: **24** = 4-monomethylaminobenzoic acid 2-ethylhexyl ester (21 %), **25** = 4-aminobenzoic acid 2-ethylhexyl ester (< 1 %) and **26** = 4-dimethylamino-(2/3)-methylbenzoic acid 2-ethylhexyl ester (5 %). Adapted from.⁶¹ 28
- Scheme 2.5.** Identified photodegradants of UV-filter **3**: **27** = 4-*t*-butyl benzoic acid, **28** = 4-methoxy benzoic acid and **29** = *t*-butyl benzene.⁶¹ 28
- Scheme 2.6.** Photodegradants of UV-filter **3** after eight hours of irradiation in cyclohexane identified by GC-MS: **30** = 4-methoxy benzaldehyde, **27** = 4-*t*-butyl benzaldehyde, **28** = 4-methoxy benzoic acid, **31** = 4-*t*-butyl benzoic acid, **32** = 4-methoxy phenylglyoxal, **33** = 4-*t*-butyl phenylglyoxal, **34** = 4-methoxy acetophenone, **35** = 4-*t*-butyl acetophenone, **36** = 4,4-di-*t*-butyl benzil, **37** = 4-*t*-butyl-4-methoxy benzil, **38** = 4,4-dimethoxydibenzoyl methane, **39** = 4-*t*-butyl-4-methoxydibenzoyl ethane. Adapted from.³⁷ 30
- Scheme 2.7.** Possible photodegradants of UV-filter **3** identified by LC-MS after an irradiation dose of 60 kJ/m² in water: **40** = (Z)-1-(4-*t*-butylphenyl)-3-hydroxy-3-(4-methoxyphenyl)prop-2-en-1-one and **41** = 1,4-*bis*(4-methoxyphenyl)butane-1,4-dione. Adapted from.⁶³ 31
- Scheme 2.8.** Photodegradants of UV-filter **6** identified by GC-MS after UVA-exposure of 100 J/cm² in petroleum jelly: **24** = 2-ethylhexyl 4-methylaminobenzoate and **42** = 4-(formylmethylamino) benzoate. Adapted from.⁴² 32
- Scheme 2.9.** Photodegradants of UV-filter **4** identified by GC-MS after UVA-exposure of 100 J/cm² in petroleum jelly: **43** = benzil, **44** = isopropylbenzil, **45** = 1-phenyl-3-(4-iso-propylphenyl)-propane-1,2,3-trione and **46** = 1,3-di(4-iso-propylphenyl)-propane-1,2,3-trione. Adapted from.⁴² 33
- Scheme 2.10.** [2+2] cycloaddition of **1** and **3**, resulting in photodegradant **49**. 34
- Scheme 2.11.** Photocycloaddition products in cyclohexane: **47** = 2-ethylhexyl-5-[4-(2,2-dimethylethyl)phenyl]-3-(4-methoxyphenyl)-2-(4-methoxybenzoyl)-5-oxopentanoate, **48** = 2-ethylhexyl-2-[4-(2,2-diethylethyl)benzoyl]-3,5-bis-(4-methoxyphenyl)-5-oxopentanoate, **49** = 2-ethylhexyl-4-[4-(2,2-

	dimethylethyl)phenyl]-3-(4-methoxyphenyl)-2-(4-methoxybenzoyl-methyl)-4-oxobutanoate and 50 = 2-ethylhexyl-3,4- <i>bis</i> -(4-methoxyphenyl)-2-[4-(2,2-dimethyl-ethyl)benzoylmethyl]-4-oxobutanoate. Adapted from. ⁶⁸	35
Scheme 2.12.	Tested benzils (36 , 37 , 43 and 53) and arylglyoxals (32 , 33 , 51 and 52) for their cytotoxicity and allergic potential using a LLNA and a cell proliferation assay. Adapted from. ⁶²	39
Scheme 2.13.	Vitamin E and vitamin E acetate.	47
Scheme 5.1.	Generation of ROS by TiO ₂	126
Scheme 5.2.	ET involving TiO ₂	127
Scheme 5.3.	Formation of vitamin E radical and regeneration to vitamin E.....	132
Scheme 5.4.	Photodegradation <i>via</i> BMDM diketo-form into BMDM-1 (Norrish-I cleavage). ⁶¹	140
Scheme 5.5.	Proposed degradation mechanism of OC (Norrish-II cleavage) after irradiation in methanol (quartz glass).....	144
Scheme 6.1.	Photodegradation of BMDM , including stabilisation by OC	165

List of Abbreviations

UV	Ultraviolet
ROS	Reactive oxygen species
BCC	Basal cell carcinoma
SCC	Squamous cell carcinoma
NMSC	Non-melanoma skin cancer
CCA	Cancer Council of Australia
TiO ₂	Titanium dioxide
ZnO	Zink oxide
SPF	Sun Protection Factor
MED	Minimum erythematous dose
UVA-PF	UVA-protection factor
PPD	Persistent-Pigment Darkening
MPD	Minimal pigmentation dose
BMDM	Butyl methoxy dibenzoylmethane
OC	Octocrylene
B3	Benzophenone-3
HPLC	High performance liquid chromatography
DSC	Differential scanning calorimetry
NMR	Nuclear magnetic resonance
IR	Infrared
LC-MS	Liquid chromatography - mass spectrometry
FTMS	Fourier transform - mass spectrometry
ICH	International Conference on Harmonisation

TGA	Therapeutic Goods Administration
ARTG	Australian Register of Therapeutic Goods
AS/NZS	Australian/New Zealand Standard
ISO	International Organisation for Standardization
CI	Confidence Interval
PMMA	Polymethylmethacrylate
FDA	Federal Drug Administration
OTC	Over-the-counter
Colipa	European Cosmetic, Toiletry and Perfumery Association
O/W	Oil in water
CIE	International Commission on Illumination
PC	Phosphatidylcholine
TBA	Thiobarbituric acid
TBARS	TBA reactive substances
GC	Gas chromatography
EPR	Electron paramagnetic resonance
GC-MS	Gas chromatography - mass spectrometry
DMSO	Dimethyl sulfoxide
THF	Tetrahydrofuran
LLNA	Local lymph node assay
UK	United Kingdom
ESR	Electron Spin Resonance
DPPH	1,1-Diphenyl-2-picrylhydrazyl
PI	Photoactivity Index

EDTA	Ethylenediaminetetraacetic acid
EPA	Eicosapentaenoic acid
MDA	Malondialdehyde
SDS	Sodium dodecyl sulphate
SED	Standard erythematol dose
SLN	Solid lipid nano-particle
NLC	Nano-structured lipid carrier
BSA	Bovine serum albumin
W/O	Water in oil
W/Si	Water in silicone
IPM	Isopropyl myristate
IPP	Isopropyl palmitate
IPS	Isopropyl stearate
PACD	Photoallergic contact dermatitis
ACD	Allergic contact dermatitis
HPTLC	High performance thin layer chromatography
NRU-PT	Neutral Red Uptake Phototoxicity Test
H3D-PT	Human 3-D Skin Model Phototoxicity Test
PDA	Photodiode array
BP	British Pharmacopoeia
PTFE	Polytetrafluoroethylene
λ_{\max}	Absorption maximum
R^2	Correlation coefficient
SD	Standard deviation

RSD %	Relative standard deviation
LOD	Limit of detection
LOQ	Limit of quantitation
S/N	Signal-to-noise
Rs	Resolution factor
H	Peak height
h	Baseline noise of the blank sample
width $\frac{1}{2}$	Widths at half height
k	Rate constant
$t_{1/2}$	Half-life
MS	Mass-spectrometer
S^0	Ground state
S^N, S^1	Excited singlet states
T^N, T^1	Excited triplet states
IC	Internal conversion
ISC	Intersystem crossing
ϵ	Molar absorption coefficient
λ	Wavelength
h_{VB}^+	Positively charged valance band
e_{CB}^-	Negatively charged conduction band
ET	Electron transfer
CB	Conduction band
t	Time
PA_t	Peak area at time t

PA ₀	Peak area at time 0
HLB	Hydrophilic-lipophilic balance
PIT	Phase inversion temperature
RH	Relative humidity
IBC	International Biosafety Committee
EMC	Ethylhexyl methoxycinnamate

Chapter 1

Introduction

1.1. Solar UV-radiation

The exposure to sunlight is part of daily life, especially in the northern regions of Australia. The monthly average ultraviolet (UV)-Index for north Queensland is between “high” and “extreme” (Table 1.1) during the whole year,¹ which is a concern in a modern, western society, where a light tan is regarded as healthy.

Table 1.1. Relationship between UV-Index and UV-exposure category.

UV-Index	Exposure Category
2 or less	Low
3 to 5	Moderate
6 to 7	High
8 to 10	Very high
11+	Extreme

Exposure to UV-light can be potentially dangerous and may result in adverse health outcomes.² UV-light is classified as UVC, UVB, UVA I and UVA II, according to wavelength range (Table 1.2).

Table 1.2. UV-classifications and their wavelengths.

UV-classifications	Wavelengths
UVC	100 - 290 nm
UVB	290 - 320 nm
UVA I	320 - 340 nm
UVA II	340 - 400 nm

While the UVC-light is filtered to a large extent by the atmosphere and thus does not reach the surface of the earth,³ UVB-radiation (1 - 10 % of the complete solar UV-radiation), although mainly restricted to penetration of the upper layers of the skin, can cause DNA-damage and sunburn. UVA-light (90 - 99 % of the complete solar radiation), however, does reach the deeper skin layers causing photoageing and DNA-damage by generation of reactive oxygen species (ROS).^{4,5}

1.2. Health Effects Caused by UV-radiation

Skin cancer is the worst outcome of excessive exposure to UV-light.^{6,7} Sunburn, eye conditions such as cataract or ocular melanoma, premature skin ageing such as wrinkles or irregular pigmentation of the skin and a compromised immune system are also potential outcomes of UV-exposure. Skin cancer can be divided into three main types: basal cell carcinoma (BCC), squamous cell carcinoma (SCC) and melanoma. The most common forms are BCC and SCC, referred to as non-melanoma skin cancer (NMSC), which are much less dangerous than melanoma, the deadliest form of skin cancer. In comparison to the NMSC, which usually appears on areas of the body that are most often exposed to the sun, such as the face or neck, melanoma may appear anywhere on the body, even on areas that are rarely exposed to the sun. According to estimations of the Cancer Council of Australia (CCA), the exposure to UV-light causes up to 95 % of the melanoma and 99 % of NMSC in Australia.⁸

Australia and New Zealand have the highest rates of skin melanoma in the world,⁹ which as estimated in 2012, is the fourth most common type of cancer in Australia.¹⁰ In 2012, the incidence rate for skin melanoma was 12,510 cases in the whole population with an estimated mortality rate of 1,560 cases.¹¹ However, these statistics do not include the NMSC, because they are less dangerous than melanoma, usually removed in doctors' surgeries and are therefore not reportable by law. Nevertheless, NMSC is by far the most commonly diagnosed cancer in Australia; it was estimated that in 2008 about 434,000 men and women were diagnosed with at least one NMSC in Australia.¹² Although the survival rates for NMSC are relatively high, with only 543 fatalities in 2011,¹² NMSC was the reason for the highest number of hospitalisations (95,312) for all cancers in 2010 and 2011.¹⁰ Before the age of 70, two out of three Australians will be diagnosed at least once with a skin cancer, which may be a melanoma or NMSC.¹³

1.3. Sunscreen Products

The most effective way to protect against the dangerous effects of UV-light is to avoid excessive exposure to sunlight and wear protective clothes. As this is not always possible, it is recommended that a sunscreen product be applied every two hours to the skin.¹⁴ The active ingredients in sunscreen products are UV-filters, which can be divided into chemical and physical UV-filters. Chemical UV-filters are organic compounds, which absorb UV-light. Titanium dioxide (TiO₂) and zinc oxide (ZnO) are two available physical UV-filters on the market, which reflect or absorb UV-light, depending on their particle size.¹⁵ Within these two groups they can be subdivided into UVA-filters which only absorb UVA-light, UVB-filters (only absorb UVB-light) and broad spectrum filters which absorb both UVA- and UVB-light.

In addition, sunscreens may contain other additives such as antioxidants, which are also thought to play a role in protecting the skin from the effects of exposure to UV-light.¹⁶

The first modern sunscreens, merchandised in the 1930s,¹⁷ were characterized by the Sun Protection Factor (SPF), which is a measure of the protection of the skin from sunburn.¹⁸ The SPF-testing method is an *in vivo* method, where protected and unprotected skin-areas are exposed to artificial sunlight for various time periods. The SPF is defined as the minimum erythemal dose (MED = time when redness of the skin is visible) on protected skin divided by the MED on unprotected skin (Equation 1.1).¹⁹

$$\text{SPF} = \text{MED}_{\text{protected}} / \text{MED}_{\text{unprotected}} \quad (1.1)$$

Because it was originally thought that sunburn (caused by UVB-light) was solely the result of exposure to UV-light, the first sunscreens did not offer protection against UVA-light. It has only been in the last few decades that the harmful and photoageing effects of UVA have been recognized and it is thus been recommended that additional protection against the UVA-light be included in sunscreens recently, resulting in the design of broad spectrum sunscreens.^{6,20-23} The UVA-protection factor (UVA-PF) can be measured *in vivo* or *in vitro*. The *in vivo*-test-method, also called Persistent-Pigment Darkening (PPD) method was applied by the Japanese industry and modified by the French Health Agency (Afssaps = Agence française de sécurité sanitaire des produits de santé) and measures the minimal darkening effect of UVA-radiation on the skin before and after exposure to UVA-light. The UVA-PF is defined as minimal pigmentation dose (MPD) on protected skin divided by the MPD on unprotected skin (Equation 1.2).^{24,25}

$$\text{UVA-PF} = \text{MPD}_{\text{protected}} / \text{MPD}_{\text{unprotected}} \quad (1.2)$$

1.4. Overall Aim, Hypothesis and Objectives

Sunscreen products, offering the optimum protection from the harmful effects of UV-radiation, often contain multiple ingredients to provide broad spectrum protection. Photoprotection provided, however, may be compromised by the photoinstability as a result of the photolysis of the component chemical UV-filters. The inclusion of the physical UV-filter TiO₂ adds complexity especially because of its photocatalytic properties, providing an additional process for the photodegradation of the chemical UV-filters. Skin penetration of the UV-filters can also reduce their UV-protective potential, in addition to causing photosensitising reactions.

The overall aim of this study was thus to investigate the photostability and skin penetration of UV-filter combinations included in a typical sunscreen product to provide broad spectrum protection.

Hypothesis

Chemical UV-filters in combination with TiO₂ in a sunscreen product decreases their photostability and the combination of chemical UV-filters increases their skin penetration.

In order to prove or disprove this hypothesis the following objectives are proposed, which inform the design of the thesis (in terms of chapters):

- To review the literature on the photostability and skin penetration of UV-filters in sunscreen products (Chapter 2)
- To characterise (chemical and physical properties) Butyl methoxy dibenzoylmethane (**BMDM**), Octocrylene (**OC**) and Benzophenone-3 (**B3**) to confirm their purity and identity (Chapter 3)
- To develop and validate a high performance liquid chromatography (HPLC) method to analyse the combination of the chemical UV-filters **BMDM** and **OC** in the presence of their photodegradants (Chapter 4)
- To investigate the photostability of **BMDM** and **OC** in the presence of TiO₂ (coated, micro- and nano-TiO₂) and vitamin E in methanol (Chapter 5)
- To determine the photostability of **BMDM** and **OC** in the presence of coated, micro- and nano-TiO₂ in a stable microemulsion (Chapter 6)
- To investigate the skin penetration *in vitro* of **BMDM**, **OC** and **B3** in a microemulsion, using Franz diffusion cells (Chapter 6)

1.5. Thesis Outline

The thesis consists of seven chapters, whose content is outlined in the table below.

Chapter 1	<p>Introduction</p> <p>This chapter provides background information about the dangerous effects of UV-light and the purpose of UV-filters in sunscreen products, highlighting the motivation for this study. The overall aim, hypothesis and the objectives for this study are presented as well as this thesis outline.</p>
Chapter 2	<p>Photostability and Skin Penetration – A Review</p> <p>In this chapter previous studies about UV-filters used in sunscreen products are reviewed, including:</p> <ul style="list-style-type: none">• Photostability of chemical UV-filters• Identity and toxicity of possible photodegradants• Effects of physical UV-filters and antioxidants on photostability of chemical UV-filters• Influence of formulation components on UV-protective performance• Skin penetration of chemical UV-filters• Photoallergic and phototoxic skin reactions caused by UV-filters <p>After reviewing the literature, candidate UV-filters were selected for the study.</p>
Chapter 3	<p>Characterisation of Chemical UV-filters</p> <p>The chemical and physical properties of the chemical UV-filters used in this study (BMDM, OC and B3) are described in this chapter. UV-filter purity is determined by melting point determinations, differential scanning calorimetry (DSC) and HPLC. Their identity is confirmed by nuclear magnetic resonance (NMR)-, infrared (IR)- and UV-spectroscopy.</p>
Chapter 4	<p>HPLC – Method Development and Validation</p> <p>This chapter includes the development and validation of an HPLC method for the simultaneous determination of the chemical UV-filters BMDM and OC in the presence of their photodegradants. The same method was also validated for the determination of UV-filter B3.</p>

Chapter 5	<p>Photostability of Chemical UV-filters</p> <p>This chapter presents the photostability studies of BMDM and OC, irradiated separately and in combination in methanol. The influence of TiO₂ (silica coated, micro- and nano-TiO₂) and vitamin E on the photostability of BMDM and OC is also investigated. Degradation kinetics are described and major photodegradants are identified by liquid chromatography - mass spectrometry (LC-MS) and Fourier transform - mass spectrometry (FTMS).</p>
Chapter 6	<p>Microemulsion – Photostability and Skin Penetration of Chemical UV-filters</p> <p>In this chapter a suitable topical microemulsion was selected from the literature, further modified and used as a model for sunscreen product for topical delivery to undertake photostability and skin penetration studies. Photostability studies of BMDM and OC, separately and in combination, in the presence and absence of silica coated, micro- and nano-TiO₂ were undertaken in the stable microemulsion and a reference cream. Finally, the skin penetration of BMDM and OC, separately and in combination, was investigated <i>in vitro</i> using Franz diffusion cells and compared to the skin penetration of B3.</p>
Chapter 7	<p>Conclusions and Recommendations</p> <p>This chapter highlights the outcomes of this project and addresses the overall aim and objectives of the study and also presents recommendations for further research in this area.</p>

Chapter 2

Photostability and Skin Penetration – A Review

2.1. Introduction

Sunscreen products are widely used worldwide to protect the skin from harmful effects of UV-light. Especially here in Australia the use of these products is widely promoted, due to the high UV-Indexes nationwide. To ensure optimum efficiency the active ingredients, the UV-filters, should remain stable to light and not penetrate the skin. Photostability testing according to the International Conference on Harmonisation (ICH) Guideline Q1B,²⁶ applied to new drug substances and products, is however not mandatory for sunscreen products in Australia, the USA and Europe.^{14,25,27} Although new guidelines in Australia (2012), the USA (2011) and Europe (2011) include a pre-irradiation of the test product, a detection and quantitation of photodegradants after UV-irradiation, under specified conditions, as in the ICH Guideline Q1B, is not required. This lack of photostability testing and the inclusion of chemical UV-filters and nano-TiO₂ in sunscreen products have highlighted the need for a review of the photostability and skin penetration of UV-filters.

2.2. Regulations

To ensure both, safety and effectivity, sunscreen products are required to be regulated. The regulation of sunscreen products differs, depending on the particular country and/or the requirements of the regulatory body. Included in these regulations is a list of approved UV-filters, the appropriate labelling of sunscreen products and requirements for the measuring of SPF, UVA-PF and water-resistance. Regulations for Australia, the USA and Europe are explained in detail below.

2.2.1. Australia - Therapeutic Goods Administration (TGA)

In Australia, although most sunscreen products are ‘listed’ medicines in the Australian Register of Therapeutic Goods (ARTG), some of these products can be ‘exempt’ or are required to be ‘registered’. ‘Listed’ sunscreen products are required to conform with the Australian/New Zealand Standard™ AS/NZS 2604:2012 and the *Australian regulatory guidelines for sunscreens* in testing and labelling.^{14,19} Active ingredients permitted in sunscreen products have to be listed in the *Australian regulatory guidelines for sunscreens* and be present within the maximum concentration.¹⁴ When the active ingredients, the UV-filters, are not listed for this purpose or the sunscreen product claims any other therapeutic effect than suncreening, the product is required to be ‘registered’. If the SPF of a sunscreen product is less than 4, does not contain any ingredients of human or animal origin, the label claim “complies to the AS/NZS

2604:2012” and has no indication for a serious disease or condition as specified in the *Therapeutic Goods Advertising Code*, it can be ‘exempt’ from being registered or listed in the ARTG. Products with sun protective ingredients, whose primary purpose is neither sunscreens nor therapeutic can be regarded as a cosmetic and are regulated by the *National Industrial Chemical Notification and Assessment Scheme*.^{14,28}

Sunscreen products are characterised using the SPF, which gives information about the UVB-protection, it offers. A further benchmark can be its water resistance or the broad spectrum (UVA and UVB) specification that gives additional protection against UVA-radiation.

General information, the classification of sunscreen products and performance requirements for water-resistance determinations and some labelling claims are described in the AS/NZS 2604:2012. Determinations of SPF and UVA-PF are referred to the standards of the International Organisation for Standardization (ISO): ISO 24444 ‘Cosmetics – Sun protection test methods – *In vivo* determination of the sun protection factor (SPF)’²⁹ and ISO 24443 ‘Determination of the sunscreen UVA photoprotection *in vitro*’,³⁰ respectively.¹⁹

The SPF-test method is an *in vivo* test-method performed on 10 - 25 fair skinned volunteers with a skin type of I to III, which implies skin that always burns easily and never tans to skin which burns moderately and tans gradually. The tested sunscreen product is placed on the back of the test subjects (2 mg/cm²) and after a waiting period of 15 to 30 minutes, the test area is exposed to solar simulated UV-light. The MED is detected by an observer 16 to 24 hours later. To obtain a valid SPF value, the 95 % confidence interval (CI) on the mean SPF measured shall be ± 17 %.²⁹ The mean SPF is calculated to one decimal place and is labelled according to a specific category (Table 2.1).¹⁹

Table 2.1. Labelled category description according to the SPF value.

Tested SPF	Labelled SPF	Category description
1 - 3	Not allowed	Not allowed
4 - 14	4, 6, 8, 10	Low
15 - 29	15, 20, 25	Medium or moderate
30 - 59	30, 40, 50	High
60 or more	50+	Very high

To determine the broad spectrum capacity, the transmission from 290 to 400 nm through a thin film of sunscreen product spread on a roughened surface (polymethylmethacrylate, PMMA) is measured. Transmittance is measured before and after UV-irradiation of a controlled,

specifically calculated dose. To claim broad spectrum protection the UVA-PF shall be equal to or greater than one third of the SPF. The 95 % CI shall not be greater than ± 17 % of the mean value of the UVA-PF,³⁰ with a critical wavelength of at least 370 nm. The critical wavelength is classified as the wavelength at which the integral of the spectral absorbance curve reaches 90 % of the integral, over the complete UV-spectrum (290 - 400 nm).¹⁹

If a sunscreen product claims water-resistance, the SPF of a sunscreen product is determined after immersion with water for at least 40 minutes in a simulated swim test device. This test device should be about 1.8 m \times 1.8 m, in which the subjects should sit comfortably. After the application of the sunscreen product, the test involves alternating 20 minutes in the water (16 minutes water circulation and four minutes air agitation) and five minutes rest period. The maximum length of time for water-resistance labelled on the product depends on the SPF determined (Table 2.2).¹⁹

Table 2.2. Maximum water resistance on product according to SPF value.

SPF after immersion	Maximum water resistance
At least 2 but less than 8	No claim
At least 8 but less than 15	40 minutes
At least 15 but less than 30	2 hours
At least 30 or above	4 hours

All sunscreen products are required to be stable, until the expiry date under the labelled storage conditions and to be free of microbiological contamination.¹⁴

2.2.2. USA - Federal Drug Administration (FDA)

In the USA, sunscreens are regulated as over-the-counter (OTC) drugs by the FDA. The *Federal Register of 1999* contains the final monograph with a list of allowed sunscreen active ingredients and their permitted maximum concentrations: *Sunscreen drug products for Over-the-counter human use*. While the *Federal Register of 2011* updated the labelling and effectiveness testing of sunscreen products, it does not include a list of allowed active ingredients with their permitted maximum concentrations. The monograph in the *Federal Register of 1999* is not mandatory and the sunscreen manufacturers are thus encouraged, but not required, to follow any of these regulations. Rules and regulations written in the *Federal Register of 2011* became effective in June 2012 with a compliance date in December 2013.^{27,31}

The *in vivo* SPF-test method is very similar to that used in Australia. A minimum of ten valid test results is required and only three subjects may be rejected; no maximum is given. Each

subject shall have a skin type between I and III. The test product is applied on the back of the subjects with a thickness of 2 mg/cm² and left to dry for at least 15 minutes before UV-irradiation. The MED is detected after 16 - 24 hours and the SPF is determined. While minimum of SPF 2 is required, no maximum allowed labelled SPF value is given.²⁷

The broad spectrum test procedure is also very similar to the Australian guideline. The transmittance of the test product, spread on a PMMA plate, after pre-irradiation of 4 MEDs is determined for each wavelength of the UV-spectrum (290 - 400 nm). To claim broad spectrum protection, a critical wavelength of 370 nm or greater must also be achieved.²⁷

For the water-resistance test, a freshwater pool, whirlpool or hot tub can be used. In contrast to the Australian guideline, where water-resistance of up to four hours can be claimed, the FDA only allows claims of 40 or 80 minutes. Test subjects should be in the water rotation for 20 minutes, followed by a rest period of 15 minutes. While in Australia subjects should not move around during the immersion time, the FDA requires moderate activity in the water.²⁷

2.2.3. Europe - European Cosmetic, Toiletry and Perfumery Association (Colipa)

In contrast to Australia and the USA, in Europe sunscreen products are regarded as cosmetics. The European Commission published a *Commission Recommendation on the efficacy of sunscreen products*, where they give advice about the hazards of UV-radiation, the need of sunscreen products and recommendations about labelling and testing.²⁵ An industry association, namely Colipa was founded to develop the industry standards on testing, labelling and consumer education. They have also published guidelines for SPF-, UVA- and water-resistance test methods.

A list of allowed UV-filters in sunscreen products and their maximum allowed concentration was published by the European parliament. While in Australia and the USA ingredients in the form of nanomaterials do not have to be specially labelled, in Europe these ingredients are required to be followed by the word 'nano' in brackets.³²

Pursuant to the *Commission Recommendation (2006)* the SPF should be measured according to the Colipa guideline *International Sun Protection Factor Test Method (2006)*, which has now been replaced by the ISO standards ISO 24444,²⁹ the same test method used in Australia.²⁵ The Colipa guideline, *In vitro method for the determination of the UVA protection factor and "critical wavelength" values of sunscreen products (2011)* has also been replaced by an ISO standard, the ISO 24443.³⁰ Details, which may not be included in the ISO standards are described in the *Commission Recommendation (2006)*, such as the recommended critical wavelengths of at least 370 nm to claim broad spectrum protection or a list of allowed labelled

SPF and categories (Table 2.3). The ratio of the UVA-PF should be at least one third of the measured SPF factor.²⁵

Table 2.3. Labelled SPF and category description according to measured SPF.

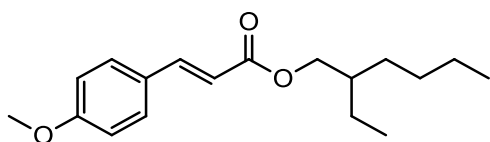
Labelled category	Labelled SPF	Measured SPF
Low protection	6	6 - 9.9
	10	10 - 14.9
Medium protection	15	15 - 19.9
	20	20 - 24.9
	25	25 - 29.9
High protection	30	30 - 49.9
	50	50 - 59.9
Very high protection	50+	60 ≤

The principle of the water-resistance test method is to compare the SPF after water immersion with the static SPF before water immersion. This is the main difference between the European and the Australian and American test methods, where only the SPF after water immersion is measured, when water resistance is claimed. The recommended equipment is a Spa Pool, Jacuzzi® or bathtub with water jets to circulate water. An alternative method with a swimming pool is also acceptable, but not described in the guideline. A sunscreen can only be claimed to be ‘water-resistant’ or ‘very water-resistant’ after a successful test of 40 or 80 minutes of immersion in water, respectively. The procedure is in turn 20 minutes immersion and 15 minutes drying time, without towelling. To attain the acceptable criteria for ‘water-resistant’ or ‘very water-resistant’, the 90 % lower unilateral confidence limit has to be greater or equal to 50 %.³³

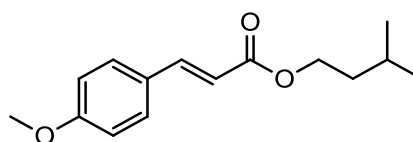
2.3. Chemical UV-filters

Figure 2.1 shows the molecular structures of the chemical UV-filters included in this review, while Table 2.4 lists their CAS-numbers, INCI-names, chemical names, UV-absorbance ranges and UV-absorbance maxima (λ_{\max}).

Cinnamates:

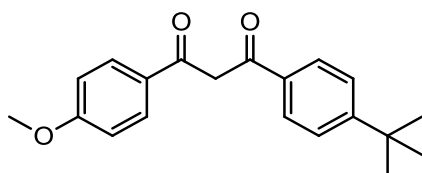


Ethylhexyl methoxycinnamate (1)

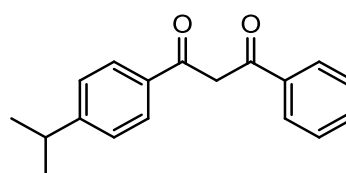


Isoamyl methoxycinnamate (2)

Dibenzoylmethanes:

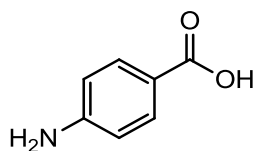


Butyl methoxy dibenzoylmethane (3)

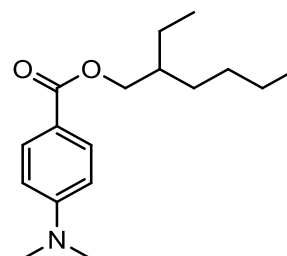


Isopropyl dibenzoylmethane (4)

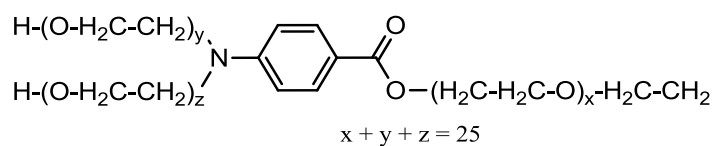
Para-amino benzoic acid and its derivatives:



Aminobenzoic acid (PABA) (5)

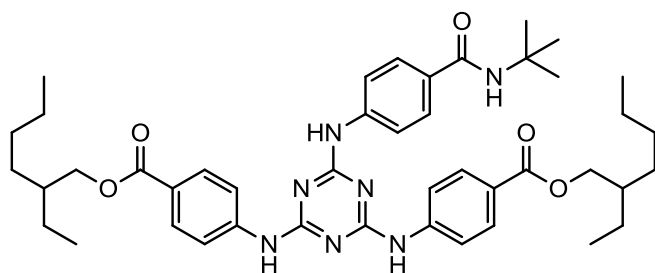


Ethylhexyl dimethyl PABA (6)

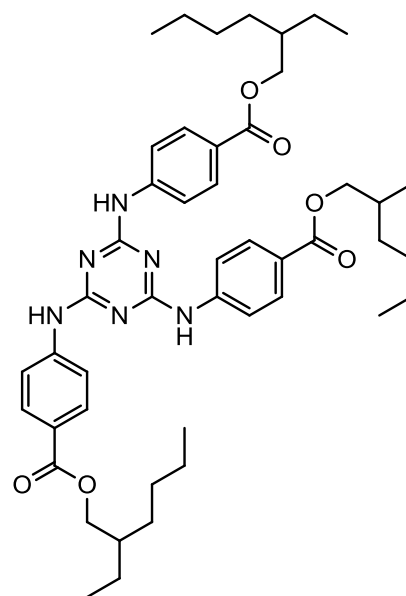


PEG-25 PABA (7)

Triaminotriazine:

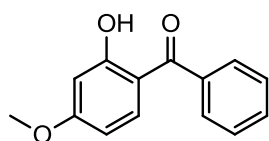


Diethylhexyl butamido triazone (8)

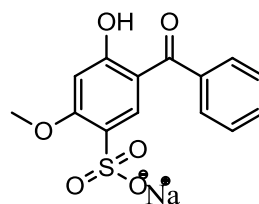


Ethylhexyl triazone (9)

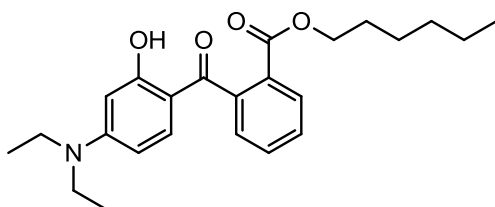
Benzophenones:



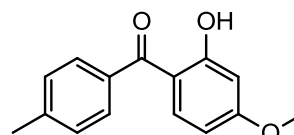
Benzophenone-3 (10)



Benzophenone-5 (11)

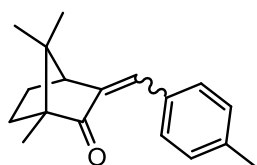


Diethylamino hydroxybenzoyl hexyl benzoate (12)

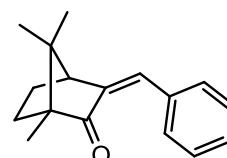


Benzophenone-10 (13)

Camphor derivatives:

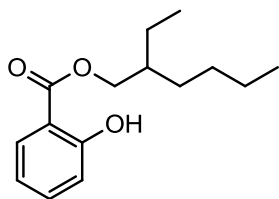


4-Methylbenzylidene camphor (14)

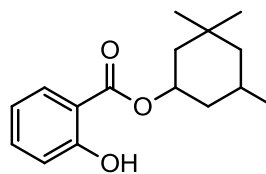


3-Benzylidene camphor (15)

Salicylate:

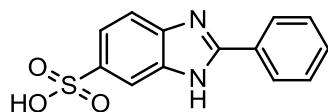


Ethylhexyl salicylate (**16**)

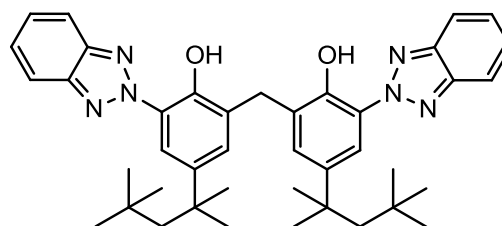


Homosalate (**17**)

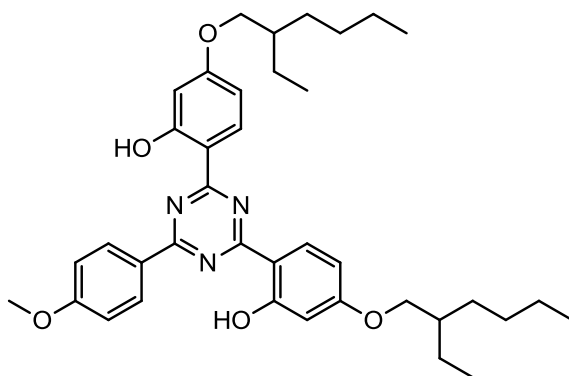
Others:



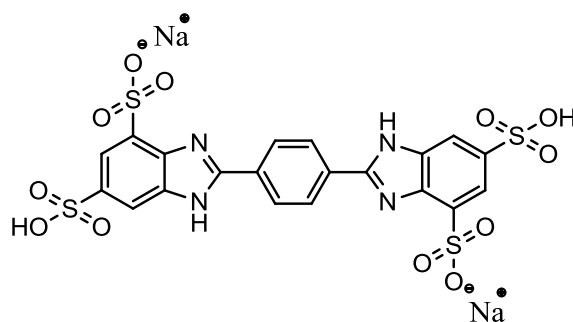
Phenylbenzimidazole sulfonic acid (**18**)



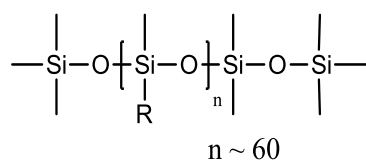
Methylene bis-benzotriazolyl tetramethylbutylphenol (**19**)



Bis-ethylhexyloxyphenol methoxyphenyl triazine (**20**)



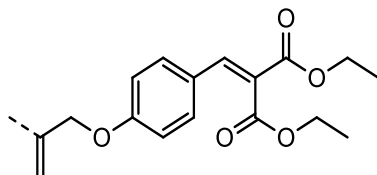
Disodium phenyl dibenzimidazole tetrasulfonate (**21**)



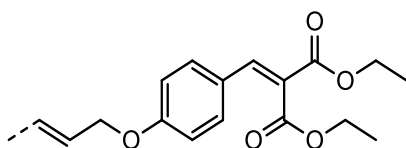
R = ~ 92.1 - 92.5%

---CH₃

and ~ 6%



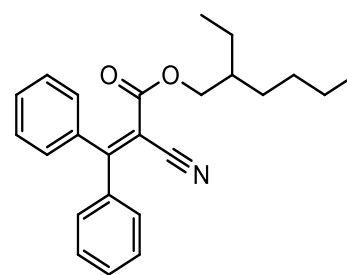
and ~ 1.5%



and ~ 0.1 - 0.4%

---H

Polysilicone-15 (**22**)



Octocrylene (**23**)

Figure 2.1. Chemical structures of chemical UV-filters.

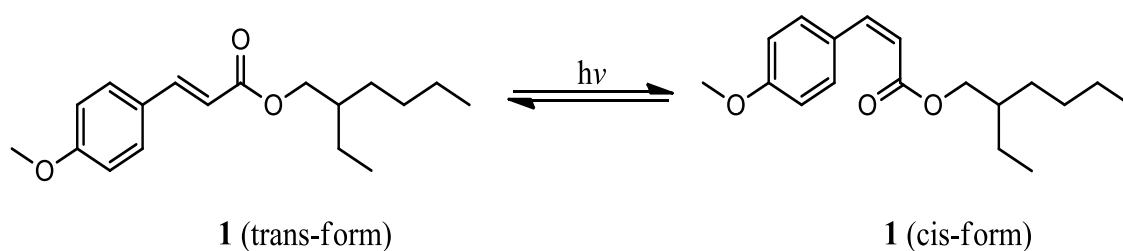
Table 2.4. Chemical UV-filters with CAS-numbers, INCI-names, chemical names, UV-absorbance (UVA/UVB), UV-absorbance maxima (λ_{\max}) with solvent and references for λ_{\max} .

No	CAS-No	INCI-name	Chemical name	UV-absorbance	λ_{\max} [nm] (Solvent)	Ref
1	5466-77-3	Ethylhexyl methoxycinnamate	2-Ethylhexyl 4-methoxycinnamate	UVB	308 (Methanol)	34
2	71617-10-2	Isoamyl methoxycinnamate	Isopentyl-4-methoxycinnamate	UVB	310 (Ethanol)	35
3	70356-09-1	Butyl methoxy dibenzoylmethane	1-(4- <i>tert</i> -Butylphenyl)-3-(4methoxyphenyl) propane-1,3-dione	UVA	357 (Ethanol)	36
4	63250-25-9	Isopropyl dibenzoylmethane	1-[4-(1-Methylethyl)phenyl]-3-phenylpropane-1,3-dione	UVA	341 (Cyclohexane)	37
5	150-13-0	PABA	4-Aminobenzoic acid	UVB	277 (Methanol)	34
6	21245-02-3	Ethylhexyl dimethyl PABA	2-Ethylhexyl 4-(dimethylamino)benzoate	UVB	311 (Methanol)	34
7	116242-27-4/ 113010-52-9	PEG 25 PABA	Ethoxylated ethyl-4-aminobenzoate	UVB	307 (Ethanol)	35
8	154702-15-5	Diethylhexyl butamido triazone	<i>Bis</i> (2-ethylhexyl) 4,4'-[(6-{[4-(<i>tert</i> -butyl-carbamoyl)phenyl]amino}-1,3,5-triazine-2,4-diyl)diimino] dibenzoate	UVB	311 (Ethanol)	35
9	88122-99-0	Ethylhexyl triazone	2,4,6-Trianiilino-(<i>p</i> -carbo-2'-ethylhexyl-1'-oxy)-1,3,5-triazine	UVB	313 (Ethanol)	38
10	131-57-7	Benzophenone-3	2-Hydroxy-4-methoxybenzophenone	UVB/UVA	287, 325 (Methanol)	34
11	6628-37-1	Benzophenone-5	2-Hydroxy-4-methoxybenzophenone-5-sulfonic acid, sodium salt	UVB/UVA	286, 323 (Not given)	39

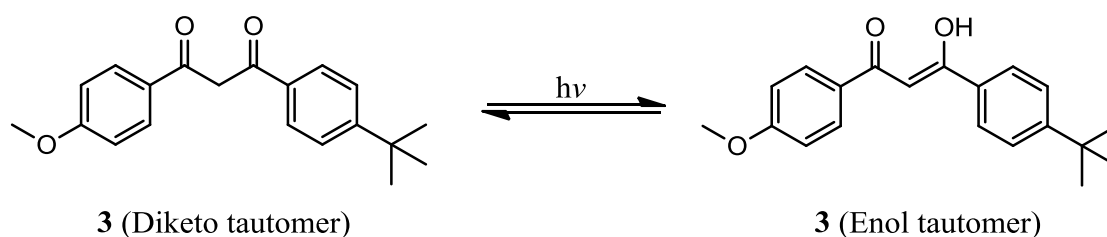
12	302776-68-7	Diethylamino hydroxybenzoyl hexyl benzoate	Benzoic acid, 2-[4-(diethylamino)-2-hydroxybenzoyl]-hexylester	UVA	354 (Ethanol)	36
13	1641-17-4	Benzophenone-10	2-Hydroxy-4-methoxy-4'-methylbenzophenone	UVB/UVA	287, 325 (Methanol)	40
14	38102-62-4/ 36861-47-9	4-Methyl-benzylidene camphor	3-(4-Methylbenzylidene)- <i>dl</i> camphor	UVB	301 (Ethanol)	38
15	15087-24-8	3-Benzylidene camphor	3-Benzylidene camphor	UVB	292 (Ethanol)	35
16	118-60-5	Ethylhexyl salicylate	2-Ethylhexyl salicylate	UVB	306 (Methanol)	35
17	118-56-9	Homosalate	3,3,5-Trimethylcyclohexyl 2-hydroxybenzoate	UVB	306 (Ethanol)	35
18	27503-81-7	Phenylbenzimidazole sulfonic acid	2-Phenylbenzimidazole-5-sulfonic acid	UVB	304 (Methanol)	34
19	103597-45-1	Methylene bis-benzotriazolyl tetramethylbutyl-phenol	2,2'-Methylene- <i>bis</i> (6-(2H-benzotriazol-2-yl)-4-(1,1,3,3-tetramethylbutyl)phenol)	UVB/UVA	306, 359 (Water)	35,41
20	187393-00-6	Bis-ethylhexyloxyphenol methoxyphenyl triazine	2,2'-[6-(4-Methoxyphenyl)-1,3,5-triazine-2,4-diyl] <i>bis</i> {5-[(2-ethylhexyl)oxy]phenol}	UVB/UVA	310, 340 (Ethanol)	36
21	180898-37-7	Disodium phenyl dibenzimidazole tetrasulfonate	Sodium salt of 2,2'- <i>bis</i> (1,4-phenylene)-1H-benzimidazole-4,6-disulfonic acid	UVA	335 (Not given)	39
22	207574-74-1	Polysilicone-15	Dimethicodiethylbenzalmalonate	UVB	313 (Ethanol)	35
23	6197-30-4	Octocrylene	2-Cyano-3,3-diphenyl acrylic acid, 2-ethylhexyl ester	UVB	304 (Ethanol)	35

2.4. Photostability of Chemical UV-filters

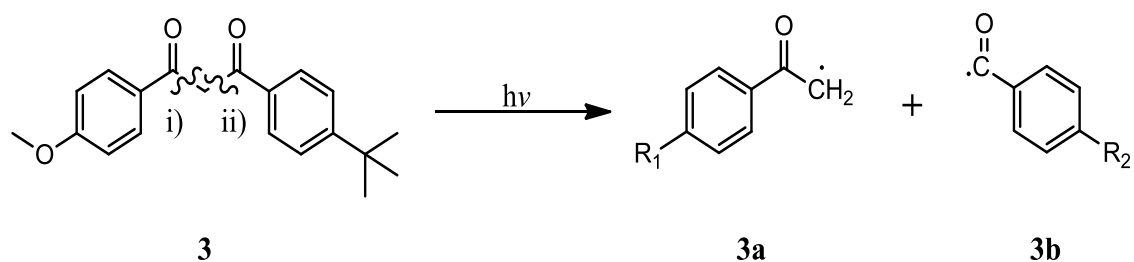
Chemical UV-filters absorb UV-light to protect the skin from dangerous UV-radiation and its damaging effects. Presently there are 27 chemical UV-filters available on the Australian market, including UVA-, UVB- and broad spectrum filters.¹⁴ The photostability of UV-filters is important for their performance as they are designed to absorb UV-light and this has to be considered during their development. The absorption of UV-light can lead to photochemical reactions of UV-filters and cause a loss in their photoprotective character. A reaction, such as trans-cis isomerisation (Scheme 2.1), where the trans-form has a higher absorption coefficient than the cis-form and has therefore a higher photoprotective effect, as in the case of UV-filter **1**, is just one example. Another possible photochemical reaction is the diketo-enol tautomerism (Scheme 2.2) as occurs in UV-filters **3** and **4**, where the enol-form absorbs in the UVA-range, while the diketo-form absorbs in the UVC-range. UV-filters also have the ability to react with other UV-filters or fragment and produce photodegradants after UV-irradiation, shown in the example for UV-filter **3** (Scheme 2.3).^{39,42}



Scheme 2.1. Trans- to cis-transformation of UV-filter **1**.



Scheme 2.2. Diketo-enol-tautomerism of UV-filter **3**.



Scheme 2.3. Fragmentation of UV-filter **3** into a phenacyl radical (**3a**) and a benzoyl radical (**3b**) with R₁ = -OCH₃ and R₂ = -C(CH₃)₃ or *vice versa*; Norris-cleavage Type I reaction at either i) or ii).

As a result of these reactions and subsequent degradation of UV-filters, their ability to absorb UVA/UVB-light may be compromised as will their ability to function as a sunscreen product.

2.4.1. Photostability of Individual Chemical UV-filters

18 UVB- and broad spectrum filters were investigated for their photostability by measuring changes in the SPF, which quantifies the effectiveness of the UV-filters in protecting from UVB-light. Each UV-filter was incorporated in an oil in water (O/W) emulsion and spread on a PMMA plate before being irradiated in a solar simulator (Suntest CPS+; Atlas, Moussy le Neuf, France) equipped with a 1500W Xenon arc lamp and special glass filters ($\lambda \geq 290$ nm). The SPF was measured *in vitro* (equation 2.1) before (SPF₀) and after various irradiation times to calculate $t_{90\%}$, which is the time in minutes when 90 % of the SPF value remained.

$$\text{SPF} = \frac{\sum_{290}^{400} E_{\lambda} S_{\lambda} d_{\lambda}}{\sum_{290}^{400} E_{\lambda} S_{\lambda} T_{\lambda} d_{\lambda}} \quad (2.1)$$

E_{λ} = CIE (International Commission on Illumination) erythemal spectral effectiveness

S_{λ} = Spectral irradiance of the UV-source

d_{λ} = Wavelength step (1 nm)

T_{λ} = Spectral transmittance

The recommended time to reapply a sunscreen product is two hours and therefore a time period of 120 minutes of irradiation was chosen to distinguish between good and poor photostability, (Table 2.5). Superior photostability was shown by the UV-filters **5** and **8** with $t_{90\%}$ of 1600 and 1520 minutes, respectively. Although UV-filter **5** has the best photostability profile of all tested UV-filters, its skin irritation potential is very high and therefore it is no longer used in sunscreen products. The four UV-filters **10**, **11**, **18** and **19** also showed a good photostability

with a $t_{90\%}$ between 180 and 320 minutes, but the majority of the twelve UV-filters showed $t_{90\%}$ values of less than 120 minutes and therefore these UV-filters have demonstrated poor photostability.⁴³

Table 2.5. SPF₀ and $t_{90\%}$ of the 18 tested UV-filters.

UV-filter	SPF ₀	$t_{90\%}$ [min]	UV-filter	SPF ₀	$t_{90\%}$ [min]
1	11.16	35	14	4.81	65
2	13.00	15	15	2.36	35
5	3.36	1600	16	2.70	10
6	8.64	20	17	3.91	45
7	4.11	20	18	9.63	215
8	13.94	1520	19	5.25	240
9	7.41	35	20	25.64	20
10	3.22	320	22	4.48	25
11	3.97	180	23	13.82	95

A similar study was undertaken by the same research group, using the change in the UVA-PF of seven UVA- and broad spectrum filters to determine their photostability. Each UV-filter was incorporated in an O/W emulsion, spread on a PMMA plate and irradiated in the solar simulator, as described above, for two hours. The UVA-PF was measured *in vitro* before and after irradiation and the difference was calculated (Δ UVA-PF (%)). The UVA-PF can be determined according the equation (2.2):

$$\text{UVA-PF} = \frac{\sum_{320}^{400} E_{\lambda} S_{\lambda} d_{\lambda}}{\sum_{320}^{400} E_{\lambda} S_{\lambda} T_{\lambda} d_{\lambda}} \quad (2.2)$$

E_{λ} = CIE erythral spectral effectiveness (often referred as P_{λ} for PPD)

S_{λ} = Spectral irradiance of the UV-source

d_{λ} = Wavelength step (1 nm)

T_{λ} = Spectral transmittance

The UV-filter was regarded as photostable, when the loss of the UVA-PF value was less than 10 % (Table 2.6). The most photostable UV-filter was UV-filter **10** with a loss of only 3 % of the UVA-PF. Regarded as not photostable were the UV-filters **11**, **19** and **21** with a loss of UVA-PF between 4 % and 9 %. The UV-filters **3**, **12** and **20** were even regarded as very photounstable with a loss in UVA-PF of 41 %, 62 % and 53 %, respectively.⁴⁴

Table 2.6. Photostability of UV-filters after irradiation.

UV-filter	UVA-PF t_{0h}	UVA-PF t_{2h}	Δ UVA-PF [%]
3	2.76	1.63	- 41 %
10	2.50	2.42	- 3 %
11	2.46	2.34	- 5 %
12	9.80	4.60	- 53 %
19	5.34	4.85	- 9 %
20	15.63	5.89	- 62 %
21	5.03	4.81	- 4 %

2.4.2. Photostability of Chemical UV-filters in Combinations

Since sunscreen products nowadays usually contain more than one UV-filter, it is necessary to observe the effects of these combinations in regards to photostability and subsequent UV-protective performance. The photostability of UVA-filter **3** alone and in the presence of six other UV-filters (**1**, **8**, **9**, **12**, **20**, and **23**) was studied by comparing the UV-filter concentrations before and after irradiation using HPLC as an analytical tool. The UV-filters alone or in combination with UV-filter **3** were dissolved in miglyol[®] 812N (caprylic/capric triglyceride, a mixture of triglycerides with 50 - 64 % C₆ and 30 - 45 % C₁₀ fatty acids) and applied on a quartz cell as a thin film before being irradiated for four hours in a solar simulator (Suntest CPS) at 35 °C and 765 Wh/m². While the UV-filters **1** and **3** clearly photodegraded with recovery yields of only 72 % and 44 %, respectively (Figure 2.2 A), the other five UV-filters showed good recovery yields after irradiation, ranging from 92 % to 100 %. Recovery of UV-filter **3** alone (44 %) was increased to 84 % in the presence of UV-filter **23**, which was the highest increase in recovery of **3** in the presence of the studied UV-filters. The presence of UV-filter **20** resulted in a recovery of 71 % for UV-filter **3**, while the recovery was only around 60 % in combination with the UV-filters **1**, **8**, **9** and **12** (Figure 2.2 B). The lowest recovery of UV-filter **3** was observed in the presence of UV-filter **12** (57 %) and even UV-filter **12** itself degraded substantially in this combination with a recovery of only 38 % compared to 100 %, when UV-filter **12** was irradiated alone.⁴⁵

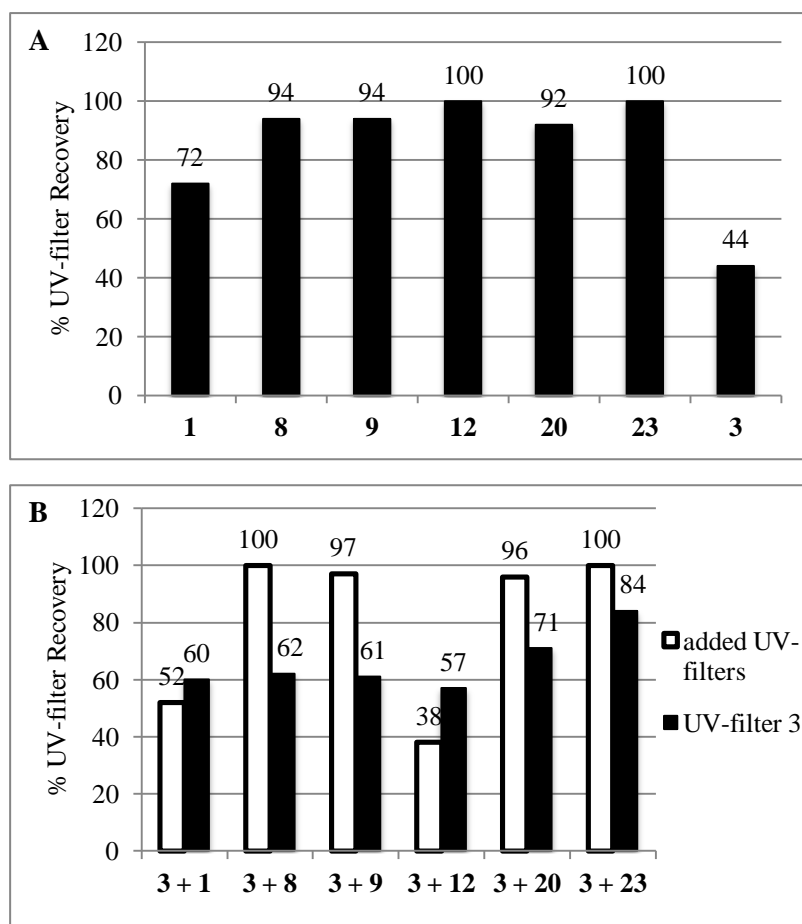


Figure 2.2. Recovery of the UV-filters **1**, **3**, **8**, **9**, **12**, **20** and **23** after four hours of irradiation in a solar simulator at 765 Wh/m². **A**: UV-filters irradiated separately and **B**: the UV-filters **1**, **8**, **9**, **12**, **20** and **23** in combination with UV-filter **3**. Adapted from.⁴⁵

Four UV-filter combinations, each with three different UV-filters (F1: **1**, **10** and **16**; F2: **1**, **3** and **14**; F3: **1**, **10** and **23**; F4: **1**, **3** and **23**), incorporated in an emulsion, were studied for their photostability. Analyses were undertaken using both, HPLC and UV-spectroscopy (280 - 400 nm). The formulations were spread on a glass plate and irradiated for three different time periods (30, 60, 120 minutes) in a solar simulator (Oriel Corporation, Stratford, CT) at 20 mW/cm², equipped with a 150W Xenon arc lamp, filtered through a dichroic mirror (280 - 400 nm) and a WG 305 long pass filter ($\lambda \geq 280$ nm). Afterwards the samples were dissolved in isopropanol and analysed by HPLC. The % recoveries of every UV-filter in each formulation are shown in Table 2.7 and were compared to each other. UV-filter **1** was present in all four formulations, but in formulation F3 it was more stable than in the other formulations, followed by F4, F1 and F2. UV-filter **3** was incorporated in formulation F2 and F4, while it was more photostable in F4. In terms of UV-filter **10**, formulation F3 was more photostable than F1 and in terms of UV-filter **23** formulation F3 was more stable than F4. Overall the most stable combination was formulation F3, followed by formulation F4.

Table 2.7. UV-filters **1**, **3**, **10**, **14**, **16** and **23** and their approximate recovery in % in the formulations F1, F2, F3 and F4.

UV-filter and their approximate (exact data not given) recovery after 120 minutes of irradiation						
Formulation	1	3	10	14	16	23
F1	50 %		90 %		85 %	
F2	40 %	25 % (irradiation time: 60 min.)		75 %		
F3	70 %		100 %			100 %
F4	55 %	40 %				85 %

For the spectrophotometric evaluation the samples were further diluted in isopropanol (1:4 v/v) and the ratio of the mean UVA- (320 - 400 nm) to the mean UVB- (280 - 320 nm) absorbance was calculated as in equation 2.3:

$$\text{UVA/UVB ratio} = \frac{\int_{320}^{400} A(\lambda) d\lambda / \int_{320}^{400} d\lambda}{\int_{280}^{320} A(\lambda) d\lambda / \int_{280}^{320} d\lambda} \quad (2.3)$$

$A(\lambda)$ = absorbance of the product at the wavelength λ [nm]

$d\lambda$ = Wavelength step (1 nm)

Formulation F4 showed the highest UVA/UVB ratio of all four tested formulations after each irradiation time. The UVA/UVB ratio of formulation F3 was lower than the ratio of the other formulations, but remained in the same range in contrast to the other formulations. Therefore it was deemed to be the most photostable of all tested four formulations (Figure 2.3). It is known that UV-filter **23** can stabilize UV-filter **3**, because their similar triplet-state energies. Since F3 and F4 were the two formulations containing the UV-filter **23**, this study suggests that UV-filter **23** has a photostabilising effect to the UV-filters **1**, **3** and **10** in the formulations F3 and F4.⁴⁶

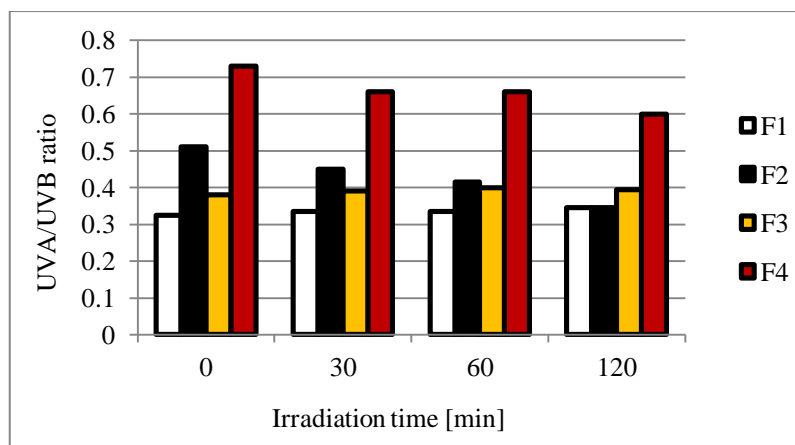


Figure 2.3. UVA/UVB ratio for the formulations F1, F2, F3 and F4, after 0, 30, 60 and 120 minutes irradiation in a solar simulator. Adapted from.⁴⁶

Since chemical UV-filters have the ability to generate ROS⁴⁷⁻⁵¹ resulting in skin damage, which is similar to that of exposure to UVA-radiation, it is important to study the capability of UV-filters and their combinations to generate these free radicals.

Several UV-filters (**1**, **3**, **9**, **12**, **19**, **20** and **23**) were studied for their ability to generate ROS after UV-irradiation. Alone and in several combinations, they were incorporated into phosphatidylcholine (PC)-based liposomes (mimicking membrane lipids) and exposed to UVA-light (400 Watt ozone-free Philips HPA lamp, UV type 3). The UV-filter/liposome suspension was filled into a 24 multi-well plate for cell cultures, before being irradiated with a complete dose of 275 kJ/m², which is equivalent to approximately 90 minutes of sunshine at the French Riviera (Nice) in summer at noon. A modified thiobarbituric acid (TBA) assay was used to determine the ROS generation after irradiation. The absorbance of the resulting product was measured at 535 nm to determine the concentration of the lipid peroxidation breakdown products (TBA reactive substances = TBARS) with a standard curve of 1,1,3,3-tetraethoxypropane. The UV-filters **3** and **9** showed a three times higher ROS generation compared to the irradiated control without UV-filters, while the ROS generation of the UV-filters **1**, **12** and **23** remained in the same range as the control. A lower TBARS concentration, and therefore ROS generation, than the control (around 20 %) was achieved by the UV-filters **19** and **20** (Figure 2.4 A). The irradiation of all tested combinations including UV-filter **3** resulted in high generation of ROS with a minimum of twice that of the ROS generation in the irradiated control without UV-filters (Figure 2.4 B). The highest rate of ROS generation was seen in the combination of UV-filter **3** with **9**, which also showed the highest rates when irradiated individually as seen in Figure 2.4 A. The combinations of UV-filter **1** with **12**, **19** and **20** showed no significant difference when compared to the control, while the combination of UV-filter **1** and **9** showed more than double the ROS generation (Figure 2.4 C).⁴⁹

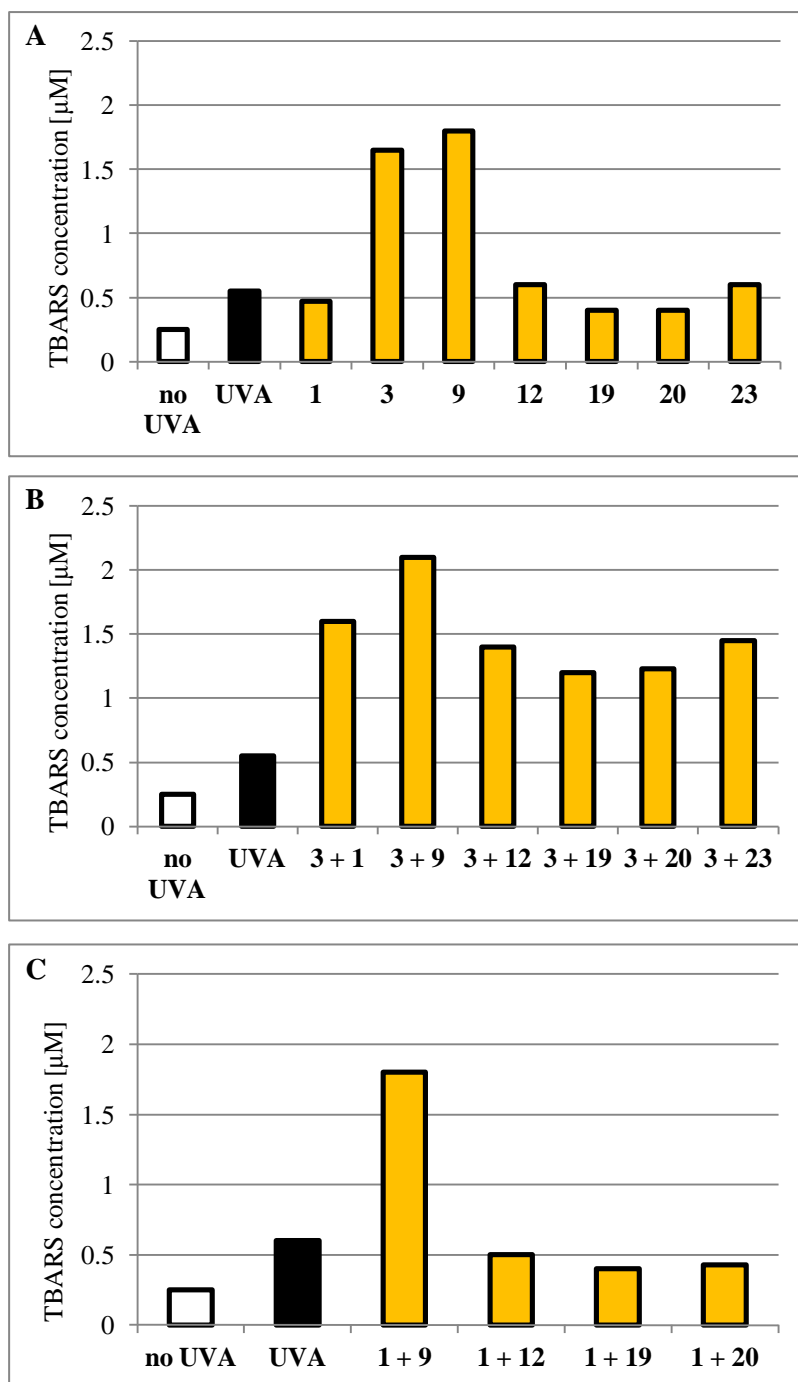


Figure 2.4. TBARS concentration in PC multilamellar liposomes after UVA-irradiation. \square = no UVA-exposure, \blacksquare = UVA-exposure, $\color{yellow}\square$ = UVA-exposure in the presence of **A**: individual UV-filters or **B** and **C**: in combinations. Adapted from.⁴⁹

To further determine UV-filter photostability, changes in the UV-absorbance spectra after irradiation were measured. The UV-absorbance maximum of UV-filter **1** decreased by about 30 % and that of UV-filter **3** by about 75 % after irradiation, confirming their instability to light. On the other hand the UV-absorbance of **19** and **23** remained unchanged, indicating photostability,⁴⁹ confirming the results of many other studies.^{43-45,52-54}

However, Couteau et al.⁴³ reported results for UV-filter **23**, which contradict these findings where this UV-filter was found to be unstable to light after irradiation in a solar simulator at 650 Wh/m². The SPF was measured after various times and compared to the SPF before irradiation. As early as after 95 minutes, the SPF value of UV-filter **23** was 10 % lower than before irradiation and therefore regarded as photounstable, because the time measured was less than two hours.⁴³ In contrast, other authors reported this UV-filter as photostable.^{45,52-54} Lhiaubet-Vallet et al.⁴⁵ and Herzog et al.⁵² reported a 100 % and nearly 100 % (exact data not given) recovery of UV-filter **23**, respectively. Data were determined by HPLC after four hours of irradiation in a solar simulator at 765 Wh/m²⁴⁵ and a total dose of 300 J/cm².⁵² Ricci et al.⁵³ and Rodil et al.⁵⁴ determined the recovery of UV-filter **23** by gas chromatography (GC) after an irradiation time of 20 hours with a UVA lamp⁵³ and after 72 hours with a halogen lamp (290 - 800 nm).⁵⁴ A recovery of UV-filter **23** of 100 % in water and acetonitrile was reported by Ricci et al.⁵³ and a recovery of about 90% (exact data not given) in water by Rodil et al.⁵⁴

There have also been conflicting reports about the photostability of the UV-filters **9**, **12** and **20**. While UV-filter **9** was regarded as photostable by Lhiaubet-Vallet et al.,⁴⁵ it was not reported as photostable by Couteau et al.⁴³ and Damiani et al.⁴⁹ Lhiaubet-Vallet et al. reported a recovery of 94 % of UV-filter **9** after irradiation of four hours in a solar simulator at 765 Wh/m² and classified it as photostable.⁴⁵ The SPF of UV-filter **9** lost 10 % of its SPF value after only 35 minutes after irradiation in a solar simulator at 650 W/m² and since the time measured was less than two hours, this UV-filter was then regarded as not photostable by Couteau et al.⁴³ A three times higher ROS generation than that of the control after irradiation under UVA-light with a dose of 275 kJ/m² confirmed the instability of UV-filter **9** studied by Damiani et al.⁴⁹

UV-filter **12** was regarded as photostable by Lhiaubet-Vallet et al.⁴⁵ and Damiani et al.⁴⁹ A recovery of 100 %, determined by HPLC, after four hours of irradiation in a solar simulator at 765 Wh/m²⁴⁵ with a ROS generation in the same range than the control after irradiation under UVA-light with a dose of 275 kJ/m²⁴⁹ led to the conclusion that **12** is photostable. On the other hand, Couteau et al.⁴⁴ showed that UV-filter **12** lost 53 % of its UVA-PF after two hours of irradiation in a solar simulator, and regarded it therefore as not photostable.

Reports on UV-filter **20** were also contradictory, with some studies regarding this UV-filter as photostable^{45,49,52} and some as not photostable.^{43,44} The recovery of UV-filter **20**, determined by HPLC after four hours of irradiation in a solar simulator at 765 Wh/m² and 300 J/cm² was reported by Lhiaubet-Vallet et al.⁴⁵ and Herzog et al.⁵² A recovery of 92 % after irradiation, reported by Lhiaubet-Vallet et al.⁴⁵ and of around 100% (exact data not given) reported by Herzog et al.⁵² resulted in the UV-filter **20** regarded as photostable. Damiani et al.⁴⁹ demonstrated the photostability of UV-filter **20** by measuring the ROS generation after

irradiation under UVA-light, with a complete dose of 275 kJ/m². About 20 % (exact data not given) less ROS generation in the presence of UV-filter **20** was reported, compared to that of the control without UV-filters.⁴⁹ Couteau et al.⁴³ reported that UV-filter **20** lost 10 % of its SPF value after only 20 minutes of irradiation in a solar simulator at 650 Wh/m² and classified it therefore as not photostable. UV-filter **20** also lost 62 % of its UVA-PF after an irradiation time of two hours in a solar simulator (650 W/m²), further indicating its photoinstability.⁴⁴

A reason why some UV-filters are more stable in the presence of other UV-filters is attributed to the ability of these UV-filters to act as singlet- or triplet-state quenchers.⁵⁵

The combination of the UV-filters **1** and **3** is an example where this triplet-triplet energy transfer occurs with the enol-form of UV-filter **3** acting as a donor and UV-filter **1** as acceptor. Electron paramagnetic resonance (EPR) and time-resolved phosphorescence spectra of both UV-filters individually and in combination confirmed this triplet-triplet energy transfer.⁵⁶ The UV-filters **14**, **20** and **23** were also described to stabilise UV-filter **3** by triplet-triplet energy transfer.^{39,52,57} Not only triplet-triplet energy transfer, but also singlet-singlet energy transfer has been reported to be a stabilisation mechanism for UV-filter **3**. Fluorescence-spectra, quantum yields and the lifetime of UV-filter **3** were determined in the presence and absence of the photostabilizer ethylhexyl methoxycrylene. Thin films of solutions were irradiated in a solar simulator to determine UV-filter recovery and *in vivo* studies to determine SPF and UVA-PF were undertaken.⁵⁸ Further studies also demonstrated the stabilisation of retinol, retinyl palmitate and trans-resveratrol by ethylhexyl methoxycrylene to occur by singlet-singlet energy transfer.^{59,60}

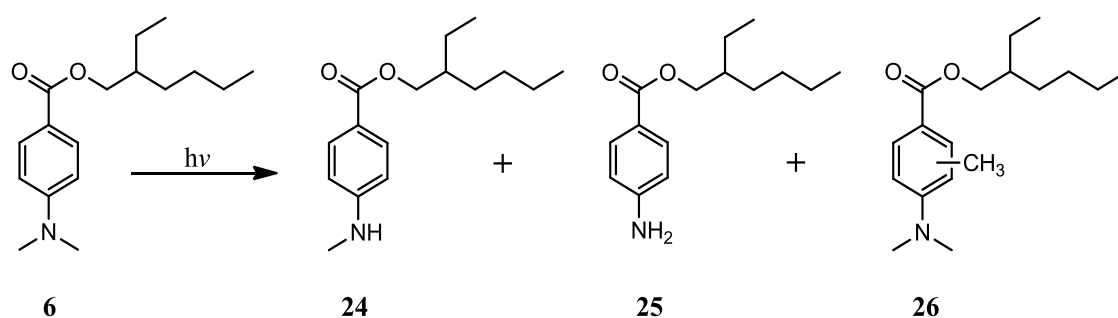
2.4.3. Possible Photodegradants of Chemical UV-filters

Some chemical UV-filters alone or in combination, resulted in photodegradation to a greater extent, which may depend on the UV-irradiation level, time or solvents used, resulting in photodegradants which may be toxic.

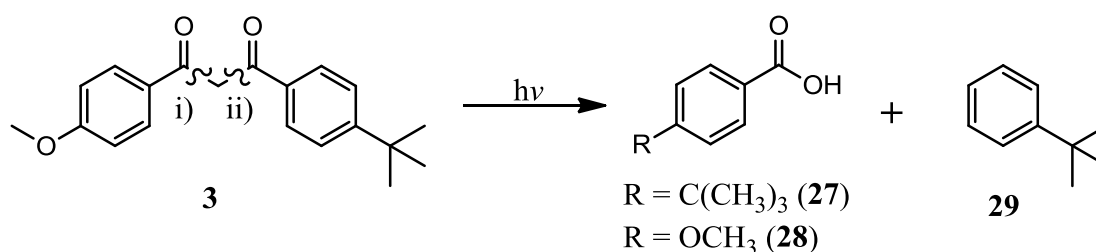
2.4.3.1. Identification of Photodegradants

The photodegradation of the three UV-filters **3**, **6** and **10** and the generation of their photodegradants was investigated in cyclohexane. The UV-filters were irradiated for 70 - 140 hours in a quartz immersion well reactor with a medium pressure mercury vapour lamp in air. UV-filter **10** remained unchanged, even after an irradiation time of 100 hours, with no photodegradants detected with gas- or liquid-chromatography in contrast to the UV-filters **3** and **6**. Three photodegradants (**24**, **25** and **26**) of UV-filter **6** were detected by gas chromatography - mass spectroscopy (GC-MS) after an irradiation time of 140 hours and identified by NMR-

spectroscopy (Scheme 2.4). Total decomposition of UV-filter **3** was observed after 100 hours of irradiation, resulting in several photodegradants. Although the Norrish-I cleavage of UV-filter **3** can occur on both sides (i and ii) of the methylene group (-CH₂), only three photodegradants were identified: two benzoic acid derivatives (**27** and **28**) and *t*-butyl benzene (**29**) (Scheme 2.5). A greater amount (two to three times) of photodegradant **27** was formed, compared to that of **28**, while 10 - 15 % of photodegradant **29** was formed.⁶¹



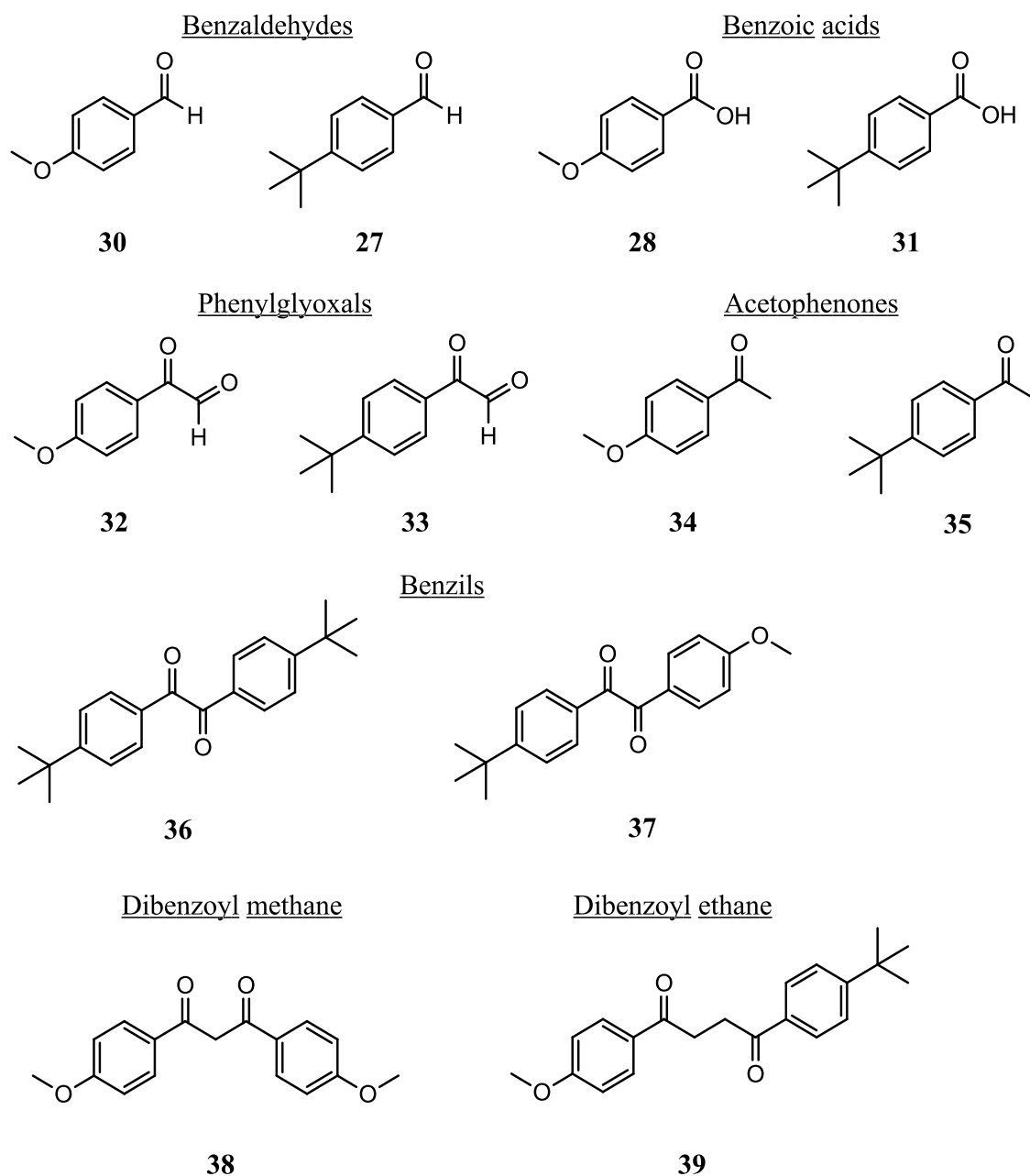
Scheme 2.4. Proposed photodegradants of UV-filter **6** after 140 hours of irradiation in cyclohexane: **24** = 4-monomethylaminobenzoic acid 2-ethylhexyl ester (21 %), **25** = 4-aminobenzoic acid 2-ethylhexyl ester (< 1 %) and **26** = 4-(2-ethylhexyl)-2-methylbenzoic acid 2-(dimethylamino)ethyl ester (5 %). Adapted from.⁶¹



Scheme 2.5. Identified photodegradants of UV-filter **3**: **27** = 4-*t*-butyl benzoic acid, **28** = 4-methoxy benzoic acid and **29** = *t*-butyl benzene.⁶¹

Isolation and detailed identification by HPLC and GC-MS of photodegradants of the UV-filters **3** and **4** were undertaken by Schwack and Rudolph.³⁷ Both UV-filters were irradiated with UV-light for eight hours in a solar simulator with two different glass filters (F1: cut off at 260 nm and F2: at 320 nm). Photodegradation was investigated in the solvents isopropanol, methanol, cyclohexane and isooctane, purged with air. In the non-polar solvents, cyclohexane and isooctane photodegradation of both UV-filters was exponential, while they were stable in the polar solvents isopropanol and methanol. The photodegradation in cyclohexane for UV-filter **3** was 14 % and for UV-filter **4** 20 %, using filter F1, while 8 % for both UV-filters was achieved

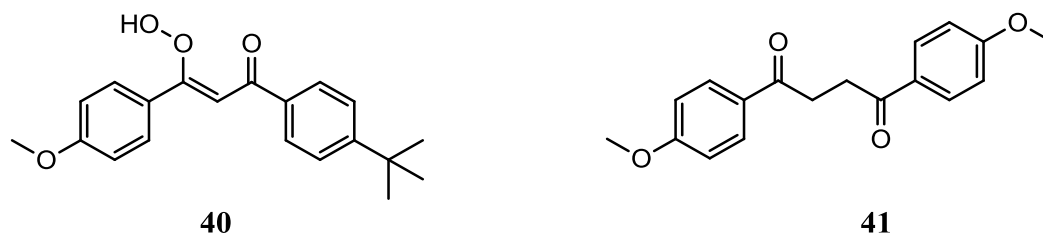
using filter F2. Photodegradation results in isooctane were not given. The first step of the photodegradation process was a cleavage of the UV-filters **3** and **4** in their diketo-form, resulting in a benzoyl and a phenacyl radical (Scheme 2.3, page 19), followed by several oxidation and/or recombination reactions. Identified photodegradants were classified into the following seven groups: benzaldehydes, benzoic acids, phenylglyoxals, acetophenones, benzils, dibenzoyl methanes and dibenzoyl ethanes as shown in Scheme 26. Diketo concentrations of both UV-filters were determined using ^1H NMR analysis in cyclohexane- d_{12} and isopropanol- d_8 . In cyclohexane- d_{12} 3.5 % of UV-filter **3** and 1.7 % of UV-filter **4** were found in their diketo-form, while in isopropanol- d_8 the diketo-form of both UV-filters was not detected. These results confirm that the photodegradation process depends on the formation of the diketo-form.³⁷ UV-filter **4** was removed from the market in 1993, due to its potential to cause photoallergic reactions.⁶²



Scheme 2.6. Photodegradants of UV-filter **3** after eight hours of irradiation in cyclohexane identified by GC-MS: **30** = 4-methoxy benzaldehyde, **27** = 4-*t*-butyl benzaldehyde, **28** = 4-methoxy benzoic acid, **31** = 4-*t*-butyl benzoic acid, **32** = 4-methoxy phenylglyoxal, **33** = 4-*t*-butyl phenylglyoxal, **34** = 4-methoxy acetophenone, **35** = 4-*t*-butyl acetophenone, **36** = 4,4-di-*t*-butyl benzil, **37** = 4-*t*-butyl-4-methoxy benzil, **38** = 4,4-dimethoxydibenzoyl methane, **39** = 4-*t*-butyl-4-methoxydibenzoyl ethane. Adapted from.³⁷

Photodegradants of UV-filter **3** in water were detected by LC-MS after irradiation in a solar simulator for four minutes intervals at 250 W/m² to a complete dose of 60 kJ/m². The photodegradants **28**, **31** and **37** detected by Schwack and Rudolph³⁷ were found as well as two

additional photodegradants, a hydroxypropenone (**40**) and a 1,4-diketone (**41**) (Scheme 2.7), generated due to a reaction with oxygen.⁶³

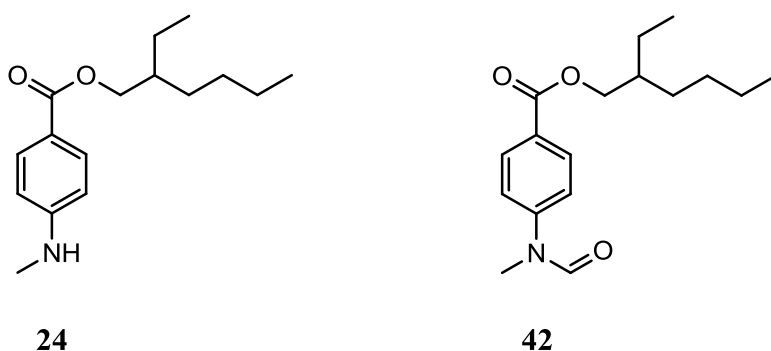


Scheme 2.7. Possible photodegradants of UV-filter **3** identified by LC-MS after an irradiation dose of 60 kJ/m² in water: **40** = (Z)-1-(4-*t*-butylphenyl)-3-hydroxy-3-(4-methoxyphenyl)prop-2-en-1-one and **41** = 1,4-*bis*(4-methoxyphenyl)butane-1,4-dione. Adapted from.⁶³

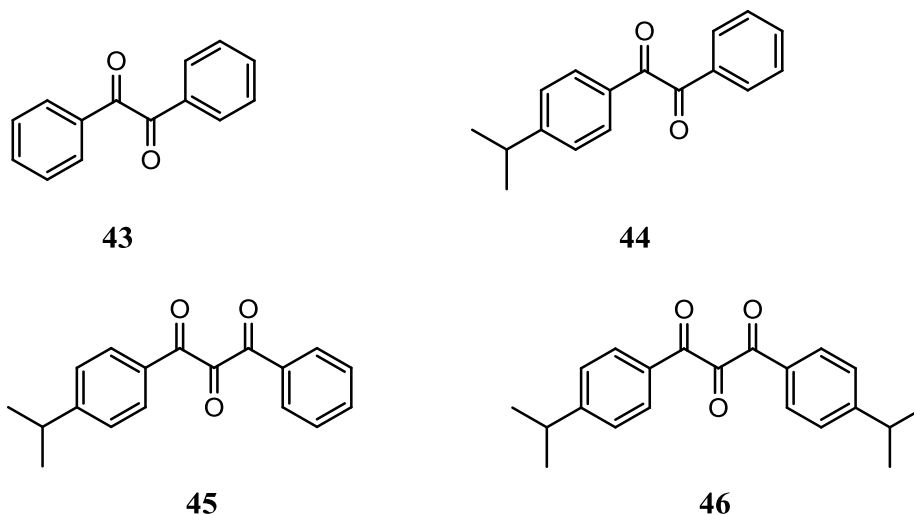
The photodegradation of UV-filter **3** was investigated after irradiation with a high pressure mercury lamp using a pyrex glass filter (≥ 300 nm) in cyclohexane, ethyl acetate and dimethyl sulfoxide (DMSO), purged with air. Photodegradants were detected by GC-MS and the results were identified using the Wiley 275 library in combination with findings by Schwack and Rudolph.³⁷ In DMSO no photodegradants were found by GC-MS after 18 hours of irradiation and the concentration of UV-filter **3** remained constant, but an HPLC analysis after 15 hours of irradiation showed a degradation of 75 % for the enol-form, while the major photodegradant was the diketo-form. These findings were not confirmed by GC-MS, because enol- and diketo-form cannot be separated by GC. In ethyl acetate two photodegradants (**33** and **37**) of UV-filter **3** were detected by GC-MS and an HPLC analysis after 15 hours of irradiation showed a decrease of 33 % of the enol-form and an increase of the diketo-form (exact data not given). In cyclohexane, previous results were confirmed by identifying the photoproducts **27**, **33**, **36**, **37** and **39** reported on by Schwack and Rudolph³⁷ and photoproduct **41** described by Huong et al.⁶³ Detailed chromatographic analyses showed that in ethyl acetate UV-filter **3** underwent photoisomeration and photodegradation to a similar extent. In DMSO the main reaction was photoisomeration, while in cyclohexane, UV-filter **3** underwent photoisomeration from the enol- to the diketo-form, followed by the formation of photodegradants.⁶⁴

The change in the UV-protective character of seven UV-filters in petroleum jelly was investigated after UVB-exposure followed by UVA-exposure. UVB-radiation was achieved by fluorescent light bulbs (peak at 313 nm), creating 20 MED and UVA-radiation by a solar simulator (320 - 400 nm) with a total dose of 100 J/cm². Photodegradants were identified by GC-MS. The UV-absorbance spectra of the UV-filters **10**, **13** and **14** did not change significantly after UVA- and UVB-exposure and were regarded as photostable. However, GC-MS analysis revealed a second peak for UV-filter **14** with the same molecular weight, and

therefore indicating the formation of its photoisomer. Because both isomers of UV-filter **14** have similar absorption spectra, both have a photoprotective character. The absorption maximum of UV-filter **1** was reduced by about one third after both, UVA- and UVB-exposure, and therefore UV-filter **1** was regarded as not photostable. One photodegradant of UV-filter **1** was detected and identified as the cis-isomer of its active trans-form (Scheme 2.1, page 18). The cis-isomer has a lower absorbance than that of the trans-form and therefore UV-filter **1** loses its photoprotective character in contrast to UV-filter **14**. The UV-absorbance spectrum of UV-filter **6** did not change significantly after UVB-exposure, however after UVA-exposure two photodegradants were identified as 2-ethylhexyl 4-methylaminobenzoate (**24**) and 4-(formylmethylamino) benzoate (**42**) (Scheme 2.8). The absorption maximum of UV-filter **3** shifted from the UVA-range (enol-form) to the UVC-range (diketo-form) confirming that UV-filter **3** underwent enol-diketo isomerisation, as described in Scheme 2.2 (page 18). UV-filter **4**, which is also a dibenzoylmethane, underwent a similar decomposition and identified photodegradants are shown in Scheme 2.9.⁴²



Scheme 2.8. Photodegradants of UV-filter **6** identified by GC-MS after UVA-exposure of 100 J/cm² in petroleum jelly: **24** = 2-ethylhexyl 4-methylaminobenzoate and **42** = 4-(formylmethylamino) benzoate. Adapted from.⁴²



Scheme 2.9. Photodegradants of UV-filter **4** identified by GC-MS after UVA-exposure of 100 J/cm² in petroleum jelly: **43** = benzil, **44** = isopropylbenzil, **45** = 1-phenyl-3-(4-isopropylphenyl)-propane-1,2,3-trione and **46** = 1,3-di(4-isopropylphenyl)-propane-1,2,3-trione. Adapted from.⁴²

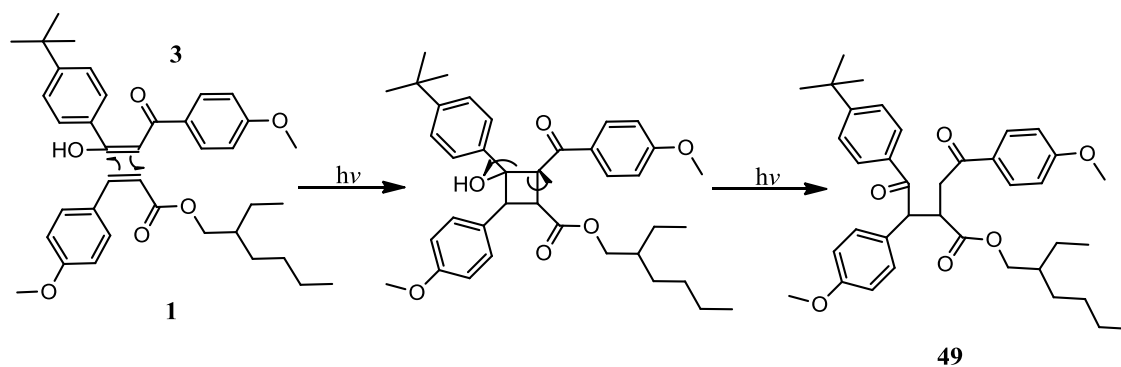
Only one photodegradant of UV-filter **1** was detected by HPLC and identified by ¹H NMR after exposure to natural sunlight in methanol. After one day of sun exposure the concentration of UV-filter **1** (1.000 ppm = 3.44 mM) was halved, while the amount of the detected photodegradant increased, maintaining molecular weight balance. Even after 30 days of sun exposure this ratio remained the same. A control sample was kept in the dark for the same amount of time and showed no change in the concentration of UV-filter **1** on HPLC analysis. Detailed investigations using online HPLC and ¹H NMR concluded that the original UV-filter **1** was the trans-isomer and the detected photodegradant its cis-isomer.⁶⁵

Molar absorption coefficients of both isomers of UV-filter **1** were measured in methanol, ethanol, hexane and a mixture of methanol and water (90/10). In all four solvents the molar absorption coefficient of the trans-isomer was about double than that of the cis-isomer, explaining the reduction of UV-absorbance after UV-irradiation of UV-filter **1**. The ratio of both isomers strongly depends on their concentration and the solvent type. The trans/cis ratios in methanol for the concentrations 0.0344, 0.344 and 3.44 mM were 0.47, 0.75 and 1.1, respectively.⁶⁶

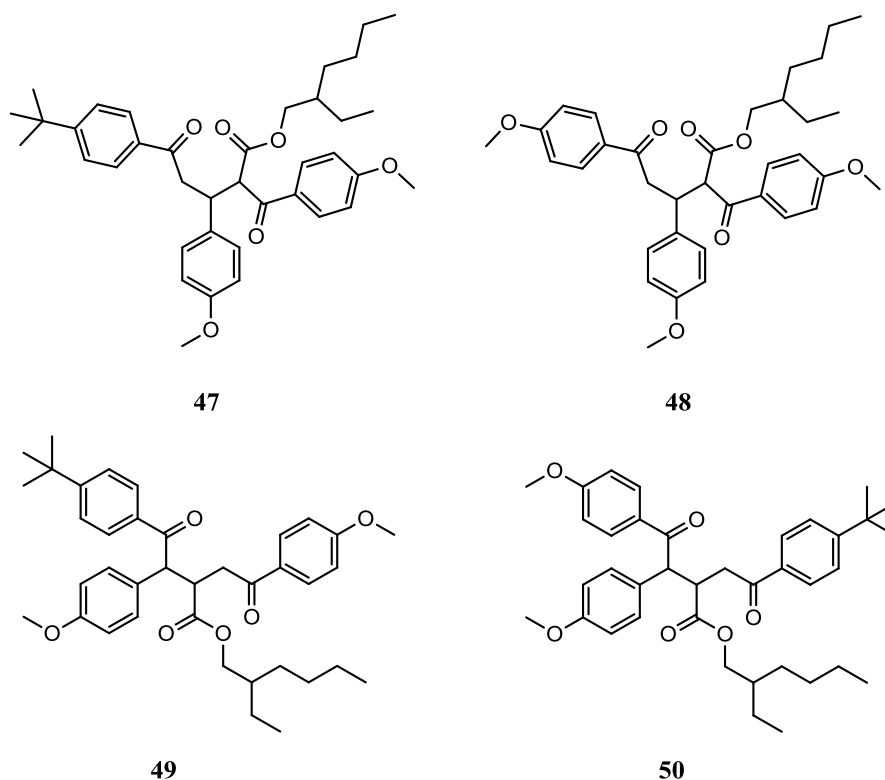
The photodegradation process of UV-filter **1** was found to be different in water from other solvents, such as heptane dioxane, ethyl acetate, tetrahydrofuran (THF), acetonitrile and isopropanol. UV-filter **1** was irradiated for ten minutes at 250 W/m² (= 150 kJ/m²) in a solar simulator. Determination of concentrations by HPLC showed that the sum of both isomers was only 71.7 % in water, while the sum in the other solvents was around 100 %. This difference

indicates the generation of other photodegradants of UV-filter **1** in water, besides the trans-cis isomerisation product. No suggestions for a particular reaction mechanism or an identification of photodegradants were given (see 2.3.1. for more details).⁶⁷

When more than one UV-filter is incorporated in a sunscreen product the photochemistry of UV-filters is altered, depending on the individual UV-filters, their concentration and the formulation: photodegradation and the generation of photodegradants. The widely used UV-filter combination **1** and **3** was investigated in cyclohexane after irradiation in a solar simulator (290 - 400 nm). After ten hours of irradiation (UV irradiance: 27 W/m²) both UV-filters underwent irreversible [2+2] cycloaddition resulting in a number of photodegradants, identified by HPLC-MS and NMR. One possible combination for this cycloaddition is given in Scheme 2.10, while the four major diketones identified are presented in Scheme 2.11.⁶⁸



Scheme 2.10. [2+2] cycloaddition of **1** and **3**, resulting in photodegradant **49**.



Scheme 2.11. Photocycloaddition products in cyclohexane: **47** = 2-ethylhexyl-5-[4-(2,2-dimethylethyl)phenyl]-3-(4-methoxyphenyl)-2-(4-methoxybenzoyl)-5-oxopentanoate, **48** = 2-ethylhexyl-2-[4-(2,2-diethylethyl)benzoyl]-3,5-bis-(4-methoxyphenyl)-5-oxopentanoate, **49** = 2-ethylhexyl-4-[4-(2,2-dimethylethyl)phenyl]-3-(4-methoxyphenyl)-2-(4-methoxybenzoyl-methyl)-4-oxobutanoate and **50** = 2-ethylhexyl-3,4-*bis*-(4-methoxyphenyl)-2-[4-(2,2-dimethyl-ethyl)benzoylmethyl]-4-oxobutanoate. Adapted from.⁶⁸

2.4.3.2. Toxicity of Photodegradants

Some UV-filters (**5**, **6** and **10**) are known to cause photosensitivity reactions in patients,^{18,69-71} which may be either phototoxic or photoallergic in nature. A phototoxic reaction occurs after exposure to sunlight in the presence of a chemical or drug (topical or systemic application) directly on the sun exposed area. Inflammatory mediators and ROS are generated, causing damage to the tissue and resulting in pain and erythema. A photoallergic reaction is a type IV immune response and can also occur on non-sun exposed areas after exposure to sunlight in the presence of a chemical or drug. A prior exposure to sunlight and the particular chemical or drug is required.⁶⁹ UV-filters can however also degrade on exposure to sunlight into various photodegradants, but the ability of these photodegradants to cause toxic reactions is not well studied.

To demonstrate the importance of the photostability of a sunscreen product, a photostable UV-filter mixture was tested against a photounstable mixture, using biological markers. The

photostable UV-filter mixture A contained UV-filters **3**, **9** and **14**, while the photounstable mixture B contained the UV-filters **1**, **3** and **9**. The photostability and instability of both UV-filter mixtures was referred to by the authors, although no definition of these terms was provided. UV-filters were incorporated into an O/W emulsion and added to human keratinocyte cells to investigate DNA damage such as direct DNA breakage, oxidative damage to purines or lemfloxacin-induced DNA damage caused by UV-light, using comet assays. The antibiotic lemfloxacin was used as model photosensitizing drug. The accumulation of the tumour suppressor protein p53 in the cells was also studied. During lemfloxacin studies samples were irradiated with UVA-light ($\lambda \geq 320$ nm), while samples in all other studies were irradiated in a solar simulator with UVA- and UVB-light ($\lambda \geq 300$ nm). The average irradiance in the solar simulator was 10 W/m^2 for UVB and 90 W/m^2 for UVA (90 kJ/m^2), while irradiance for UVA-light alone was 70 W/m^2 (60 kJ/m^2). Before the UV-filter mixtures were added to the human cells and irradiated under the described conditions, they were pre-irradiated for one hour at 360 kJ/m^2 . In all experiments the photostable UV-filter mixture A had a higher protective effect towards the keratinocyte cells than mixture B. The comet assay showed that keratinocyte nuclei maintain their round shape after UV-irradiation in the presence of mixture A, while a tail could be observed in the presence of mixture B, which indicates DNA breakage in the nuclei. After 24 hours post UV-exposure, western plots showed a two to three times stronger intensity of the protein p53-band in keratinocyte nuclei in the unstable UV-filter mixture B than in the stable mixture A. The comet assay in the presence of lemfloxacin showed a three times greater tail formation of the keratinocyte cells after UVA-exposure in the presence of mixture B than that of mixture A, demonstrating more DNA breakage in mixture B. These results show that unstable UV-filters have a negative impact on cell mechanisms such as DNA breakage and a higher p53 production. Whether the genotoxic events in the human keratinocyte cells were due to the loss of their UV-protective character or to the toxic effect of photodegradants was not determined.⁷²

The UV-filters **1** and **3** were studied for their toxicity to mouse cells after UV-irradiation in a solar simulator, compared to a dark control. UV-filters were dissolved in ethanol and irradiated for two or 20 hours before being added to a mouse cell suspension and incubated for a total of 22 hours. After the incubation time, the survival of mouse cells in percent was determined, using trypan blue. The unexposed UV-filter **1** showed a decreasing cell survival rate from about 95 % (at 2 ppm) to nearly 0 % at a concentration of 10 ppm, while unexposed UV-filter **3** maintained the high survival rate of about 95 % until a concentration of 5 ppm, but then decreased to about 30 % at 10 ppm. In a small volume of 5 μL the survival rate of UV-filter **1** decreased from nearly 100 to 90 % after UV-exposure of two hours, maintaining this percentage after 20 hours of UV-exposure. UV-filter **3** showed no significant difference in cell

survival between the irradiated and non-irradiated sample. It can thus be concluded that both, UV-filter **1** and **3**, are toxic towards mouse cells. However, although the toxicity of UV-filter **1** was higher after UV-exposure, UV-filter **3** showed no different toxicity between the dark and after UV-exposure.⁷³

The UV-filters **1**, **2** and **6** were studied for their algal toxicity in water after exposure to simulated sunlight, using a halogen lamp (290 - 800 nm). The reproduction inhibition of the algae *S. vacuolatus*, which implies toxicity, was measured before and after UV-irradiation in the presence of the UV-filters and related to the UV-filter concentration. In the presence of the UV-filters **1** and **2** the reproduction inhibition decreased after UV-exposure correlating to a decrease of the UV-filter concentration (Figure 2.5 **A** and 2.5 **B**), assuming that the photodegradants of **1** and **2** are less toxic towards the tested algae than the UV-filters **1** and **2**. As photodegradants, the dimer of each filter, which formed due to [2+2] cycloaddition reactions, and the cis-isomers of both UV-filters were identified. In the presence of UV-filter **6**, the reproduction inhibition remained in the same range after 14 hours of UV-exposure as before, although half of UV-filter **6** was degraded (Figure 2.5 **C**), implying that the photodegradants of UV-filter **6** after 14 hours have the same toxicity as the UV-filter. Three photodegradants (**24**, **25** and **26**) were identified for UV-filter **6** (Scheme 2.4). Photodegradant **24** showed the highest concentration after 14 hours of UV-exposure and it was thus proposed to be the reason for the high toxicity. Reproduction inhibition and therefore algal toxicity decreased after a longer irradiation time, which indicates that the other photodegradants are less toxic than UV-filter **6**.⁵⁴

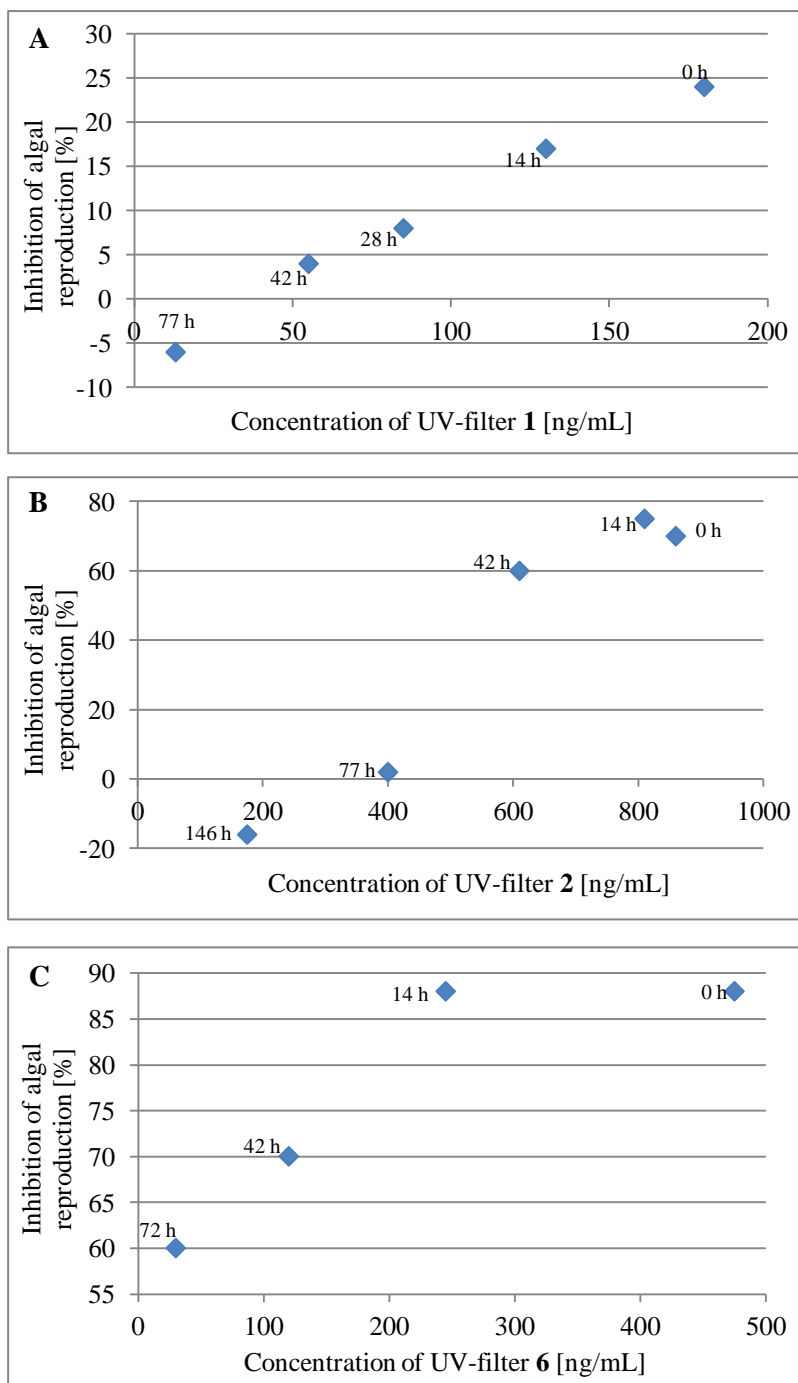
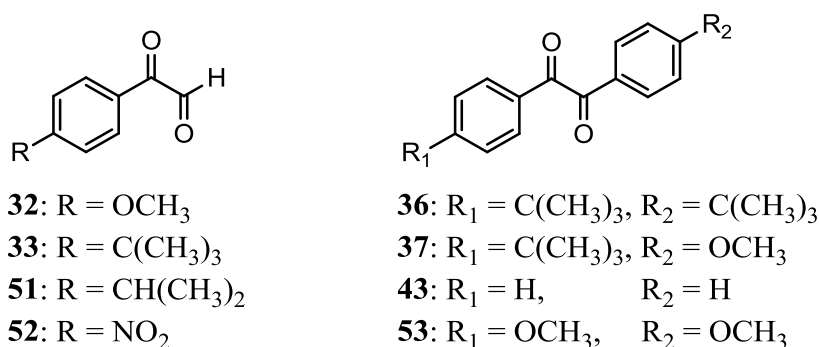


Figure 2.5. Algal toxicity of the mixture of UV-filters and their photodegradants: **A: 1**, **B: 2**, and **C: 6**. Reproduction inhibition of the algae *S. vacuolatus* in % plotted against the remaining UV-filter concentration after UV-exposure. Adapted from.⁵⁴

UV-filter **3** is very unstable, and results in the formation of benzils and arylglyoxals in addition to other photodegradants, as described previously.^{37,63,64} Four benzils (**36**, **37**, **43** and **53**) and four arylglyoxals (**32**, **33**, **51** and **52**) (Scheme 2.12) were investigated for their photosensitising effect using the local lymph node assay (LLNA) and cytotoxic effect towards the acetyl-protected amino acid arginine (cell proliferation assay). Only the compounds **36** and **43** gave a

response in the LLNA, but detailed analysis led to the conclusion that this response was due to their cytotoxicity and not photosensitivity. On the other hand, all four arylglyoxals were shown to be strong sensitizers, based on the LLNA and although the chemical properties of the arylglyoxal moieties were very different, no significant difference in their sensitizing capacity was detected. The cell proliferation assay results indicated that the benzils **36**, **37** and **43** are highly toxic, while it was not possible to determine the cytotoxicity of compound **53**. The authors however still concluded that all four benzils could be regarded as cytotoxic. Only the reactivity of the arylglyoxals **32**, **51** and **52** towards acetyl-protected arginine was tested in the cell proliferation assay, because of the chemical similarities of **33** and **51**. All three arylglyoxals showed no difference in reactivity towards the arginine, which strengthens the conclusion from the LLNA results, that the presence of the arylglyoxal moiety is not relevant in terms of their allergic potential. Conversely it can be said that the benzils are cytotoxic rather than photosensitive, while the arylglyoxals are strong sensitizers.⁶²



Scheme 2.12. Tested benzils (**36**, **37**, **43** and **53**) and arylglyoxals (**32**, **33**, **51** and **52**) for their cytotoxicity and allergic potential using a LLNA and a cell proliferation assay. Adapted from.⁶²

2.5. Effects of UV-filter Photostability by the Addition of other Active Ingredients

2.5.1. Addition of Physical UV-filters (Metal Oxides)

Although there is a wide range of chemical UV-filters, only two physical UV-filters are available: TiO₂ and ZnO, which are both broad spectrum filters. In sunscreen products chemical and physical UV-filters are often used in combination. A review undertaken in 2005 in the United Kingdom (UK) showed that 3.6 %, of 308 surveyed sunscreen products, contained only a physical UV-filter (TiO₂ and/or ZnO), 41.6 % contained a mixture of chemical and physical UV-filters and the remaining 54.8 % contained only chemical UV-filters. It can therefore be concluded that nearly half of the sunscreen products contain metal oxides, with 90.2 % of these containing TiO₂ and 9.8 % ZnO.⁷⁴ A more recent review undertaken in 2010 in

the UK reported similar findings, although only TiO₂ was included as physical UV-filter. According to this survey 49 % of the 337 sunscreen products contained TiO₂.⁷⁵

TiO₂ is available in two different crystal forms, rutile and anatase. The anatase form is more photoreactive and this has resulted in its use as a photocatalyst in photocatalytic reactions.⁷⁶⁻⁷⁹ Depending on the particle size, TiO₂ and ZnO absorb or reflect UV-light. Particles smaller than 370 nm mainly absorb UV-light and practically no light is reflected. In sunscreen products TiO₂ and ZnO are widely used in particles smaller than 100 nm, classified as nano-particles, because they cause less skin irritation and therefore are more suitable for sensitive skin and for children.¹⁵ In the past TiO₂ or ZnO were used in larger particle sizes, micro-particles, which were white and clearly visible on the skin and therefore not aesthetically pleasing. With the advent of TiO₂ or ZnO nano-particles, the acceptance in society has increased for these types of UV-filters, because of their transparent nature on the skin.¹⁵ Although there has been some concern that these particles are small enough to penetrate to the viable layers of the skin, it has not been proven.^{15,18,80-82} The disadvantage of TiO₂ and ZnO is that they may have a negative effect on the photostability of chemical UV-filters, because of their ability to generate ROS when exposed to UV-light.⁸³

The photocatalytic effect of TiO₂ and the resulting photodegradation of chemical UV-filters were studied in acetonitrile. A complete degradation of the UV-filters **1** and **3** in the presence of TiO₂ was shown after irradiation of ten hours in the solar simulator Solarbox 1500e (Co.FO.ME.GRA s.r.l., Milan), which was equipped with an outdoor filter with IR-treatment to filter out infrared radiation. HPLC analyses showed that the concentration of both chemical UV-filters in the presence of TiO₂ was less than 10 % than that of the irradiated solution not including TiO₂.⁶⁸ It has also been reported that TiO₂ induced mineralization of the UV-filters **1**, **10**, **16** and **23** irradiated in water for 20 hours. A multilamp photoreactor with Luzchem UVA lamps, a total exposure of about 2.5 mJ/cm² and following spectral distribution were used: 95.05 % UVA, 0.98 % UVB, 0.27 % UVC and 3.70 % visible radiation.⁵³

2.5.1.1. Coated Metal Oxides

To reduce the photocatalytic activity of TiO₂ and ZnO, particles can be coated for example with silica, aluminium or dimethicone. Nowadays, in particular TiO₂ particles are often coated, because the photocatalytic reactivity of TiO₂ is much higher than that of ZnO. The photoreactivity of silica and dimethicone coated TiO₂ and ZnO was compared to uncoated materials by measuring the photocatalytic oxidation of isopropanol to propanone under oxygenated conditions. The metal oxides were irradiated in a batch photoreactor under constant focused photon flux from a 500 W medium pressure mercury arc lamp (Priel Products Ltd.) at

24 °C (irradiation time not given) and propanone concentrations were determined by GC. The photoreactivity is represented in terms of moles of isopropanol converted to propanone per gram of metal oxide per hour of irradiation and represented as rate of isopropanol oxidation (Figure 2.6). It is clear that the photoreactivity of ZnO is much lower than that of TiO₂. Both coatings were less photoreactive than the uncoated forms, however, the decrease of photoreactivity of ZnO remained within the experimental error for this test.⁸⁴

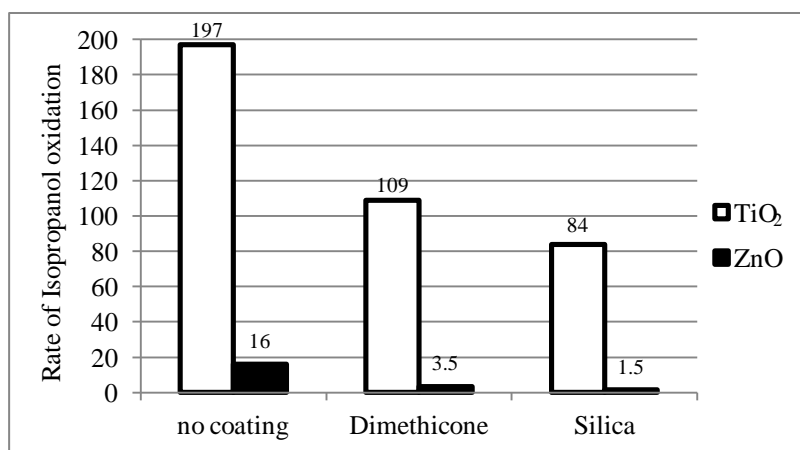


Figure 2.6. Relative photoreactivity of ZnO and TiO₂, coated and uncoated, measured by the photocatalytic oxidation of isopropanol to propanone. Adapted from.⁸⁴

TiO₂ coated with silica, aluminium hydroxide, dimethicone/methicone copolymer and ZnO coated with diphenyl capryl methicone were used to investigate SPF changes in several UV-filter combinations. The SPF for a combination of UV-filters was predicted and compared to the value achieved on measurement. The UV-filter combinations were incorporated in an O/W emulsion and spread on a PMMA plate before the SPF was measured *in vitro* and carried out according to equation (2.1), page 19. In Table 2.8 and 2.9 the SPF of each individual chemical UV-filter, the SPF of the combinations with TiO₂ or ZnO and the decrease or increase of the SPF compared to the predicted value are listed. The SPF of a cream with 25 % TiO₂ was 37.65 while with 25 % ZnO the value was 7.14. In nine out of the 18 combinations with TiO₂, no significant difference between the predicted and measured SPF was noted. Six combinations showed a lower SPF (loss between four and 25 SPF units) compared to the predicted outcome and only the two UV-filters **6** and **20** appeared to be more promising than predicted with an increase of seven and six SPF units, respectively. No combination with ZnO showed a lower SPF than predicted, in contrast, the majority (eleven out of 18) showed a higher SPF value with up to 31 units more for the combination with UV-filter **8**.

Table 2.8. Combination of chemical UV-filters and TiO₂.⁸⁵

UV-filter	SPF_{UV-filter} (mean)	SPF_{UV-filter+TiO2} (mean)	Difference of measured and predicted SPF (SPF units)
1	12.09	53.12	-
2	13.49	52.84	-
5	5.48	41.04	-
6	8.98	53.55	+ 7
7	4.09	35.87	- 6
8	10.73	47.27	-
9	12.54	36.57	- 14
10	5.10	39.07	- 4
11	5.59	35.77	- 7
14	6.44	43.38	-
15	2.84	33.47	- 7
16	2.89	38.81	-
17	4.25	38.09	- 4
18	13.39	49.37	-
19	6.68	19.50	- 25
20	29.63	73.06	+ 6
22	4.25	38.77	-
23	9.40	43.42	-

Table 2.9. Combination of chemical UV-filters and ZnO.⁸⁵

UV-filter	SPF_{UV-filter} (mean)	SPF_{UV-filter+ZnO} (mean)	Difference of measured and predicted SPF (SPF units)
1	12.09	26.63	+ 7
2	13.49	29.07	+ 8
5	5.48	10.94	-
6	8.98	28.51	+ 12
7	4.09	15.06	+ 4
8	10.73	49.28	+ 31
9	12.54	25.88	+ 6
10	5.10	13.42	-
11	5.59	15.28	+ 3
14	6.44	15.16	-
15	2.84	12.72	+ 3
16	2.89	9.08	-
17	4.25	11.94	-
18	13.39	24.76	+ 4
19	6.68	12.92	-
20	29.63	36.89	-
22	4.25	15.55	+ 4
23	9.40	25.74	+ 9

Overall the combinations with TiO₂ were shown to be more effective than with ZnO, with a resulting higher SPF value. However only two combinations with TiO₂ showed a higher SPF than predicted, whereas eleven combinations with ZnO showed the synergy of the combination.⁸⁵

Given that there is a wide range of different coatings, the effectiveness of ten uncoated and coated commercial TiO₂ nano-particle formulations was studied. The lipid peroxidation of linoleic acid, in indication of the generation of ROS, was measured after 120 minutes of irradiation with a UVB lamp (G40T10E, Sankyo Denko, Kanagawa, Japan) at 2.4 W/m². Some of the TiO₂ formulations were then further investigated using Electron Spin Resonance (ESR) spectroscopy and the spin trapping technique was used to evaluate the potential to generate ROS and the presence of surface active sites. Only molecules with unpaired electrons, such as ROS, can be detected by ESR. It was concluded that the coating of the TiO₂ nano-particles with

silica appeared to be the most effective in regards to the protection from the generation of ROS.⁸⁶

2.5.1.2. Doped Metal Oxides

A new innovation to protect these metal oxides is the use of dopants such as manganese to reduce the extent of ROS generation.⁸⁷⁻⁸⁹ Manganese doped TiO₂ showed additional benefits to that of coated TiO₂ (BASF Uvinul = octylsilylated TiO₂ and Tayca MT-100SA = silica-alumina coated TiO₂) when tested comparatively in terms of their effect on UV-filter **3** degradation. The determination was undertaken by HPLC after two hours of irradiation by a Spectral Energy Xenon arc solar simulator equipped with a Schott WG320 filter (≥ 290 nm) in an O/W emulsion. In the presence of manganese doped TiO₂, 79 % of UV-filter **3** remained, while in the formulation with UV-filter **3** alone only 63 % remained. No enhanced photostability of UV-filter **3** was observed with the two other coated TiO₂ samples (Figure 2.7).

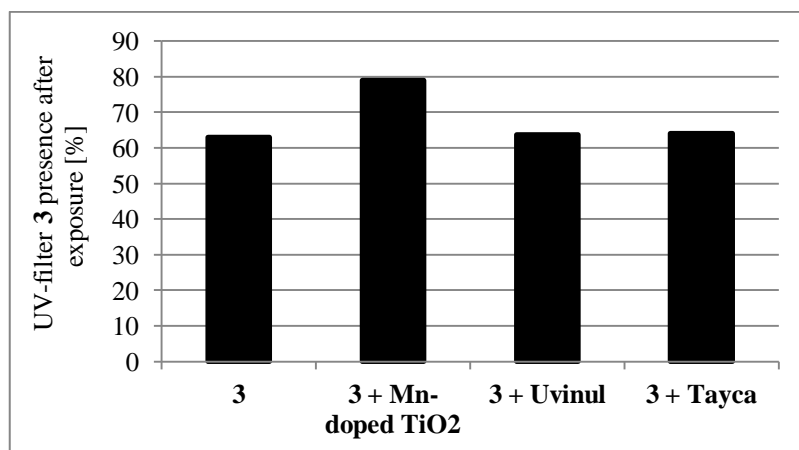


Figure 2.7. Presence of UV-filter **3** in combination with TiO₂ after exposure of 10 mW/cm² for 120 minutes in a solar simulator. Adapted from.⁸⁷

Furthermore, ROS formation from the uncoated, undoped TiO₂ was reduced by over 90 % with the manganese doped TiO₂ and only by 30 % with the silica-alumina coated TiO₂ measured by ESR after irradiation at 2 mW/cm² (octylsilylated TiO₂ was not tested).⁸⁷

Manganese doped TiO₂ was tested against octylsilane coated rutile TiO₂ for its effect on the degradation of two UV-filters (**1** and **3**) and two antioxidants (vitamin E and C). They were incorporated in an O/W emulsion and irradiated for two hours in a Honle Sol-2 solar simulator ($\lambda = 290 - 400$ nm) with an output energy of 10 mW/cm². After irradiation the recovery of UV-filter **3** was 20 % without TiO₂, 36 % with the coated metal oxide and 63 % with the manganese doped TiO₂. The same trend was observed with UV-filter **1**, which had a recovery of 24 % without TiO₂, 49 % with the coated TiO₂ and 83 % with the manganese doped metal oxide.

These results show a significant advantage of the manganese doped TiO₂ against the coated TiO₂. Vitamin E and C were evaluated at different concentrations and showed a recovery of over 90 % of both antioxidants in a 10 % emulsion in the presence of manganese doped TiO₂, while the control without TiO₂ showed a recovery of 77 - 78 % for both vitamins. The coated metal oxide did not protect the antioxidants and showed a lower recovery compared to the control, with the remaining concentration of vitamin E even lower (24 %) than that of vitamin C, about 60 %.⁹⁰

The photoactivity of undoped and doped ZnO was tested by a colorimetric method which measures the photobleaching of the radical 1,1-diphenyl-2-picrylhydrazyl (DPPH). The reciprocal of the time it takes to transform the purple radical to its reduced form, which is yellow, was defined as the Photoactivity Index (PI) in units of min⁻¹. While all four dopants (iron, nickel, copper and manganese) showed a reduction in photoactivity compared to the undoped ZnO, nickel, copper and manganese appeared to be most effective in reducing photoreactivity (Table 2.10).⁸⁹

Table 2.10. Doped and undoped ZnO: Crystal size, the time it takes to reduce the DPPH radical and PI.

Compound	Crystal size [nm]	Time of decay of DPPH radical [min]	PI [min ⁻¹]
ZnO	24	12	0.0833
ZnO/Fe (0.44 wt.%)	14	30 +	< 0.0333
ZnO/Ni (0.64 wt.%)	20	100	0.0100
ZnO/Co (0.7 wt.%)	16	150 +	< 0.0066
ZnO/Mn (1.1 wt.%)	21	150	0.0066

An acrylic polymer (Nanocryl S) film containing manganese doped ZnO was tested for its ability to improve the fading rate of a dyed fabric exposed to UV-light compared to a film containing undoped ZnO. The 100 % plain weave polyester fabric was dyed before being irradiated in a MBTF light box (Australian Standard S 2001.4.21 - 2006) at 65 % relative humidity and 40 °C. A benzopyran-based dye (D1) with a lightfastness on polyester of four to five and an anthraquinone-based dye (D2) with a lightfastness on polyester of six to seven were used in the study. In the UV region the main wavelengths of the light box were 364, 271, 246 and 249 nm. The colour change of the two tested dyes was measured by a Datacolour SF 600 Plus-CT Spectraflash spectrometer. The best protection of the fabric was achieved when the polymer films were separated from the fabric by a quartz slide, where the protection was 2.9

fold higher for D1 and 4.75 fold higher for D2 compared to the untreated fabric. When the ZnO containing film was in direct contact with the dyed fabric, the fading rate was dye dependent. Dye D2 could not be protected by the undoped ZnO, while the fading rate of Dye D1 decreased significantly (exact data not given). This difference can be explained by the photoreactivity of ZnO towards the different chromophores of the two dyes. The manganese doped ZnO showed a significant decrease in the fading rate in both dyes (exact data not given).⁹¹

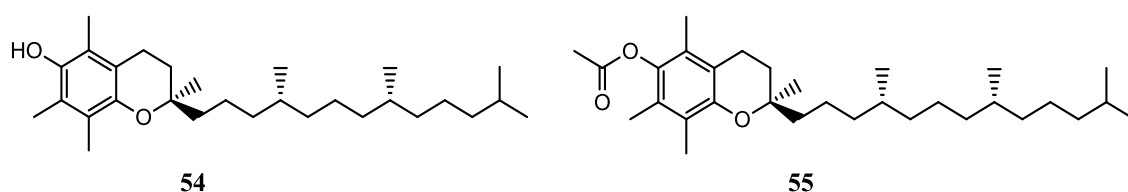
Although the physical UV-filters are not exchangeable, while TiO₂ has a stronger absorption in the UVB-range, ZnO protects better in the UVA-range, especially in the UVA I-range.^{85,92} The SPF, which is an indicator for UVB-protection, of a 25 % TiO₂ cream was about 38, while it was only seven for a 25 % ZnO cream reported in a study by El-Boury et al.⁸⁵ The UV-absorbance spectrum of ZnO showed increased absorbance in the UVA-range. While TiO₂ lost its absorbance capacity at about 340 nm, ZnO remained stable until about 370 nm. In this range (340 - 370 nm), ZnO had a higher absorbance than TiO₂ with a maximum difference shown at 370 nm.⁹²

2.5.2. Addition of Antioxidants

In order to protect the skin from UV-irradiation and the subsequent formation of ROS, the skin contains non-enzymatic antioxidants, such as α -tocopherol (vitamin E) and ascorbic acid (vitamin C), and enzymatic antioxidants, such as superoxide dismutase or glutathione peroxidase. Under increasing oxidative stress, such as UV-light, the skin's own antioxidants may be overwhelmed and no longer capable of protecting the skin. Decreased levels of these antioxidants were reported in mice and even suberythrogenic UV doses resulted in a depletion of these antioxidants in humans.⁹³ To overcome this problem, antioxidants such as vitamin E or C can be added to a sunscreen product to reduce the amount of ROS in the skin. These antioxidants have the ability to scavenge ROS before they can reach the cells and cause molecular or cellular skin damage.^{16,77}

The protective effect of vitamin E, in the presence of the chemical UV-filters **1**, **3** and **23**, has been reported by measuring the reduction of lipid peroxidation *via* TBARS formation. The chemical UV-filters (incorporated in multilamellar PC liposomes), vitamin E, vitamin E acetate and their combinations were dispersed in 5 mM phosphate buffer, 0.9 % NaCl, 0.1 mM Ethylenediaminetetraacetic acid (EDTA), at pH 7.4, transferred into multi-well plates and irradiated with UVA-light for 20 minutes. As light source, a Philips Original Home Solarium (model HB 406/A; Philips, Groningen, Holland) equipped with a 400 W ozone-free Philips HPA lamp, UV type 3, delivering a flux of 23 mW/cm² between 300 and 400 nm was used. A control sample of a liposomal suspension without UV-filters and antioxidants was used, which

showed a three times higher lipid peroxidation after UVA-exposure than in the dark. UV-filter **23** had no influence on the TBARS concentration compared to the irradiated control, while the presence of UV-filter **3** resulted in a notably higher and UV-filter **1** in a slightly lower TBARS concentration (Figure 2.8). In the presence of vitamin E the lipid peroxidation was reduced nearly to the level of the non-irradiated sample, while in presence of vitamin E acetate it was similar to that of the irradiated control. This difference can be explained by the antioxidant activity of vitamin E, which is caused by a hydrogen donation from the hydroxyl group on the benzene ring to a radical, with this hydroxyl group replaced by an acetoxy group in the acetate (Scheme 2.13). Experiments in viable human skin showed, however, that vitamin E acetate bioconverts into vitamin E and is assumed to show the same ROS reduction in viable skin.



Scheme 2.13. Vitamin E and vitamin E acetate.

The TBARS concentration in the presence of vitamin E and UV-filter **3** in combination is about double that of vitamin E only, but still significantly less than in the sample with UV-filter **3** alone. In a combination of the UV-filters **1**, **3** and **23** with vitamin E lipid peroxidation was even further decreased, which can be explained by the stabilising effect of UV-filter **23** on UV-filter **3** (Figure 2.8).⁹⁴

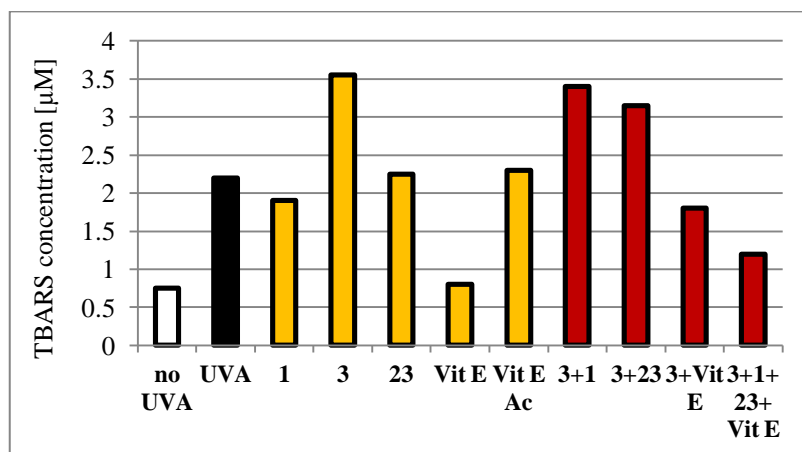


Figure 2.8. ROS generation, measured *via* TBARS concentration. □ : no UVA-exposure, ■ : UVA-exposure, ■ : UVA-exposure in the presence of UV-filters **1**, **3**, **23**, vitamin E (Vit E), vitamin E acetate (Vit E Ac) and their combinations (■). Adapted from.⁹⁴

The protective effect of the two vitamins E and C against lipid peroxidation was studied in the presence of eicosapentaenoic acid (EPA) on porcine skin. EPA was used because it protects against UV-induced immunosuppression and photocarcinogenesis, but this protective effect is limited by oxidative degradation. Dissolved in acetone, EPA was applied onto the porcine skin and after a short drying time different concentrations of vitamin E, vitamin C or a combination of both in 20 % (v/v) DMSO in ethanol was applied. The skin was then dried for 60 minutes to allow the components to penetrate into the skin before being irradiated for 18.5 minutes using a 40W/12 lamp light source (spectral region 260 - 390 nm; peak at 310 nm; Philips, Eindhoven, The Netherlands). After irradiation the malondialdehyde (MDA)-concentrations, which is an indication of lipid peroxidation, in the viable epidermis were determined by HPLC. Each vitamin alone protected the EPA treated skin from lipid peroxidation completely, resulting in a reduction of the MDA-concentration to the level of the non-irradiated sample without antioxidants. However, a 500-fold higher concentration of vitamin C (5000 nmol/cm²) than that of vitamin E (10 nmol/cm²) was required to achieve this result, which could be explained by the higher antioxidant potential of vitamin E, compared to vitamin C. The difference of the vitamin localisation might also play an important role, since vitamin E is located in the membrane, like EPA, and vitamin C in the aqueous phase. The combination of both vitamins also resulted in a total protection, even with lower doses for vitamin C (100 nmol/cm²) and vitamin E (5 nmol/cm²). Lower doses of vitamin E and C are required when used in combination due to a combined action of both antioxidants. Vitamin C regenerates the vitamin E radical, which is formed when vitamin E quenches ROS.⁹⁵

The antioxidants phenylalanine, sodium ascorbyl phosphate and ascorbyl palmitate were also investigated for their effect on the oxidation of linoleic acid and porcine skin in the presence and absence of TiO₂ (0.05 % w/w). They were added separately to a 4.0 % sodium dodecyl sulphate (SDS) aqueous solution (pH 4.0) containing 1.0 % linoleic acid or pieces of porcine skin and irradiated for two hours with a UVB lamp (G40T10E, Sankyo Denki, Kanagawa, Japan) at 2.4 W/m². Each antioxidant was irradiated without TiO₂ and with six different variations of this photocatalyst (Table 2.11), whose activities were investigated in a previous study.⁸⁶ The formation of MDA, the linoleic peroxidation product, was determined by a 2-TBA assay and determined by UV/Vis-spectroscopy. The amino acid phenylalanine did not protect against linoleic peroxidation in the absence of TiO₂ and in the presence of three TiO₂ variations (Maxlight F-TS20, Tego Sun TS plus, T-Lite SF-S). In the presence of the three most active TiO₂ nano-particles (Aeroxide P 25, T-Lite SF, PW Covasil S-1) phenylalanine showed a protective effect against the formation of MDA after irradiation. The two ascorbic acids, sodium ascorbyl phosphate and ascorbyl palmitate, behaved similarly in that, both had a protective effect on linoleic acid, without TiO₂ as well as with all six TiO₂ variations. Different

antioxidant concentrations were tested with linoleic acid and only the concentration showing the best protective effect was tested with porcine skin. Also, only two different TiO₂ variations, one with a high (PW Covasil S-1) and one with a low photocatalytic activity (Tego Sun TS plus), according to results from a previous study,⁸⁶ were tested in the experiments using porcine skin (Figure 2.9). In contrast to the results with linoleic acid, phenylalanine showed a protective effect without and with both TiO₂ powders in porcine skin. In the absence of TiO₂, sodium ascorbyl phosphate resulted in about one third lower MDA formation than without antioxidants (Figure 2.9). These results are in contrast to those involving peroxidation of linoleic acid, where the protective effect of this antioxidant was nearly 100 %. Ascorbyl palmitate showed a notable (one third to one fifth) reduction in peroxidation in all three samples (with and without TiO₂) compared to the samples without antioxidants, which is attributed to its lipophilic character, allowing a good skin penetration. Ascorbyl palmitate appeared to be the best of the three tested antioxidants because of its stability, lipophilicity and scavenging potential.⁹⁶

Table 2.11. TiO₂ samples, commercial name, composition and crystal phase in %.

Commercial name	Composition [%]	Crystal phases [%]
Maxlight F-TS20	TiO ₂ = 75, SiO ₂ = 22	100 rutile
PW Covasil S-1	TiO ₂ > 95, trymethoxycaprylylsilane < 5	80 anatase, 20 rutile
Tego Sun TS plus	TiO ₂ > 50, SiO ₂ = 10 - 25, TMCS = 4.5	80 anatase, 20 rutile
T-Lite SF	TiO ₂ = 84, Al(OH) ₃ = 7, Dimethicone = 4.5	100 rutile
T-Lite SF-S	TiO ₂ = 78, Al(OH) ₃ = 3.5, Silica = 7.5, Dimethicone = 5.5	100 rutile
Aeroxide P 25	TiO ₂ = 100	80 anatase, 20 rutile

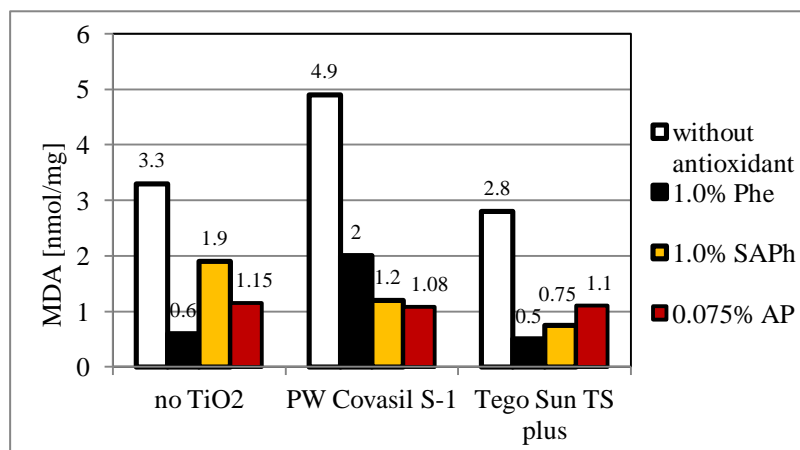


Figure 2.9. MDA concentration in the absence and presence of TiO₂ (PW Covasil S-1 and Tego Sun TS plus), with or without the antioxidants phenylalanine (Phe), sodium ascorbyl phosphate (SAPH) and ascorbyl palmitate (AP). Adapted from.⁹⁶

2.6. Change of UV-protective Performance by Formulation Components

2.6.1. Different Solvents and Formulations

It has been reported that the photostability of chemical UV-filters is solvent dependant.^{34,37,63,64} To investigate this solvent dependant photoreactivity of UV-filter **3**, the UV-filter was dissolved in several solvents with various polarities (dioxane, acetonitrile, ethyl acetate, THF, ethanol, isopropanol, hexane, heptane, cyclohexane and water). Samples were irradiated in a solar simulator (Suntest CPS+ from Atlas Material Testing Technology, Moussy Le Neuf, France) equipped with a Xenon lamp delivering a complete dose of 60 kJ/m² (four minutes interval at 250 W/m²). Filled into spectroscopic 1-cm quartz cuvettes and capped by Teflon[®] stoppers, the absorbance spectra of UV-filter **3** were determined before and after irradiation. In the solvents dioxane, acetonitrile, ethyl acetate, THF, ethanol and isopropanol UV-filter **3** was regarded as stable due to a minimal loss of absorbance of only 1 - 2 %. On the other hand, in the non-polar solvents hexane, heptane and cyclohexane, UV-filter **3** was unstable after irradiation with much higher losses in UV-absorbance. In heptane, the absorption maximum of UV-filter **3** was about 75 % lower after irradiation than before, while the loss in UV-absorbance in hexane and cyclohexane was also recognised but exact data were not given. Interestingly, the instability of UV-filter **3** in the non-polar solvents was reversible after twelve hours in the darkness, but completely inhibited by the addition of 1 % isopropanol. In water, although photodegradation of UV-filter **3** occurred, the phenomenon of the reversibility was not

detected. Although it was suggested that under the described conditions in water degradation of UV-filter **3** into photoproducts occurs, a mechanism was not proposed.⁶³

The photostability of UV-filter **3** in polar solvents and its instability to light in non-polar solvents was confirmed by the results from other studies (Table 2.12).^{37,64} Schwack and Rudolph³⁷ reported the photodegradation of UV-filter **3** in the non-polar solvents, cyclohexane and isooctane, and its photoinstability in the polar solvents isopropanol and methanol. The dissolved UV-filter was irradiated with UVA-light in a solar simulator and analysed by HPLC and GC-MS. Two different glass-filters were employed in the solar simulator: filter F1 ($\lambda \geq 260$ nm) resulting in an irradiance of 12.4 mW/cm² UVA- and 0.54 mW/cm² UVB-light; and filter F2 ($\lambda \geq 320$ nm) resulting in an irradiance of 11.1 mW/cm² UVA-light. In cyclohexane the degradation was exponential using both glass-filters, but while the degradation of **3** was 14 % with filter F1, it was only about 8 % with filter F2. Data for the photodegradation in isooctane were not given.³⁷

Mturi and Martincigh⁶⁴ reported the stability of UV-filter **3** (0.01 M) to light in methanol, but its photodegradation in the non-polar solvents DMSO, ethyl acetate and cyclohexane (Table 2.12). UV-filter **3** was irradiated with a high pressure mercury lamp using a pyrex glass filter (≥ 300 nm) in the presence of air and analysed by HPLC, GC-MS, UV- and NMR-spectroscopy. After an irradiation time of 18 hours of UV-filter **3** in cyclohexane, no photodegradants or photodegradation were detected by GC. Although, it is important to mention that with the employed GC-column a separation of the diketo- and enol-form was not possible. In ethyl acetate two photodegradants were detected, while in cyclohexane nine photoproducts were found. In DMSO a decrease of 75 % for the enol-form of UV-filter **3** resulted after 15 - 18 hours of irradiation, while 56 % was detected in cyclohexane, 33 % in ethyl acetate and only 7 % in methanol. Comparison of the ¹H NMR spectra of UV-filter **3** before and after 21 hours of irradiation in DMSO showed an increase of the methylene proton-signal, which indicates a photoisomerisation of the enol- to the diketo-form. In cyclohexane ¹H NMR spectra indicated the presence of three major photodegradants after an irradiation time of 25 hours, while in methanol no difference between the non-irradiated and the irradiated sample was observed. In methanol the presence of air had no effect on the photostability of UV-filter **3**, while for the other three solvents (cyclohexane, ethyl acetate and DMSO) the UV-filter was more stable without air. Though, the difference was not significant in cyclohexane and ethyl acetate, in DMSO 97 % of UV-filter **3** degraded after 40 minutes of irradiation in the presence of air, while only 7 % degraded in the absence of air.⁶⁴ The instability of UV-filter **3** in ethyl acetate was not consistent with results by Huong et al.⁶³ who reported the stability of UV-filter **3** after irradiation in a solar simulator at four minute intervals at 250 W/m² to a complete dose of 60 kJ/m² in air. However, although Huong et al.⁶³ only used the UV-spectroscopy to study the

photostability of UV-filter **3** in the different solvents, Mturi and Martincigh⁶⁴ used a combination of analytical instruments. ¹H NMR spectra showed that UV-filter **3** forms 3.5 % of its diketo-form in cyclohexane-d₁₂, while no diketo was detected in isopropanol-d₈. Given that UV-filter **3** is unstable in cyclohexane and stable in isopropanol, these results show that the photodegradation strongly depends on the formation of the 1,3-diketo-form.³⁷

Table 2.12. Comparative photostability of UV-filter **3** in different solvents.^{37,63,64}

Solvents	Huong et al. ⁶³	Schwack and Rudolph ³⁷	Mturi and Martincigh ⁶⁴
Acetonitrile	stable		
Dioxane	stable		
Ethyl acetate	stable		unstable
THF	stable		
Ethanol	stable		
Isopropanol	stable	stable	
Methanol		stable	stable
Hexane	unstable		
Heptane	unstable		
Cyclohexane	unstable	unstable	unstable
Isooctane		unstable	
DMSO			unstable

Photostability of the UV-filters **1**, **5**, **6**, **10** and **18** was investigated in water, methanol, hexane and acetonitrile after irradiation with an Hg/Xe lamp ($\lambda \geq 290$ nm) excluding infrared light. After 30 minutes of irradiation (equilibrated with air), UV-filter **1** degraded in all four solvents with the extent of degradation 90 % in water, 40 % in methanol, 40 % in hexane and 45 % in acetonitrile. After two hours of irradiation the degradation of UV-filter **1** was nearly complete (approximately 95 %) in hexane, the least polar solvent. In all solvents the photodegradation was attributed to a trans-cis isomerisation reaction (Scheme 2.1, page 18). Not only the photodegradation, but also were the UV-absorbance spectra found to be solvent dependent. In water, the absorbance maximum of UV-filter **1** was at 320 nm, while in hexane it was shifted to 289 nm. In addition, the absorption maximum in water shifted to about 280 nm after 30 minutes of irradiation. This shift in the UV-absorbance after irradiation may impact the UV performance in a sunscreen product. UV-filter **10**, on the other hand, was more photostable after two hours of irradiation compared to UV-filter **1**. The degradation was about 20 % in water, around 95 % in methanol, 15 % in hexane and 5 - 10 % in acetonitrile, implying instability in methanol, but photostability in the other three solvents. In contrast to UV-filter **1**,

the absorbance maxima shifts of UV-filter **10** were relatively small, remaining in the range of 283 - 287 nm and 321 - 325 nm. UV-filter **5** degraded in all four solvents with photodegradation rates of 65 % in water, 60 % in methanol 87 %, in hexane and 45 % in acetonitrile after 60 minutes of irradiation. The onset of the UV-absorbance spectrum was shifted from 325 nm in water, to 305 nm in hexane, resulting in a loss of the photoprotective character of UV-filter **5** in the UVB-range. UV-filter **6** almost completely degraded after only 20 minutes of irradiation in hexane (97 %) and acetonitrile (94 %), while in water the degradation was 75 % and in methanol it was the lowest with 15 %. The absorption maxima of UV-filter **6** shifted after irradiation in all four solvents, in water from 311 to 277 nm after 30 minutes, in methanol from 311 to 292 nm after 80 minutes, in hexane from 299 to 259 nm after 20 minutes and in acetonitrile from 309 to 266 nm after 30 minutes of irradiation. These shifts decrease the UV-protective effect of UV-filter **6**, similarly to the UV-filters **1** and **5**. The photostability of UV-filter **18** was only determined in water, methanol and acetonitrile, due to its low solubility in hexane. After only ten minutes of irradiation in water UV-filter **18** showed a degradation of 90 %. In acetonitrile, 50 % of UV-filter **18** was degraded after 20 minutes, while after two hours the degradation rate reached 70 %. Absorption maxima and absorption ranges of UV-filter **18** showed no differences between the solvents, in contrast to the other tested UV-filters.³⁴

UV-filter **1** was investigated for its isomerisation in the solvents heptane, dioxane, ethyl acetate, THF, acetonitrile, isopropanol and water. The percentage of both isomers (trans- and cis-isomers) was determined by HPLC. The UV-filter was dissolved in each solvent and irradiated in a solar simulator for ten minutes at 250 W/m² (= 150 kJ/m²). The trans-isomer is the active form of UV-filter **1** and its recovery was the highest in water and heptane with 55.4 % and 53.0 %, respectively, while it was the lowest in isopropanol and acetonitrile with 34.2 % and 33.6 %, respectively. HPLC analysis in the solvents dioxane, ethyl acetate and THF resulted in similar percentage recoveries of the trans-isomer with 41.5 %, 43.5 % and 40.6 %, respectively. The sum of the trans- and cis-isomer was in all solvents was about 100 %, except in water where it was lower (71.7 %), which indicates a structural degradation of UV-filter **1**.⁶⁷

Investigation of the photostability of 16 commercial sunscreen products showed that the same UV-filter combinations are photostable in some formulations and unstable to light in others. The sunscreen products were spread on a quartz plate and irradiated in a solar simulator (COLIPA Dermasun Dr Honle 400F/5, Planegg, Germany) with a radiometrically (Solar Light SL 5D, Solar Light, Philadelphia, PA) defined, homogeneous field of irradiance according to different (5, 12.5, 25, 50) standard erythema doses (SED). One SED is equivalent to an erythemal effective radiant exposure of 100 J/m². The spectral absorbance before and after the different exposures was measured for the UVA- and UVB-range separately with using UV-

spectroscopy. In all tested sunscreen products, the mean difference of the absorbance before and after UV-exposure of 25 SED (ΔA) was ≤ 1 % in the UVB-range. On the other hand, in the UVA-range some sunscreen products showed a ΔA of up to 48.4 % after a UV-exposure of 25 SED. Sunscreen products with a $\Delta A \leq 1$ % were regarded as photostable. Out of three sunscreen products (A1, A2, A3), with the same UV-filter combination (TiO₂, **1**, **3**, **9**, **14**), two were regarded as photostable in the UVA-range with $\Delta A = 0.0$ and 0.6 %, respectively and one was regarded as not photostable with $\Delta A = 26.5$ % after UV-exposure (Table 2.13). A different UV-filter combination (TiO₂, **1**, **3**, **14**) was found in four sunscreen products (B1, B2, B3, B4), where three were unstable to light with $\Delta A = 28.1$, 24.3 and 31.8 %, respectively and one was photostable with $\Delta A = 0.5$ % (Table 2.13). Six of these products were sun milks, except for sunscreen product A3, a lotion, which was photostable with $\Delta A = 0.6$ %. Further details about the differences in the formulation or the reasons for the difference in photostability were not provided.⁹⁷

Table 2.13. Absorbance of seven commercial sunscreen products before UV-exposure and photoinactivation after increasing UV-exposure in the UVA-range.

Sunscreen product	Absorbance A [%]	Photoinactivation, ΔA [%]			
		5	12.5	25	50
A1	97.7	5.3	13.8	26.5	32.7
A2	99.9	0.1	0.0	0.0	
A3	99.9	0.0	0.1	0.6	
B1	99.4		15.7	28.1	29.7
B2	98.4	7.7	13.2	24.3	
B3	99.9	0.0	0.1	0.5	
B4	95.5	8.3	18.2	31.8	

2.6.2. New Formulation Additives to Reduce Photodegradation of UV-filters

As described in section 2.2 the photostability of some chemical UV-filters is problematic, separately and also in combination with other chemical UV-filters. Recent studies have reported an increased photostability of chemical UV-filters after incorporation into solid lipid nano-particles (SLNs),^{98,99} nano-structured lipid carriers (NLCs)⁹⁸ or other structures, such as mesoporous silicate MCM-41.¹⁰⁰

UV-filters **3** and **23** were co-encapsulated in SLNs and NLCs and incorporated in a cream before being irradiated with UV-light. A light source, in a BioSun irradiation system (Vilver Lourmat, France) was used, irradiating the samples at 365 (UVA) nm and 312 nm (UVB) with an energy of 19.5 J/cm². Samples were irradiated in two intervals, the first interval was for one hour and 30 minutes of UVA-irradiation and two hours 30 minutes of UVB-irradiation. The second interval was longer with three hours UVA- and five hours UVB-irradiation. After each interval the SPF and UVA-PF were measured *in vitro*. As a reference a cream with non-encapsulated UV-filters was irradiated. Both, encapsulation in SLNs and NLCs resulted in higher SPF and UVA-PF values after irradiation compared to the reference cream. The highest photoprotection was reported with the NLCs, which absorbed 98 % of the UVA- and 94 % of the UVB-radiation.⁹⁸

To increase photostability of UV-filter **1** it was incorporated into the pores of mesoporous silicate MCM-41 and trapped by closing the pore openings. Solid samples were irradiated for 120 minutes with a Xenon lamp at 330 nm, selected by a monochromators, and analysed by UV-spectroscopy (Cary4000, Varian). As a reference UV-filter **1** was incorporated in vaseline and irradiated. UV-spectra of all samples before and after irradiation showed that the incorporation into mesoporous silicate MCM-41 significantly increased the photostability of UV-filter **1**, compared to that of the reference sample.¹⁰⁰

2.7. Skin Penetration of Chemical UV-filters and Sunscreen Formulations

Chemical UV-filters are required to remain on the surface of the skin in order to maintain their photoprotective character. Skin penetration of these UV-filters in sunscreen products should therefore be avoided. In addition to reduction in UV-protection as the result of skin penetration, photosensitivity reactions may also occur.^{81,101}

To study the skin penetration of UV-filters, several *in vivo* and *in vitro* methods are available. *In vivo*, the radioactivity of a topically applied radioactive compound, such as carbon-14 or tritium, can be determined in blood or excreta. Other *in vivo* methods are the tape stripping method, microdialysis or multiphoton microscopy.⁸¹ *In vitro* skin penetration studies are often performed using diffusion cells, such as Franz cells,¹⁰² but the tape stripping method and electron microscopy have also been used.^{81,103} Since skin penetration of chemical UV-filters *in vitro* is studied using Franz diffusion cells in Chapter 6, the literature was only reviewed for this technique.

2.7.1. Skin Penetration of Chemical UV-filters *in vitro*

Skin penetration of the UV-filters **1**, **3**, **7**, **10** and **23** has been studied *in vitro* using Franz diffusion cells. UV-filters were incorporated in mineral oil (0.5 and 1.0 %) and between 17.6 and 18.2 mg was placed on human epidermal skin for 24 hours. As receptor fluid phosphate buffer (pH: 7.4) containing 4 % bovine serum albumin (BSA) was used. After washing the skin surface with DMSO/water (1/1) and plotting dry, two tape strips were used to remove non-penetrated material before the epidermis was separated from the viable cells by the enzyme digestion technique. Tape strips, epidermis, viable cells and receptor fluid were analysed for their UV-filter content by HPLC. Between 95 and 98 % of the UV-filter was recovered on the skin surface and the two tape strips, classified as non-penetrated material. UV-filter **10** showed the highest penetration with a recovery of 4 % in the receptor fluid.¹⁰⁴

Three typical sunscreen formulations (cream, lotion, cream gel) were employed to study the skin penetration of the three UV-filters **1** (7.5 % w/w), **10** (4.0 % w/w) and **16** (5.0 % w/w). Excised porcine ear skin was mounted onto Franz diffusion cells with phosphate buffer (pH: 7.2) containing 0.5 % v/v Tween[®] 20 as receptor fluid. 300 mg of the formulation was placed onto the skin for six hours, before excess formulation was wiped off and the stratum corneum was removed by 15 adhesive tapes. The remaining skin (epidermis and dermis) was cut into small pieces, extracted with methanol and analysed for the UV-filter content by HPLC. The extraction method was validated with three different concentrations of the three UV-filters. Recovery for UV-filter **1** was between 87.03 and 99.33 %, for UV-filter **10** between 73.32 and 79.19 % and for UV-filter **16** between 70.81 and 98.41 %. The amount of UV-filter retained in the skin (epidermis and dermis) after extraction was the highest in the cream gel for all three UV-filters, with 0.41 % for UV-filter **10**, 0.26 % for **1** and 0.22 % for **16** of the applied dose. The retained UV-filter **10** was not only the highest in the cream gel, but also for the cream and the lotion.¹⁰¹

The UV-filters **1**, **6**, **12**, **16** and **20** were studied *in vitro* for their penetration through human skin using Franz diffusion cells. All five UV-filters were incorporated into a water in oil (W/O) emulsion, but only **1** and **19** were additionally studied for their penetration from a water in silicone (W/Si) emulsion. A precise quantity of 2 mg/cm² was applied onto the skin. UV-filter concentrations were determined in the receptor fluid (4 % BSA in phosphate buffered saline), non-penetrated material on the skin surface and the skin (dermis and epidermis) by a developed and validated HPLC method. Before analysis, the skin was ground and UV-filters were extracted with a mixture of THF/acetonitrile (80/20). To precipitate the proteins from the BSA in the receptor fluid 2 mL sample were mixed with 4 mL acetonitrile, sonicated and centrifuged before being analysed by HPLC. The recovery of all five UV-filters both from receptor fluid

and formulations were studied and results showed that between 90 and 105 % of UV-filter content was recovered from the receptor fluid and between 92 and 105 % from the formulations. Only two UV-filters were detected in the receptor fluid, **1** and **19**. Skin penetration of UV-filter **19** showed no difference between the two formulations, with the level of skin penetration of $0.12 \mu\text{g/mL cm}^2$ for the W/O emulsion and $0.14 \mu\text{g/mL cm}^2$ for the W/Si emulsion. On the other hand, the nature of the formulation had an impact on the level of skin penetration of UV-filter **1**, with $1.21 \mu\text{g/mL cm}^2$ for the W/O emulsion and $0.87 \mu\text{g/mL cm}^2$ for the W/Si emulsion. About 25 to 30 % of all five UV-filters was detected in the skin (exact data not given).¹⁰⁵

Skin penetration of the UV-filters **1**, **3**, **10**, **16** and **17** was studied *in vitro* using Franz diffusion cells and *in vivo* using the tape stripping method. For *in vitro* studies human full-thickness skin and an aqueous saline solution (0.9 %) with 1.5 % BSA as receptor fluid were used. UV-filters were incorporated in an O/W emulsion and petrolatum jelly, which were applied on the skin with a thickness of 3 mg/cm^2 . After 30 minutes or six hours the skin was washed with methanol/water (60/40) containing 0.5 % Tween[®] 80, while the epidermis and dermis were separated by the hot plate method and ground. UV-filter content was extracted with methanol from the skin and analysed by HPLC. The skin extraction recovery of the UV-filters was > 95 %, while the total recovery was between 85 and 95 %. After six hours UV-filter penetration was more pronounced from petrolatum jelly than the emulsion. Skin penetration of UV-filter **10** was the highest with 1.5 % of the applied dose in the epidermis and 2.0 % in the dermis, after six hours. Only UV-filter **1** and **10** penetrated into the dermis and no UV-filter was detected in the receptor fluid. For the *in vivo* studies 2 mg/cm^2 formulation was applied to the forearm of volunteers and after 30 minutes access formulation was removed with cotton wipes and the skin was tape-stripped 16 times. UV-filter content from the tapes was extracted with methanol with an extraction recovery of > 97 %. Content from the first tape was regarded as not penetrated. UV-filter content in the tapes 2 - 16 of all five UV-filters was about the same with an average of 25.8 % of the applied dose for the emulsion and 10.3 % for the petrolatum jelly.¹⁰⁶

2.7.2. Microemulsions as Sunscreen Formulation

Sunscreen products are available as various formulations, including creams, lotions, milks, sprays and gels. They should spread easily and uniformly on the skin to provide protection from UV-exposure. Achieving a uniform film on the skin is usually easier with emulsified systems such as creams and lotions in contrast to gels, whose sheer-thinning is often much lower. However, due to the greasy nature of creams and lotions attributed to the oily component, they are not very popular with consumers. The advantage, however, of O/W lotions and creams is that they are less greasy, compared to W/O emulsions. Alcohol- or water-based sprays or gels

are even less greasy and therefore highly favoured by consumers working outdoors. In addition, they have a cooling effect on the skin and are completely transparent after application. The disadvantage of these products is that they are more susceptible to microbial contamination due to the high water content and an uneven application is more likely to occur due to evaporation of the alcoholic or aqueous base.^{107,108} In recent years, microemulsions have been increasingly considered as possible bases for sunscreen products, due to their transparent appearance, although they do contain both oily and aqueous components. Formulation of these microemulsions requires the inclusion of surfactants and often co-surfactants.¹⁰⁹

With a variable combination of oil, surfactant and co-surfactant, the drug delivery of a microemulsion can be decreased or increased. It was reported that the dermal and transdermal penetration of different drugs could be improved using a microemulsion as formulation.^{110,111} An acyclovir containing microemulsion showed a 1.7 fold higher permeation coefficient than the commercially available creams and ointments.¹¹² Skin permeation in mice was significantly higher for a penciclovir containing microemulsion and a microemulsion-based hydrogel than for a cream available on the market. A higher permeation into dermis and epidermis was shown.¹¹³ A microemulsion containing azelaic acid showed a superior penetration through mouse skin compared to a gel.¹¹⁴

While an increased skin penetration is optimum for drugs requiring transdermal delivery the opposite is the case in terms of UV-filters in sunscreen products. In order to keep their photoprotective character and absorb UV-light, chemical UV-filters have to stay on the surface of the skin or in the stratum corneum.¹⁰¹

The UV-filters **1** and **14** were incorporated separately into a microemulsion containing C₁₂-C₁₅ alkylbenzoate as lipid, soyalecithin and decylpolyglucose as surfactants and 1,2-hexanediol as co-surfactant. Beside these main ingredients other adjuvants (cyclomethicone, ethanol, allantoin, stearyl methicone and menthol) were added to produce a non-sticky, waterproof, fresh and moisturizing product. The permeation through a double membrane, a lipophilic membrane and Silastic[®] membrane was investigated for both UV-filter containing microemulsions using a two-compartment horizontal cell. The analysis was undertaken by UV-spectroscopy. After 150 minutes 0.1×10⁻⁵ M of UV-filter **14** were penetrated through the double membrane, while the penetration rates through a lipophilic and Silastic[®] membrane were ten times higher. The kinetics for all penetrations followed pseudo zero-order. UV-filter **1** showed similar results compared to UV-filter **14**. Although no reference formulation was tested for penetration in this study, the authors concluded that the microemulsions were examples of formulations exhibiting very low penetration rates.¹¹⁵

A microemulsion containing the UV-filter **3** was analysed for its drug release through a cellulose membrane using Franz diffusion cells. Different combinations of surfactant, co-surfactant and oily compound were analysed. While glyceryl oleate was used as co-surfactant in every combination, two different surfactants were employed (oleth-20 and isoceteth-20) and three different lipids, namely isopropyl myristate (IPM), isopropyl palmitate (IPP) and isopropyl stearate (IPS). The percentage of the surfactant/co-surfactant mixture was very low (7.7 % w/w) in all microemulsions. No drug release in any of the microemulsion combinations was detected after six hours, while the released amount of UV-filter **3** varied after 22 hours, depending on the composition of the microemulsion. The cumulative drug amount after 22 hours was detected in the receiving phase of the Franz cell (4.5 mL) by HPLC. The cumulative amounts in all of the tested microemulsions together with the different compositions can be found in Table 2.14, with microemulsion 1 showing the highest drug release and microemulsion 5 the lowest. It was demonstrated that not only the type of surfactant, but also the type of lipid can influence the release of UV-filter **3** from a microemulsion.¹¹⁶

Table 2.14. Surfactant and lipid compositions of microemulsions 1-5 with the corresponding cumulative amount released after 22 hours (Q_{22}).¹¹⁶

Micro-emulsion	Oleth-20 [% w/w]	Isoceteth-20 [% w/w]	IPM [% w/w]	IPP [% w/w]	IPS [% w/w]	Q_{22} [μ g]
1	5.5	-	5	-	-	234.5
2	5.5	-	-	5	-	200.6
3	5.5	-	-	-	5	19.3
4	-	5.5	5	-	-	78.1
5	-	5.5	-	5	-	5.4

The drug release and skin penetration of a microemulsion containing UV-filter **1** were investigated. Several surfactants, co-surfactants and lipids were used as ingredients for different microemulsions (Table 2.15). The drug release was studied with cellulose membrane in Franz diffusion cells, while human skin was used to investigate the penetration of UV-filter **1**. Microemulsions 1 - 6 contained isoceteth-20 as surfactant and glyceryl oleate as co-surfactant, combined with six different lipids. The cumulative drug amount in the receptor fluid (water/ethanol: 50/50 % v/v) of the Franz cell (4.5 mL) was detected by HPLC after 24 hours for both, the release study and the penetration study. Microemulsion 6, containing triglyceride caprylic/capric as lipid, showed the lowest amount of released drug (2.2 μ g) and penetrated drug (2.0 μ g) after 24 hours. Therefore triglyceride caprylic/capric was chosen as lipid for the microemulsions 7 - 13 and was mixed with different surfactants and co-surfactants. The drug

release and penetration of UV-filter **1** from microemulsions 7 - 13 are also given in Table 2.15. During the drug release and the skin penetration studies low amounts of UV-filter **1** were detected in the receptor fluid for microemulsions 7 - 9, while the concentration for microemulsion 10 was about three times higher (Table 2.15). No drug release was observed from microemulsions 11 - 13 and therefore there was no penetration through the skin (Table 2.15). Based on these data, it was assumed that the main ingredients of a microemulsion, surfactants, co-surfactants and lipids, play an important role in drug release and penetration characteristics, especially in relation to the lipophilicity of the ingredients. This conclusion is supported by the fact that oleth-20 was the most lipophilic analysed surfactant and no microemulsion containing this surfactant (11 - 13) showed any drug release. In contrast microemulsion 10 showed a higher drug release than 8 and 9, although its co-surfactant (glyceryl monostearate) has a higher lipophilicity than the other two (glyceryl oleate and glyceryl isostearate). Therefore it is strongly supported that the structure of these molecules together with the structure of the drug, in this case UV-filter **1**, plays an important role in terms of both drug release and penetration.¹¹⁷

Table 2.15. Surfactant, co-surfactant and lipid compositions of microemulsions 1 - 13 with the corresponding cumulative amount released after 24 hours (Q_{24r}) and penetrated through the skin after 24 hours (Q_{24p}).¹¹⁷

ME	Surfactant [% w/w]	Co-surfactant [% w/w]	Lipid [% w/w]	Q_{24r} [μ g]	Q_{24p} [μ g]
1	Isoceteth-20 (5.5)	Glyceryl oleate (2.2)	Octyl dodecanol (5.0)	259.2	44.1
2	Isoceteth-20 (5.5)	Glyceryl oleate (2.2)	Cetyl stearyl isononanoate (5.0)	39.3	10.6
3	Isoceteth-20 (5.5)	Glyceryl oleate (2.2)	Decyl oleate (5.0)	248.3	12.9
4	Isoceteth-20 (5.5)	Glyceryl oleate (2.2)	IPM (5.0)	600.0	20.7
5	Isoceteth-20 (5.5)	Glyceryl oleate (2.2)	IPM (5.0)	544.7	12.8
6	Isoceteth-20 (5.5)	Glyceryl oleate (2.2)	Triglyceride caprylic/capric (5.0)	2.2	2.0
7	Isoceteth-20 (5.5)	Glyceryl isostearate (2.4)	Triglyceride caprylic/capric (5.0)	2.0	1.7
8	Ceteth-20 (5.5)	Glyceryl oleate (2.2)	Triglyceride caprylic/capric (5.0)	3.0	2.7
9	Ceteth-20 (5.5)	Glyceryl isostearate (2.4)	Triglyceride caprylic/capric (5.0)	2.7	2.6
10	Ceteth-20 (5.5)	Glyceryl monostearate (2.6)	Triglyceride caprylic/capric (5.0)	11.8	9.9
11	Oleth-20 (5.5)	Glyceryl oleate (2.2)	Triglyceride caprylic/capric (5.0)	-	-
12	Oleth-20 (6.0)	Glyceryl isostearate (2.4)	Triglyceride caprylic/capric (5.0)	-	-
13	Oleth-20 (5.5)	Glyceryl monostearate (2.6)	Triglyceride caprylic/capric (5.0)	-	-

2.7.3. Photoallergic and Phototoxic Skin Reactions

UV-filters may cause photoallergic or phototoxic skin reactions, as stated previously. However, the results from different studies are often controversial due to the use of different methods and models. Therefore caution has to be exercised when interpreting the results from these studies. Due to these reactions consumers may reduce their use of sunscreen products resulting in a higher UV-exposure and thus increasing the rates of melanoma or NMSC.⁷¹

A multicentre photopatch test study has been undertaken to investigate 19 UV-filters for their potential to cause photoallergic contact dermatitis (PACD) and allergic contact dermatitis (ACD). 1031 patients in 30 centres across twelve European countries took part in this study. The photopatch application time was 24 hours in 670 (65.9 %) patients and 48 hours in 347 (33.7 %), while no application time was specified in the remaining five patients. The UVA-irradiation dose for the majority of 977 (94.8 %) patients was 5 J/cm², while the irradiation dose was lower in the remaining patients. 148 PACD reactions occurred in 95 patients (9.2 %) and 55 ACD reactions were recorded in 47 patients (4.6 %). The UV-filters most commonly leading to PACD were the UV-filters **10** and **23**, followed by **3**, **2**, **1** and **19**. UV-filter **19** showed the highest number in ACD reactions, followed by **23**, **10**, **14** and **3**. The high reactivity of UV-filter **19** might not be directly related to the UV-filter itself, but to its suspending agent. It is formulated as nano-particles in the surfactant decyl glucoside, which has been reported previously to cause ACD.¹¹⁸

Another multicentre photopatch test study was undertaken in the UK, including eleven UV-filters. From the 1155 patients 51 (4.4 %) showed PACD reactions, 64 (5.5 %) ACD reactions and 15 (1.3 %) showed both reactions. UVA-irradiation dose to investigate PACD reactions was 5 J/cm² in most cases, but photosensitive patients were irradiated with lower UVA doses (2.5 or 1 J/cm²). The critical reading was undertaken 48 hours after irradiation, but if possible additionally after 24 and 72 hours. The highest rate in PACD reactions were caused by the UV-filter **10**, followed by UV-filter **3**, **2** and **1**. UV-filters **14**, **6**, **9** and **5** also showed limited PACD reactions. UV-filters **3** and **10** showed the highest reactions in ACD, followed by **6**, **14**, **1**, **2**, **9** and **5**.¹¹⁹

During a photopatch test study in the USA, 76 patients were tested for PACD caused by ten UV-filters and other products. After application of the potential photoallergen the patients were subject to UVA-irradiation of 10 J/cm² or less and photopatch test sites were evaluated after 24, 72 or 120 hours. 16 (23.2 %) patients showed PACD caused by the UV-filters **3**, **5**, **6** and **10** to a similar extent.¹²⁰

Eleven UV-filters were studied to estimate their possible reactivity with amino groups as they are present in skin components. Applied on high performance thin layer chromatography (HPTLC) glass plates amino F₂₅₄ the UV-filters were heated to 33 °C and irradiated in the solar simulator Suntest CPS+ (Atlas Testing Technology, Linsengericht, Germany) or in natural sunlight for one hour. The solar simulator was equipped with a Xenon lamp and a special UV-glass filter, simulating the outdoor solar radiation. The average light dose in the solar simulator was 1260 kJ/m² and under natural sunlight 1843 kJ/m². HPTLC amino plates consist of propylamine chains, which are attached to the silica surface. The studied UV-filters provide

ketone or ester groups, which may react with primary amines resulting in the formation of azomethines or amides, respectively. After irradiation, UV-filter standards were applied on the plates and chromatography was carried out in a twin-trough chamber with petroleum ether/*t*-butyl methyl ether/methanol (70/20/10 % v/v) + 1 % triethylamine as mobile phase. For UV-filter **11**, a mobile phase of methanol/acetic acid (90/10 % v/v) was employed. To ensure that eventual reactions were related to the amino groups, control irradiations were undertaken using HPTLC glass plates silica gel 60 F₂₅₄ and RP₁₈ WF₂₅₄ in addition to dark controls. The UV-filters **1**, **3**, **10**, **11** and **23** showed the highest reactivity with the amino plates, indicating possible allergic reactions in the skin. Results were then compared to photopatch data from the literature, showing that these UV-filters were also the most common allergens in these photopatch tests.¹²¹

Of all currently marketed UV-filters, UV-filter **10** is regarded as the most common cause for PACD,^{18,81} which was confirmed by the above described studies.

The phototoxicity of the UV-filters **1**, **3**, **10**, **14**, **16** and **23** was evaluated *in vitro* by the 3T3 Neutral Red Uptake Phototoxicity Test (3T3-NRU-PT) and the Human 3-D Skin Model Phototoxicity Test (H3D-PT). As light source, a doped mercury metal halide lamp (SOL 500, Dr. Hönle, Germany) was used, which simulates the spectral distribution of natural sunlight above 320 nm. For the 3T3-NRU-PT UV-filters were tested individually in DMSO and in combinations in DMSO or in an O/W formulation, while for the H3D-PT UV-filters were only studied in combination with DMSO solutions diluted in C₁₂-C₁₅ alkyl benzoate. Only UV-filter **3** was considered phototoxic in the 3T3-NRU-PT, with increasing phototoxicity correlating to higher UVA doses. This phototoxicity was reported for UV-filter **3** dissolved in DMSO individually and in combination with other UV-filters, but not in the formulation. The H3D-PT showed no phototoxicity in any UV-filter combination.¹²²

2.8. Summary

Sunscreen products play an important role in protecting the skin from the harmful effects of UV-light. It is therefore important for regulatory bodies worldwide, including Australia, to ensure not only the safety, but also the ability of the active ingredients, the UV-filters, to provide broad spectrum protection.

This review presents an in-depth investigation into the photostability of UV-filters and what influence UV-filter combinations and the presence of other ingredients have. Photostability is important and in fact should be regulated, although this is currently not the case. Skin penetration of UV-filters should be limited and they should stay on the surface of the skin in order to be photoprotective and limit the occurrence of photosensitivity reactions. Microemulsions are presented as good formulation choice for sunscreen products to minimise skin penetration of chemical UV-filters. The UVA-filter Butyl methoxy dibenzoylmethane (**3**) and the UVB-filter Octocrylene (**23**) were chosen for photostability and skin penetration studies to provide broad spectrum protection. UV-filter Benzophenone-3 (**10**) was chosen as control during skin penetration studies, as it is known to penetrate the skin.

All three chemical UV-filters were investigated in detail in Chapter 3 to confirm their identity (by NMR-, IR- and UV-spectroscopy) and purity (by melting point determinations, DSC and HPLC) prior their use in subsequent chapters.

Chapter 3

Characterisation of Chemical UV-filters

3.1. Introduction

Characterisation of the three UV-filters, Butyl methoxy dibenzoylmethane (**BMDM**), Octocrylene (**OC**) and Benzophenone-3 (**B3**) to be used in this study, was undertaken. Different experimental methods were used to confirm both the identity and purity of these UV-filters, before further studies were undertaken. One chromatographic and three spectroscopic methods were employed: HPLC, NMR-, IR- and UV-spectroscopy. In addition to these analytical methods, DSC, solubility and melting point determinations were also undertaken.

To perform some of the analytical methods described in this chapter (NMR, UV, HPLC) and a requirement for the formulation development in Chapter 6, is that the UV-filters have to be dissolved in an appropriate solvent. Therefore, the solubility of these UV-filters in different solvents and formulation excipients was investigated.

Although UV-spectroscopy is not specific for the determination of substances in the presence of impurities, it can be used as additional method for identification.¹²³ The absorption maximum, determined from the complete UV-spectrum, is used during the rapid and simple quantitation of these UV-filters. This determination is also important for HPLC analyses, as most of these analyses are undertaken at the absorption maximum. The UV-spectral determination of the four UV-filters was undertaken as first step of the characterisation, due to the availability of reference data in the literature. These reference data were then compared with the measured values for the absorption maxima, which were then further used as the detection wavelength for the HPLC analyses.

The high specificity of the HPLC method allows the determination of a chemical substance in the presence of both degradation products and impurities.¹²⁴ The silica-filling (bonded or unbonded) of an HPLC column interacts with injected substances for a certain time period, depending on their structure and polarity. The difference in interaction times results in the separation of the components of a mixture. The photodiode array (PDA) detector allows the measurement of the absorbance at one or more chosen wavelengths, which is expressed in a chromatogram over a time period. Thus, even small amounts of impurities can be separated from the main substance and visualised. The HPLC is one of the most commonly used analytical techniques nowadays especially for pharmaceuticals because of its high precision and its almost unlimited applications. A wide range of different available equipment excludes only

a few substances from being analysed by this technique.¹²⁵ The HPLC analyses were undertaken to determine the purity of the UV-filters.

The melting point determination, although not specific for a particular substance, can act as additional method for identification and purity, if reference data are available. In the British Pharmacopoeia (BP), the melting point measurement is often represented as identification method. Reference data for all solid UV-filters were available and therefore the experimental data could be compared to those in the literature.

DSC was also undertaken, which measures the energy change of a substance when it is heated, cooled or held isothermally. The heat flow, which is the flow of energy per time, is measured and every change indicates an event such as the glass transition temperature, the melting or crystallisation process. The DSC measurement is very fast and easy, requiring little preparation necessary before analysis.¹²⁶ The analysed UV-filters were heated and the melting process was compared to reference data in the literature and the classic melting point determination. The DSC indicates the purity of a substance.

NMR-spectroscopy is a very useful method to confirm the structure of a molecule, known or unknown. Placed in a magnetic field a substance can absorb electromagnetic radiation in the radio frequency region. This absorption is based on the magnetic properties of certain atomic nuclei, however not all nuclei absorb electromagnetic radiation. The most commonly analysed nuclei are proton (¹H NMR) and carbon (¹³C NMR) nuclei. In the NMR-spectrum the frequencies of the absorption are plotted against the peak intensity.¹²⁷ A ¹H NMR was undertaken for all four UV-filters in this chapter to confirm their identity. In the ¹H NMR spectrum the type and number of proton containing functional groups can be identified.

Another valuable tool for the identification of substances is the IR-spectroscopy, with every substance having a distinctive IR-spectrum. Each atom absorbs infrared light of different wavelengths, which leads to molecular vibrations between atomic bonds. The absorption wavelengths, which are expressed as wavenumbers [cm⁻¹] in the IR-spectrum, depend on the force constants of the bonds, the relative molecular weights and geometry of the atoms. Functional groups can be identified by characteristic peaks in the absorption range between 4000 and 400 cm⁻¹. The lower wavenumbers (1300 - 900 cm⁻¹) are regarded as the fingerprint region, which is unique for each substance. The identity can be proven if a reference IR-spectrum is available, to undertake a peak-to-peak correlation.¹²⁸ In the BP, the use of IR-spectroscopy is often listed as identification method, providing comparative spectra, but unfortunately none of the used UV-filters are listed in the BP. Only incomplete IR-data were available in the literature and therefore the IR-spectroscopy could not be used as proof for identification for the UV-filters, only as additional method.

3.2. Materials and Methods

3.2.1. Solvents and Reagents

The UV-filters Butyl methoxy dibenzoylmethane (Eusolex[®] 9020) and Octocrylene (Eusolex[®] OCR) were purchased from Merck (Darmstadt, Germany). Chloroform-*d*₁ (CDCl₃, 99.8 atom %) and the UV-filter Benzophenone-3 (2-Hydroxy-4-methoxybenzo-phenon, 98%) were purchased by Sigma-Aldrich (St. Louis, USA). Methanol (HPLC-Grade) and glacial acetic acid were obtained from RCI Labscan (Bangkok, Thailand) and methanol-*d*₄ (CD₃OD, 99.8 atom %) was supplied by Cambridge Isotope Laboratories, Inc. (Tewksbury, USA). Water was prepared with a Millipore[®] Elix 10 reverse osmosis filter system from Millipore SAS (Molsheim, France).

3.2.2. Instrumentation

An OptiMelt Automated Melting Point System with digital image processing technology from Stanford Research Systems (Sunnyvale, USA) and a DSC 822^c equipped with the STARE-software, purchased from Mettler Toledo (Schwerzenbach, Switzerland), were used.

For the spectroscopic methods, a Varian Cary[®] 50 UV-spectrometer (Varian Inc., Melbourne, Australia), a Thermo Scientific Nicolet 6700 FTIR-spectrometer (Thermo Fisher Scientific Inc., Waltham, USA) and a Bruker Avance 600 NMR-spectrometer (Bruker Biosciences Pty. Ltd., Melbourne, Australia) were used.

A Varian ProStar[®] HPLC system (Varian Inc., Melbourne, Australia) consisting of a 240 quaternary solvent delivery module, 210 autosampler and a 330 PDA detector was used for the HPLC analyses.

3.2.3. Methodology

3.2.3.1. Solubility

Solubility determinations of the UV-filters were undertaken using the so-called Saturation Shake-Flask Method.¹²⁹ An excess amount of the UV-filters in the chosen solvent in a 25 mL conical flask was sonicated for about one minute prior equilibration to increase the surface area of the UV-filter. This suspension was stirred with a magnetic stirrer for 24 hours, covered with aluminium foil, and then filtered prior to analysis. A 15 mm - syringe filter with a 0.45 µm regenerated cellulose - membrane (Phenomenex Inc. Sydney, Australia) was used to filter the aqueous suspension and a syringe filter with a 0.45 µm Polytetrafluoroethylene (PTFE) membrane for all other solvents. The samples were analysed by UV-spectroscopy and the

concentration of the UV-filter of the saturated solution calculated. The solubility of all UV-filters in water was too low to be detected by UV-spectroscopy and therefore are described as not soluble.

3.2.3.2. Ultraviolet (UV)-spectroscopy

The absorption spectra of the dissolved UV-filters were measured at different concentrations to attain an absorption between 0.3 and 1.0. In this range, the risk for noise and stray light, which can cause a deviation from linearity, is marginal.¹³⁰ For the detection the solution was filled in a quartz cuvette (d = 1 cm). In Table 3.1 the UV-filter concentrations and solvents are presented.

Table 3.1. Concentration and solvent of UV-filters used in UV-spectroscopy.

UV-filter	Concentration [$\mu\text{g/mL}$]	Solvent
BMDM	6	Methanol
OC	20	Methanol
B3	10	Methanol

3.2.3.3. High Performance Liquid Chromatography (HPLC)

All three UV-filters **BMDM**, **OC** and **B3** were dissolved in methanol. The samples were filtered through a 15 mm - syringe filter with a 0.45 μm PTFE membrane before injection onto the HPLC. The full HPLC-method development and validation is described in Chapter 4 with the following chromatographic conditions applied to analyse UV-filters:

- Column: SunFire™ C18 (4.6 x 250 mm, 5 μm) from Waters Corp., Rydalmere, Australia
- Mobile Phase: Methanol/water/acetic acid (89/10/1 % v/v)
- Flow-rate: 1 mL/minute
- Injection volume: 10 μL
- Column temperature: 30 °C
- Detector settings: 303 nm (λ_{max} of UV-filter **OC**)
324 nm (λ_{max} of UV-filter **B3**)
358 nm (λ_{max} of UV-filter **BMDM**)
- Retention times: UV-filter **B3**: ~ 5.0 minutes
UV-filter **OC**: ~ 8.5 minutes
UV-filter **BMDM**: ~ 12.2 minutes

3.2.3.4. Melting Point Measurement

To measure the melting range of the UV-filters Method VI, specified in the BP,¹³¹ was used. In this method the dried powder (dried over silica) was filled in a glass capillary, sealed at one end, to a height of 3 - 4 mm and then placed into the melting point apparatus.¹³¹ The melting range is given by the onset point, the start of the melt, and the clear point, which is the point when the substance is completely melted. The melting range measurement was started about 5 °C under the expected onset point, and the UV-filter slowly heated at a rate of 1 °C/minute for **BMDM** and **B3** only, since **OC** is an oily liquid at room temperature. The melting ranges were determined in triplicate.

3.2.3.5. Differential Scanning Calorimetry (DSC)

No further preparation of the UV-filters was necessary for the DSC experiments. The exactly weighted (2 - 5 mg) UV-filter was placed in a 40 µL aluminium crucible and sealed, while a hole in the lid allowed the replacement of air with nitrogen in the DSC. The flow rate of nitrogen was approximately 80 mL/minute. Table 3.2 gives the weight and the heating range of the UV-filters, which were all heated at a rate of 10 °C/minute. The difference between the heat flow of the UV-filters and an empty crucible was measured as a function of temperature. The software automatically determined the area between the heat flow curve and the extrapolated baseline. With the value of this area and the weight of the sample, the change in enthalpy (ΔH) can be calculated. UV-filter **OC** is liquid at room temperature and therefore it was not analysed by DSC.

Table 3.2. UV-filters with weight and DSC-heating range.

UV-filter	Weight [mg]	Heating range [°C]
BMDM	3.35	40 - 120
B3	4.69	35 - 100

3.2.3.6. Nuclear Magnetic Resonance (NMR)-spectroscopy

To identify the UV-filters and to assign proton-binding atoms to chemical shifts a ¹H NMR in chloroform-*d*₁ was performed for all four UV-filters. ¹H NMR and ¹³C NMR measurements were performed for **BMDM** in methanol-*d*₄ as well, to determine the ratio of the diketo-enol-forms, given that photostability studies were determined in methanol. 1D and 2D NMR spectra were collected at 600 MHz for ¹H and 125 MHz for ¹³C. The *t*-butyl-group signals and the aromatic signals were integrated for both forms. These measurements were undertaken 15 times for both signals and an average value was calculated.

3.2.3.7. Infrared (IR)-spectroscopy

About 10 mg of the pure UV-filters were placed in the FTIR-spectrometer to measure the IR-spectra.

3.3. Results and Discussion

3.3.1. Butyl methoxy dibenzoylmethane (BMDM) [70356-09-1]

BMDM, one of the most commonly used UVA-filters,^{18,39} is a white to yellowish-white fine crystalline powder. It has the empirical formula $C_{20}H_{22}O_3$ and a molecular weight of 310.4 g/mol.¹³² This UV-filter undergoes keto-enol tautomerism (Figure 3.1), where the enol-form absorbs in the UVA-range while the diketo-form absorbs in the UVC-range, with this transformation rendering **BMDM** no longer effective as a sunscreen.⁴²

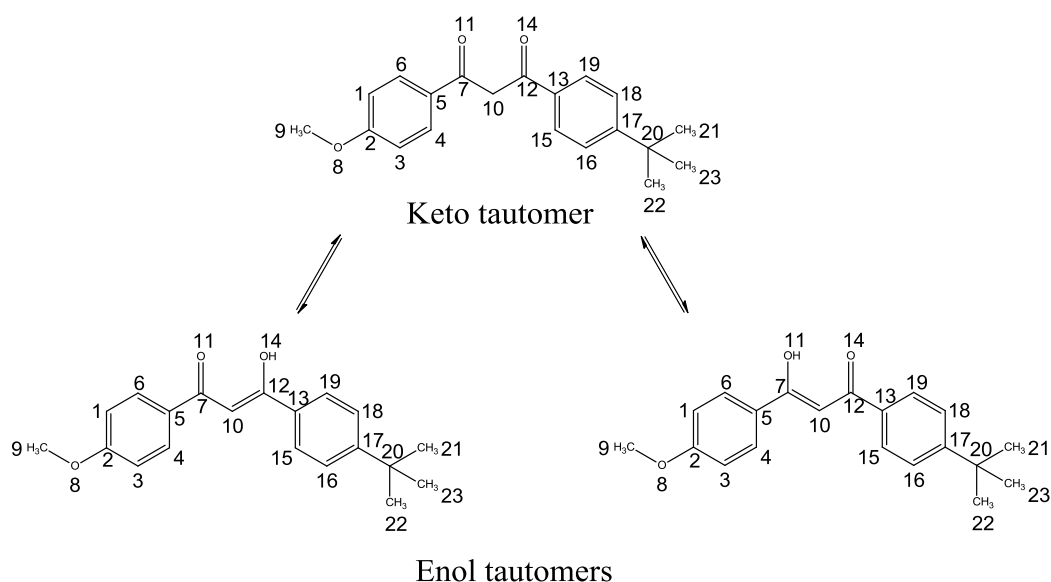


Figure 3.1. Chemical structure of **BMDM** showing the diketo- and the two enol-forms.

3.3.1.1. Solubility

The solubility of **BMDM** in different solvents and formulation excipients is given in Table 3.3.

Table 3.3. Solubilities of **BMDM**.

Solvent	Solubility [mg/mL]	
	Experimental	Literature
Water	Not soluble	0.027 ¹³²
Methanol	19.93	-
Mygliol® 812	137.05	-
Phosphate buffer (pH: 7.4) + 4 % BSA	16.79	-

3.3.1.2. Ultraviolet (UV)-spectroscopy

BMDM showed an absorption maximum (λ_{\max}) at 358.0 nm with an absorbance (A) of 0.718 (Figure 3.2). In the literature λ_{\max} was given at 357 nm in ethanol.³⁶ With λ_{\max} in the UVA-range, this result indicates that **BMDM** is present predominantly in its enol-form in methanol.

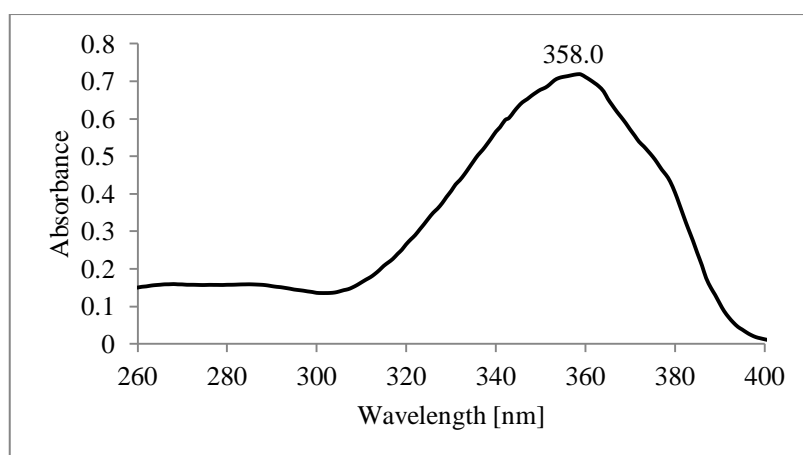


Figure 3.2. UV-absorption spectrum of **BMDM**.

3.3.1.3. High Performance Liquid Chromatography (HPLC)

During HPLC analysis of **BMDM**, five additional peaks were noted at 3.5, 4.6, 5.2, 6.1 and 22.2 minutes. Therefore the UV-filter was recrystallised from methanol and water, reducing the presence of these impurities in the sample. In Figure 3.3 the complete chromatogram of **BMDM** (0.04 mg/mL) is shown after (A) and before recrystallisation (B) at a wavelength detection of 358 nm.

One of the additional peaks (4.6 minutes) in the HPLC-chromatogram was identified as the keto-form of **BMDM**, with the other four peaks regarded as impurities. The sum of all impurities was calculated at 2.42 % with the largest impurity at 1.94 % before recrystallisation. After recrystallisation the impurity % varied slightly from batch to batch, the largest impurity was about 0.62 % and the sum of impurities about 0.66 %. The official monograph of **BMDM** of the United States Pharmacopoeia allows an individual impurity of 3 % and a sum of all impurities of 4.5 %.¹³³ **BMDM** was recrystallised before use, because one of the impurities (22.2 minutes), which was eliminated by recrystallisation, eluted after **BMDM** in the HPLC-chromatogram. This was undertaken to reduce the run-time, preventing overlapping peaks with subsequent injections.

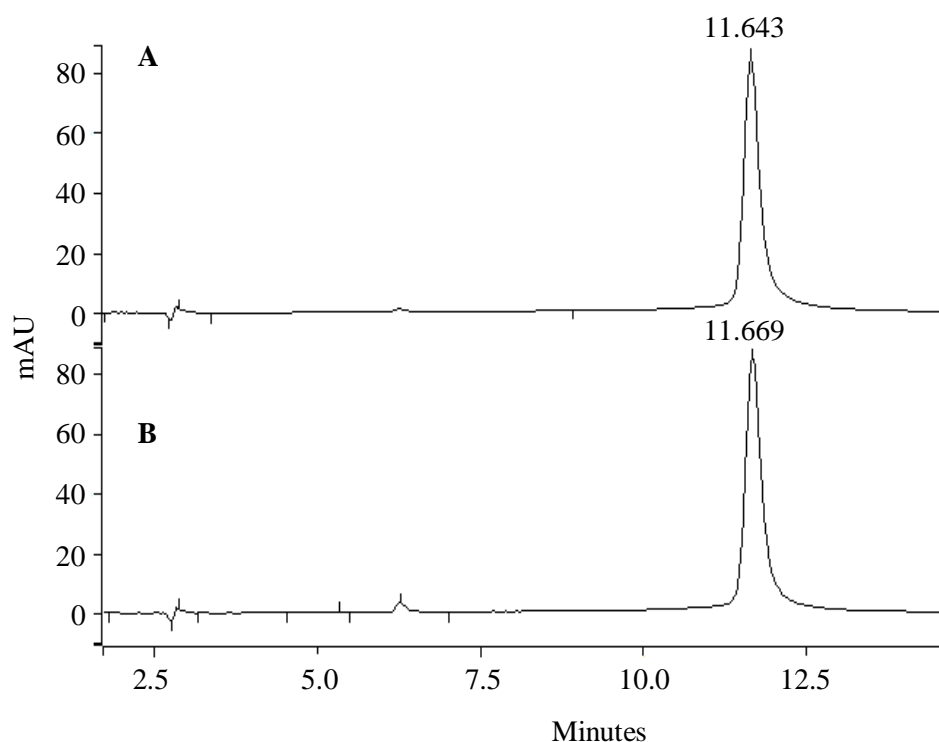


Figure 3.3. HPLC-chromatogram of **BMDM** measured at 358 nm. A: after recrystallisation, B: before recrystallisation.

3.3.1.4. Melting Point Measurement

The melting range of **BMDM** was 82.7 - 84.3 °C before recrystallisation and 84.4 - 85.5 °C after recrystallisation, which are both in accordance with the values quoted in the literature (81 - 86 °C).¹³³ After recrystallisation of **BMDM** the melting range is higher and narrower than before, indicating a higher purity of the sample, which is to be expected after a recrystallisation.

3.3.1.5. Differential Scanning Calorimetry (DSC)

The melting range measured in the DSC gave an onset point of 85.47 °C and an end point of 88.70 °C with a peak at 86.65 °C (-20.97 mW) (Figure 3.4). A reference melting peak was given as 86.8 °C in the literature.¹³⁴ With the area under the curve and the exact weight of **BMDM** (3.35 mg) the change of enthalpy (ΔH) was 79.5 J/g.

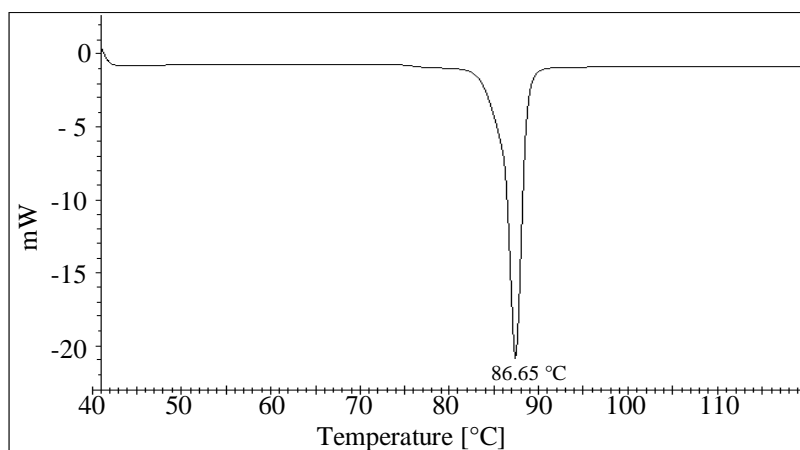


Figure 3.4. DSC-thermogram of **BMDM**.

3.3.1.6. Nuclear Magnetic Resonance (NMR)-spectroscopy

The data of the ¹H NMR-spectrum for **BMDM** are given in Table 3.4, including comparative literature data.¹³⁵ The positions of the proton-binding atoms are indicated in Figure 3.1 on page 70.

Table 3.4. ^1H spectral assignment and chemical shifts of **BMDM**.

Position and type of proton-binding atoms	Chemical shift [ppm]		Multiplicity	Coupling constant J [Hz]
	Experimental (CDCl_3)	Literature ¹³⁵ (CDCl_3)		
3 x CH_3 (21-23)	1.36	1.36	s	-
OCH_3 (9)	3.88	3.88	s	-
COCHCO (10)	6.78	6.78	s	-
2 x H_{arom} (1, 3)	6.98	6.98	d	9.0
2 x H_{arom} (16, 18)	7.5	7.5	d	8.4
2 x H_{arom} (15, 19)	7.92	7.91	d	8.4
2 x H_{arom} (4, 6)	7.98	7.97	d	8.7
OH (14)	17.04	17.02	s	-

s = singlet

d = doublet

 H_{arom} = aromatic proton

The assignment of the four aromatic proton-groups was possible due to the measurement of a COSY NMR, which showed which identified the proton groups belonging to the same aromatic ring.

The presence of the hydroxyl group in the ^1H NMR-spectrum (17.04 ppm) indicates that UV-filter **BMDM** is found mainly in its enol-form in CDCl_3 . Further evidence for this assumption is the strong left shift of the proton binding C-atom at the methylene group (atom 10). In the diketo-form this C-atom would have two protons with a peak further upfield in the spectrum. A reference for the diketo-form could be found in the literature for the solvents C_6D_6 at 5.1 ppm (enol-form at 6.65 ppm) and for DMSO-d_6 at 4.75 ppm (enol-form at 7.23 ppm).⁶⁴

3.3.1.6.1. Determination of the Diketo-enol Ratio

UV-filter **BMDM** undergoes keto-enol tautomerism (Figure 3.1, page 70), as described earlier. To determine the diketo- and enol-ratio, ^1H NMR measurements were undertaken in methanol- d_4 , given that **BMDM** was dissolved in methanol during photostability studies. Two sets of proton signals from both forms occur, the *t*-butyl-group protons on $\text{C}_{21}\text{-C}_{23}$ (enol at 1.380 - 1.357 ppm and diketo at 1.355 - 1.350 ppm) and the aromatic ring protons on C_1/C_3 and C_4/C_6 (enol at 8.08 - 8.04 ppm and diketo at 7.965 - 7.925 ppm). The protons on C_{10} could not be considered for integration because of an interference with the methanol- d_4 signal at 3.31 ppm in the ^1H NMR spectrum. Additional 2D NMR measurements also confirmed that the aromatic protons on C_1/C_3 and C_4/C_6 in both forms were clearly resolved and were suitable for

integration. In both instances the integral of the enol signals were normalised to 100 % (Figure 3.5). Integration of each of the two resonances for each tautomeric form gave an average of 9.1 % for the diketo- and 90.9 % for the enol-form.

The percentage of the diketo-form in cyclohexane- d_{12} was reported to be 3.5 %³⁷ and is therefore lower than in the experimental results in methanol- d_4 . This difference is in accordance with another study where the diketo-enol ratios were calculated for different solvents, showing that with increasing solvent polarity the equilibrium increasingly shifted to the diketo-form.¹³⁶

During ^1H NMR analyses the disappearance of the proton signal from the methylene group on C_{10} (6.99 ppm) over time was observed. This phenomenon can be explained by the keto-enol tautomerism of **BMDM**. In the enol-tautomers the keto and enol groups form hydrogen bonds with methanol- d_4 , resulting in a slow exchange of the proton (^1H) in the molecule with the deuterium (D ; ^2H). As shown in Figure 3.1 (page 70) the diketo- and both enol-forms constantly interconvert, resulting in the complete exchange of the ^1H with the D at C_{10} . This is the main reason why most ^1H NMR investigations of **BMDM** are conducted in non-exchangeable deuterated solvents, however, as shown here, the signal resolution at 600 MHz is adequate for quantification.

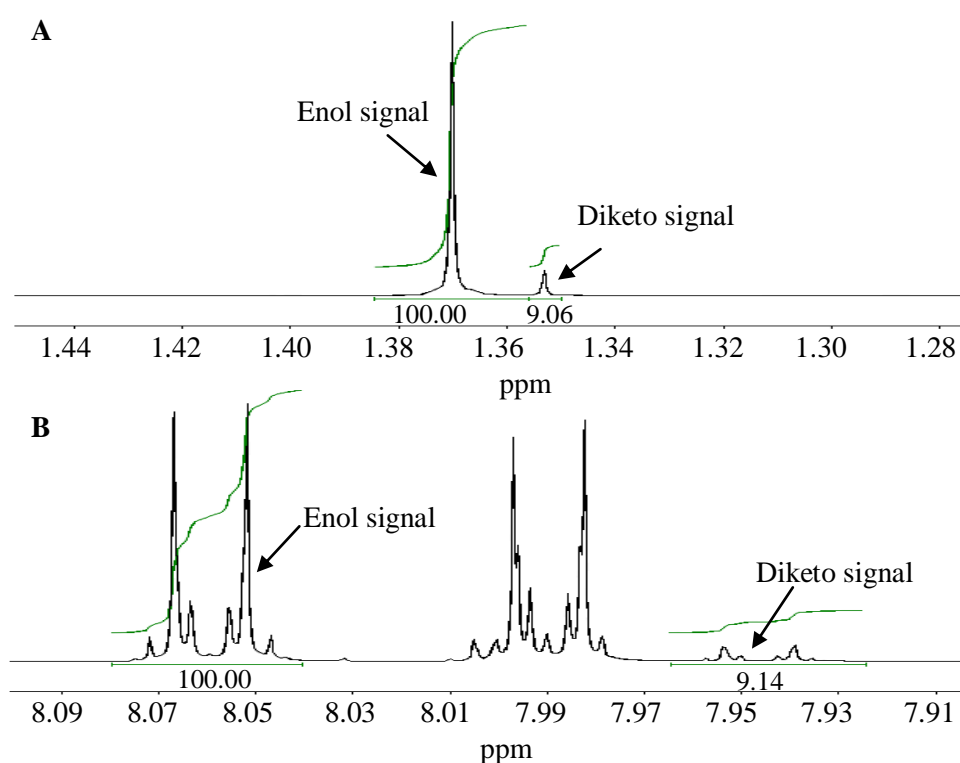


Figure 3.5. ^1H NMR spectrum sections of **BMDM** showing integration of proton signals of the enol- and diketo-form; **A**: proton signals of the *t*-butyl-group and **B**: proton signals of the aromatic ring protons on C_1/C_3 and C_4/C_6 .

3.3.1.7. Infrared (IR)-spectroscopy

The IR-spectrum of **BMDM** is shown in Figure 3.6. Significant peaks are assigned to chemical groups and are presented with their wavenumbers in Table 3.5. The absorption band of the carbonyl peak at 1584 cm^{-1} indicates the presence of the enol-form of **BMDM**, since the diketo-form would present an absorption band around 1700 cm^{-1} . Unfortunately, no literature could be found as reference for the IR-spectrum.

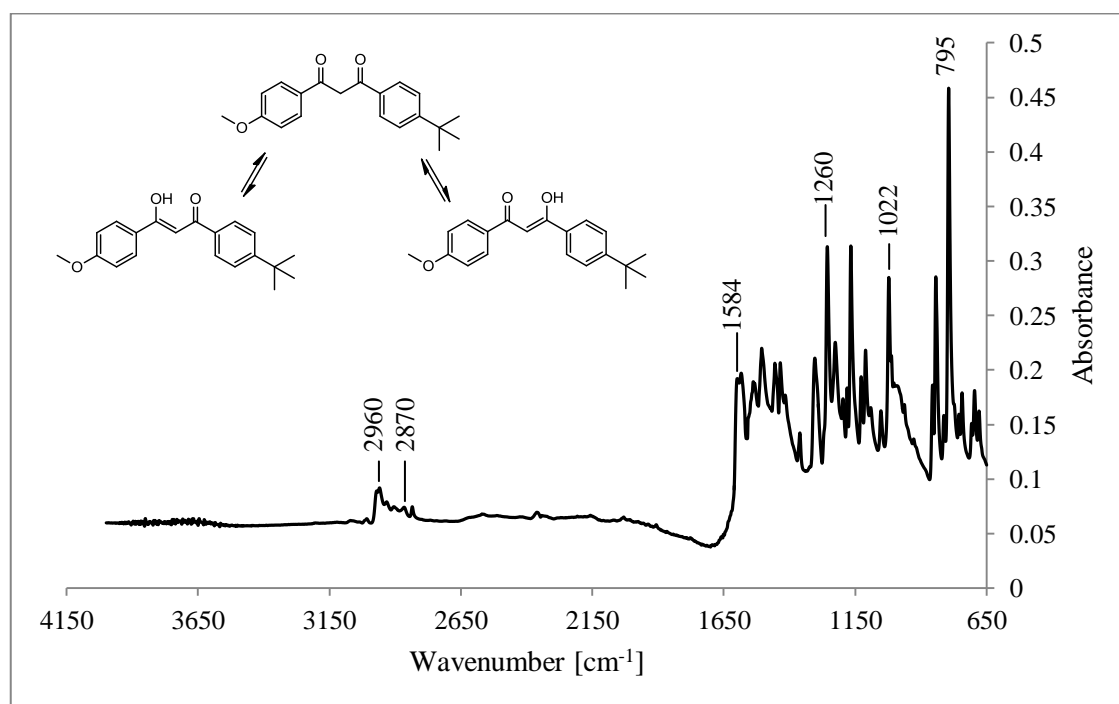


Figure 3.6. IR-spectrum of **BMDM**.

Table 3.5. Infrared absorption bands of **BMDM**.

Chemical group	Wavenumber [cm^{-1}]	
	Experimental	Literature
$\text{C}_{\text{arom}}\text{-H}$	795	-
C-O-C	1022, 1260	-
C=O	1584	-
CH_3	2870, 2960	-

3.3.2. Octocrylene (OC) [6197-30-4]

UV-filter **OC**, which occurs as a thick oily liquid, is a widely used UVB-filter (Figure 3.7).^{18,39} It is a yellow liquid with the empirical formula $C_{24}H_{27}NO_2$ and a molecular weight of 361.5 g/mol.¹³⁷

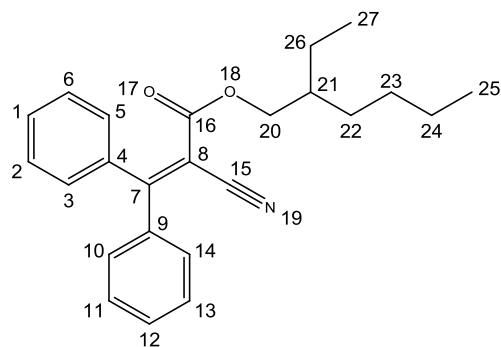


Figure 3.7. Chemical structure of **OC**.

3.3.2.1. Solubility

The solubilities of **OC** in different solvents and formulation excipients are listed in Table 3.6.

Table 3.6. Solubilities of **OC**.

Solvent	Solubility [mg/mL]	
	Experimental	Literature
Water	Not soluble	0.0013 ¹³⁷
Methanol	Miscible	-
Mygliol [®] 812	Miscible	-
Phosphate buffer (pH:7.4) + 4 % BSA	93.22	-

3.3.2.2. Ultraviolet (UV)-spectroscopy

OC showed an absorption maximum at 302.9 nm with an absorbance of 0.710 in methanol (Figure 3.8). In the literature the absorption maximum is reported at 304 nm in ethanol.³⁵

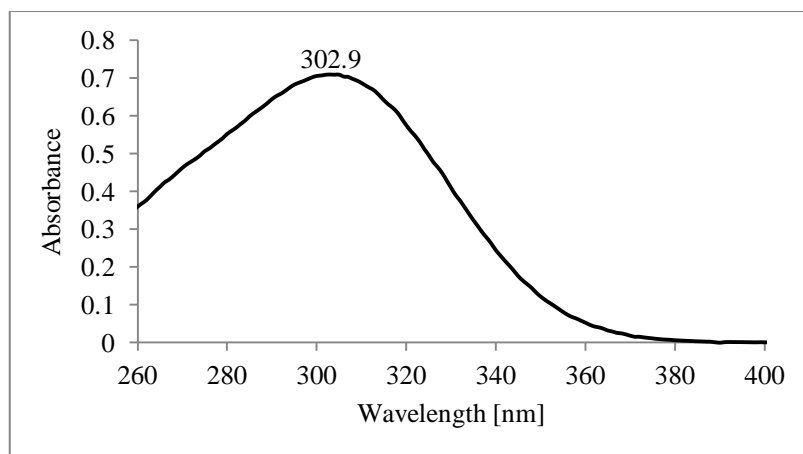


Figure 3.8. UV-absorption spectrum of **OC**.

3.3.2.3. High Performance Liquid Chromatography (HPLC)

The HPLC-chromatogram of **OC** (0.05 mg/mL) with wavelength detection at 303 nm is shown in Figure 3.9.

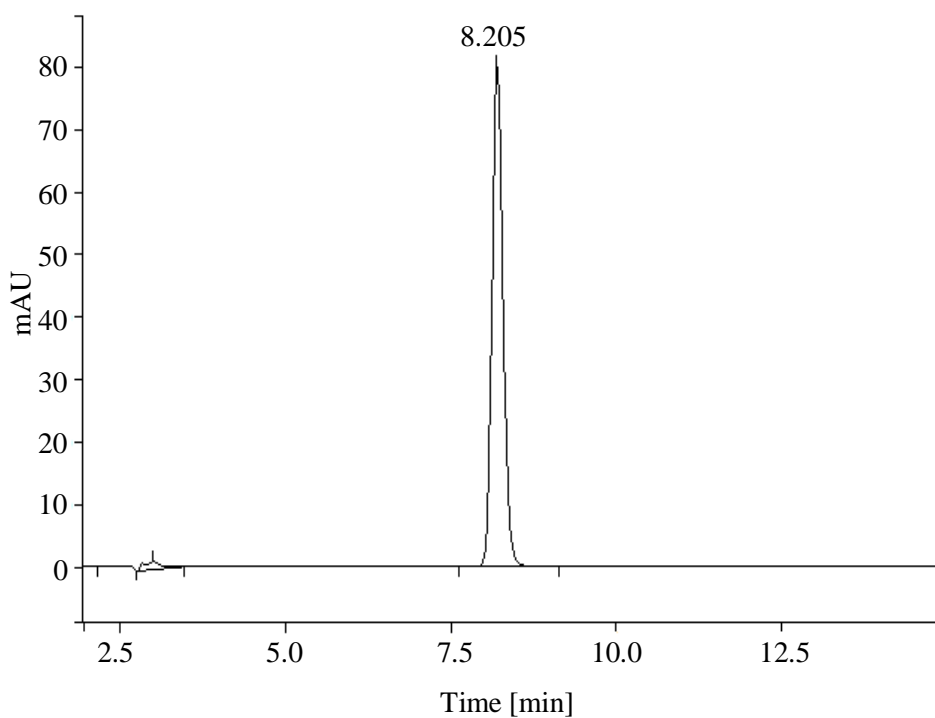


Figure 3.9. HPLC-chromatogram of **OC**.

3.3.2.4. Nuclear Magnetic Resonance (NMR)-spectroscopy

In Table 3.7 the ^1H NMR-data of **OC** are listed with the position of the proton-binding atoms shown in Figure 3.7 (page 77). No reference data were found in the literature.

Table 3.7. ¹H spectral assignment and chemical shifts of **OC**.

Position and type of proton-binding atoms	Chemical shift [ppm]		Multiplicity	Coupling constant J [Hz]
	Experimental (CDCl ₃)	Literature		
CH ₃ (25 or 27)	0.84	-	t	7.5
CH ₃ (25 or 27)	0.90	-	t	7.2
4 x CH ₂ (22-24, 26)	1.19 - 1.3	-	br m	-
CH (21)	1.47	-	sep	6
OCH ₂ (20)	4.01	-	dd	5.9, 11
OCH ₂ (20)	4.05	-	dd	5.6, 10.9
4 x H _{arom} ((2,6 or 11,13) and (3,5 or 10,14))	7.16	-	m	-
5 x H _{arom} (1,12 and (2,6 or 11,13) and (3,5 or 10,14))	7.36 - 7.49	-	br m	-

t = triplet	sep = septet	m = multiplet
br m = broad multiplet	dd = doublet of doublet	H _{arom} = aromatic proton

The aromatic protons could not be assigned to particular shifts, even a COSY NMR and a gradient selective TCOSY did not provide any detailed information.

3.3.2.5. Infrared (IR)-spectroscopy

In Figure 3.10 the IR-spectrum of **OC** is shown with some characteristic peaks illustrated out and labelled. The exact wavenumber at the absorption maximum of these peaks are listed in Table 3.8. Unfortunately no reference IR-spectrum could be found for **OC**.

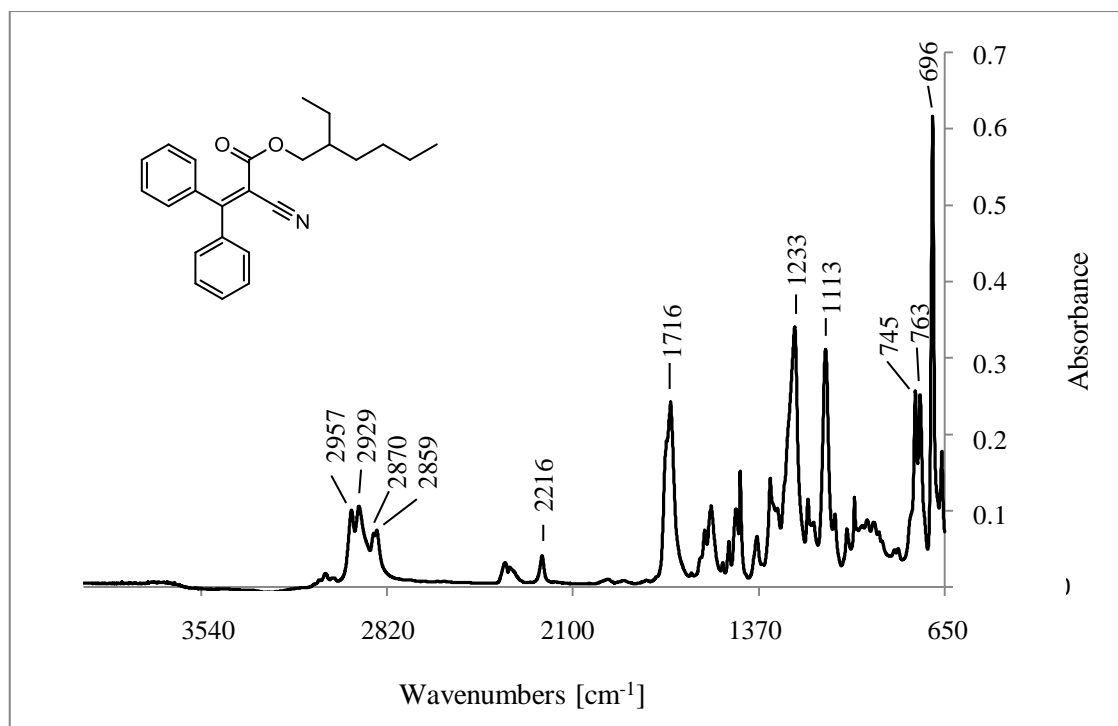


Figure 3.10. IR-spectrum of **OC**.

Table 3.8. Infrared absorption bands of **OC**.

Chemical group	Wavenumber [cm ⁻¹]	
	Experimental (pure)	Literature
C=C (arom)	696	-
C _{arom} -H	745, 763, 1113	-
C-O-C _{carbonyl}	1233	-
C=O	1716	-
C≡N	2216	-
-CH ₂	2859, 2929	-
-CH ₃	2870, 2957	-

3.3.3. Benzophenone-3 (B3) [131-57-7]

The widely used UV-filter **B3**, also known as Oxybenzone, is regarded as broad spectrum filter (Figure 3.11), even though it only absorbs UV-light in the UVB- and UVA II-range.^{18,39} It is a pale yellow powder with the empirical formula C₁₄H₁₂O₃ and a molecular weight of 228.3 g/mol.¹³⁸

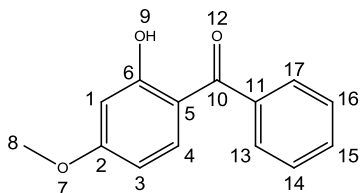


Figure 3.11. Chemical structure of **B3**.

3.3.3.1. Solubility

The solubilities of **B3** in different solvents and formulation excipients are listed in Table 3.9.

Table 3.9. Solubilities of **B3**.

Solvent	Solubility [mg/mL]	
	Experimental	Literature
Water	Not soluble	0.0037 ¹³⁸
Methanol	67.61	-
Mygliol® 812	172.92	-
Phosphate buffer (pH:7.4) + 4 % BSA	358.00	-

3.3.3.2. Ultraviolet (UV)-spectroscopy

B3 showed two absorption maxima, one at 324.0 nm with A = 0.435 and the other one at 287.0 nm with A = 0.668, measured in methanol (Figure 3.12). These values are confirmed by literature reports.³⁴

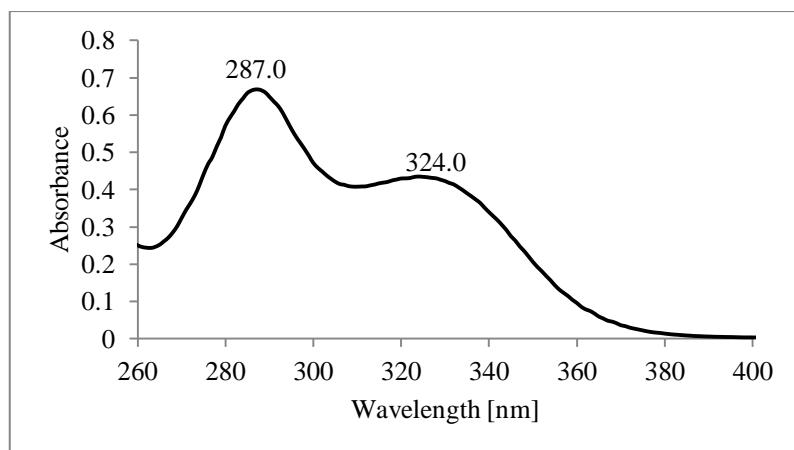


Figure 3.12. UV-absorption spectrum of **B3**.

3.3.3.3. High Performance Liquid Chromatography (HPLC)

The HPLC chromatogram of **B3** (0.03 mg/mL) is shown in Figure 3.13 at 324 nm.

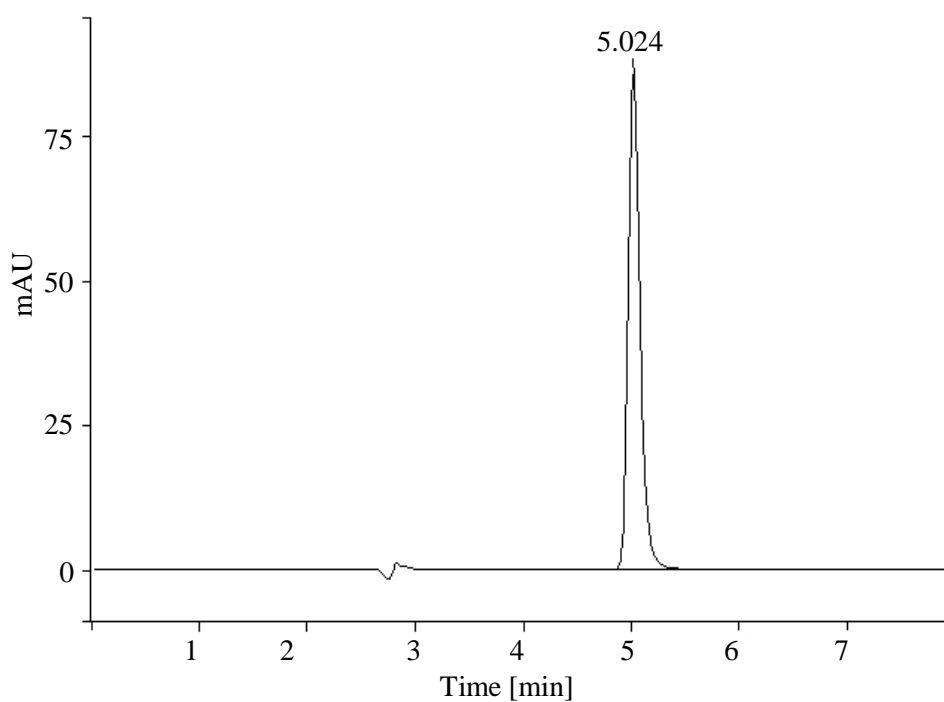


Figure 3.13. HPLC-chromatogram of **B3**.

3.3.3.4. Melting Point Measurement

The melting range of **B3** was found to be between 63.0 and 63.9 °C. The literature reported a range of 63 - 65 °C, which is in accordance with the melting range measured.¹³⁹

3.3.3.5. Differential Scanning Calorimetry (DSC)

In the DSC, **B3** shows a melting range from 62.92 °C to 67.32 °C and a peak at 64.42 °C with a value of -30.83 mW (Figure 3.14). The change of enthalpy during the melting process was $\Delta H = 94.4 \text{ J/g}$.

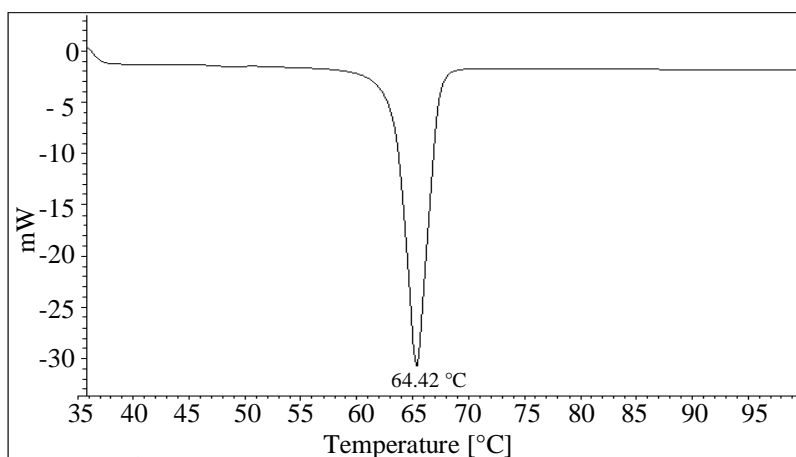


Figure 3.14. DSC-thermogram of **B3**.

3.3.3.6. Nuclear Magnetic Resonance (NMR)-spectroscopy

The results of the ^1H NMR spectroscopy determinations for **B3** are listed in Table 3.10 with the data for the literature measured in deuterated chloroform and acetone. The assignments of the positions of the protons are according to Figure 3.11 on page 81.

Table 3.10. ^1H spectral assignment and chemical shifts of **B3**.

Position and type of proton- binding atoms	Chemical shift [ppm]			Multiplicity	Coupling constant J [Hz]
	Experimental (CDCl_3)	Literature ¹⁴⁰ (CDCl_3)	Literature ¹⁴¹ (acetone- d_6)		
OCH_3 (8)	3.86	3.86	3.91	s	-
H_{arom} (3)	6.41	6.41	6.52	dd	8.9, 2.5
H_{arom} (1)	6.52	6.53	6.55	d	2.5
2 x H_{arom} (14,16 or 13,17)	7.49	-	-	m	-
H_{arom} (4)	7.50	-	7.46	d	8.9
H_{arom} (15)	7.56	-	-	m	
2 x H_{arom} (14,16 or 13,17)	7.63	7.64	-	m	
OH (9)	12.69	-	12.67	s	-

s = singlet

d = doublet

 H_{arom} = aromatic proton

dd = doublet of doublet

m = multiplet

3.3.3.7. Infrared (IR)-spectroscopy

Figure 3.15 illustrates the IR-spectrum of **B3**, while Table 3.11 lists the wavenumbers of the characteristic absorption peaks. Only the wavenumbers of the carbonyl-group and an approximate value of the hydroxyl-group were reported in the literature.¹⁴²

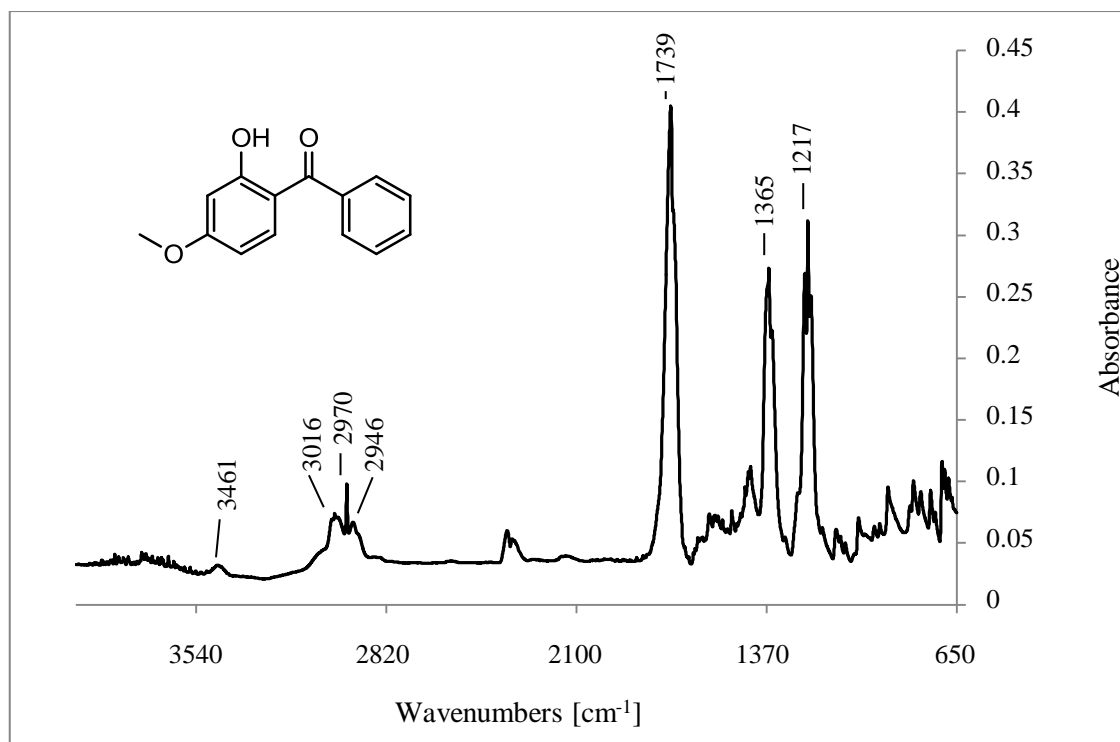


Figure 3.15. IR-spectrum of **B3**.

Table 3.11. Infrared absorption bands of **B3**.

Chemical group	Wavenumber [cm ⁻¹]	
	Experimental (pure)	Literature (KBr-disc) ¹⁴²
C-O-C	1217	-
C=O	1365, 1739	1720
-CH ₃	2946, 2970	-
C _{arom} -H	3016	-
-OH	3461	about 3300

3.4. Summary

Characterisations of the chemical UV-filters **BMDM**, **OC** and **B3**, using a combination of several analytical techniques confirmed their identity and purity.

The solubility determinations of the UV-filters in certain solvents and formulation excipients facilitated the appropriate choice of solvents for the use in both the photostability and formulation studies. The determination of the absorption maxima, which were in accordance with reference data reported in the literature, informed the detection wavelength to be used in the HPLC analysis. The purity of the UV-filters was confirmed by HPLC. With the use of the PDA detection the purity was not only determined at one wavelength, the whole UV-range (200 - 400 nm) was monitored. While two of the three UV-filters were proved to be pure, several small impurities were detected for **BMDM**. Though not all impurities could be entirely removed by recrystallisation, an enhancement of the purity was achieved, apparent not only in the HPLC-chromatogram, but by narrowing of the melting point range. The melting range determination and DSC were employed as additional methods to analyse the purity of the UV-filters and consistent results were achieved for the melting point. ¹H NMR-spectroscopy was undertaken to confirm the molecular structures of the UV-filters. Each functional group showed a characteristic peak in the NMR-spectra, which were compared to literature data for the UV-filters, insofar as they were available. IR-spectroscopy was only used as additional method for identification, confirming the presence of characteristic functional groups of the UV-filters.

The identity and purity of **BMDM**, **OC**, and **B3** were satisfactory proven by the combination of methods employed and by comparison with reference data, where available. Some of the results, especially the solubility and UV-absorbance maxima, will be utilised in the following chapter which is to develop and validate an HPLC method for the simultaneous determination of **BMDM** and **OC** in the presence of their photodegradants.

Chapter 4

High Performance Liquid Chromatography (HPLC)

- Method Development and Validation

4.1. Introduction

Sunscreen products usually contain a combination of UV-filters in order to achieve broad spectrum protection. Because of their ability to absorb light, there is potential for degradation, resulting in the formation of photodegradants. The more UV-filters are included in a sunscreen product the more photodegradants are likely to be formed, presenting as multi-component samples. The separation and quantification of these components in the samples requires an analytical method that is both selective and specific. This can be achieved using an HPLC method.¹²⁵

Guidelines for the validation of analytical procedures were published by the ICH.¹⁴³ In these guidelines, the determination of linearity, accuracy, precision, specificity, sensitivity and robustness are recommended. Although these guidelines are general and not specific to HPLC methods, they provide useful information about ranges and limits for the described procedures.¹⁴³

In this study, HPLC methods are required to analyse the UV-filters: Butyl methoxy dibenzoylmethane (**BMDM**), Octocrylene (**OC**) and Benzophenone-3 (**B3**). One method was developed to analyse both **BMDM** and **OC** in the presence of their photodegradants, which was then also used to analyse UV-filter **B3**. Reverse-phase chromatography, using a C18 column was employed.

The concentration of UV-filters **BMDM** and **OC** are required to be determined during photostability studies alone and in combination, necessitating the method to be valid for both UV-filters in the presence of their photodegradants. Validation in terms of robustness and specificity was undertaken, after irradiation in a photoreactor using a pyrex glass filter ($\lambda \geq 300$ nm).

Several researchers have studied the behaviour of **B3** in the presence of light and demonstrated its photostability.^{42-44,61,144} The UVA-PF⁴⁴ and SPF⁴³ did not change significantly after an irradiation time of two hours in a solar simulator. UV-filter **B3** was reported to be stable after irradiation in cyclohexane with a mercury vapour immersion lamp (185 - 4000 nm)⁶¹ and in petroleum jelly after irradiation with a UVA and UVB lamp (290 - 400 nm).⁴² Even after irradiation of 24 hours with simulated sunlight, the concentration of **B3** remained unchanged.¹⁴⁴

As result of these literature findings, this UV-filter was not included in this study to investigate its photostability. However, because of its reported skin penetration and ability to cause photoallergic reactions,^{101,118} it was included in the skin penetration studies. Therefore, the method was not validated for specificity and robustness, by irradiating **B3** with UV-light.

Several HPLC methods for the analysis of the UV-filters **BMDM**, **OC** and **B3** are available in the literature.^{46,62-64,105,134,145-154} The analysed UV-filters, type of column and mobile phase composition of these methods are listed in Table 4.1. To analyse the UV-filters **BMDM**, **OC** and **B3** alone, in combination with each other or with other UV-filters, a C18 column was the column of choice in the reviewed literature (Table 4.1). In most cases the mobile phase contained a mixture of methanol and water, with or without other solvents, such as acetonitrile^{62,147,151} or THF.^{147,151} Some mobile phases were acidified with acetic acid,^{145,147,150,154} formic acid⁶² or phosphoric acid.⁶³ Although some HPLC methods from Table 4.1 were developed for the determination of all three UV-filters simultaneously,^{46,148,149,154} a new method was developed and validated in this chapter. The reason behind this was to increase the HPLC run time to achieve an adequate separation of photodegradants from each other and the parent UV-filters for further LC-MS analysis.

Mobile phase ingredients were also chosen in order that the method could be applied to the identification of photodegradants by LC-MS in Chapter 5.

This HPLC method represents the first method developed for the simultaneous determination of **BMDM** and **OC** in the presence of their photodegradants, which is rapid and simple and can be applied to LC-MS studies.

Table 4.1. Relevant HPLC method components for UV-filters.

UV-filters	Column	Mobile Phase [% v/v]	Reference
BMDM	C18	Methanol/water (85/15)	64
BMDM	C18	Methanol/water (92/8)	134
BMDM, OC, B3 , Ethylhexyl methoxycinnamate (EMC), Ethylhexyl salicylate (ES), 4-Methylbenzylidene camphor (MBC)	C18	Methanol/water (88/12)	46
BMDM, EMC	C18	Methanol/water/acetic acid (83/17/0.01)	145
BMDM, B3, EMC	C18	Methanol/1 % acetic acid (82/18)	150
BMDM	C18	Methanol/acetonitrile/water/THF (60/15/15/10)	151
BMDM, OC, B3, MBC , Ethylhexyl dimethyl PABA (EDP), EMC, ES	C18	Ethanol/1 % acetic acid (gradient)	154
BMDM , 4-Isopropylidibenzoylmethane (IDM) + degradation products	C18	Acetonitrile/water; both with 0.01 % formic acid (gradient)	62
BMDM, B3, BMT, EMC	C18	Acetonitrile/THF/0.1 % acetic acid (gradient)	147
BMDM, OC, MBC, EMC , Ethylhexyl triazone (ET), BMT, Methylene bis-benzotriazolyl tetramethylbutylphenol (MBBT)	C18	Methanol/0.1 % phosphoric acid (gradient)	63
OC, EMC, ES, MBBT	C18	Methanol/acetonitrile (90/10)	153
BMDM, B3, EMC, ES, MBC, EDP , Phenylbenzimidazole sulphonic acid (PSA), MBBT	CN	Methanol/acetonitrile/THF/0.5 % acetic acid (55/15/10/20)	152
BMDM, OC, B3, MBC, EDP, EMC, ES , Homosalate (HO), BMT, MBBT	C18	Ethanol/1 % acetic acid (gradient)	148
BMDM, OC, B3, PSA , Isoamyl methoxycinnamate (IMC), DHHB, EMC, ES, ET, Diethylhexyl butamido triazone (DBT), BMT, MBBT	C18	Ethanol/1 % phosphoric acid (gradient)	149

4.2. Materials and Instrumentation

4.2.1. Solvents and Reagents

The UV-filters Butyl methoxy dibenzoylmethane (Eusolex[®] 9020) and Octocrylene (Eusolex[®] OCR) were purchased from Merck (Darmstadt, Germany). Benzophenone-3 (2-Hydroxy-4-methoxybenzophenone, 98%), acetophenone, toluene, methylbenzoate and naphthalene were obtained from Sigma-Aldrich (St. Louis, USA). Glacial acetic acid was acquired from RCI Labscan (Bangkok, Thailand) and methanol (HPLC-Grade) from Thermo Fisher Scientific (Waltham, USA). Reverse osmosis water was prepared with a Millipore[®] Elix 10 from Millipore SAS (Molsheim, France).

4.2.2. Instrumentation

The Varian ProStar[®] HPLC system (Varian Inc., Melbourne, Australia), consisting of a 240 quaternary solvent delivery module, 410 autosampler and a 330 PDA detector was used for analysis. The Software is equipped with the PolyView 2000[™] spectral Processing Application (Varian Inc., Melbourne, Australia).

The immersion well photoreactor (400 mL) used was supplied by Heraeus Noblelight GmbH (model UV-RS-1), Hanau, Germany, equipped with a UV immersion lamp TQ 150 (medium pressure mercury lamp, 150 W). A pyrex glass vessel ($\lambda \geq 300$ nm) was used during method validation, which served as cooling jacket to maintain the temperature of the reaction mixture at 20 - 25 °C.

A Varian Cary[®] 50 UV-spectrometer (Varian Inc., Melbourne, Australia) was used for filter validation.

4.3. HPLC Method Development

4.3.1. Choice of Analytical Column

In most studies, determination of the concentrations of the UV-filters **BMDM**, **OC** and **B3** alone, in combination with each other or with other UV-filters involved the use of C18 columns (Table 4.1). A SunFire[™] C18 column (4.6 × 250 mm, 5 μm) from Waters Corp., Milford, USA was thus chosen for this study.

Column efficiency was assessed by calculating the theoretical plate numbers (N) for the substances of a test mixture. This test mixture contained acetophenone (20 μg/mL), toluene (300 μg/mL), methylbenzoate (200 μg/mL) and naphthalene (40 μg/mL), dissolved in

acetonitrile/water (60/40), which was also used as mobile phase. With a flow rate of 1 mL/min and an injection volume of 10 μ L this mixture was injected in triplicate onto the column at an ambient temperature (25 ± 1 °C). The detection wavelength was set at 254 nm. The theoretical plate numbers (N) provide information about the column performance and were calculated as follows:¹⁵⁵

$$N = 5.54 (t_r/W_{0.5})^2 \quad (4.1)$$

with: t_r = retention time

$W_{0.5}$ = peak width at half height

A suitable value for N can be calculated as follows:¹⁵⁵

$$N \sim 3000 L/dp \quad (4.2)$$

with: L = column length [cm]

dp = particle diameter [μ m]

An acceptable plate number, N, would be at least 15 000 for the SunFire™ C18, which was achieved with N between 14 470 and 20 850.

4.3.2. Choice of Mobile Phase

Table 4.1 shows the various mobile phase compositions from the literature for the analysed UV-filters **BMDM**, **OC** and **B3** alone, in combination with each other or with other UV-filters. The common HPLC solvent methanol was found in most mobile phases, together with acetonitrile,¹⁵¹⁻¹⁵³ water^{46,145,150,151} and/or THF.^{147,151,152} In some studies an acid was added to the mobile phase, such as acetic acid,^{147,150,152} formic acid⁶² or phosphoric acid.^{63,149} The objective was to develop an HPLC method for the determination of a combination of **BMDM** and **OC** in the presence of their photodegradants, which is also appropriate to analyse UV-filter **B3** alone.

As first step to the method development, a mobile phase of 100 % methanol was evaluated for the UV-filters **BMDM** and **OC**, resulting in **OC** being eluted after 4.25 minutes, while **BMDM** eluted after 5.36 minutes. As described in Chapter 3, UV-filter **BMDM** contains a small amount of impurities and one of these impurities eluted after 4.26 minutes, which resulted in inadequate separation from **OC**. A combination of both UV-filters, using a mobile phase of methanol with 5 % water, did not result in a satisfactory resolution of UV-filter **OC** (5.65 minutes) from the impurity at 5.23 minutes (Figure 4.1A), with a resolution factor of only 0.2. In order to separate this impurity from the **OC** peak, the water content of the mobile phase was further increased to 10 % (Figure 4.1B). With this altered mobile phase, the retention time of

the impurity was 7.41 minutes and of UV-filter **OC** 8.64 minutes, resulting in a resolution factor of 4.6 for **OC**. In order to sharpen the **BMDM** peak and reduce tailing, acetic acid was added to the mobile phase in a concentration of 0.01 and 1 %, as shown in Figure 4.2B and Figure 4.2C, respectively. When 1 % acetic acid was added to the complete mobile phase, **BMDM** showed the lowest peak width $\frac{1}{2}$ (10.4) and the tailing factor was acceptable (1.22). The final mobile phase was therefore chosen to be methanol/water/acetic acid with the ratio of 89/10/1 % v/v. A sample containing both UV-filters after irradiation and analysed with the chosen mobile phase showed that both UV-filters were adequately separated from all degradation products, with a resolution factor of 3.5 for **OC** and 8.8 for **BMDM**. Figure 4.3 shows the chromatogram at 358 nm, the detection wavelength of **BMDM**, and at 303 nm, the detection wavelength of **OC**.

An acceptable retention time and peak shape was also achieved for UV-filter **B3** using the same mobile phase and chromatographic conditions (Figure 4.4).

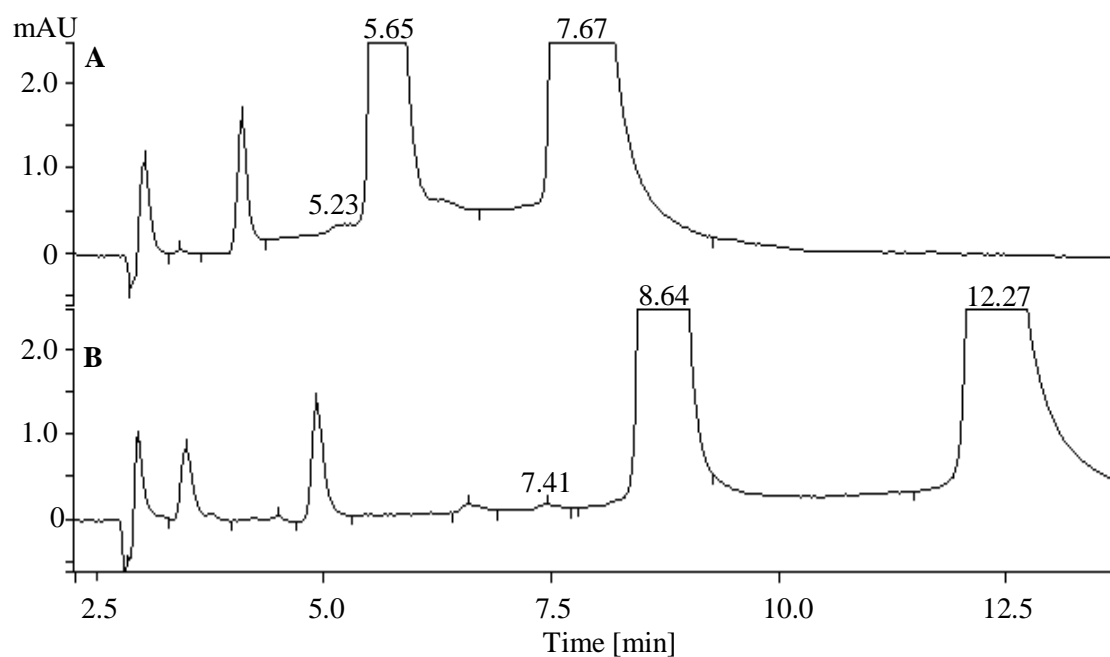


Figure 4.1. HPLC chromatogram of **BMDM** and **OC** in combination, using the mobile phase **A** methanol/water (95/5 % v/v): **OC** at 5.65 min, **BMDM** at 7.67 min and **B** methanol/water (90/10 % v/v): **OC** at 8.64 min, **BMDM** at 12.27 min.

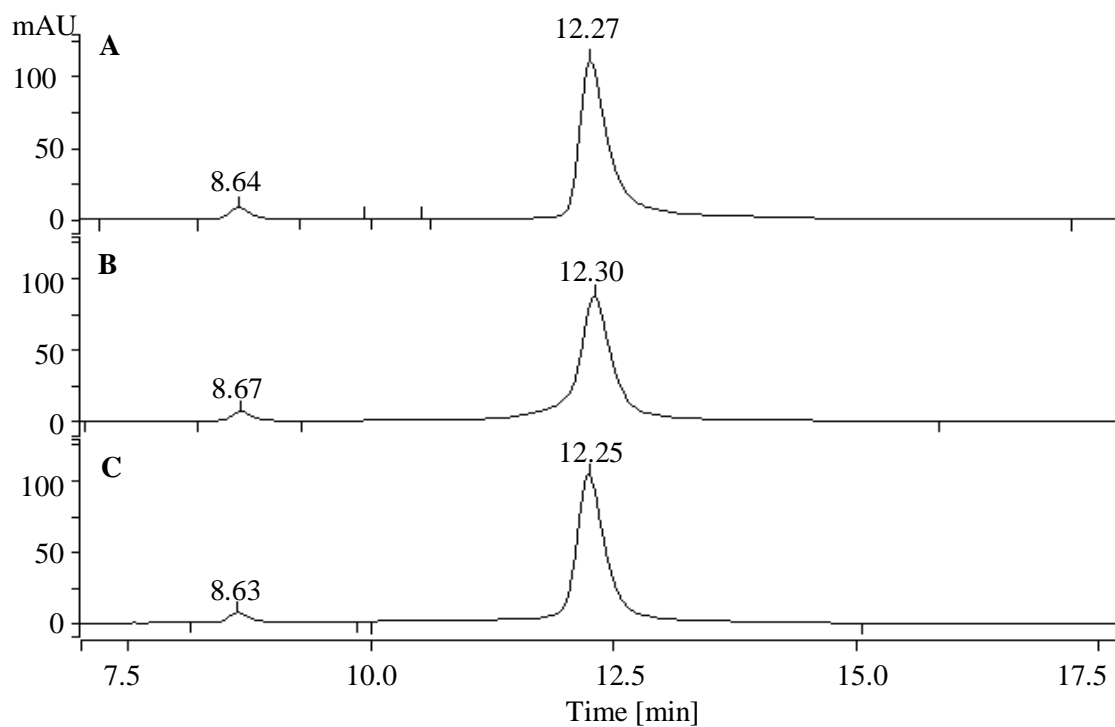


Figure 4.2. HPLC chromatogram of **BMDM** and **OC** in combination, detected at 358 nm; **A** mobile phase: methanol/water (90/10 % v/v): **BMDM** elution at 12.27 min, tailing factor: 1.99 and peak width $\frac{1}{2}$: 17.9 sec; **B** mobile phase: methanol/water/acetic acid (90/9.99/0.01 % v/v): **BMDM** elution at 12.30 min, tailing factor: 0.93 and peak width $\frac{1}{2}$: 19.8 sec; **C** mobile phase: methanol/water/acetic acid (89/10/1 % v/v): **BMDM** elution at 12.25 min, tailing factor: 1.22 and peak width $\frac{1}{2}$: 10.4 sec.

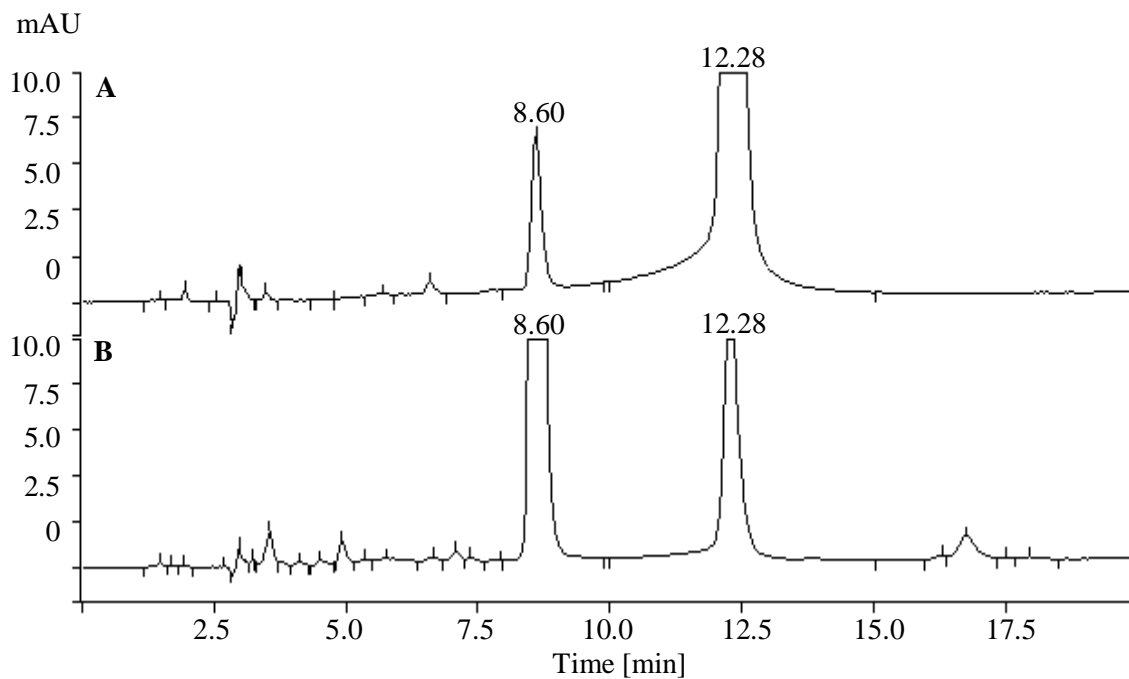


Figure 4.3. HPLC chromatogram of the UV-filters **BMDM** and **OC** in the presence of photodegradants, detected at **A** 358 nm and **B** 303 nm.

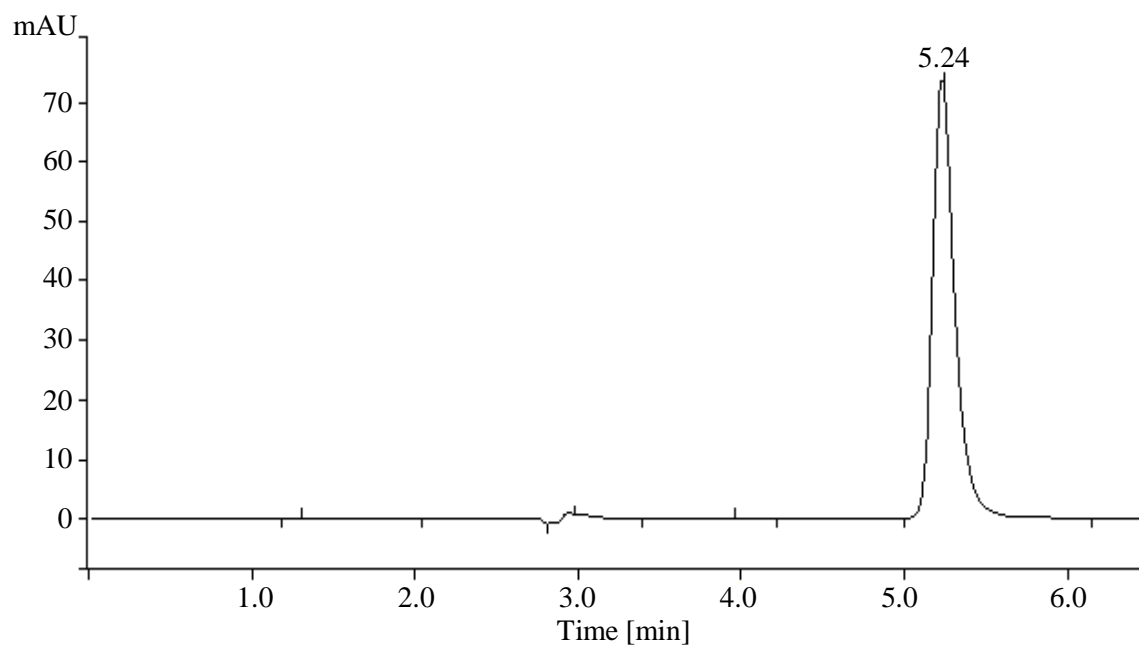


Figure 4.4. HPLC chromatogram of UV-filter **B3** (retention time: 5.24), using the mobile phase: methanol/water/acetic acid (89/10/1), detected at 324 nm.

4.3.3. Chromatographic Conditions

- Column: SunFire™ C18 (4.6 × 250 mm, 5 µm) from Waters Corp., Milford, USA
- Mobile Phase: Methanol/water/acetic acid (89/10/1 % v/v) (pH = 3.4)
aqueous phase: pH = 2.2
- UV-filter solvent: Methanol
- Flow-rate: 1 mL/minute
- Injection volume: 10 µL
- Column temperature: 30 °C ± 1 °C
- Detector settings: 303 nm (λ_{max} of UV-filter **OC**)
324 nm (λ_{max} of UV-filter **B3**)
358 nm (λ_{max} of UV-filter **BMDM**)
- Retention times: UV-filter **B3**: ~ 5.2 minutes
UV-filter **OC**: ~ 8.6 minutes
UV-filter **BMDM**: ~ 12.2 minutes

4.4. HPLC Method Validation

The HPLC method validation was undertaken according to the ICH Guideline Q2(R1),¹⁴³ requiring the determination of linearity, accuracy, precision, specificity, sensitivity and robustness. In addition to the ICH recommendation, a filter evaluation was undertaken, because all samples were filtered before injected onto the HPLC.

4.4.1. Filter Evaluation

Before a sample can be injected onto an HPLC-system any undissolved or insoluble particles should be removed by filtration.¹⁵⁶ A filter evaluation was undertaken to determine whether any of the UV-filters adsorb to the filter, potentially altering their concentration in the filtered solution. The UV-absorption spectrum of an unfiltered sample was compared to that of a filtered sample. The filtered sample was further divided into two batches: the first batch contained the first 5 mL of filtrate and the second batch contained the second 5 mL of filtrate (Figure 4.5), to determine if adsorption could be avoided by discarding the first millilitres of the filtrate.

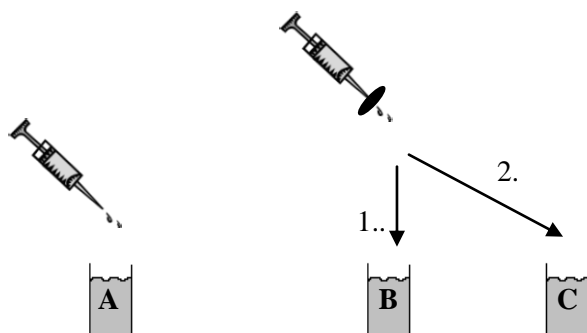


Figure 4.5. Three samples analysed **A** unfiltered sample, **B** first 5 mL of filtrate and **C** second 5 mL of filtrate.

Two concentrations for each UV-filter were prepared and filtered through a 15 mm syringe filter with a 0.45 μm PTFE membrane (Phenomenex Inc. Sydney, Australia). For each sample the UV-spectrum was recorded and the absorbance at the absorption maximum of the unfiltered sample was compared to the absorbance of the two filtered batches. A difference of less than 5 % is regarded as acceptable.¹⁵⁷

4.4.2. Linearity

The linearity of the UV-filters was determined by the construction of a calibration curve. The UV-filters **BMDM** and **OC** were analysed in the concentration range of 20.0 - 100.0 $\mu\text{g/mL}$ and **B3** in the range of 10.0 - 50.0 $\mu\text{g/mL}$. The mean of three peak area measurements was plotted against the known concentration. The linear regression line, the regression equation and the correlation coefficient (R^2) were calculated with Microsoft Office Excel 2007.

4.4.3. Accuracy and Precision

For precision and accuracy three concentrations, each with three replicates, were analysed. The lowest, the middle and the highest concentration from the calibration curve were chosen. Accuracy describes the closeness of the measured compound concentration to the known added amount of compound. The percent recovery ($n = 3$) was calculated using the regression equation. The precision expresses the repeatability of the method and is reported by the standard deviation (SD), relative standard deviation (RSD %) and the 95 % CI.¹⁴³

4.4.4. Specificity

To demonstrate specificity of a method for a particular compound, it is required that the peak response is due to only one compound and does not contain any co-eluting compounds.¹⁵⁸ For the developed HPLC methods, the purity of a peak was analysed using a PDA detector and

PolyView 2000™ Version 6.41. Several points of an HPLC peak can be selected with the PolyView program, to provide the corresponding UV-spectrum. After normalisation, these UV-spectra should show an exact overlay, in order for the method to be specific for that particular compound.

4.4.5. Sensitivity

The limit of detection (LOD) and limit of quantitation (LOQ) were measured to demonstrate sensitivity of the HPLC method. While the LOD is the lowest amount of compound which can be detected, the LOQ is the lowest amount which can be quantitated. Therefore the RSD % is given for the LOQ values. Both limits were carried out by using the signal-to-noise (S/N) approach. The baseline noise was measured of a blank sample in the area, where the compound peak would be present and compared to the peak height of the compound of known concentration (n = 10). As a blank sample, only the UV-filter solvent was injected. The time frame of the baseline noise measurement should be at least five times the width at half-height of the substance peak.¹⁵⁹ The S/N ratio should be between two and three for the LOD and about 10 for the LOQ.¹⁴³ This ratio was calculated with the following equation:¹⁵⁹

$$S/N = 2H/h \quad (4.3)$$

with: H = height of substance peak
h = baseline noise of blank sample

4.4.6. Robustness

To validate the HPLC method for robustness experimental conditions, such as flow rate, column temperature, pH and organic-aqueous ratio, were altered. Samples were also injected 24 hours after their first injection to determine the stability of the sample solution in the HPLC autosampler. The effect on peak resolution for the UV-filters was determined using the Star Chromatography Workstation Version 6.41. The resolution factor (Rs), which should be > 2.0 to confirm robustness, was calculated by the following equation:¹⁵⁵

$$R_s = \frac{tR1 - tR2}{0.5(W_{0.5(1)} + W_{0.5(2)})^{1.7}} \quad (4.4)$$

with: $tR1$ = retention time of peak 1
 $tR2$ = retention time of peak 2
 $W0.5(1)$ = peak width at half height of peak 1
 $W0.5(2)$ = peak width at half height of peak 2

The flow rate (1 mL/min) was changed by ± 0.2 mL/min, the temperature (30 °C) was increased by 5 °C and the pH of the aqueous phase was increased from 2.2 to 5.4. The organic-aqueous ratio was altered by increasing the organic phase by 3 %, without changing the pH of the aqueous phase. The UV-filters **BMDM** and **OC** were irradiated for five hours in combination to determine the extent of their photodegradation, in order to validate the method for the determination of these two UV-filters in the presence of their photodegradants.

4.5. Results and Discussion

4.5.1. Butyl methoxy dibenzoylmethane (BMDM) and Octocrylene (OC)

4.5.1.1. Filter Evaluation

The filter evaluation was carried out on two concentrations of the UV-filters **BMDM** (2.0 and 8.0 $\mu\text{g/mL}$) and **OC** (4.0 and 20.0 $\mu\text{g/mL}$) in methanol. For **BMDM**, λ_{max} was at 358 ± 2 nm and for **OC** at 303 ± 1 nm. The mean absorbance, SD and the RSD % for **BMDM** and **OC** are given in Tables 4.2 and 4.3, respectively, as well as the % difference between the filtered and the unfiltered samples.

Table 4.2. Filter Evaluation data for **BMDM**.

Concentration [$\mu\text{g/mL}$]	Mean absorbance [A] (n = 6)	SD [A]	RSD %	Difference compared to unfiltered sample [%]
No filtration				
2.0	0.241	± 0.000837	0.35	
8.0	0.948	± 0.001169	0.12	
First 5 mL				
2.0	0.238	± 0.000408	0.17	- 1.25
8.0	0.945	± 0.001633	0.17	- 0.32
Second 5 mL				
2.0	0.238	± 0.000516	0.22	- 1.25
8.0	0.947	± 0.001506	0.16	- 0.11

Table 4.3. Filter Evaluation data for **OC**.

Concentration [µg/mL]	Mean absorbance [A] (n = 6)	SD [A]	RSD %	Difference compared to unfiltered sample [%]
No filtration				
4.0	0.140	± 0.000894	0.64	
20.0	0.702	± 0.001329	0.19	
First 5 mL				
4.0	0.140	± 0.000408	0.29	0.00
20.0	0.701	± 0.001835	0.26	- 0.14
Second 5 mL				
4.0	0.141	± 0.000816	0.58	+ 0.71
20.0	0.701	± 0.002251	0.32	- 0.14

The difference in the absorbance between the filtered and the unfiltered samples of both UV-filters was less than 5 %. These results showed no significant adsorption for **BMDM** and **OC** onto the filter.

4.5.1.2. Linearity

Butyl methoxy dibenzoylmethane (BMDM)

A calibration curve was established for **BMDM** by plotting the mean peak area at 358 nm against the known concentration. Their values are shown in Table 4.4 and the calibration curve in Figure 4.6. The SDs for each point are presented as error bars in Figure 4.6, but are too small to be visualised. The equation of the linear regression line was calculated as $y = 45.634x$, with a correlation coefficient of $R^2 = 0.9997$. Table 4.4 also shows the 95 % CI, the SD and RSD %.

Table 4.4. Linearity data for **BMDM**.

Concentration [$\mu\text{g/mL}$]	Peak Area [mAU \cdot sec] (n = 3)	95 % CI [mAU \cdot sec]	SD [mAU \cdot sec]	RSD %
20.0	895	± 22.8	± 9.2	1.024
30.0	1342	± 0.0	± 0.0	0.000
40.0	1798	± 16.5	± 6.7	0.370
50.0	2262	± 20.2	± 8.1	0.360
60.0	2732	± 3.8	± 1.5	0.056
80.0	3670	± 15.0	± 6.0	0.164
100.0	4584	± 18.0	± 7.2	0.158

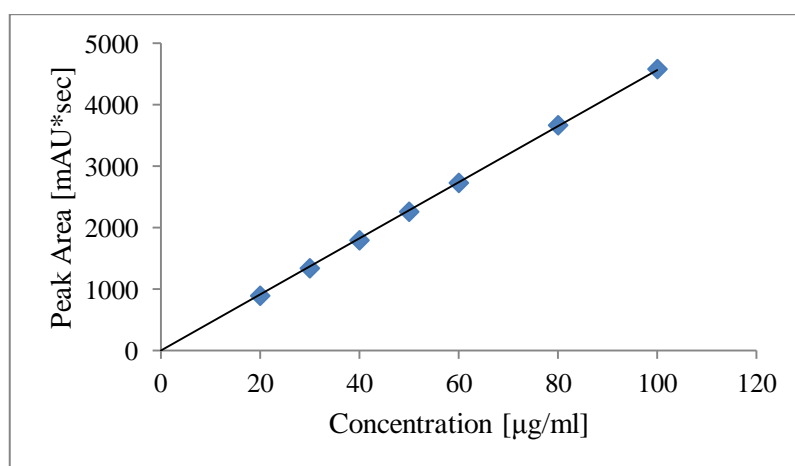


Figure 4.6. Calibration curve for **BMDM**.

Octocrylene (OC)

Linearity of **OC** was determined by constructing a calibration curve as described for UV-filter **BMDM**. The peak area values were measured at 303 nm and are shown in Table 4.5 together with the 95 % CI, SD and RSD % of UV-filter **OC**. Figure 4.7 shows the calibration curve, which has a linear regression equation of $y = 18.939x$ and a correlation coefficient of $R^2 = 1.0000$. The SDs of each data point are represented as error bars in Figure 4.7, but too small to be visualised.

Table 4.5. Linearity data for **OC**.

Concentration [$\mu\text{g/mL}$]	Peak Area [mAU \cdot sec] (n = 3)	95 % CI [mAU \cdot sec]	SD [mAU \cdot sec]	RSD %
20.0	379	± 1.4	± 0.58	0.15
30.0	566	± 1.4	± 0.58	0.10
40.0	755	± 2.5	± 1.00	0.13
50.0	947	± 3.8	± 1.53	0.16
60.0	1141	± 5.7	± 2.31	0.20
80.0	1516	± 5.2	± 2.08	0.14
100.0	1892	± 9.9	± 4.00	0.21

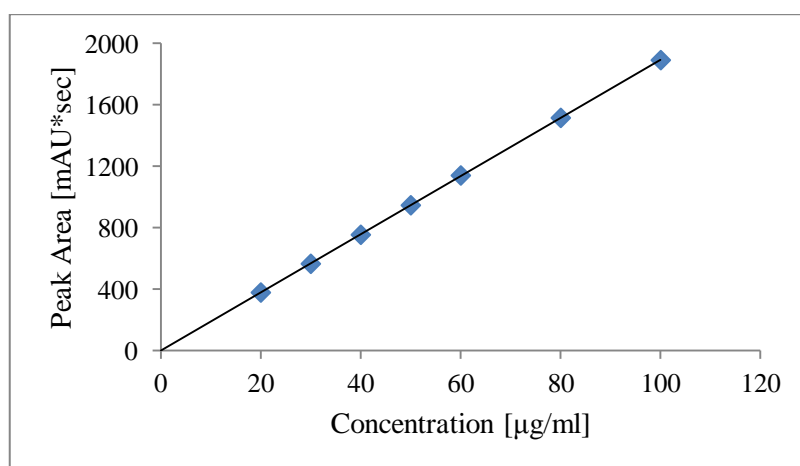


Figure 4.7. Calibration curve for **OC**.

4.5.1.3. Accuracy and Precision

Butyl methoxy dibenzoylmethane (BMDM)

For the precision and accuracy determinations, the concentration of **BMDM** was calculated for three samples using the linear regression equation (Table 4.6).

The accuracy was determined by calculating the % recovery of the measured mean concentration compared to the real concentration (Table 4.6), which remained in the required range (98.0 - 102.0 %), confirming the accuracy of the method.¹⁶⁰

The precision of the HPLC method was confirmed, with all values for the RSD % remaining under the limit of 2 % (Table 4.6).¹⁶⁰ Table 4.6 also shows the data for the 95 % CI and the SD.

Table 4.6. Accuracy and Precision data for **BMDM**

Real conc. [$\mu\text{g/mL}$]	Peak Area [mAU·sec] (n=3)	Measured conc. with $y = 45.634x$ [$\mu\text{g/mL}$] (n=3)	Recovery [%]	95 % CI [$\mu\text{g/mL}$]	SD [$\mu\text{g/mL}$]	RSD %
20.0	898	19.678	98.4	± 0.249	± 0.100	0.508
50.0	2260	49.524	98.9	± 0.108	± 0.044	0.089
100.0	4583	100.437	100.3	± 0.082	± 0.033	0.033

Octocrylene (OC)

The concentrations of three samples (in triplicate) were calculated to show precision and accuracy (Table 4.7).

The % recoveries of the measured mean concentration compared to the real concentration are presented in Table 4.7, which represent the accuracy of the method. For all measured concentrations the % recovery remained in the required range (98.0 - 102.0 %) and thus confirmed the accuracy of the method.¹⁶⁰

Table 4.7 also presents the 95 % CI, SD and the RSD % of the data set. The values for the RSD% remained under the limit of 2 %, confirming the precision of the method.¹⁶⁰

Table 4.7. Accuracy and Precision data for **OC**.

Real conc. [$\mu\text{g/mL}$]	Peak Area [mAU·sec] (n=3)	Measured conc. with $y = 18.939x$ [$\mu\text{g/mL}$] (n=3)	Recovery [%]	95 % CI [$\mu\text{g/mL}$]	SD [$\mu\text{g/mL}$]	RSD %
20.0	379	20.029	100.2	± 0.075	± 0.030	0.150
50.0	948	50.073	100.2	± 0.330	± 0.133	0.265
100.0	1892	99.917	99.9	± 0.273	± 0.110	0.110

4.5.1.4. Specificity

Specificity of both UV-filters, **BMDM** and **OC**, was determined by using the PDA detector and PolyView 2000™. For both UV-filters in combination at 358 nm for **BMDM** and at 303 nm for **OC**, seven points on each UV-filter peak were selected and the UV-spectra were recorded. These UV-spectra were normalised and overlaid, as shown in Figure 4.8 for **BMDM** and in Figure 4.9 for **OC**.

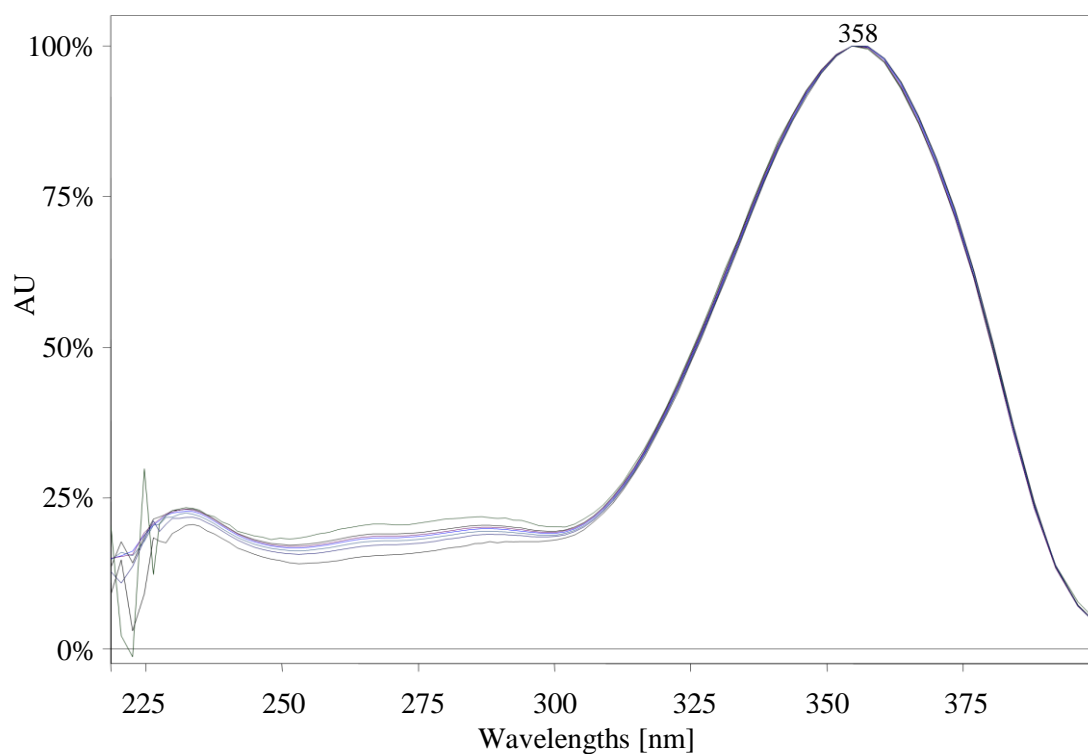


Figure 4.8. UV-spectra at selected points of **BMDM** peak in the chromatogram after normalisation.

Although the UV-spectra of **BMDM** overlay between 310 and 400 nm, differences are evident between 230 and 310 nm. These differences are attributed to the presence of different amounts of the diketo-form of UV-filter **BMDM**, attributed to the ability of this UV-filter to undergo keto-enol tautomerism. While the enol-form is the dominant and active form, with a retention time of about 12.2 minutes, at an absorption maximum of 358 nm, the diketo-form elutes earlier (~ 4.8 minutes) and has an absorption maximum of 266 nm. These forms exist in equilibrium and undergo conversion on the column. The differences in the UV-spectra (Figure 3.12) are attributed to the decreasing amounts of the diketo-form and therefore the **BMDM**-peak can be regarded as pure.

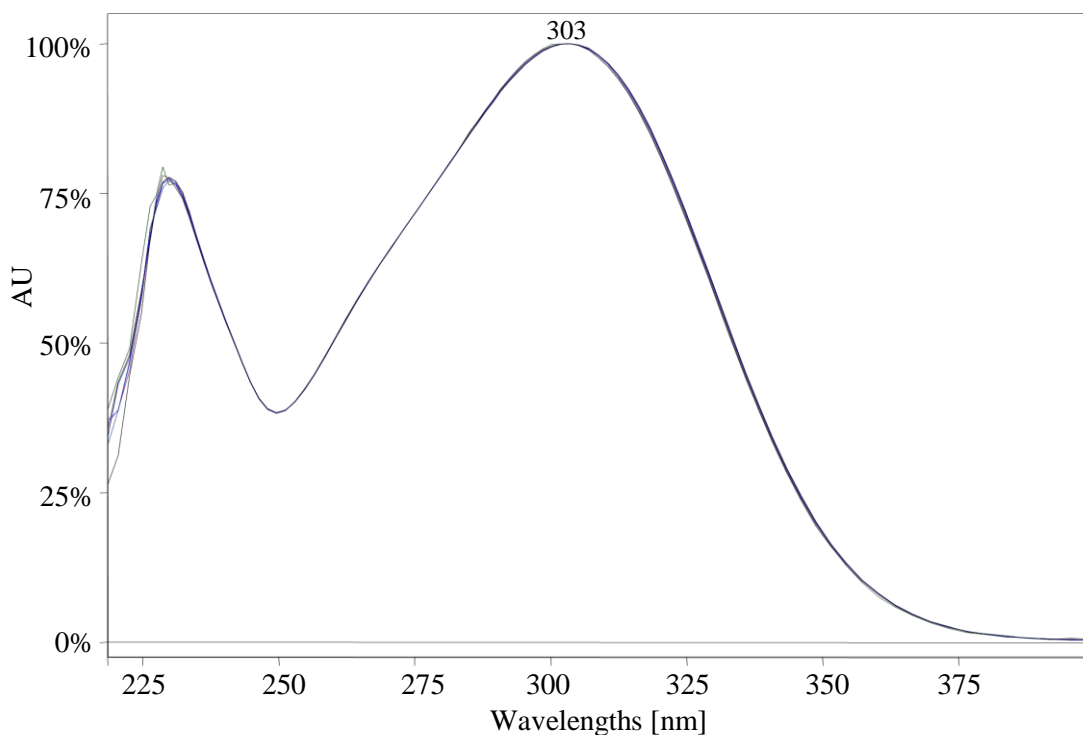


Figure 4.9. UV-spectra at selected points of **OC** peak in the chromatogram after normalisation.

All overlaid UV-spectra of UV-filter **OC** are identical between about 230 and 400 nm, confirming the purity of the **OC**-peak and the specificity of the method for the determination of **OC**, in the presence of **BMDM** and their photodegradants.

4.5.1.5. Sensitivity

Sensitivity of the method is represented by the LOD and the LOQ. The wavelength of detection for **OC** was 303 nm and for **BMDM** 358 nm. For **OC** the LOD was 0.03 µg/mL and the LOQ 0.1 µg/mL, with a RSD % of 4.5 %. **BMDM** had the same LOD (0.03 µg/mL) but a LOQ of 0.15 µg/mL with a RSD of 5.2 %. Peak heights (H), baseline noises of the blank sample (h), widths at half height (width $\frac{1}{2}$) and S/N ratios for both UV-filters are presented in Table 4.8.

To be valid for sensitivity the RSD % of the LOQ should be lower than 5.0 %, ¹⁶⁰ which is the case for UV-filter **OC**. The RSD % of the LOQ for **BMDM** is 5.2 %.

Table 4.8. LOD and LOQ data for **OC** and **BMDM**.

Conc. [$\mu\text{g/mL}$]	OC		BMDM	
	0.03 (LOD)	0.10 (LOQ)	0.03 (LOD)	0.15 (LOQ)
H [μAU]	47.8	139	72.0	283
h [μAU]	29	29	46	46
Width $\frac{1}{2}$ [mm]	12.6	13.5	14.8	17.1
S/N	3.30	9.59	3.13	12.3

4.5.1.6. Robustness

To evaluate the robustness of an HPLC method, several conditions were altered and the resolution factors were calculated. In Table 4.9 the resolution factors of **BMDM** and **OC** are listed under optimum and altered conditions. The optimum conditions were: flow rate: 1.0 mL/min, temperature: 30 °C, pH: 2.2 and a mobile phase ratio of methanol/water/acetic acid (89/10/1 % v/v). For both UV-filters the resolution factors remained over 2.0 for all altered conditions, which confirms the robustness of the method for **BMDM** and **OC** in the presence of their photodegradants.

Table 4.9. Rs for **BMDM** and **OC**.

Change of condition	Rs	
	BMDM	OC
Optimum	8.8	3.5
Flow rate: 0.8 mL/min	8.7	6.4
Flow rate: 1.2 mL/min	7.9	3.3
Temp.: 35 °C	8.1	3.6
pH: 5.4	8.4	3.4
Mobile phase: methanol: 92 % v/v	7.5	3.7

Samples were injected 24 hours after their first injection to determine the stability of the sample solutions in the HPLC autosampler. Less than 0.5 % decrease in concentration confirmed the stability of both UV-filters, since samples were not maintained in the autosampler for longer than 20 hours.

4.5.2. Benzophenone-3 (B3)

4.5.2.1. Filter Evaluation

The filter evaluation for **B3** was undertaken at two concentrations (4.0 and 20.0 µg/mL) in methanol. The absorbance was measured at $\lambda_{\text{max}} = 325 \pm 2$ nm and the mean absorbance, the SD, RSD % and the % difference between the filtered and unfiltered samples are presented in Table 4.10.

Table 4.10. Filter Evaluation data for **B3**.

Concentration [µg/mL]	Mean absorbance [A] (n = 6)	SD [A]	RSD %	Difference compared to unfiltered sample [%]
No filtration				
4.0	0.177	± 0.000548	0.31	
20.0	0.881	± 0.001897	0.22	
First 5 mL				
4.0	0.176	± 0.000408	0.23	- 0.57
20.0	0.879	± 0.002098	0.24	- 0.23
Second 5 mL				
4.0	0.176	± 0.000516	0.29	- 0.57
20.0	0.880	± 0.001265	0.14	- 0.11

The % difference in absorbance between the filtered and unfiltered samples is under the limit of 5 %, showing that UV-filter **B3** does not adsorb onto the filter.

4.5.2.2. Linearity

A calibration curve was constructed for UV-filter **B3** by plotting the mean peak areas against the corresponding concentrations. The mean peak area, 95 % CI, SD and RSD % are given in Table 4.11, while the calibration curve is represented in Figure 4.10 with the SDs as error bars. Though, error bars are too small to be visualised. The linear regression equation was calculated as $y = 22.616x$ with a correlation coefficient of $R^2 = 0.9999$.

Table 4.11. Linearity data for **B3**.

Concentration [$\mu\text{g}/\text{mL}$]	Peak Area [mAU \cdot sec] (n = 3)	95 % CI [mAU \cdot sec]	SD [mAU \cdot sec]	RSD %
10.0	228	± 1.4	± 0.58	0.253
15.0	342	± 3.8	± 1.53	0.447
20.0	457	± 1.4	± 0.58	0.126
25.0	568	± 3.8	± 1.53	0.269
30.0	679	± 1.4	± 0.58	0.085
40.0	906	± 5.2	± 2.08	0.230
50.0	1125	± 2.9	± 1.15	0.103

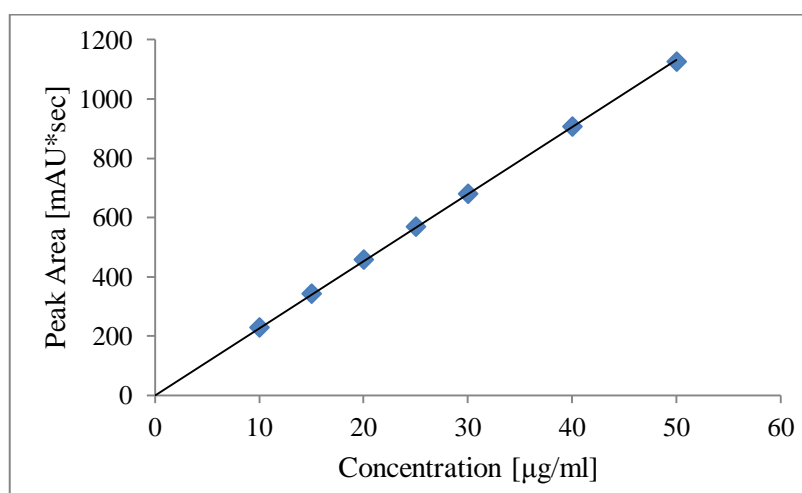


Figure 4.10. Calibration curve for **B3**.

4.5.2.3. Accuracy and Precision

For the accuracy and precision determinations of UV-filter **B3**, the concentrations of three samples (in triplicate) were calculated, using the linear regression equation (Table 4.12).

The accuracy was described by the % recovery of the measured mean concentration compared to the real concentration (Table 4.12). For all three concentrations the % recovery remained between 98.0 and 102.0 %, confirming the accuracy of the method.¹⁶⁰

With the RSD % values remaining under the limit of 2 %, the precision of the method was confirmed.¹⁶⁰ The SD, RSD % and 95 % CI of the **B3** data are presented in Table 4.12.

Table 4.12. Accuracy and Precision data for **B3**.

Real conc. [µg/mL]	Peak Area [mAU·sec] (n=3)	Measured conc. with $y = 22.616x$ [µg/mL] (n=3)	Recovery [%]	95 % CI [µg/mL]	SD [µg/mL]	RSD %
10.0	230	10.155	101.6	0.063	± 0.025	0.250
25.0	567	25.086	100.3	0.167	± 0.067	0.268
50.0	1127	49.832	99.7	0.219	± 0.088	0.177

4.5.2.4. Specificity

Specificity of UV-filter **B3** was determined using the same method as for the UV-filters **BMDM** and **OC**. Figure 4.11 shows the normalised and overlaid UV-spectra of UV-filter **B3** at 324 nm.

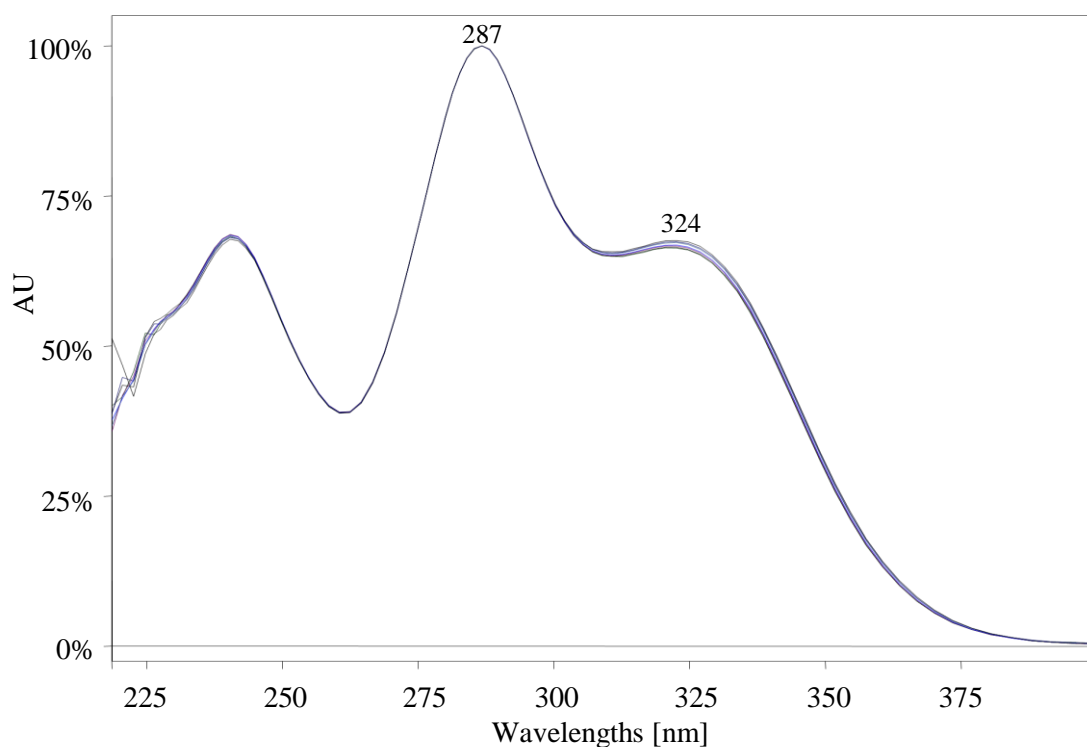


Figure 4.11. UV-spectra of selected points of **B3** chromatogram after normalisation.

Between 230 and 400 nm all overlaid UV-spectra are identical and confirm that no co-eluting substances are present. The HPLC method is therefore specific for the determination of UV-filter **B3**.

4.5.2.5. Sensitivity

The LOD for UV-filter **B3** was found to be 0.015 µg/mL and the LOQ 0.06 µg/mL with a RSD of 4.8 % at 324 nm. Relevant data (H, h, width ½ and S/N ratio) are given in Table 4.13.

Table 4.13. LOD and LOQ data for **B3**.

Conc. [µg/mL]	0.015 (LOD)	0.06 (LOQ)
H [µAU]	51.7	181
h [µAU]	39	39
Width ½ [mm]	6.84	7.06
S/N	2.65	9.28

4.5.2.6. Robustness

In Table 4.14 the resolution factors of **B3** are listed under optimum and altered conditions. The following conditions are the optimum: flow rate: 1.0 mL/min, temperature: 30 °C, pH: 2.2 and a mobile phase ratio of methanol/water/acetic acid (89/10/1 % v/v). A resolution factor > 2.0 confirmed the robustness of the method for **B3**.

Table 4.14. Rs for **B3**.

Change of condition	Rs
Optimum	5.9
Flow rate: 0.8 mL/min	6.3
Flow rate: 1.2 mL/min	6.1
Temp.: 35 °C	5.8
pH: 5.4	5.8
Mobile phase: methanol: 92 %	6.1

4.6. Summary

An HPLC method was developed and validated to quantitatively analyse the UV-filters **BMDM** and **OC** simultaneously in the presence of their photodegradants. The same method was also validated for UV-filter **B3**, since this UV-filter will be studied for skin penetration in Chapter 6.

The HPLC column was chosen based on literature reports. The mobile phase selection was kept as simple as possible, resulting in an isocratic mobile phase containing water, methanol and acetic acid, which is suitable for LC-MS analyses. A sample injected containing **BMDM** and **OC** including photodegradants showed a good resolution for both UV-filters with a resolution factor of 8.8 for **BMDM** and 3.5 for **OC**. A low mobile phase pH of 2.2 was necessary to achieve the best possible peak shape for UV-filter **BMDM**.

Method validation for **BMDM**, **OC** and **B3** was undertaken and linearity, accuracy, precision, sensitivity, specificity and robustness determined. Specificity and robustness was confirmed in the presence of the photodegradants. Filter evaluation tests showed that the three UV-filters did not adsorb significantly onto the filter material used. Accuracy and precision of the method were confirmed and correlation coefficients remained over 0.9997, confirming linearity. The sensitivity of the method was reported by the determination of LOD and LOQ. Co-eluting compounds were not detected, and resolution remained over 2.0, after alteration of method parameters, confirming the specificity and robustness of the method.

The developed and validated method can therefore be used to determine the concentration of UV-filters during photostability and skin penetration studies in the following two chapters.

Chapter 5

Photostability of Chemical UV-filters

5.1. Introduction

UV-filters, which can be divided into physical and chemical UV-filters, are the active ingredients of sunscreen products. The photostability of these UV-filters is important to ensure protection from dangerous health effects caused by UV-light, such as skin cancer or immunosuppression.⁵ While physical UV-filters are photostable, chemical UV-filters may be unstable to light, and as a result of this instability may lose their photoprotective character. As described in Chapter 2, the SPF and UVA-PF of several chemical UV-filters decreased up to 62 % after only two hours of UV-irradiation.^{43,44} Two physical UV-filters, TiO₂ and ZnO, and 27 chemical UV-filters, including UVA-, UVB- and broad spectrum filters, are available on the Australian market.¹⁴ Physical and chemical UV-filters, in addition to other ingredients, such as antioxidants, are often used in combination in sunscreen products. It is recommended that sunscreen products are reapplied every two hours during use.¹⁴

The regulation of sunscreen products in Australia, Europe and the USA is described in detail in Chapter 2. Important to mention here is the lack of the requirement for photostability testing for sunscreen products in these countries, as described in the ICH Guideline Q1B for photostability testing of new drug substances and products.^{14,25-27} This ICH guideline would require that a quantitative analysis of the UV-filter content and a detection of photodegradants after UV-irradiation be undertaken, under specified conditions. Despite this lack of required photostability testing for sunscreen products, a number of studies have reported on the photostability of chemical UV-filters.^{43-46,49,52,54}

Combinations of chemical UV-filters and TiO₂ seem to present a particular challenge in terms of photostability, due to the photocatalytic properties of TiO₂ and its ability to generate ROS.⁸⁷ TiO₂ is often used as a photocatalyst to induce the degradation of organic molecules in wastewater treatment and to remove pollutants.¹⁶¹ Since chemical UV-filters are organic molecules, this degradation might be problematic. A reduction in the photoreactivity of TiO₂ can be achieved by coating^{84,86} or doping^{87,90} of TiO₂ particles. The inclusion of antioxidants, such as vitamin E, into sunscreen products also has the potential to reduce ROS generation.^{16,77,95}

In this chapter the photostability of the two chemical UV-filters, Butyl methoxy dibenzoylmethane (**BMDM**) and Octocrylene (**OC**) in the presence of TiO₂ and vitamin E will be reported.

UV-filter **BMDM**, often referred to by its synonym Avobenzone or its trade name Parsol® 1789, is a commonly used UVA-filter, offering protection especially in the UVA I-range. There have however been reports of its instability to light;^{18,39} **BMDM** undergoes keto-enol tautomerism (Figure 5.1), where the enol-form absorbs in the UVA-range and the diketo-form in the UVC-range. Photodegradation involves conversion of the enol- to the diketo-form with the subsequent formation of several photodegradants.^{42,64} UV-filter **OC**, a thick oily liquid, is a commonly used UVB-filter and was chosen as a candidate for this study because of its photostability and potential to stabilize other UV-filters, mainly **BMDM**.^{18,39} In addition, this combination provides broad spectrum protection and often occurs as such in commercial sunscreen products. A survey undertaken in the UK in 2010, identified **BMDM** and **OC** as the two most commonly used UV-filters in commercial sunscreen products. In 96.4 % of the 337 surveyed sunscreen products, **BMDM** was one of the active ingredients, while 90.5 % contained **OC**.⁷⁵

The physical UV-filter TiO₂, which is a broad spectrum UV-filter, was chosen because it is often added to chemical UV-filters in sunscreen products to increase the SPF and UVA-PF. In the study mentioned above, 49.0 % of the surveyed sunscreen products contained TiO₂.⁷⁵ Absorption of UV-light depends on the TiO₂ particle size, it absorbs mainly in the UVB- and UVA II-range, but is less effective in the UVA I-range.⁵ The effect of the antioxidant vitamin E on the photostability of **BMDM** and **OC** has been investigated because of its ability to reduce ROS generation. These ROS are known to cause cell damage and have the potential to degrade chemical UV-filters in sunscreen products.⁸⁷

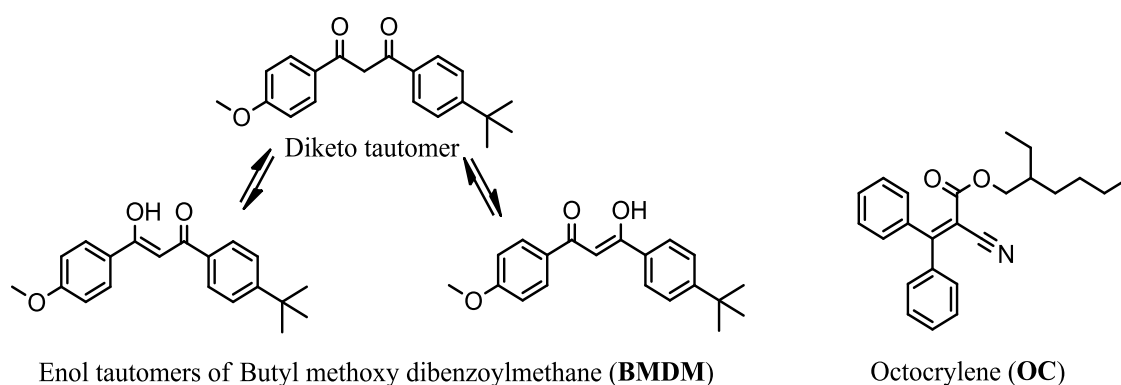


Figure 5.1. Chemical structures of **BMDM** and **OC**.

The photodegradation of a number of chemical UV-filters is described in detail in Chapter 2. Relevant studies on **BMDM**, **OC**, TiO₂ and vitamin E are summarised in this chapter. The

UVA-protection factor of **BMDM** was reduced by 41 % in an O/W emulsion⁴⁴ and a degradation of 56 % in mygliol[®] 812 was reported after UV-irradiation,⁴⁵ while other UV-filters showed only minimal degradation under the same conditions. Generation of ROS on exposure of **BMDM** to UV-light was three times that of other UV-filters and an irradiated control without UV-filter.⁴⁹ After UV-irradiation of **OC**, no degradation was reported in a number of studies^{45,52,53} and the ROS generation remained in the same range as that of the irradiated control.⁴⁹ However, a 10 % loss of the SPF after only 95 minutes of UV-irradiation was reported as a result of the instability of **OC** to UV-light.⁴³ Although the physical UV-filter TiO₂ is photostable, the complete degradation of **BMDM** and **OC** after UV-irradiation in the presence of untreated TiO₂ is attributed to ROS generation.^{53,68} Doping or coating of TiO₂-particles reduced ROS generation and resulted in the protection of chemical UV-filters from degradation.^{86,87} Reduction of ROS generation may also be achieved by the addition of vitamin E, as mentioned above. The generation of ROS on exposure to UV-light in the presence of **BMDM** was reduced by 50 % on the addition of vitamin E.⁹⁴

In this chapter the effect of TiO₂ and vitamin E on the photostability of **BMDM** and **OC** in methanol was determined. Methanol was chosen because of the solubility of both chemical UV-filters and because it is commonly used in direct photolysis studies.^{37,64,66} In the first part of the study, the effect of TiO₂ particle size on the photostability of **BMDM** and **OC** was investigated by using untreated TiO₂. Silica coated TiO₂ appears to be one of the most effective ways to reduce the photodegradation of chemical UV-filters^{84,86} and was therefore chosen for the second part of the study. Given that such coating does not completely prevent the generation of ROS or that coated TiO₂ may lose its protective nature due to aging,^{84,87} the rationale for the addition of vitamin E was to further reduce UV-filter degradation.

After UV-irradiation of both chemical UV-filters, the major photodegradants generated were identified by LC-MS and FTMS.

5.2. Materials and Methods

5.2.1. Solvents and Reagents

The UV-filters Butyl methoxy dibenzoylmethane (Eusolex[®] 9020), Octocrylene (Eusolex[®] OCR) and the silica coated TiO₂ (Eusolex[®] T-AVO) were purchased from Merck (Darmstadt, Germany). Vitamin E ((+)- α -tocopherol), anatase TiO₂ micro- (\geq 99 % trace metals basis, particle size \sim 0.6 μ m) and nano-particles (99.7 % trace metals basis, particle size $<$ 25 nm) were purchased from Sigma Aldrich (St. Louis, USA). Glacial acetic acid and methanol

(HPLC-Grade) were purchased from RCI Labscan (Bangkok, Thailand). Reversed osmosis water was prepared with a Millipore® Elix 10 from Millipore SAS (Molsheim, France).

5.2.2. Instrumentation

The immersion well photoreactor (400 mL) used was supplied by Heraeus Noblelight GmbH (model UV-RS-1), Hanau, Germany, and was equipped with a UV immersion lamp TQ 150 (medium pressure mercury lamp, 150 W). Two glass vessels, quartz ($\lambda \geq 200$ nm) and pyrex ($\lambda \geq 300$ nm), were used during the study, which served as cooling jacket to maintain the temperature of the reaction mixture at 20 - 25 °C.

The Varian ProStar® HPLC system (Varian Inc., Melbourne, Australia), consisting of a 240 quaternary solvent delivery module, 410 autosampler and a 330 PDA detector was used for analysis. Data collection was undertaken with the Star Chromatography Workstation System Control version 6.41, which was equipped with the PolyView 2000™ spectral Processing Application (Varian Inc., Melbourne, Australia).

An Eppendorf centrifuge 5810R (Eppendorf South Pacific, Sydney, Australia) was used to centrifuge samples containing TiO₂.

A Stuart® flask shaker SF1 (Bibby Scientific Ltd., Staffordshire, UK) was used for the adsorption experiments.

The LC-MS was an Agilent 1100 HPLC system (Agilent Technologies Pty. Ltd., Melbourne, Australia) comprising a degasser, quaternary pump, autoinjector and PDA detector which was connected to a Bruker Daltonics Esquire3000plus mass spectrometer (ESI MS) with an Apollo source operating at 40 eV (Bruker Biosciences Pty. Ltd., Melbourne, Australia). Low resolution mass spectral data were measured with this system. All LC-MS data was collected using Bruker Daltonics Esquire Control v5.3 and Hystar v3.1 software (Bruker Biosciences Pty. Ltd., Melbourne, Australia).

High resolution mass spectral data were collected using a Bruker BioApex 47 FTMS with an electrospray (ESI) Analytica of Brandford source. All experimental event sequences were controlled and data reduction performed using Bruker Daltonics XMASS version 7.0.3.0 software (Bruker Biosciences Pty. Ltd., Melbourne, Australia).

5.2.3. Preparation of Standards

The standard solutions were prepared by dissolving 100 mg of **BMDM** and **OC** in 50 mL methanol, separately or in combination. This stock solution was then further diluted with methanol to achieve seven standards, within the calibration range 20 - 100 µg/mL, which was

consistent with the concentration of the standards found in the literature for **BMDM** and **OC** (up to 60 or 100 $\mu\text{g/mL}$).^{146,149,162}

5.2.4. Photostability Studies

Photodegradation profiles of **BMDM** and **OC** were determined in a pyrex glass vessel in the photoreactor, under constant magnetic stirring (400 rpm). Pyrex glass has a transmission of $\lambda \geq 300$ nm, which resembles the UV-emission of the natural sun, reaching the surface of the earth ($\lambda \geq 290$ nm).⁸⁷ Solutions were prepared at a concentration of 60 $\mu\text{g/mL}$ for **BMDM** and **OC** alone or in combination in methanol, avoiding the necessity for dilution prior to analysis. UV-filter combinations without TiO_2 were filtered through a 15 mm syringe filter with a 0.45 μm PTFE membrane (Phenomenex Inc. Sydney, Australia), while samples with TiO_2 were centrifuged at 4000 rpm for 30 minutes, and the supernatant analysed. All experiments were undertaken in triplicate.

5.2.4.1. Photostability Studies in the Presence of Different TiO_2 Particle Sizes

To study the effect of TiO_2 particle size on the photodegradation of **BMDM** and **OC** untreated anatase TiO_2 (100 $\mu\text{g/mL}$) with two different particle sizes was used: micro- TiO_2 with an average particle size of 0.6 μm and nano- TiO_2 with a particle size smaller than 25 nm. The concentration of TiO_2 was 1.7 times that of the chemical UV-filters. However, 2.5 times the amount of TiO_2 compared to the studied chemical UV-filter concentrations has been reported.^{87,90} A concentration higher than 100 $\mu\text{g/mL}$ was, however, not suitable because of reflection and blocking the UV-light from reaching the complete sample suspension. Samples were taken before irradiation and then every 30 minutes after irradiation for four hours.

5.2.4.2. Photostability Studies in the Presence of Coated TiO_2 and Vitamin E

Coated TiO_2 and vitamin E were added to **BMDM** and **OC** in order to reduce photodegradation, using the same concentrations for **BMDM**, **OC** and TiO_2 . The average particle size of the silica coated TiO_2 (100 % rutile) was 119 nm, as informed by the manufacturer. The vitamin E concentration to be used was adopted from a study,⁹⁵ where its protective effect towards the UV-induced lipid peroxidation in the presence of EPA was investigated. Topical application of at least 1 mM vitamin E solution completely protected against the UV-induced lipid peroxidation in an *ex vivo* porcine skin.⁹⁵ The molar concentration was converted to $\mu\text{g/mL}$ (430.7 $\mu\text{g/mL}$) and rounded up to 440 $\mu\text{g/mL}$. To establish the degradation profiles, samples were taken before irradiation and then after every hour of irradiation for four hours. With the employed mobile phase, vitamin E was not eluted in an appropriate time (128 minutes) and it was necessary to add isopropanol to the mobile phase

(50/50) for ten minutes. HPLC mobile phases containing isopropanol have been previously reported to determine vitamin E.^{163,164} If samples were taken every 30 minutes the total HPLC run would exceed 24 hours, which is due to the retention time of vitamin E and the re-equilibration time. An HPLC run exceeding 24 hours could not guarantee UV-filter stability in the HPLC vials, as described in Chapter 4 during robustness validation.

5.2.4.3. Adsorption Studies

UV-filters may be adsorbed to the surface of TiO₂ particles and may then reduce the detectable UV-filter concentration. Only free, non-adsorbed UV-filters, dissolved in solution, can be determined by HPLC. Adsorption is also a crucial step in photocatalysis. Therefore, adsorption studies of **BMDM** and **OC** with coated, micro- and nano-TiO₂ were undertaken to investigate adsorption of chemical UV-filters over 24 hours in the dark. Mixtures of **BMDM** and **OC** with all three TiO₂ forms, in the same concentration as above, were wrapped in aluminium foil and shaken for 24 hours at a speed of 600 osc/min. Samples taken before the addition of TiO₂ were designated as 100 % and compared to samples taken after one, six and 24 hours.

5.2.5. Kinetic Studies

To make an unequivocal delineation about degradation kinetic data, a degradation reaction should proceed at least to 50 % conversion. In order to get to a UV-filter degradation of 80 % or more, **BMDM** and **OC** were irradiated separately and in combination in the photoreactor using a quartz glass vessel. The UV-filter concentration (60 µg/mL = 16.60×10^{-5} mol/L **OC** and 19.33×10^{-5} mol/L **BMDM**), using the same method, was employed as for the photostability studies in the absence of TiO₂. Irradiated alone, **BMDM** samples were withdrawn every five minutes during the initial 30 minutes and then every two minutes for a total irradiation time of 80 minutes. When **OC** was irradiated alone, samples were taken every three minutes for the initial 21 minutes and then every 1.5 minutes for a total irradiation time of 48 minutes. The combination of **BMDM** and **OC** was irradiated for 120 minutes and samples were withdrawn every six minutes for the first 36 minutes and then every three minutes. Degradation rate constants (k) and half-lives ($t_{1/2}$) were calculated for the following degradation range: **OC**: 10 - 70 %, **BMDM**: 20 - 70 %, **OC** in combination: 10 - 60 %, **BMDM** in combination: 20 - 60 %.

5.2.6. Data Analysis

Concentrations of **BMDM** and **OC** were determined, using the HPLC method developed and validated in Chapter 4. The % recovery for **BMDM** and **OC** was calculated, based on the sample taken before irradiation, which was designated as 100 %. The mean % recovery was

then plotted against time and the SD was displayed as error bars. Each sample was injected in triplicate. For statistical analysis a One-way ANOVA was calculated using the IBM® SPSS® statistics software Version 20 with the level of significance at $p < 0.05$. For equal variances the Bonferroni Post Hoc test was undertaken, while for unequal variances the Games-Howell Post Hoc test was applied.

5.2.7. Identification of Major Photodegradants using LC-MS and FTMS

LC-MS is a commonly used method for the analyses for known and unknown substances.¹⁶⁵ A liquid chromatograph, an HPLC, is coupled to a mass spectrometer (MS), which acts as detector. The LC-MS used in this work was coupled to a PDA detector, allowing every peak in the HPLC chromatogram to be assigned to a molecular weight detected by the MS. The employed LC-MS system measured low resolution mass data, delivering molecular weights only to the nearest whole number. On the other hand, the employed FTMS delivered high resolution mass data to four significant figures, resulting in much more precise data. The FTMS was not coupled to a chromatographic system.

The LC-MS was optimised in positive and negative mode with standard solutions of each UV-filter. Samples selected from the photostability studies were those with a maximum level of the major photodegradants and were then analysed by LC-MS, using the HPLC method, developed and validated in Chapter 4. The injection volume was the only parameter which was changed, from 10 μL to 40 μL for samples containing **OC** alone and 100 μL for samples containing **BMDM**. After preliminary test runs, the data collection for the LC-MS was set for the range m/z 50 - 850 and the data were collected in positive and negative mode.

All major photodegradants were also determined by FTMS, to confirm their molecular weights. Before analyses, the instrument was calibrated with a solution of sodium trifluoroacetate in methanol (0.1 mg/mL). Ions were detected in positive and negative mode with a molecular weight range of m/z 50 - 2000 by direct infusion of the sample (0.02 mg/mL; Cole Palmer 74900 syringe pump at 120 $\mu\text{L}/\text{h}$). The same samples were used for both the LC-MS and FTMS analyses.

5.3. Results and Discussion

5.3.1. Influence of TiO_2 Particle Size on Photodegradation

Both chemical UV-filters **BMDM** and **OC** were irradiated separately and in combination without TiO_2 , with micro- and nano- TiO_2 .

5.3.1.1. Butyl methoxy dibenzoylmethane (BMDM)

Degradation profiles for **BMDM**, irradiated alone (Figure 5.2) show higher recovery rates for **BMDM** in the absence, than in the presence of TiO_2 . It is also apparent that **BMDM** in the presence of micro- TiO_2 degraded less than in the presence of nano- TiO_2 . After four hours of irradiation the % recovery of **BMDM**, without TiO_2 was 94.08 %, with micro- TiO_2 78.39 % and with nano- TiO_2 65.02 % (Table 5.1). For the first 1.5 hours, the degradation profiles of **BMDM** in the presence of micro- and nano- TiO_2 are very similar (Figure 5.2). Thereafter **BMDM** degradation in the presence of nano- TiO_2 is increasingly higher than in the presence of micro- TiO_2 , with a difference of almost 13 % after four hours of irradiation. The % recovery after four hours of irradiation between all samples is significantly different ($F_{2,6} = 680.555$, $p < 0.000$).

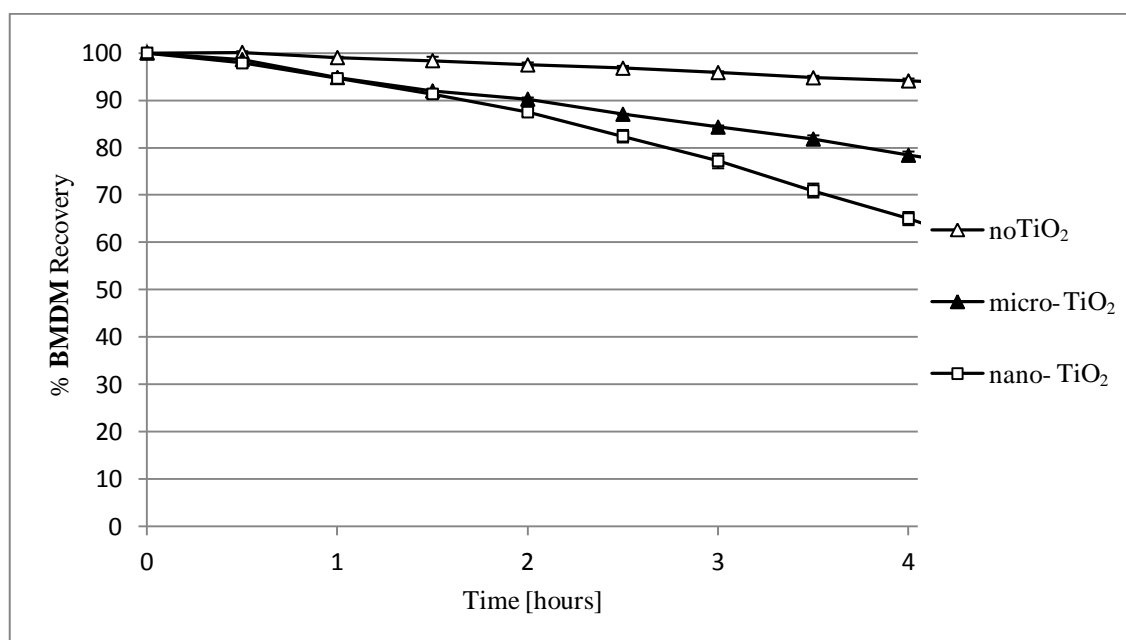


Figure 5.2. Photodegradation profile of **BMDM** in the presence and absence of TiO_2 .

Table 5.1. % Recovery \pm SD of **BMDM** in the presence and absence of TiO₂.

Time [hours]	% Recovery of BMDM (n = 3) \pm SD		
	no TiO ₂	micro-TiO ₂	nano-TiO ₂
0.0	100.00	100.00	100.00
0.5	100.11 \pm 0.24	98.59 \pm 0.31	97.85 \pm 0.20
1.0	99.01 \pm 0.18	94.80 \pm 0.27	94.61 \pm 0.48
1.5	98.36 \pm 0.83	91.97 \pm 0.23	91.34 \pm 0.46
2.0	97.46 \pm 0.52	90.23 \pm 0.35	87.50 \pm 0.86
2.5	96.77 \pm 0.49	87.04 \pm 0.10	82.41 \pm 1.32
3.0	95.85 \pm 0.26	84.33 \pm 0.34	77.18 \pm 1.55
3.5	94.75 \pm 0.42	81.81 \pm 0.78	70.94 \pm 1.47
4.0	94.08 \pm 0.51	78.39 \pm 0.78	65.02 \pm 1.39

Figure 5.3 shows the degradation profiles of **BMDM**, irradiated in combination with **OC**, in the presence and absence of TiO₂. Corresponding % recovery \pm SD for **BMDM** is represented in Table 5.2.

During the first 1.5 hours of irradiation, in the absence of TiO₂ more than 99 % of **BMDM** was recovered, while after the irradiation time of four hours, the recovery was 95.18 %. In the presence of nano-TiO₂, the recovery of **BMDM** was significantly lower after four hours of irradiation than in the absence of TiO₂ (28.31 %) or the presence of micro-TiO₂ (8.18 %), as shown in Table 5.2 ($F_{2,6} = 1013.278$, $p < 0.000$).

Also notable is that for the first 2.5 hours of irradiation the degradation profiles for **BMDM** in the presence of micro- and nano-TiO₂ were very similar, and are almost superimposable.

Data for the recovery after four hours of irradiation and degradation profiles of **BMDM** irradiated in combination with **OC** are similar to the data for **BMDM** irradiated alone. **OC** does not influence the photodegradation of **BMDM** in this study, although it has been reported that **OC** is a protecting agent for **BMDM**.⁴⁵ This discrepancy to the literature can be explained by the low UV-filter concentration (0.006 % w/v) in this study compared to the UV-filter concentration in the literature (3 % w/v).⁴⁵ The protecting effect of **OC** is less effective at low concentrations and quenching through collision does not occur within the very short lifetime of the triplet excited states of **BMDM**.⁵⁸

No adsorption of **BMDM** to micro- or nano-TiO₂ was detected neither after one, six nor 24 hours. Compared to a sample containing no TiO₂, **BMDM** concentration was 100.91 % in the

presence of micro-TiO₂ and 100.65 % in the presence of nano-TiO₂ after 24 hours. Physical adsorption, thus does not explain the decreased recovery in the presence of TiO₂.

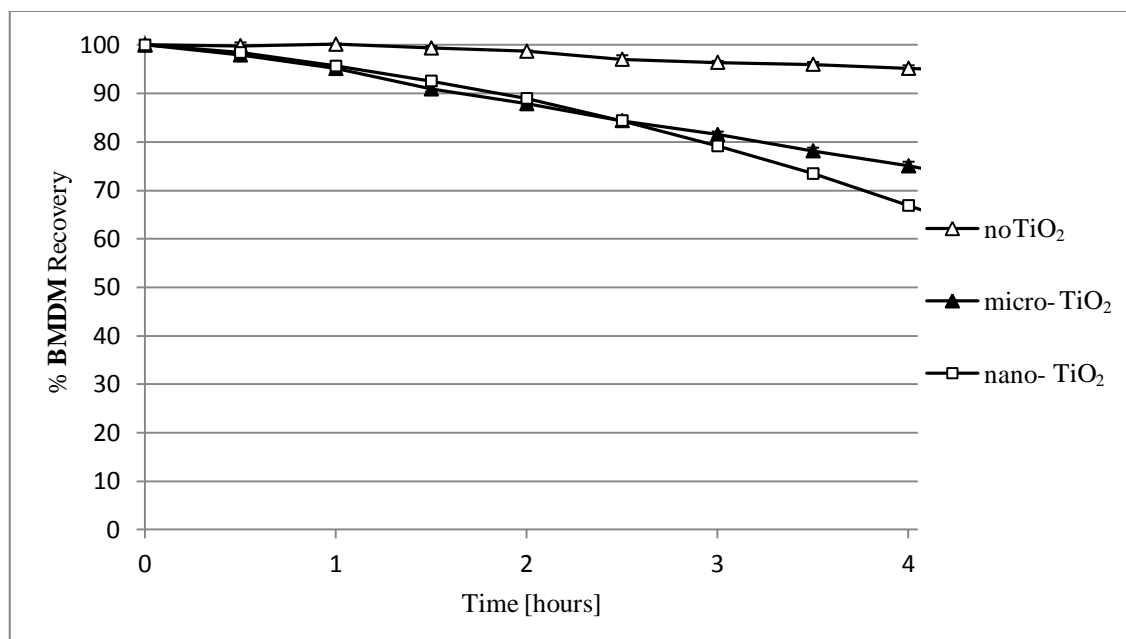


Figure 5.3. Photodegradation profile of BMDM in combination with OC in the presence and absence of TiO₂.

Table 5.2. % Recovery ± SD of BMDM in combination with OC in the presence and absence of TiO₂.

Time [hours]	% Recovery of BMDM (n = 3) ± SD		
	no TiO ₂	micro-TiO ₂	nano-TiO ₂
0.0	100.00	100.00	100.00
0.5	99.83 ± 0.68	97.93 ± 0.33	98.43 ± 0.81
1.0	100.15 ± 0.13	95.15 ± 0.87	95.64 ± 0.23
1.5	99.37 ± 0.40	90.92 ± 0.61	92.56 ± 0.31
2.0	98.71 ± 0.14	87.87 ± 0.54	88.96 ± 0.43
2.5	97.04 ± 0.81	84.39 ± 0.67	84.39 ± 0.49
3.0	96.42 ± 0.28	81.52 ± 0.60	79.15 ± 0.71
3.5	96.02 ± 0.44	78.15 ± 0.64	73.45 ± 0.83
4.0	95.18 ± 0.60	75.05 ± 0.85	66.87 ± 0.90

5.3.1.2. Octocrylene (OC)

UV-filter **OC** showed no significant photodegradation after four hours of irradiation without TiO_2 and in the presence of micro- TiO_2 (Figure 5.4). On the other hand, a significant photodegradation of 37.79 % for **OC** was found to occur in the presence of nano- TiO_2 ($F_{2,6} = 355.819$, $p < 0.000$).

The % recovery \pm SD are listed in Table 5.3. A difference of nearly 40 % **OC** degradation shows the increased effect on photodegradation of nano- TiO_2 compared to the same amount of micro- TiO_2 .

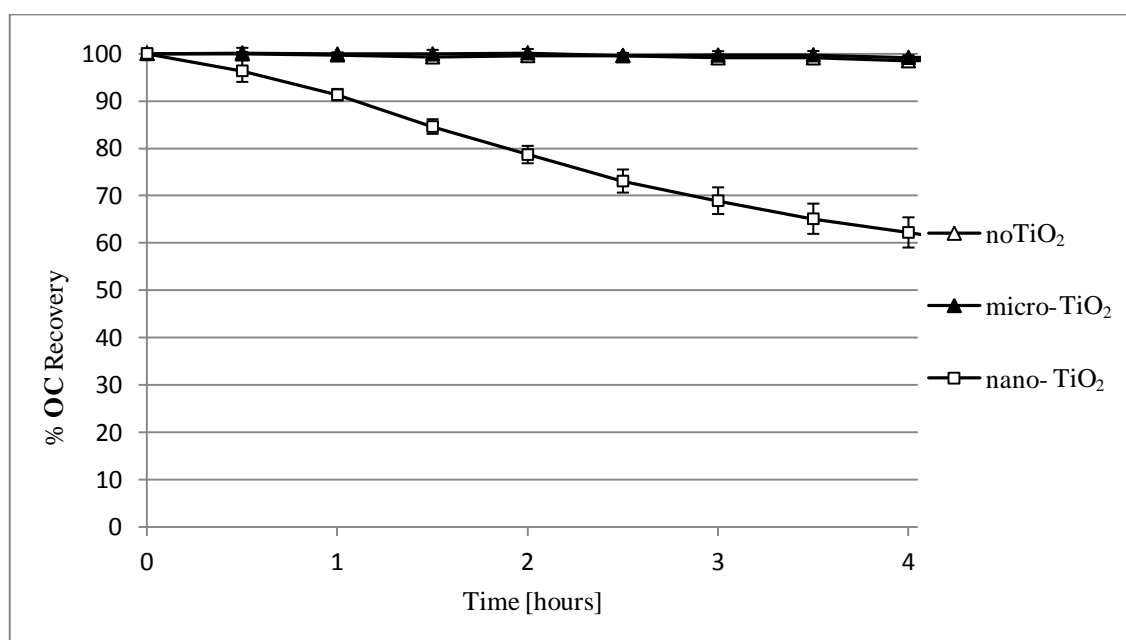


Figure 5.4. Photodegradation profile of **OC** in the presence and absence of TiO_2 .

Table 5.3. % Recovery \pm SD of **OC** in the presence and absence of TiO_2 .

Time [hours]	% Recovery of OC (n = 3) \pm SD		
	no TiO_2	micro- TiO_2	nano- TiO_2
0.0	100.00	100.00	100.00
0.5	99.91 \pm 0.41	100.14 \pm 1.05	96.34 \pm 2.35
1.0	99.70 \pm 0.37	99.88 \pm 0.36	91.29 \pm 1.22
1.5	99.28 \pm 0.28	99.91 \pm 0.85	84.57 \pm 1.54
2.0	99.55 \pm 0.18	100.14 \pm 0.80	78.65 \pm 1.84
2.5	99.52 \pm 0.53	99.59 \pm 0.53	73.06 \pm 2.44
3.0	99.07 \pm 0.73	99.67 \pm 0.82	68.91 \pm 2.82
3.5	99.07 \pm 0.44	99.73 \pm 0.79	65.10 \pm 3.19
4.0	98.46 \pm 0.95	99.18 \pm 0.45	62.21 \pm 3.19

Degradation profiles of **OC**, irradiated in combination with **BMDM**, are shown in Figure 5.5 with % recovery \pm SD for **OC** listed in Table 5.4.

UV-filter **OC** showed no degradation in the absence and presence of micro- TiO_2 . The presence of nano- TiO_2 , however, resulted in a small, but significant, photodegradation of nearly 3 % after four hours of irradiation ($F_{2,6} = 61.091$, $p < 0.000$).

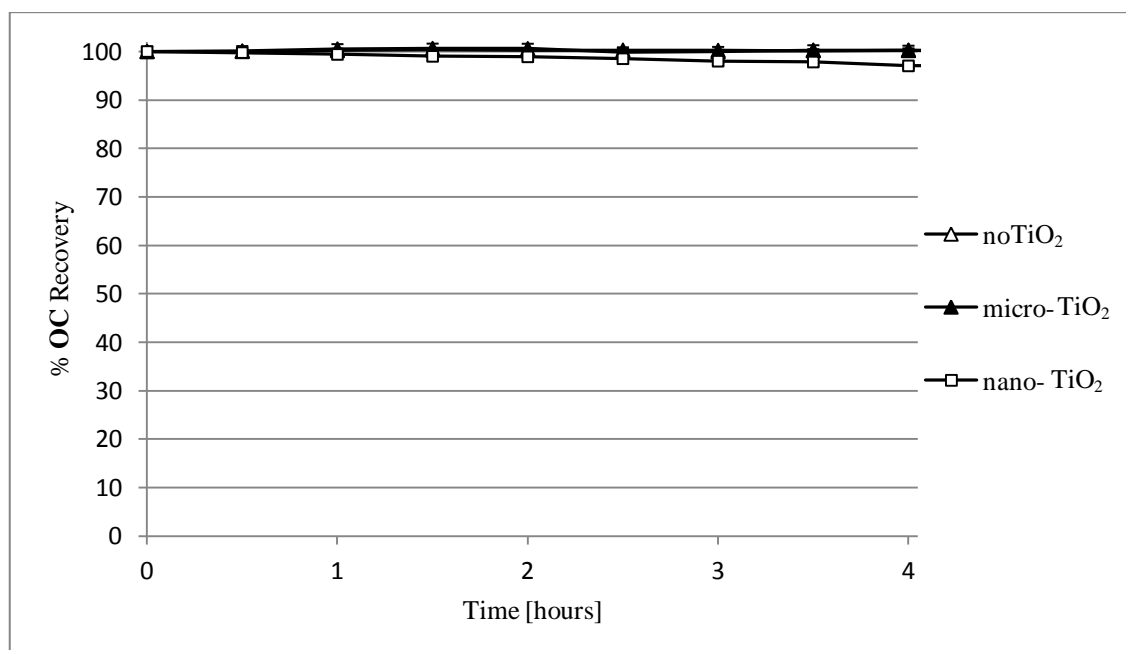


Figure 5.5. Photodegradation profile of **OC** in combination with **BMDM** in the presence and absence of TiO_2 .

Table 5.4. % Recovery \pm SD of **OC** in combination with **BMDM** in the presence and absence of TiO_2 .

Time [hours]	% Recovery of OC (n = 3) \pm SD		
	no TiO_2	micro- TiO_2	nano- TiO_2
0.0	100.00	100.00	100.00
0.5	100.12 \pm 0.54	100.00 \pm 0.29	99.77 \pm 0.52
1.0	100.52 \pm 0.48	100.20 \pm 0.40	99.40 \pm 0.09
1.5	100.63 \pm 0.21	100.35 \pm 0.31	99.00 \pm 0.14
2.0	100.60 \pm 0.40	100.29 \pm 0.30	98.90 \pm 0.37
2.5	99.86 \pm 0.10	100.29 \pm 0.36	98.51 \pm 0.63
3.0	99.95 \pm 0.91	100.23 \pm 0.13	98.00 \pm 0.39
3.5	100.29 \pm 0.52	100.17 \pm 0.31	97.83 \pm 0.72
4.0	100.20 \pm 0.44	100.29 \pm 0.36	97.03 \pm 0.43

These results are similar to the degradation profiles of UV-filter **OC** irradiated without **BMDM**. The only difference is the extent of **OC** degradation in the presence of nano- TiO_2 . While the recovery of **OC** is only 62.21 % when irradiated without **BMDM**, it is 97.03 % when irradiated in the presence of **BMDM**.

Photostability of **OC** without TiO_2 and its photodegradation in the presence of nano- TiO_2 confirms the findings of Ricci et al.⁵³, who however, did not investigate the photodegradation of **OC** in the presence of micro- TiO_2 . UV-filter **OC** (5.0×10^{-4} M) was studied in water in the presence and absence of anatase nano- TiO_2 (1.0 mg/mL) with an average particle size of 32 nm. The suspension was irradiated for 20 hours in pyrex tubes using a multilamp chamber photoreactor equipped with Luzchem UVA fluorescent tubes. Without TiO_2 100 % of **OC** was recovered, while in the presence of nano- TiO_2 only 55 % of **OC** were recovered, as determined by GC.⁵³

Adsorption studies after one, six and 24 hours showed no adsorption of **OC** to micro- and nano- TiO_2 . Compared to a sample without TiO_2 , **OC** concentration was 100.29 and 99.42 % in the presence of micro- and nano- TiO_2 , respectively, after 24 hours. Physical adsorption thus does not contribute to the removal of **OC**.

Under the experimental conditions two degradation processes for **BMDM** and **OC** are possible, direct photolysis and TiO_2 photocatalysis. While both processes took place during photodegradation of **BMDM**, **OC** only degraded *via* a photocatalytic reaction in the presence of nano- TiO_2 .

Photoprotection and direct photolysis can be explained using the Jablonski diagram (Figure 5.6). Continuous UV-irradiation leads to an excitation of UV-filter molecules from the ground state (S^0) to excited singlet states (S^N , S^1) and subsequent conversion to the triplet states (T^N , T^1) via intersystem crossing (ISC). From their S^1 or T^1 states, molecules may either return back to the S^0 state through heat release (internal conversion, IC) or light emission (fluorescence or phosphorescence) thus maintaining photoprotection. As there was no photodegradation of **OC** detected in the absence of TiO_2 , this cycle is very efficient, confirming the stability of UV-filter **OC**.^{45,55} On the other hand, photodegradation of **BMDM** was observed, which occurs from the unstable T^1 state,⁵⁸ resulting in a number of photodegradants.^{37,61,63}

Figure 5.7 shows the molar absorption coefficients (ϵ) of **BMDM** and **OC**, plotted against the wavelengths (λ), together with the main emission lines of the mercury lamp and the UV-transmittance of the pyrex glass vessel. The red line shows the transmittance of the pyrex glass, which reaches its maximum plateau at about 350 nm. Although the mercury lamp has five main emission lines, only two are relevant (313 and 366 nm), because at 254 nm no light is transmitted through the glass and at 405 and 436 nm both chemical UV-filters do not absorb any light. At 313 nm only about 40 % of the UV-light is transmitted through the pyrex glass, while at 366 about 70 % is transmitted.

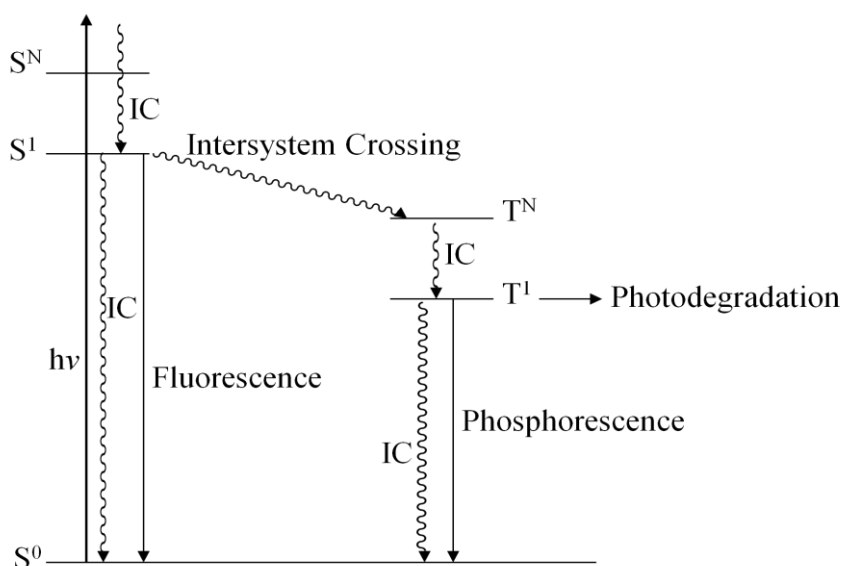


Figure 5.6. Simplified Jablonski Diagram.¹⁶⁶

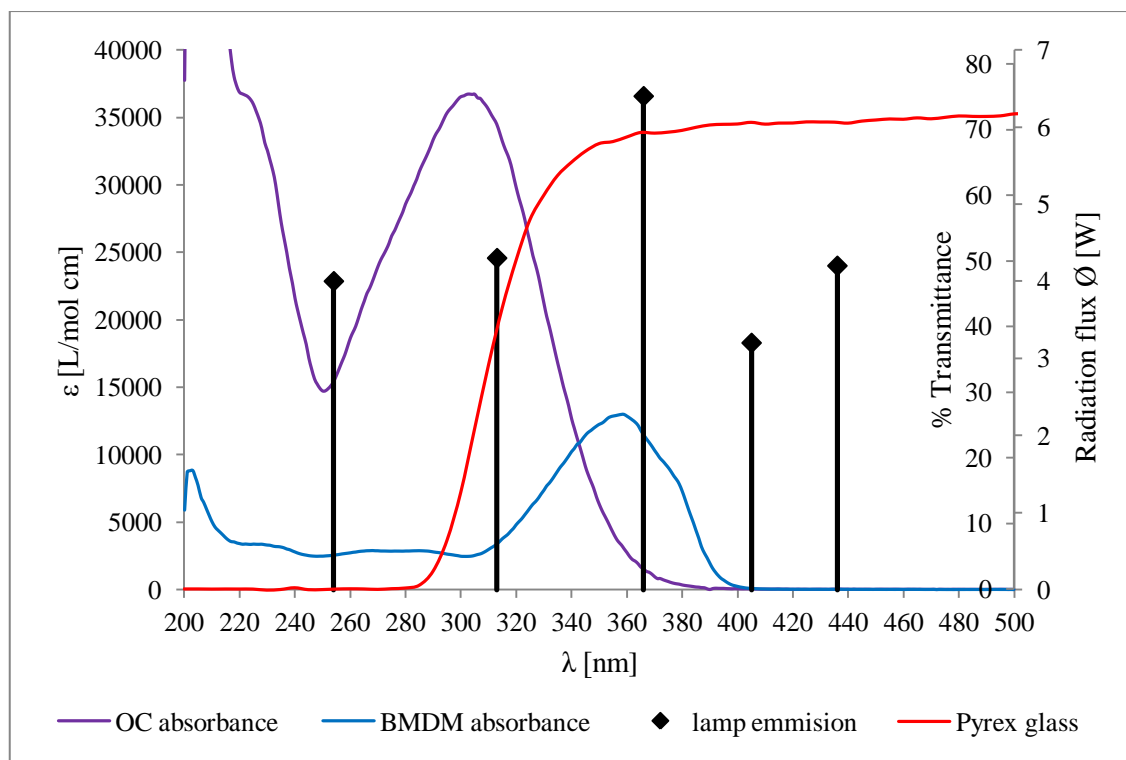


Figure 5.7. Molar absorption coefficients (ϵ) of **BMDM** and **OC**, main emission lines of TQ 150 mercury lamp (radiation flux) and % transmittance of pyrex glass vessel.

In the presence of TiO_2 , photocatalytic reactions involving various ROS may compete with direct photolysis. During the photocatalytic reaction (Figure 5.8 and Scheme 5.1)¹⁶⁷ energy from UV-light ($< 400 \text{ nm}$) is absorbed by the TiO_2 particle resulting in the migration of an electron from the electron-filled valence band to the vacant conduction band. This migration creates a positive hole in the valence band (h_{VB}^+) and a negatively charged electron in the conduction band (e_{CB}^-), the so called electron-hole-pair. ROS, mainly hydroxyl radicals OH^\bullet and superoxide radical anions $\text{O}_2^{\bullet -}$ can be formed in subsequent redox reactions (Scheme 5.1),^{77,78,91} although other oxidative species, such as hydrogen peroxide H_2O_2 or singlet oxygen $^1\text{O}_2$ can also be formed.^{78,168} These ROS may cause degradation of other sunscreen ingredients, skin damage or both.⁸⁷ The methanolic reaction mixture was not degassed prior to UV-irradiation, therefore it can be expected that O_2 was present in the solution. The solubility of O_2 in methanol is 2.1 - 2.2 mmol/L (atmospheric O_2).¹⁶⁹ Although only trace amounts of water are present in methanol (0.02 %), a small amount of OH^\bullet may still be formed. However, since methanol is known to efficiently quench hydroxyl radicals,¹⁷⁰ they may not play a role in degradation. Alternatively, methanol derived radical species ($\text{CH}_3\text{O}^\bullet$ or $^\bullet\text{CH}_2\text{OH}$) may themselves participate in degradation processes. The greater photoreactivity of nano- TiO_2 compared to micro- TiO_2 is attributed predominately to the larger surface area of the nano- TiO_2 ,

a reduced, deactivating e_{CB}^-/h_{VB}^+ recombination and a faster charge transfer.¹⁷¹ Due to the fact that ROS are generated on the surface of TiO₂ particles, a larger surface area generates more ROS, which may induce the degradation of chemical UV-filters.¹⁷² The larger surface area also offers more active sites, although physical adsorption of the UV-filters was not observed.

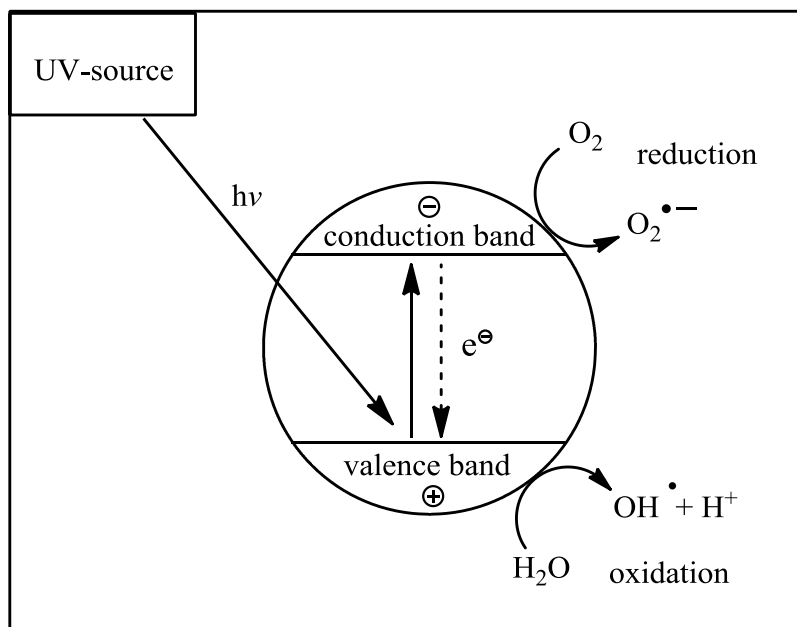
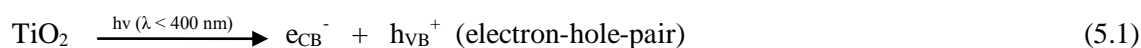


Figure 5.8. Formation of electron-hole pair on surface of TiO₂ particle.



Scheme 5.1. Generation of ROS by TiO₂.

Alternatively, the degradation in the presence of TiO₂ involves an electron transfer (ET) process (Scheme 5.2).¹⁷³ Direct excitation of the UV-filters leads to an ET from their triplet excited states into the vacant conduction band (CB) of TiO₂. The e_{CB}^- can subsequently generate $\text{O}_2^{\bullet -}$ (equation 5.2), which can initiate photodecomposition. Likewise, the unstable radical cation of the UV-filter molecule formed can photodegrade.



Scheme 5.2. ET involving TiO₂.

The enhanced photolability of **BMDM** in the presence of TiO₂ suggests that this ET process preferentially, if not exclusively, occurs with this UV-filter. In contrast, triplet excited **OC** is not able to inject an electron into the valence band of the semiconductor TiO₂, thus retaining its photostability.

The significantly reduced photodegradation of **OC** in the presence of **BMDM** and nano-TiO₂ has not been reported in the literature. These results suggest a selective reactivity of nano-TiO₂ for **BMDM**. The concentrations of **BMDM** and **OC** are relatively low, resulting due to dilution with methanol. Although there is no direct adsorption of either **BMDM** or **OC** onto TiO₂, the hydroxyl groups of the enol-forms of **BMDM** may result in H-bonding or electrostatic interactions with TiO₂ resulting in an attraction of **BMDM** for the TiO₂ molecules.¹⁷⁴ **BMDM** would thus accumulate close to the TiO₂ particles. As described in Chapter 3, **BMDM** is available at 90.9 % in its enol-form in methanol. The short-lived generated ROS on the surface of TiO₂ may therefore react preferentially with **BMDM**, because of its close proximity. This unprecedented selectivity may alternatively be explained through the ET scenario described above and by the ability of **BMDM** to act as an electron donor in this process.

OC remained largely photostable with the exception of its individual irradiation in the presence of nano-TiO₂, which is attributed predominantly to its larger surface area, reduced e_{CB}⁻/h_{VB}⁺ recombination and faster charge transfer.¹⁷¹ Due to the small particle size of nano-TiO₂ an even dispersion in methanol occurs, thus allowing for competitive absorption of light. Since ROS are generated on the surface of the TiO₂ particles, a larger surface area and the associated smaller particle size consequently result in a reduced photostability.¹⁷² However, in the presence of **BMDM**, **OC** retained photostability, even in the presence of nano-TiO₂.

5.3.2. Influence of Coated TiO₂ and Vitamin E on Photodegradation

The aim was to improve the photostability of **BMDM** and **OC**, by the inclusion of silica coated TiO₂ and the addition of vitamin E to the chemical UV-filters, separately and in combination.

5.3.2.1. Butyl methoxy dibenzoylmethane (BMDM)

Photodegradation profiles of **BMDM**, together with the coated TiO₂ and vitamin E, are shown in Figure 5.9. The corresponding recovery data \pm SD are listed in Table 5.5. Statistical analysis showed that there is a significant difference in recovery between all three analysed samples after four hours of irradiation ($F_{2,6} = 276.675$, $p < 0.000$).

The presence of coated TiO₂ decreased the **BMDM** recovery by about 15 %, while the addition of vitamin E resulted in a further, significant decrease in **BMDM** recovery of about 4 %.

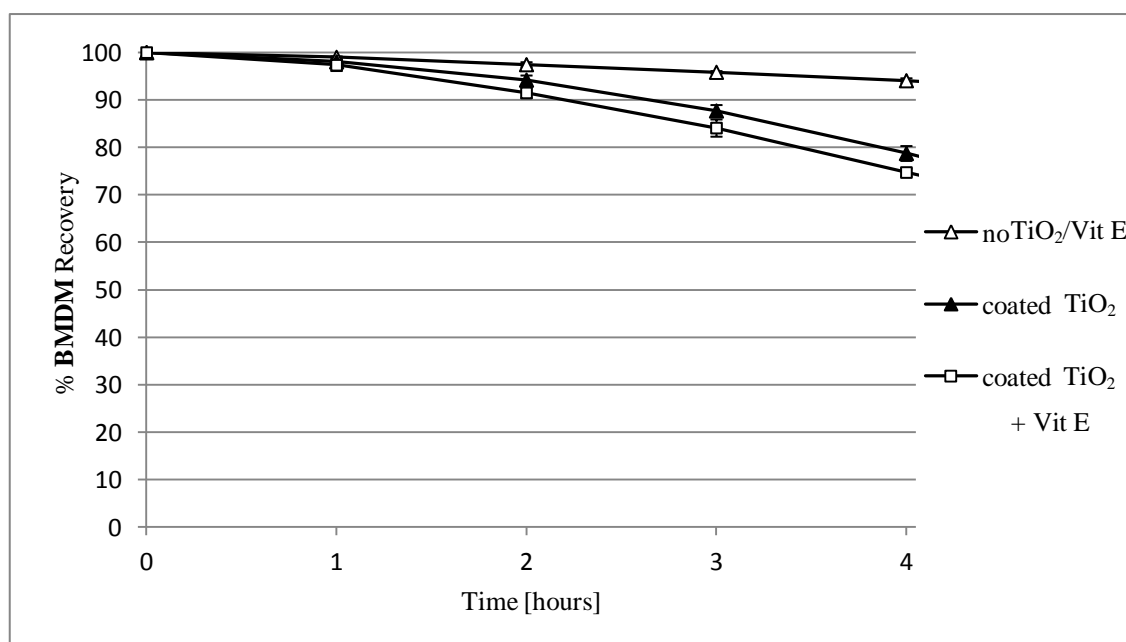


Figure 5.9. Photodegradation profile of **BMDM** in the presence and absence of coated TiO₂ and vitamin E (Vit E).

Table 5.5. % Recovery \pm SD of **BMDM** in the presence and absence of coated TiO₂ and vitamin E (Vit E).

Time [hours]	% Recovery of BMDM (n = 3) \pm SD		
	no TiO ₂ / Vit E	coated TiO ₂	coated TiO ₂ + Vit E
0	100.00	100.00	100.00
1	99.01 \pm 0.18	98.05 \pm 0.47	97.34 \pm 1.22
2	97.46 \pm 0.52	94.21 \pm 0.96	91.51 \pm 1.11
3	95.85 \pm 0.26	87.71 \pm 1.24	84.10 \pm 1.81
4	94.08 \pm 0.51	78.75 \pm 1.57	74.74 \pm 0.83

Degradation profiles and corresponding recovery data of **BMDM**, irradiated in combination with **OC**, in the presence of coated TiO₂ and vitamin E are shown in Figure 5.10 and Table 5.6.

After four hours of irradiation, the recovery of **BMDM** was 95.18 %, which was decreased by the addition of coated TiO₂ by 17.52 %. Further addition of vitamin E increased the recovery again by about 3 % (Table 5.6). These differences in degradation rates are all statistically significant ($F_{2,6} = 468.392$, $p < 0.000$).

In the presence of silica coated TiO₂, no adsorption of **BMDM** was detected after one, six or 24 hours, with a **BMDM** concentration of 100.07 % after 24 hours, compared to a sample containing no TiO₂. Physical adsorption is thus negligible and does not contribute to the removal of **BMDM**.

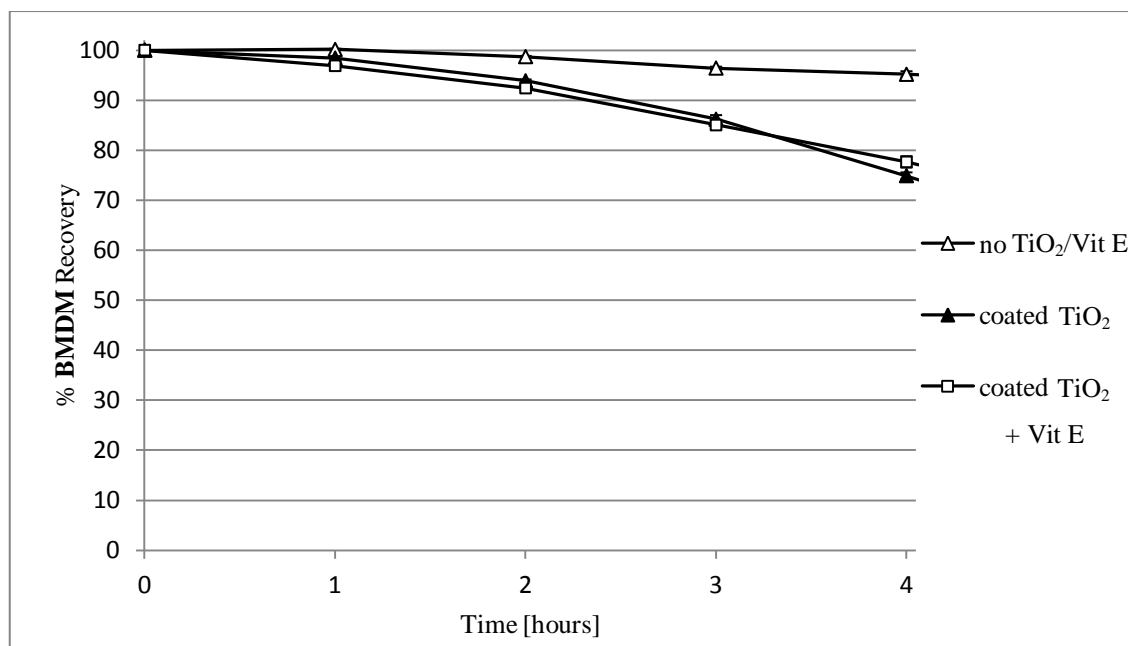


Figure 5.10. Photodegradation profile of **BMDM** in a combination with **OC** in the presence and absence of coated TiO₂ and vitamin E (Vit E).

Table 5.6. % Recovery ± SD of **BMDM** in a combination with **OC** in the presence and absence of coated TiO₂ and vitamin E (Vit E).

Time [hours]	% Recovery of BMDM (n = 3) ± SD		
	no TiO ₂ / Vit E	coated TiO ₂	coated TiO ₂ + Vit E
0	100.00	100.00	100.00
1	100.15 ± 0.13	98.43 ± 0.46	96.88 ± 0.34
2	98.71 ± 0.14	93.87 ± 0.28	92.42 ± 0.38
3	96.42 ± 0.28	86.19 ± 0.82	85.03 ± 0.39
4	95.18 ± 0.60	74.91 ± 0.65	77.66 ± 1.13

Addition of the antioxidant vitamin E to a combination of coated TiO₂ and **BMDM**, irradiated with and without **OC**, did not result in an increased **BMDM** recovery. While in combination with **OC**, the **BMDM** recovery was increased by about 3 % due to vitamin E, the irradiation without **OC** resulted in a reduced **BMDM** recovery of 4 %. Only a small increase in **BMDM** recovery was expected because the addition of vitamin E only has an effect on the oxidation reactions. However, due to the presence of TiO₂, many other competing degradation reactions may occur. Figure 5.11 shows the UV-absorption spectrum of vitamin E.

It is important to note that vitamin E in methanol degraded completely within the first hour of irradiation. This rapid degradation provides another explanation as to why vitamin E increased **BMDM** recovery only by 3 % in combination with **OC**. A rapid degradation of vitamin E in methanol was also reported by Sabliov et al.¹⁷⁵ After six hours of irradiation only about 20 % of vitamin E, dissolved in methanol, was recovered, while irradiated in its pure, undissolved form 83 % and dissolved in hexane 68 % were recovered. As light source a Blak Ray 1B 100P MDSK long wave UV-lamp (100 W) at 365 nm was used. This light source emits UV-light only in the UVA-range, while the UV immersion lamp TQ 150, used in this study, emits various wavelengths over 300 nm, resulting in a greater overlap with the λ_{max} of vitamin E (290 nm). This, in combination with the increased power output of the TQ 150 lamp, resulted in a more rapid vitamin E degradation.¹⁷⁵

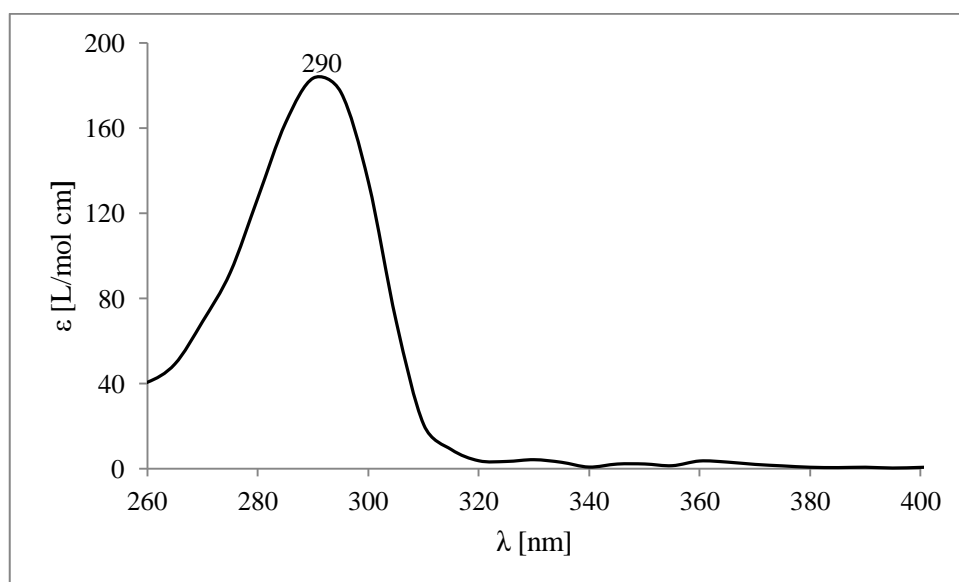
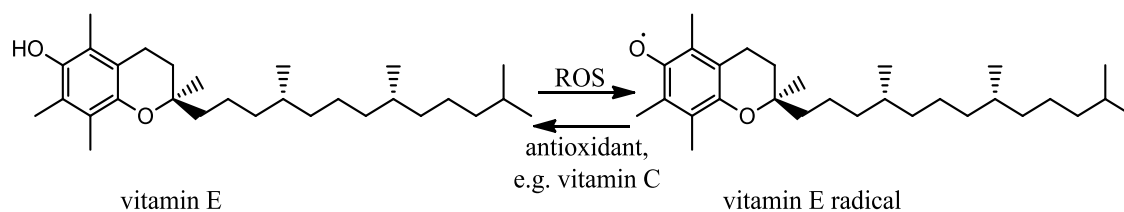


Figure 5.11. UV-absorption spectrum of vitamin E.

The antioxidant vitamin E, its ability to scavenge ROS and its subsequent regeneration is shown in Scheme 5.3. Due to the rapid photodegradation of vitamin E in this study, its antioxidant effect was not observed and it was therefore unable to function as ROS scavenger. In order to regenerate vitamin E from the radical a second antioxidant is required. Most commonly vitamin C is used in combination for this purpose⁹⁵, but EDTA⁹⁴ has also been used. The absence of an antioxidant to regenerate vitamin E in this study also explains the lack of an increase in **BMDM** recovery in the presence of vitamin E, both with and without **OC**.

Although the differences in **BMDM** recovery, with and without **OC**, are significant, they are negligible and can be disregarded.



Scheme 5.3. Formation of vitamin E radical and regeneration to vitamin E.

5.3.2.2. Octocrylene (**OC**)

Degradation profiles and corresponding data for the irradiation of **OC** can be found in Figure 5.12 and Table 5.7. Addition of coated TiO_2 and vitamin E resulted in no significant difference in the degradation of the UV-filter **OC** ($F_{2,6} = 1.228$, $p = 0.357$).

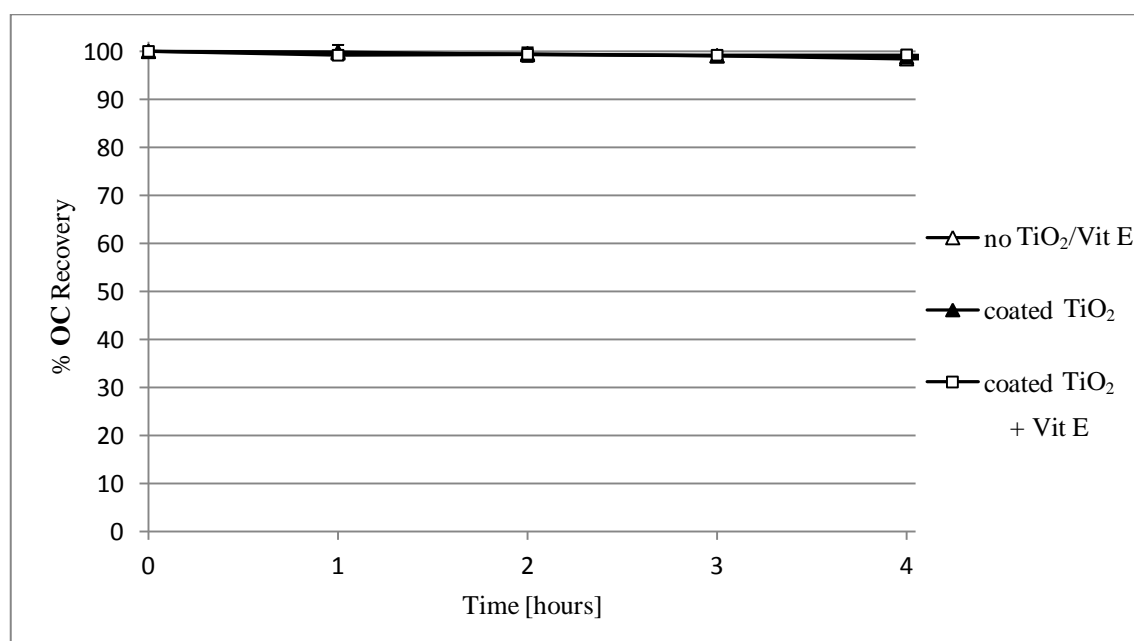


Figure 5.12. Photodegradation profile of **OC** in the presence and absence of coated TiO_2 and vitamin E (Vit E).

Table 5.7. % Recovery \pm SD of OC in the presence and absence of coated TiO₂ and vitamin E.

Time [hours]	% Recovery of OC (n = 3) \pm SD		
	no TiO ₂ / Vit E	coated TiO ₂	coated TiO ₂ + Vit E
0	100.00	100.00	100.00
1	99.70 \pm 1.37	99.98 \pm 1.36	99.20 \pm 0.62
2	99.55 \pm 0.18	99.33 \pm 1.50	99.40 \pm 0.65
3	99.07 \pm 0.73	99.09 \pm 0.21	99.20 \pm 0.77
4	98.46 \pm 0.95	98.85 \pm 0.44	99.28 \pm 0.36

The irradiation in combination with **BMDM** also resulted in no significant photodegradation of UV-filter OC in the presence or absence of coated TiO₂ and vitamin E, as seen in Figure 5.13 and Table 5.8 ($F_{2,6} = 4.786$, $p = 0.057$).

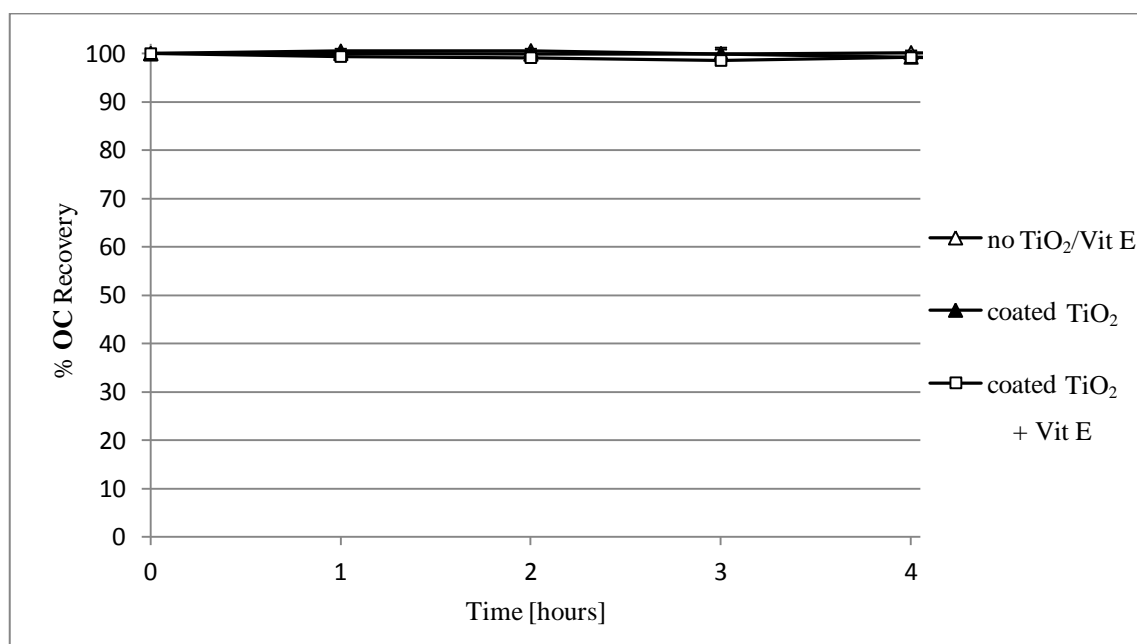


Figure 5.13. Photodegradation profile of OC in a combination with **BMDM** in the presence and absence of coated TiO₂ and vitamin E (Vit E).

Table 5.8. % Recovery \pm SD of **OC** in a combination with **BMDM** in the presence and absence of coated TiO₂ and vitamin E (Vit E).

Time [hours]	% Recovery of OC (n = 3) \pm SD		
	no TiO ₂ / Vit E	coated TiO ₂	coated TiO ₂ + Vit E
0	100.00	100.00	100.00
1	100.52 \pm 0.48	100.05 \pm 0.51	99.40 \pm 0.29
2	100.60 \pm 0.40	99.91 \pm 0.26	99.17 \pm 0.77
3	99.95 \pm 0.91	99.97 \pm 1.26	98.58 \pm 0.35
4	100.20 \pm 0.44	99.30 \pm 0.38	99.18 \pm 0.50

Dark experiments showed that there was no adsorption of **OC** onto coated TiO₂ after one, six or 24 hours, with exactly the same **OC** concentration measured before and after 24 hours in the presence of coated TiO₂. Results indicate that physical adsorption does not contribute to the removal of **OC**.

In the first part of this study **OC** only degraded in the presence of highly reactive nano-TiO₂, but not in the presence of the less reactive micro-TiO₂. Coated TiO₂ is designed to cause less (if any) photodegradation of chemical UV-filters compared to that of the untreated TiO₂.⁸⁶ Therefore it was expected that **OC** would remain stable in the presence of coated TiO₂ and vitamin E, but these experiments were carried out for completeness.

5.3.3. Kinetic Studies

Photodegradation kinetics for **BMDM** and **OC** were determined using the same UV-filter concentration (60 mg/mL = OC: 16.60×10^{-5} mol/L and BMDM: 19.33×10^{-5} mol/L) and photoreactor as in above described studies. Instead of the pyrex glass ($\lambda \geq 300$ nm) vessel, a quartz glass ($\lambda \geq 200$ nm) vessel was used to accelerate the photodegradation, due to exposing the UV-filters to a wider UV-irradiation range. Photodegradation profiles of both UV-filters, from which kinetic data were calculated, are shown in Figure 5.14 (page 136) and 5.15 (page 137), respectively. The initial part of all degradation profiles is linear and therefore follows zero-order kinetics. Due to a high initial UV-filter concentration, the degradation was influenced only by the rate of photon supply i.e. the light intensity, resulting in the described linear profile. During irradiation, the UV-filter concentration decreased and this reduced concentration then became the rate controlling factor. The kinetics of the degradation profiles follow a mixed zero- and first-order and k and $t_{1/2}$ for **BMDM** and **OC** are calculated for the first-order reaction.

The first-order rate law is:

$$k[A] = -\frac{d[A]}{dt} \quad (5.7)$$

with: k = rate constant [min^{-1}]

$[A]$ = UV-filter concentration at time t

t = time [min]

and after integration:

$$\ln\left(\frac{[A]}{[A]_0}\right) = -kt \quad (5.8)$$

with: $[A]_0$ = concentration at time zero

When $\ln([A]/[A]_0)$ is plotted against t , the slope of the straight line is $-k$.

The half-life $t_{1/2}$ can be determined from the equation:

$$t_{\frac{1}{2}} = \frac{\ln 2}{k} \quad (5.9)$$

Instead of using concentrations at time zero and time t , the peak areas, at time zero and time t were used to determine the degradation kinetics.

5.3.3.1. *Butyl methoxy dibenzoylmethane (BMDM)*

Degradation profiles of **BMDM**, irradiated alone and in combination with **OC**, show linearity up to 20 minutes of irradiation (Figure 5.14). Irradiated alone, the change of the kinetic order occurs at this time and 90 % of **BMDM** remained. At a **BMDM** recovery of about 70 % the concentration becomes the only rate controlling factor and the degradation follows first-order kinetics. When irradiated in combination with **OC**, this change in the kinetic order occurs after about 50 minutes, when about 80 % of **BMDM** remained. The degradation starts to follow first-order kinetics, when a **BMDM** recovery of 60 % is achieved.

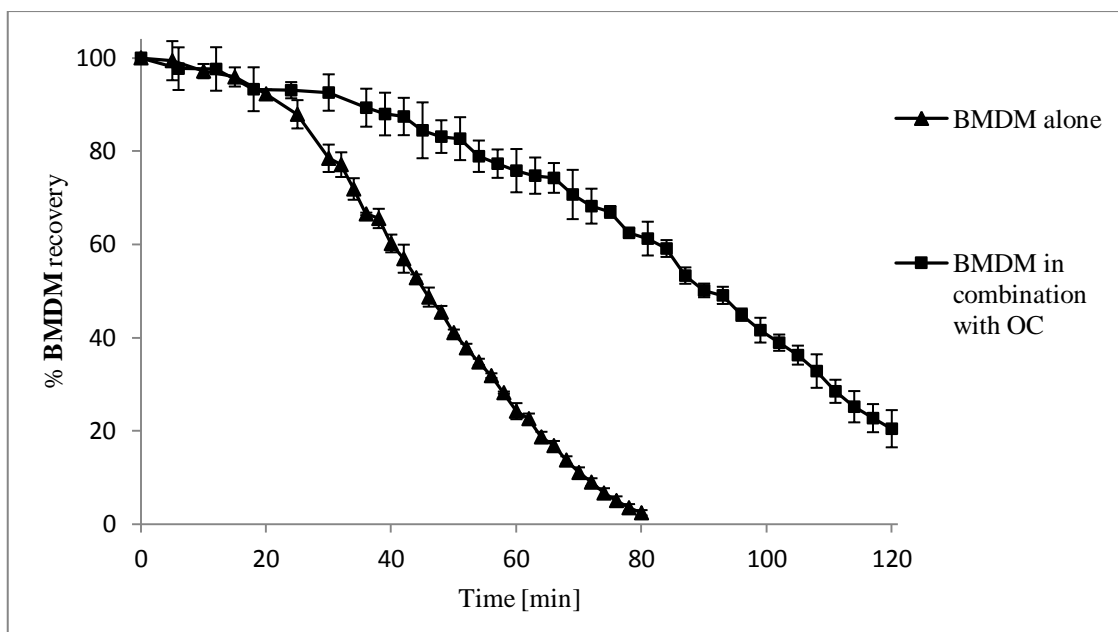


Figure 5.14. BMDM recovery in % \pm SD, alone and in combination with OC.

5.3.3.2. Octocrylene (OC)

Figure 5.15 shows the degradation profiles of OC, irradiated alone and in combination with BMDM. Again, the first 20 minutes of irradiation, no difference in the degradation profiles was observed, which were linear. The degradation profile for OC, irradiated alone, remains linear until about 85 % of OC remained, and to 80 %, when irradiated in combination with BMDM. The concentration becomes the only rate controlling factor and degradation follows first-order kinetics at OC recoveries of 70 and 60 %, irradiated alone and in combination with BMDM, respectively.

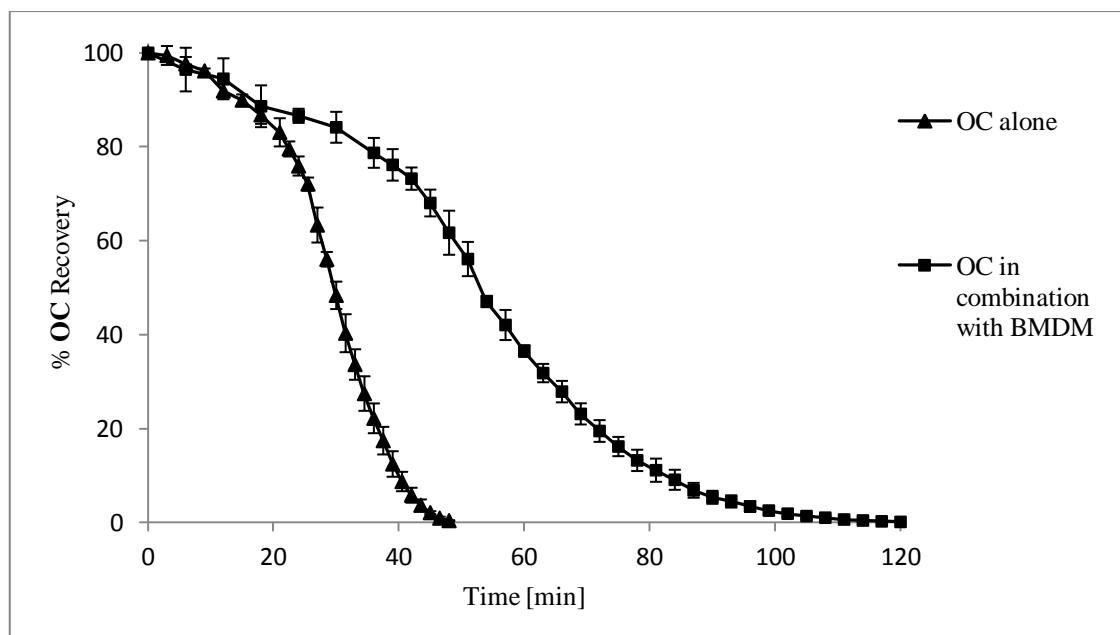


Figure 5.15. OC recovery in % \pm SD, alone and in combination with **BMDM**.

For both UV-filters, irradiated alone and in combination, the peak area at time t (PA_t) is divided by the peak area at time zero (PA_0) and the \ln of this value is then plotted against time (Figure 5.16). Using equation (5.8) and (5.9) k and $t_{1/2}$ (page 135) were calculated and are listed in Table 5.9. It is notable that the rate constants of **BMDM** and **OC** irradiated alone are about double that of the rate constants of **BMDM** and **OC**, than when irradiated in combination.

This difference can be explained in terms of the UV-filter concentration. As described above, the initial degradation rate was influenced only by the rate of photon supply, due to the high UV-filter concentration. When both UV-filters were irradiated in combination the overall UV-filter concentration was double, with both UV-filters competing for the same number of photons supplied. Therefore the time until the critical concentration is reached and the kinetic order changes, is longer than when UV-filters were irradiated separately. This is confirmed by the $t_{1/2}$ values, which are about double for **BMDM** and **OC** in the combination, compared to $t_{1/2}$ for both UV-filters irradiated separately.

The degradation order of **BMDM** confirmed findings by Mbah,¹⁷⁶ who studied the degradation of **BMDM** at 60 °C in phosphate buffer (pH 7.4 - 10.0), showing first order degradation kinetics. The degradation was found to be hydroxide ion dependant and at lower pH-values (2.0 - 5.0) **BMDM** was stable. A mixed zero- and first-order was however not found although the initial **BMDM** concentration was higher ($160 \mu\text{g/mL} = 51.55 \times 10^{-5} \text{ mol/L}$)¹⁷⁶ than in this study

(60 $\mu\text{g/mL} = 19.33 \times 10^{-5}$ mol/L). No degradation kinetic studies for UV-filter **OC** have been reported.

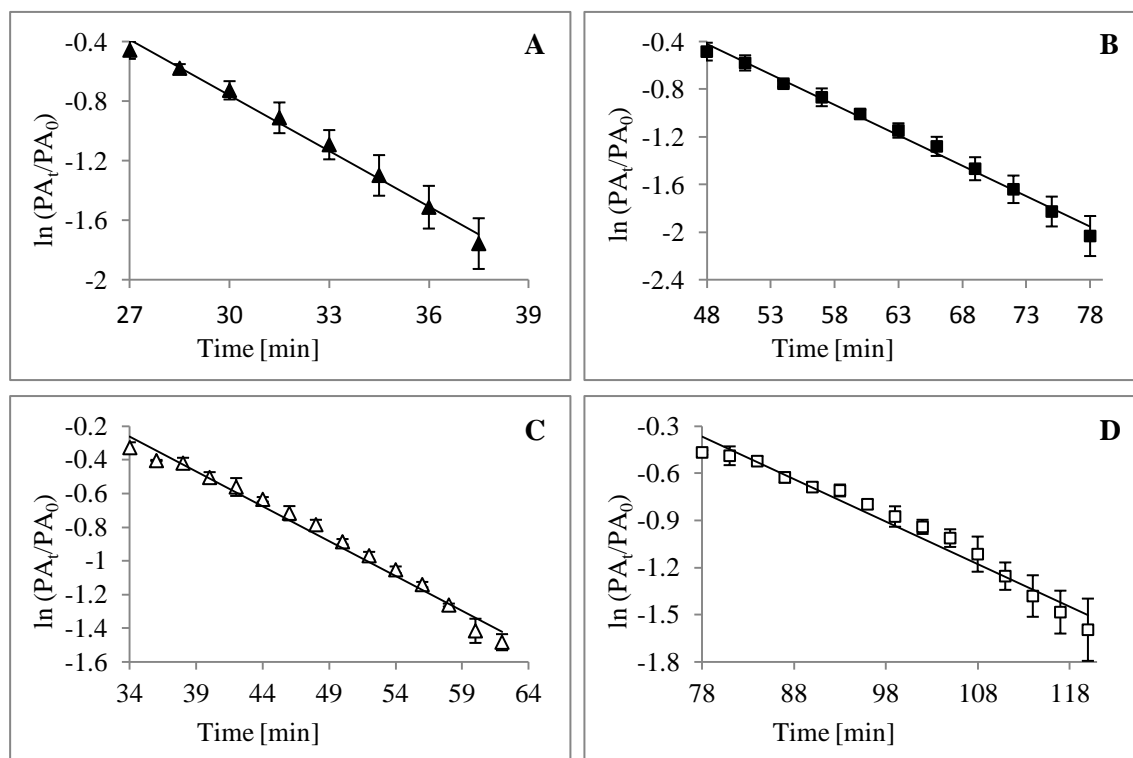


Figure 5.16. First order kinetic plots of **A: OC** alone; **B: OC** in combination; **C: BMDM** alone; **D: BMDM** in combination, plotted as $\ln(PA_t/PA_0) \pm SD$ against time.

Table 5.9. First-order kinetic data for **BMDM** and **OC**.

UV-filter	$k \pm SD$ [min^{-1}]	$t_{1/2} \pm SD$ [min]	R^2
BMDM	0.0415 ± 0.0018	16.73 ± 0.70	0.9844
BMDM in combination	0.0270 ± 0.0044	26.07 ± 3.97	0.9718
OC	0.1242 ± 0.0148	5.63 ± 0.70	0.9909
OC in combination	0.0511 ± 0.0031	13.61 ± 0.85	0.9929

5.3.4. Identification of Major Photodegradants using LC-MS and FTMS

Irradiation of **BMDM** in the photoreactor, using pyrex and quartz glass vessels, resulted in the generation of two major and several minor photodegradants (Figure 5.17). Analyses of both, the positive and negative mode LC-MS and FTMS data, confirmed the molecular weights of two photodegradants: **BMDM-1** (4-methoxy benzoic acid) at a retention time of 3.5 minutes (λ_{max} 253 nm, negative ion 151 m/z) and **BMDM-2** (4-*t*-butyl benzoic acid) at a retention time of 4.5

minutes (λ_{max} 237 nm, negative ion 177 m/z). In Table 5.10 (page 140), the observed ions in positive and negative mode, the expected molecular weights, the proposed formulas and structures of both photodegradants are presented. Both structures have been reported in previous studies and thus the proposed formulas and structures are confirmed.^{37,61,63} As described previously, the degradation mechanism involves the conversion of the enol-form of **BMDM** to the diketo-form. Scheme 5.4 shows the mechanism of photodegradation of **BMDM** to **BMDM-1**, t-butylbenzene and acetic acid *via* the diketo-form (i). The Norrish-I cleavage can also occur on the other side (ii) of the methylene group, resulting in the second detected photodegradant **BMDM-2** and methoxy benzene. Both monosubstituted benzenes, which were expected to be present, could not be detected.

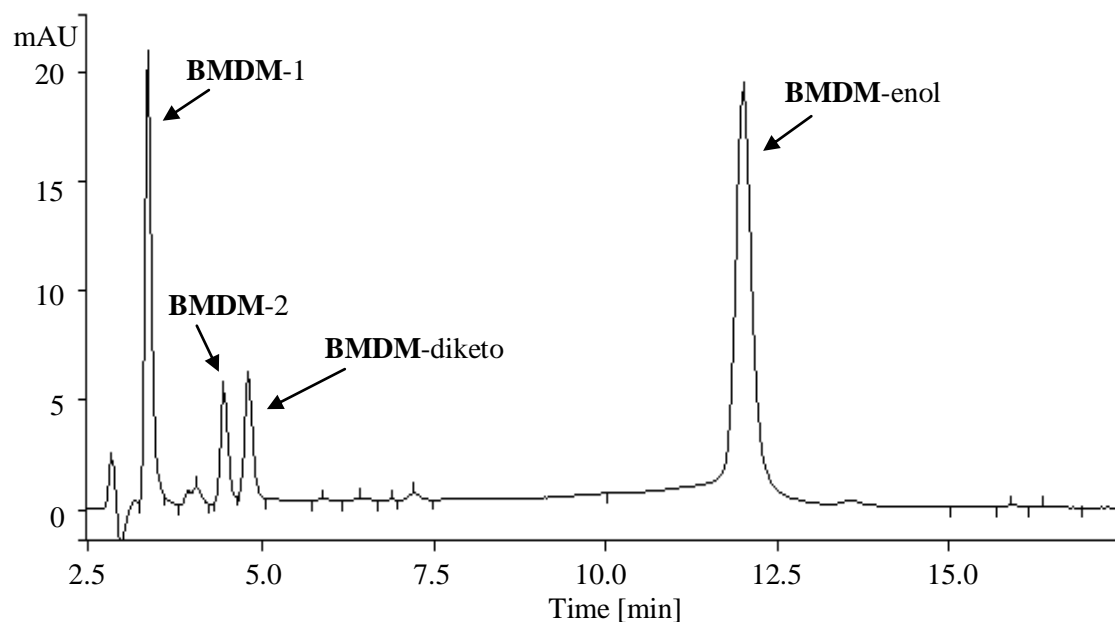
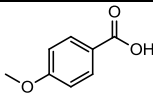
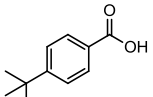
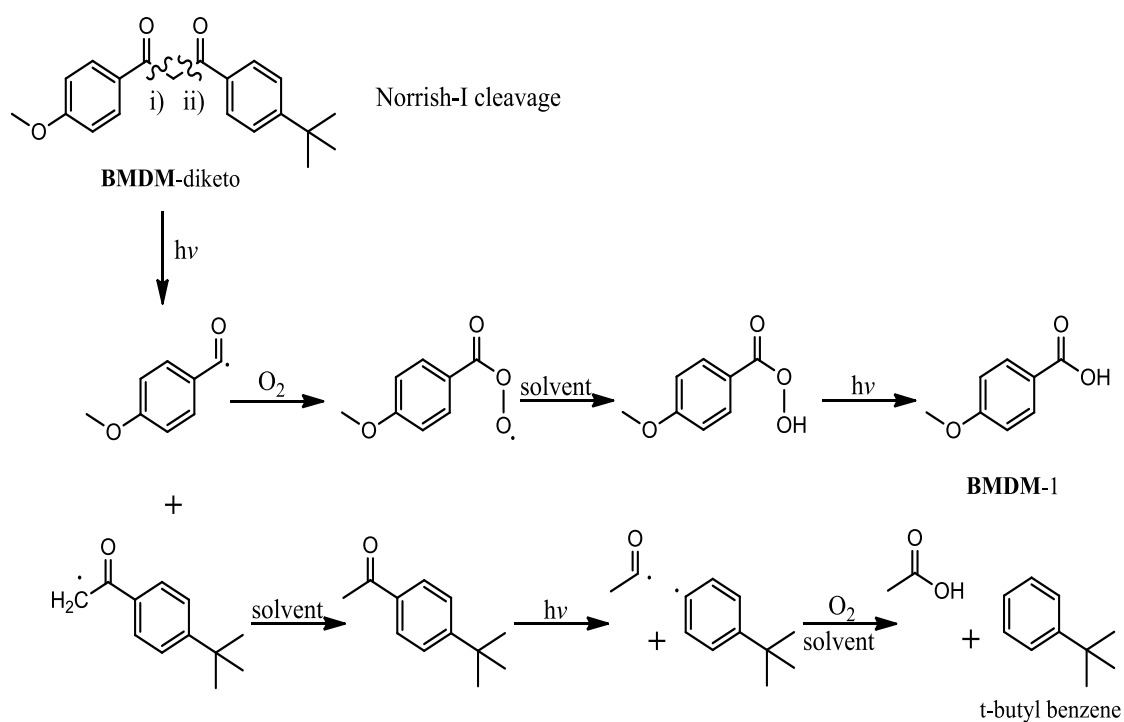


Figure 5.17. HPLC chromatogram of **BMDM** after four hours irradiation, detected at 253 nm.

Table 5.10. Major photodegradants of **BMDM**.

Photodegradant	Observed ions LC-MS/FTMS [<i>m/z</i>]	Expected molecular weights [<i>m/z</i>]	Proposed molecular formula	Proposed molecular structure
BMDM-1	150.9/151.0399 (negative mode)	151.0401 (Δ 1 ppm) [M-H] ⁻	C ₈ H ₈ O ₃	
BMDM-2	177.0/177.0920 (negative mode)	177.0921 (Δ 1 ppm) [M-H] ⁻	C ₁₁ H ₁₄ O ₂	
	nd/201.0898 (positive mode)	201.0886 (Δ 6 ppm) [M+Na] ⁺		

nd = not detected



Scheme 5.4. Photodegradation *via* **BMDM** diketo-form into **BMDM-1** (Norrish-I cleavage).⁶¹

The LC-MS system, equipped with a PDA detector allowed an overlay of the total ion chromatogram with the UV-chromatogram. Photodegradant peaks from the UV-chromatogram were assigned to peaks in the total ion chromatogram and mass spectra for **BMDM-1** and

BMDM-2 were detected and are shown in Figures 5.18 and 5.19, respectively. Both mass spectra were detected in negative mode.

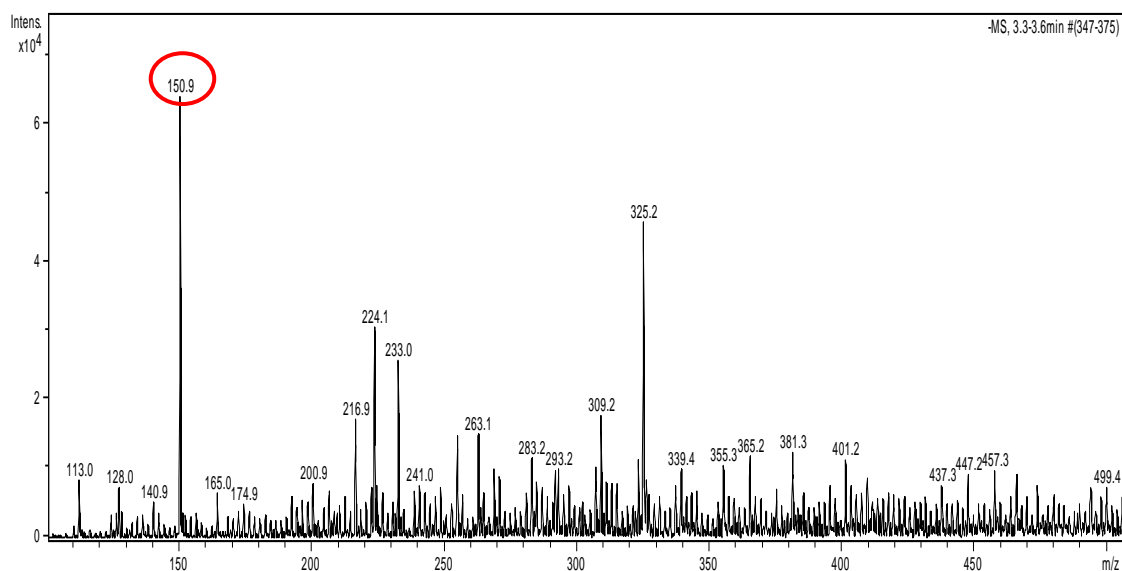


Figure 5.18. Mass spectrum with the observed ion for **BMDM-1** (m/z 150.9).

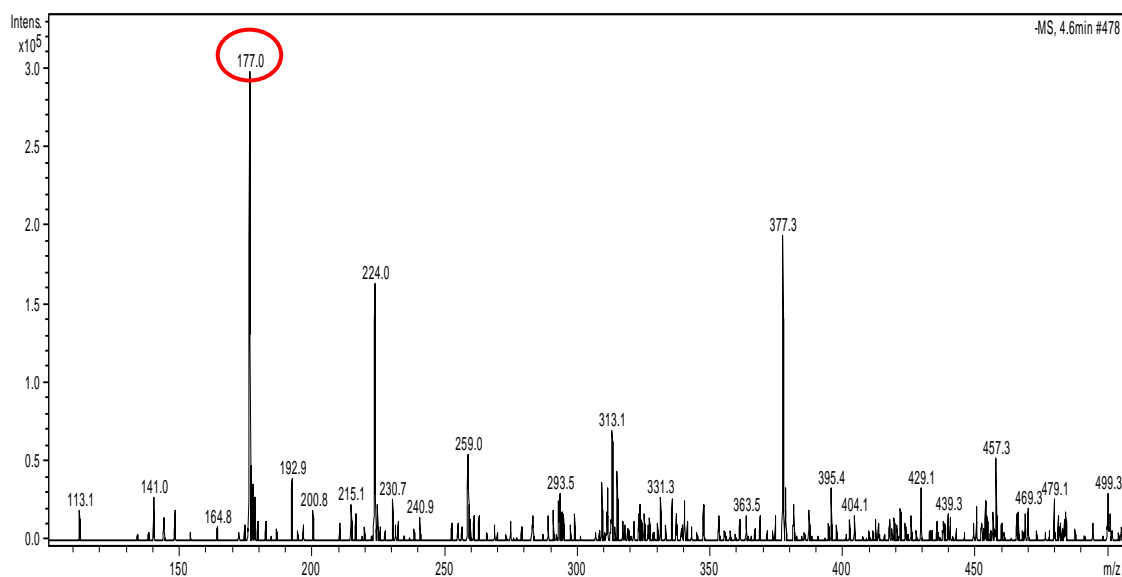


Figure 5.19. Mass spectrum with the observed ion for **BMDM-2** (m/z 177.0).

After irradiation of UV-filter **OC** through quartz glass, one major photodegradant was detected (**OC-1**), namely methyl-2-cyano-3,3-diphenylacrylate (Figure 5.20, page 142). The molecular

weight of this photodegradant was determined by LC-MS, and the molecular formula and structure proposed (Table 5.11). To confirm the molecular formula the sample was analysed by FTMS. The observed weight of m/z $[M+Na]^+$ 286.0845 shows a difference of only 2.4 ppm and thus within the error of the measurement from the expected weight (m/z 286.0838), confirming its identity. In Scheme 5.5 (page 144) a possible degradation mechanism, *via* a Norrish-II cleavage is proposed, where **OC-1** is generated after a self-catalysed thermal Fisher esterification in the presence of methanol.¹⁷⁷ 2-Ethylhex-1-ene, as a proposed by-product, could neither be detected with the UV-detector nor by LC-MS/FTMS. On irradiation through pyrex glass the photodegradant **OC-1** was not detected, although the addition of nano-TiO₂ resulted in 37.79 % degradation after four hours of irradiation. Pyrex glass blocks UV-light under 300 nm, while quartz glass transmits UV-light over 200 nm, which is able to excite the $n \rightarrow \pi^*$, necessary for the Norrish-II cleavage. No major photodegradants for **OC** were identified during irradiation studies, using the pyrex glass vessel, which was confirmed by findings of Ricci et al.⁵³ After UV-irradiation in pyrex tubes using Luzchem UVA lamps in the presence of nano-TiO₂, no photodegradants for **OC** were detected by GC or TLC, although a degradation of 45 % occurred. However, elemental analysis of the solid TiO₂, which was recovered after irradiation, showed the presence of carbon, indicating that photodegradants were present, but were not detectable by GC or TLC.⁵³ The generation of **OC-1** after irradiation with UV-light ≥ 200 nm was confirmed by Karlsson et al.¹⁷⁸ As light source a falling film photoreactor, equipped with a medium pressure mercury lamp (200 - 600 nm) and an irradiation time of six hours (temperature 20 - 25 °C) was employed by these authors. **OC** was irradiated in ethanol and in cyclohexane in the presence of benzylamine forming ethyl-2-cyano-3,3-diphenylacrylate and N-benzyl-2-cyano-3,3-diphenylacrylamide, respectively, similarly to the photodegradant methyl-2-cyano-3,3-diphenylacrylate detected in this study. In the reported study¹⁷⁸ the same photodegradants were detected using a Solarlux™ solar simulator (300 - 400 nm) at an irradiation time of 30 hours (temperature 43 - 45 °C). As UV-light over 300 nm cannot cause the $n \rightarrow \pi^*$ transition and thus the Norrish-II cleavage, these same photodegradants may occur *via* another mechanism. Karlsson et al. did not propose a degradation mechanism, but due to the high temperature and the long irradiation time, a thermal transesterification may have occurred.¹⁷⁸ These results are not comparable with those conditions in pyrex glass in this study, as the temperature in the photoreactor only reached 20 ± 1 °C and the irradiation time was four hours.

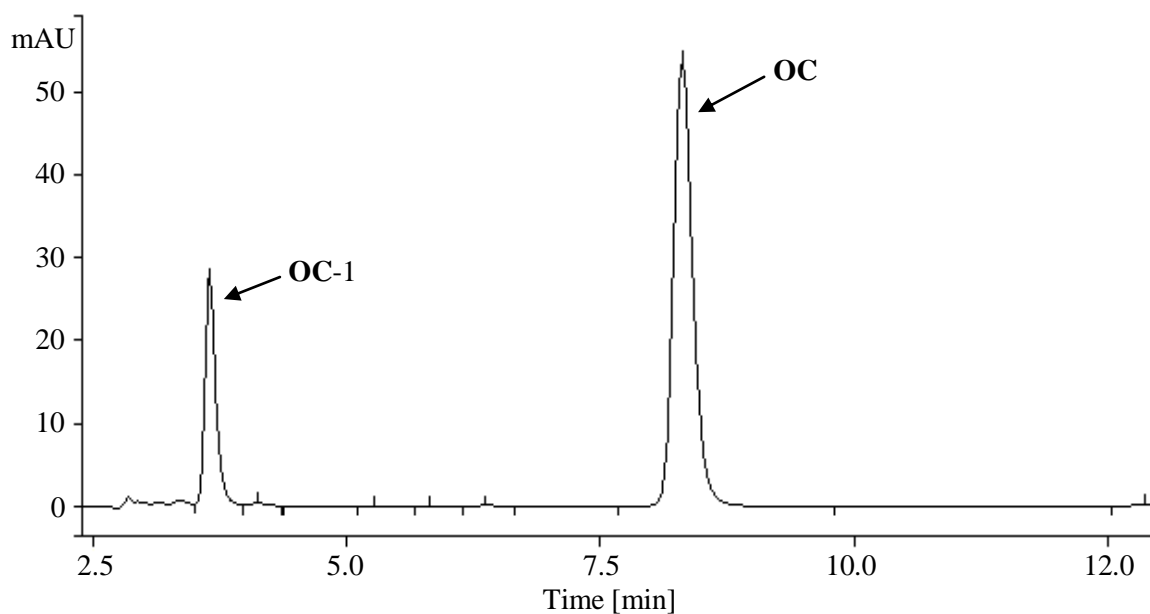
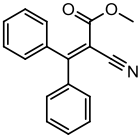
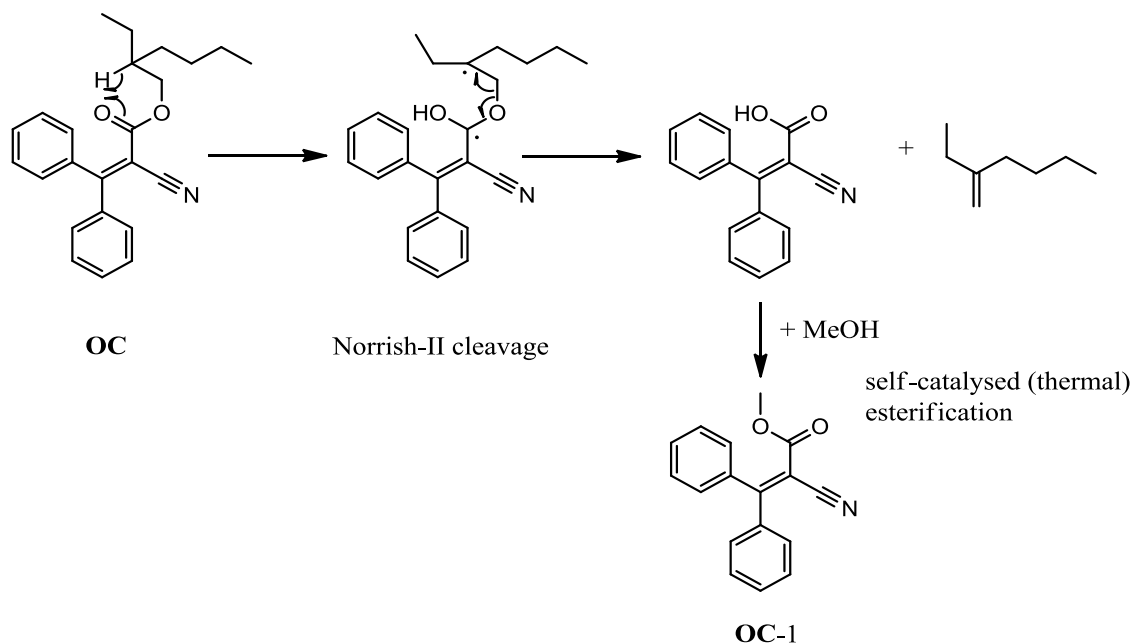


Figure 5.20. HPLC chromatogram of **OC** after 24 minutes irradiation, detected at 303 nm.

Table 5.11. Photodegradant of **OC**.

Photodegradant	Observed ions LC-MS/FTMS [<i>m/z</i>]	Expected molecular weight [<i>m/z</i>]	Proposed molecular formula	Proposed molecular structure
OC-1	286.3/286.0845	286.0838 (Δ 2 ppm) [M+Na] ⁺	C ₁₇ H ₁₃ O ₂ N	



Scheme 5.5. Proposed degradation mechanism of **OC** (Norrish-II cleavage) after irradiation in methanol (quartz glass).

OC-1 (m/z 286.3), was detected in positive mode and Figure 5.21 shows its mass spectrum. A pattern of molecular weights (m/z 261.3, 305.4, 349.5, 393.5) was detected throughout the mass spectrum, which is attributed to contaminants in the solvent and/or the system. Due to the very high sensitivity of the MS the presence of contaminants, such as plastics, are a common problem. Acetic acid, which was part of the mobile phase, increased the conductivity of the ions in the MS and therefore also increased the likelihood for contaminants.

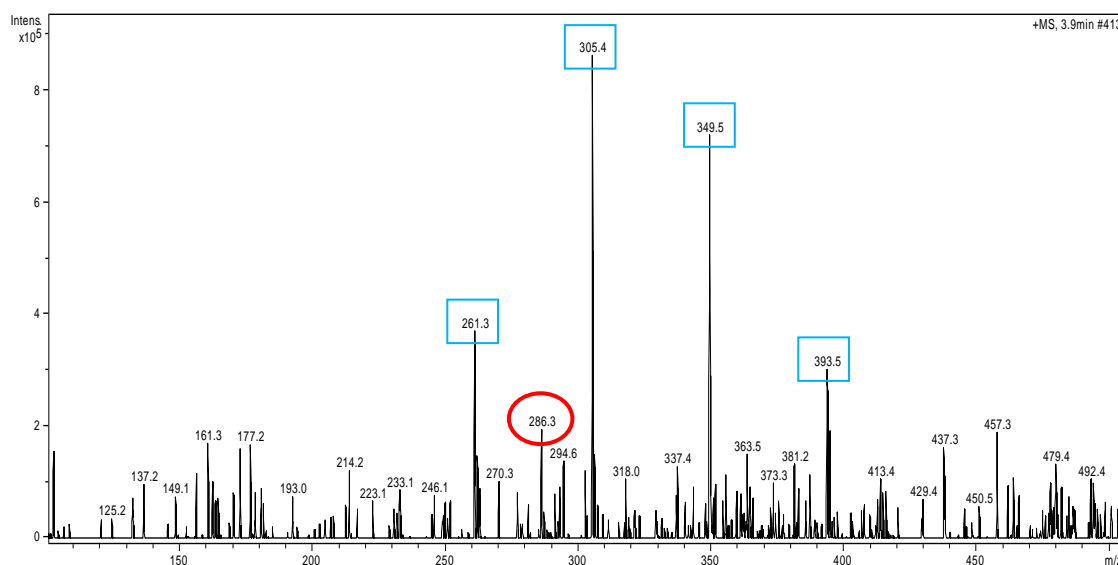


Figure 5.21. Mass spectrum with the observed ion for **OC-1** (m/z 286.3) and other detected molecular weights, which are part of a pattern (m/z 261.3, 305.4, 349.5, 393.5).

5.4. Summary

The photostability of **BMDM** and **OC**, alone and in combination, in the presence of TiO₂ and vitamin E was investigated in methanol. In addition, photodegradation kinetics of both chemical UV-filters and the identity of their major photodegradants are reported.

TiO₂ particle size influenced the photostability of **BMDM** and **OC**, with micro-TiO₂ having less of an effect on their photodegradation than the nano-TiO₂. Irradiated separately and in combination, the presence of nano-TiO₂ resulted in a significant lower recovery rate for **BMDM** and **OC** than for the micro-TiO₂. While **BMDM** degraded without TiO₂, with micro-, nano- and coated TiO₂, **OC** only degraded in the presence of nano-TiO₂. The antioxidant vitamin E was added to the combination of chemical UV-filters as was coated TiO₂ to investigate their potential to reduce photodegradation. Due to the rapid degradation of vitamin E itself, no meaningful influence of vitamin E on the photodegradation of **BMDM** or **OC** occurred.

Kinetic analyses showed that degradation profiles of **BMDM** and **OC** follow mixed zero- and first-order. Initial zero-order reactions were due to the high UV-filter concentration and degradation was only influenced by the rate of photon supply.

Photodegradation of **BMDM** resulted in the generation of two major and several minor photodegradants, while the generation of one major **OC** photodegradant occurred only after irradiation with lower wavelengths, through quartz glass ($\lambda \geq 200$ nm). Major photodegradants, identified as 4-methoxy benzoic acid and 4-*t*-butyl benzoic acid for **BMDM** and methyl-2-cyano-3,3-diphenylacrylate for **OC**, were determined by LC-MS and confirmed by FTMS.

The findings in this chapter clearly show that the TiO₂ particle size influences the photostability of the chemical UV-filters **BMDM** and **OC** in methanol. The following chapter will present photostability studies with both chemical UV-filters and all three types of TiO₂, incorporated into a developed topical microemulsion, using a solar simulator as light source.

Chapter 6

Microemulsion - Photostability and Skin Penetration of Chemical UV-filters

6.1. Introduction

A stable topical microemulsion was prepared and the photostability and skin penetration of its component chemical UV-filters investigated.

Microemulsions are transparent, containing both oily and aqueous components, surfactants and in some cases co-surfactants. Surfactants are characterised by the hydrophilic-lipophilic balance (HLB), which indicates their miscibility in the oily or aqueous component of the emulsion. Low HLB values signify lipophilic surfactants, which are generally used for W/O systems, while surfactants with a HLB value over 12 are hydrophilic and are required in O/W systems. Co-surfactants are added to a microemulsion to further reduce the interfacial tension and to ensure that the concentrations of the surfactant are within appropriate limits.¹⁰⁹ Microemulsions offer a number of advantages over coarse emulsions or macroemulsions, including the ease of preparation, due to spontaneous formation and thermodynamic stability.^{110,179} Table 6.1 compares important variables between these two emulsions. The dynamic structure of a microemulsion results in constant and spontaneous fluctuations, which makes it impossible to divide the microemulsion into an oily or aqueous phase, even when the water- or oil-rich fractions are often described as “phases”.¹¹⁰ One disadvantage of the formulation of microemulsions for pharmaceutical use is, that it is difficult to find appropriate surfactants and co-surfactants, which are both non-toxic and are able to produce a thermodynamically stable microemulsion.¹⁷⁹

Table 6.1. Comparison of micro- and macroemulsions.

	Macroemulsion	Microemulsion
Droplet size	> 500 nm	10 - 100 nm
Colour	milky	transparent
Thermodynamic	unstable	stable
Energy needed to form	high energy input	easy to form
Microstructure	static	dynamic

Several papers and patents have reported on the use of a microemulsion as a suitable formulation for sunscreen products. These reports have included mention of a number of

different components of the microemulsion as well as several UV-filters.^{115-117,180-182} Detailed information for incorporating UV-filters into microemulsions is given in Chapter 2. An example for a commercial sunscreen product in the form of a microemulsion is *Red vine hair sun protection* manufactured by Korres S.A. Natural Products.¹⁸³

Microemulsions designed for oral administration often have a low viscosity and need to be thickened appropriately for topical application. A sunscreen product is required to be applied with a thickness of 2 mg/cm² in order to reach the labelled protection factors.¹⁴ It is important that the thickener does not alter the desirable features of the microemulsion, such as the transparent appearance or the stability. Several thickeners for microemulsions have been proposed, such as xanthan gum,¹⁸⁴⁻¹⁸⁶ aerosil 200¹⁸⁷ and gelatine.¹⁸⁸ In this study xanthan gum was chosen as thickener, which is used in concentrations between 0.5 and 1.0 % in microemulsions.^{185,186} The UVA reference sunscreen S2, described in the ISO standard for the determination of sunscreen UVA photoprotection *in vitro*, which is also used as reference in the AS/NZS 2604:2012: Sunscreen products - Evaluation and classification, contains xanthan gum (0.6 %).^{19,30} Xanthan gum is a polysaccharide with a high molecular weight, containing D-glucose, D-mannose and D-glucuronic acid, prepared as the sodium, potassium or calcium salt. It is produced by fermentation of a carbohydrate with the bacterium *Xanthomonas campestris*, followed by purification.¹⁸⁹ In the pharmaceutical and food industry, xanthan gum is used as suspending, stabilising, thickening, and emulsifying agent,¹⁹⁰ due to its stability during heat treatment and high shear on mixing, freezing and thawing.¹⁹¹ One of the main food applications for xanthan gum is in salad dressings, which are O/W emulsions.¹⁹¹

Human skin can be divided into three major layers, the epidermis, the dermis and the subcutaneous. The outermost layer, the epidermis, can further be subdivided into the stratum corneum and the viable epidermis. Also known as horny layer, the stratum corneum consists of dead epidermal cells, the corneocytes, which are embedded in a lipid matrix and overlap each other. This characteristic formation is often referred to as the so-called brick and mortar model. As the lipophilic phase of the epidermis, the stratum corneum can act as a reservoir for lipophilic substances. The viable epidermis does not have blood vessels itself, but is supplied with oxygen and nutrients by the vascular system in the dermis. The subcutaneous layer of the skin contains mainly fatty tissue and serves as reserve energy source, thermal insulator and trauma protector.^{81,192}

In order to penetrate through the skin a substance or drug has to pass through the stratum corneum, the main barrier of the skin. A substance can be transported either by the intercellular or transcellular pathway. Transport by the intercellular route follows the 0.1 µm wide winding path around the corneocytes and is the major transport route for most substances. The

transcellular route through the skin cells is often hindered by the dense, cross-linked protein structures.¹⁹²

UV-filters in sunscreen products are required to remain on the skin surface or in the stratum corneum in order to maintain their UV-protective character.¹⁰¹ On exposure to the viable skin tissue, they may cause photosensitivity reactions, which may be phototoxic or photoallergic, as described in Chapter 2.

To study the skin penetration of chemical UV-filters, *in vitro* Franz diffusion cells were used. The Franz cell is a static diffusion cell, where the donor and acceptor chamber are arranged vertically and are separated by an artificial membrane or excised human or animal skin (Figure 6.1). The sample is placed in the donor chamber, while the acceptor chamber contains the receptor fluid, a thermostatically controlled solution mimicking physiological fluids. Samples are usually taken from the side arm and replaced with pre-warmed receptor fluid.^{81,192} To mimic the physiological fluid, phosphate buffer (pH: 7.4),^{103,104} citrate buffer¹⁸⁵ or 0.9 % saline solution¹⁹³ are used. The analysed substance is required to be soluble in this buffer solution, which could be problematic for lipophilic substances, such as the UV-filters studied in this chapter. To improve sink conditions, additives such as BSA,^{103,104,193} surfactants,^{101,103} propylene glycol¹⁰³ or ethanol¹⁰³ have been added. Propylene glycol and ethanol are however not optimum, due to their ability to act as permeation enhancers, with the potential to alter the diffusion rates of substances across the skin.¹⁰³

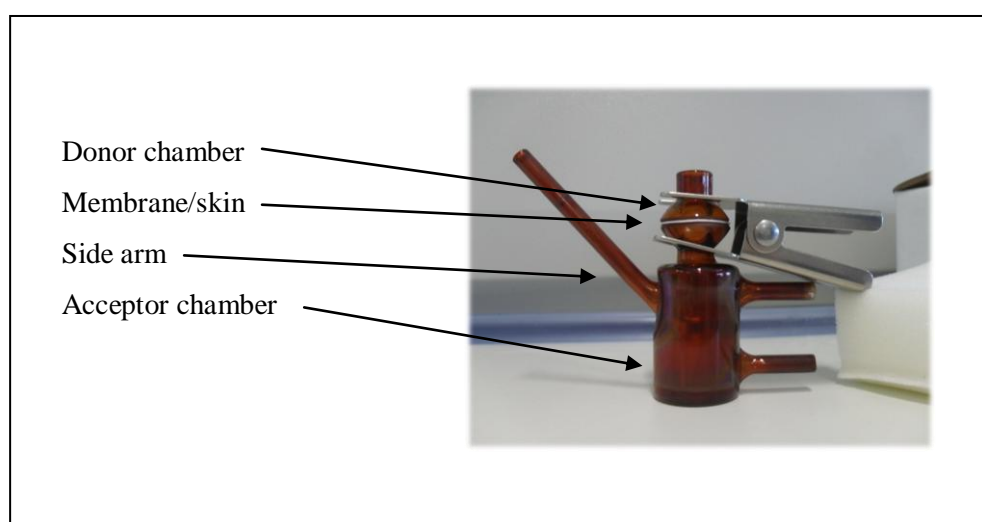


Figure 6.1. Franz diffusion cell.

Human or animal skin can be used as full-thickness skin, containing stratum corneum, viable epidermis and dermis, or split-thickness skin, where the lower dermis has been removed.

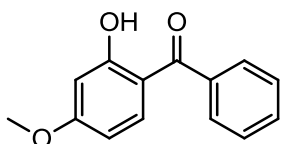
Human skin is obviously the best model for *in vitro* skin penetration studies, but the use of animal skin is also acceptable, with the best alternative being porcine ear skin.¹⁹⁴ Although split-thickness skin is more suitable for percutaneous absorption studies, the use of full-thickness porcine skin has been reported to be acceptable, because of the difficulty to obtain intact split-thickness porcine skin.¹⁹⁴

Separation of the stratum corneum from the epidermis is often undertaken by the tape stripping method. This simple and easy method can be used *in vivo*,¹⁹⁵⁻¹⁹⁷ because it is less invasive, or *in vitro*, either on a whole porcine ear^{195,197} or after the skin penetration studies using Franz diffusion cells.^{101,193,198} Different types of adhesive tapes have been used varying from simple Scotch® tape^{193,198} over Transpore® tape¹⁹⁹ to the specially designed Corneofix® tape¹⁹⁵ in order to remove corneocytes.

A microemulsion for the use as sunscreen product is described in this chapter. The purpose was not to undertake the comprehensive formulation of a microemulsion, including a stability profile towards a commercial product as an outcome, but based on available information choose the appropriate components to prepare a stable and transparent microemulsion. Photostability of the UV-filters Butyl methoxy dibenzoylmethane (**BMDM**) and Octocrylene (**OC**) alone, in combination and in the presence and absence of TiO₂ in the microemulsion was determined. The photostability of **BMDM** and **OC** was compared to their photostability in a reference cream.²⁰⁰ Photostability studies were undertaken according to ICH Guidelines Q1B,²⁶ as the recommended dose in these guidelines (21 MJ/m²) is in the range of the daily exposure in an Australian summer (20 - 28 MJ/m²).²⁰¹ The preliminary stability studies on the microemulsion were informed by ICH Guideline Q1A (R2).²⁰²

Skin penetration studies were undertaken for **BMDM** and **OC** separately and in combination as well as for the chemical UV-filter Benzophenone-3 (**B3**). **B3**, also known as Oxybenzone, which is regarded as broad spectrum filter (Figure 6.2), even when it only absorbs UV-light in the UVB- and UVA II-range. **B3** was chosen to comparatively evaluate the skin penetration of **BMDM** and **OC**, due to its reported capability to penetrate through the skin.^{101,104}

Photoallergic skin reactions caused by exposure to the UV-filters **BMDM** and **B3** have been reported widely,^{18,70,118-120} Despite being the most photoallergic UV-filter on the market **B3** is often used in sunscreen products.^{18,81} In 2010, 15.1 % of tested sunscreen products in the UK contained UV-filter **B3**.⁷⁵ Skin penetration of **BMDM** was reported to be equal to or less than 1 % of the applied dose, up to 10 % for **B3** was reported.¹⁸ For UV-filter **OC** no skin penetration, phototoxic or photoallergic reactions have been previously reported.¹⁸ However, more recent studies, on the other hand, reported the incidence of photoallergic skin reactions after application of UV-filter **OC**.^{118,121,203}



Benzophenone-3 (**B3**)

Figure 6.2. Chemical structure of **B3**.

6.2. Materials and Methods

6.2.1. Solvents and Reagents

Butyl methoxy dibenzoylmethane (Eusolex[®] 9020), Octocrylene (Eusolex[®] OCR) and the silica coated titanium dioxide (Eusolex[®] T-AVO) were purchased from Merck (Darmstadt, Germany). Benzophenone-3 (2-Hydroxy-4-methoxybenzophenon, 98%), albumin from bovine serum (≥ 98 % (agarose gel electrophoresis), lyophilized powder) (BSA), anatase TiO₂ nano- (99.7 % trace metals basis, particle size < 25 nm) and micropowder (≥ 99 % trace metals basis, particle size ~ 0.6 μm) were purchased from Sigma Aldrich (St. Louis, USA). Glacial acetic acid and methanol (HPLC-Grade) were obtained from RCI Labscan (Bangkok, Thailand). Acetonitrile (HPLC-Grade) was sourced from Scharlau Chemie S.A. (Sentmenat, Spain) and Di-Sodium hydrogen orthophosphate (Na₂HPO₄) and potassium di-hydrogen orthophosphate (KH₂PO₄) from Ajax Finechem (Australia). Reverse osmosis water was prepared using a Millipore[®] Elix 10 from Millipore SAS (Molsheim, France). Propylene glycol, phenoxyethanol, lanolin (wool fat), stearic acid, white soft paraffin, methylparaben and propylparaben were all obtained from Chem-Supply (Gillman, Australia) and xanthan gum, triethanolamine (trolamine) and mygliol[®] 812 (caprylic/capric triglycerides) from PCCA (Houston, USA). Glycerol oleate was purchased from Tokyo Chemical Industry Co., Ltd. (Tokyo, Japan) and oleth-20 (Brij[®] 98) from Acros Organics (New Jersey, USA).

6.2.2. Instrumentation

Photostability studies were undertaken in a SunTest XLS+ (I) (Atlas Material Testing Technology GmbH, Linsengericht, Germany) equipped with a Xenon arc lamp (2.2 kVA), with variable irradiance from 250 to 765 W/m². The temperature in the reaction chamber reached up to 42 ± 1 °C during UV-irradiation. The glass filter used was the Special UV-glass-filter D65, which transmits wavelengths over 290 nm and is the “internationally recognised standard for outdoor daylight”.²⁶

Preliminary stability studies were undertaken in a climatic chamber KBF 720 from Binder GmbH (Tuttlingen, Germany) with program control, a temperature range from -10 to 100 °C and a humidity range from 10 to 90 % RH and a refrigerated incubator from Thermoline L+M Australia (Northgate, Australia).

Skin penetration studies were carried out using a Franz diffusion cell with a 5 mL receptor chamber (amber glass) and a surface area of 0.64 cm² (PermeGear, Inc., Hellertown, PA, USA).

The Varian ProStar[®] HPLC system (Varian Inc., Melbourne, Australia), consisting of a 240 quaternary solvent delivery module, 210 autosampler and a 330 PDA detector was used for analysis. Data collection was undertaken with the Star Chromatography Workstation System Control version 6.41, which was equipped with the PolyView 2000[™] spectral Processing Application (Varian Inc., Melbourne, Australia).

6.2.3. Preparation of Standards

Standard solutions of **BMDM** and **OC** were prepared by dissolving 100 mg UV-filter in 50 mL methanol separately or in combination. This stock solution was then further diluted with methanol to achieve seven standards, within the calibration range 0.15 - 20 µg/mL. To prepare standard solutions for **B3** 100 mg was dissolved in 100 mL methanol and then further diluted to achieve a calibration range between 0.06 and 25 µg/mL (seven standards).

6.2.4. Preparation of Microemulsion

Microemulsions were prepared by using the phase inversion temperature (PIT) method as described by Azeem et al.¹⁰⁹

Table 6.2 contains microemulsion ingredients for all prepared microemulsions. Each microemulsion containing TiO₂ was prepared with coated, micro- and nano-TiO₂.

To prepare a blank microemulsion, water and the oily ingredients (mygliol[®] 812, glyceryl oleate, oleth-20) were separately heated to 85 - 90 °C and then combined. The microemulsion was cooled to about 40 °C and then phenoxyethanol (90 µL) and xanthan gum were added with stirring, after which water was added to weight (10 g). The UV-filters **BMDM**, **OC** and **B3** were added to the oily ingredients before heating, while TiO₂ was added to the cooled microemulsion and the amount of the water adjusted appropriately.

Table 6.2. Microemulsion formulae containing UV-filters.

Formulation ingredient	Amount of ingredient [g] in microemulsion containing the UV-filters:						
	BMDM	BMDM + TiO ₂	OC	OC + TiO ₂	BMDM + OC	BMDM + OC + TiO ₂	B3
BMDM	0.10	0.10	-	-	0.10	0.10	-
OC	-	-	0.15	0.15	0.15	0.15	-
B3	-	-	-	-	-	-	0.15
Coated, micro- or nano-TiO ₂	-	0.20	-	0.20	-	0.20	-
Mygliol® 812	1.00	1.00	1.00	1.00	1.00	1.00	1.00
Oleth-20 (HLB: 15.3) ¹¹⁷ - surfactant ¹¹⁷	1.10	1.10	1.10	1.10	1.10	1.10	1.10
Glyceryl oleate (HLB: 3.8) ²⁰⁴ - co-surfactant ¹¹⁷	0.44	0.44	0.44	0.44	0.44	0.44	0.44
Phenoxyethanol (ρ = 1.10 g/mL)	0.10	0.10	0.10	0.10	0.10	0.10	0.10
Xanthan gum	0.06	0.06	0.06	0.06	0.06	0.06	0.06
Water	7.20	7.00	7.15	6.95	7.05	6.85	7.15

6.2.5. Preparation of Cream

To compare photostability results of the microemulsion to another topical formulation the low SPF formula P7 from the international standard ISO 24444-2010 was slightly modified and used as cream base.²⁰⁰ Ingredients of each cream are listed in Table 6.3. Each cream containing TiO₂ was prepared with coated, micro- and nano-TiO₂.

The oil and aqueous phase were heated separately to about 80 °C under constant stirring and then combined. The cream was cooled, while stirring and water was added to the final weight. The UV-filters were added to this formulation before heating and the amount of soft white paraffin and water were adjusted appropriately.

Table 6.3. Cream formulae containing UV-filters.

Formulation ingredient	Amount of ingredient [g] in microemulsion containing the UV-filters:					
	BMDM	BMDM + TiO ₂	OC	OC + TiO ₂	BMDM + OC	BMDM + OC + TiO ₂
BMDM	0.10	0.10	-	-	0.10	0.10
OC	-	-	0.15	0.15	0.15	0.15
Coated, micro- or nano-TiO ₂	-	0.20	-	0.20	-	0.20
Lanolin	0.50	0.50	0.50	0.50	0.50	0.50
Stearic acid	0.40	0.40	0.40	0.40	0.40	0.40
Soft white paraffin	0.95	0.95	0.90	0.90	0.80	0.80
Propylene glycol ($\rho = 1.036$ g/mL, containing 2 % methylparaben and 1 % propylparaben)	0.52	0.52	0.52	0.52	0.52	0.52
Triethanolamine ($\rho = 1.124$ g/mL)	0.10	0.10	0.10	0.10	0.10	0.10
Water	7.43	7.23	7.43	7.23	7.43	7.23

6.2.6. Preliminary Stability Studies

Preliminary stability testing of the microemulsion was undertaken to determine the quality of the microemulsion and the chemical stability of UV-filters over time under the influence of environmental factors, such as heat and humidity.

Three microemulsions were evaluated for shelf-life stability of the microemulsion:

- blank microemulsion (without UV-filters)
- microemulsion containing **BMDM** and **OC**
- microemulsion containing **BMDM**, **OC** and silica coated TiO₂

A bulk of 270 g for each microemulsion was prepared and filled in airtight jars (20 g). Samples of each microemulsion were stored for six months at 25 °C and for three months under accelerated storage conditions (40 °C /75 % relative humidity, RH) in the dark.²⁰² Every month, one sample of each microemulsion was evaluated for colour changes, transparency, pH and the chemical stability of **BMDM** and **OC**. The pH was determined with a labChem-CP pH-meter (TPS Pty. Ltd., Brisbane, Australia) using an intermediate junction pH electrode (model: IJ44C) from Ionode Pty. Ltd. (Brisbane, Australia). All microemulsions were analysed visually for any colour change, while only microemulsions without TiO₂ were evaluated for their transparency. Chemical stability of **BMDM** and **OC** was determined by using the extraction method described for photostability studies and the HPLC method described in Chapter 4.

6.2.7. Photostability Studies

About 20 mg (exactly weighed) of microemulsion or reference cream was spread on the bottom of a glass beaker onto an area of 10 cm², using a plastic inoculating loop. It has been reported that there is no difference in UV-filter performance after UV-exposure, spread on glass as compared to a biological membrane, such as human or porcine skin.²⁰⁵ Thus, the glass surface is confirmed to be appropriate for the photostability studies. The beaker was then placed directly under the light source in the solar simulator. At 400 W/m², the samples were irradiated for 14.6 hours (1.2 million lux hours), according to ICH Guideline Q1B,²⁶ reaching a total irradiance of 21,000 kJ/m². After irradiation, about 10 mL methanol was filled into the beaker and sonicated for ten minutes. The sample suspension was then transferred to a 25 mL volumetric flask, the beaker was rinsed with methanol (3 × 4 mL) and these rinsings were then transferred to the volumetric flask, which was made up to volume with methanol. Samples were filtered through a 15 mm syringe filter with a 0.45 µm PTFE membrane (Phenomenex Inc. Sydney, Australia) before analysis using the developed and validated HPLC method in Chapter 4. Non-irradiated samples (controls) were extracted the same way as described above. Each

photostability experiment was undertaken at least three times and samples were analysed in triplicate.

6.2.8. Skin Penetration Studies

The Franz cell receptor chamber was filled with phosphate buffer (pH: 7.4) containing 4 % BSA to mimic physiological fluid and to ensure sink conditions for the UV-filters. Sink conditions are increased due to the ability of the protein BSA to bind lipophilic substances, such as the employed UV-filters.²⁰⁶ The receptor fluid (5 mL) was constantly stirred and maintained at 37 °C. Samples of 200 µL were withdrawn directly after the microemulsion application, after one, six and 24 hours and replaced with pre-warmed buffer solution. Before analysis, these samples were pre-treated to remove the BSA content. The sample (160 µL) and 320 µL acetonitrile were mixed before being centrifuged using an Eppendorf centrifuge 5810R (Eppendorf South Pacific, Sydney, Australia) for 15 minutes at 4000 rpm at 15 °C to minimise evaporation.

Porcine ears from “Landmark” pigs were obtained from a local abattoir and collected as soon as possible after slaughtering. The International Biosafety Committee (IBC) Approval for the following procedure is attached as Appendix A. The skin was removed from the ears, freed from hair with scissors and cut into ready-to-use pieces (~ 4 cm²) before being kept at -80 °C until use (maximum two months). The porcine ear skin was mounted on the Franz cell and left to equilibrate for 30 minutes, before an exact amount of microemulsion (~ 30 mg) was spread onto the skin. The chamber was covered with Parafilm[®] paper to protect the skin from drying out.

The following extraction methods for the UV-filters were adapted from Vilela et al.¹⁰¹

- After 24 hours the skin was blotted dry with cotton wipes and washed once with methanol to remove excess microemulsion. The cotton wipes were combined, sonicated for ten minutes in methanol and regarded as containing the non-penetrated material.
- To separate the stratum corneum from the remaining epidermis and dermis, the skin was stripped 25 times with Transpore[™] surgical tape (3M Health Care, St. Paul, MN, USA). All tapes were combined and also sonicated for ten minutes in methanol.
- The remaining skin (dermis and viable epidermis) was then cut into small pieces, sonicated for ten minutes in 2 mL methanol and supernatant transferred to a 10 mL volumetric flask. This extraction procedure was repeated four times, supernatants combined and the volumetric flask filled up to volume with methanol.

- Samples were filtered through a 15 mm syringe filter with a 0.45 µm PTFE membrane (Phenomenex Inc. Sydney, Australia), and analysed using the developed and validated HPLC method in Chapter 4. Each experiment was undertaken six times.

6.3. Results and Discussion

6.3.1. Microemulsion Development

Four microemulsions (one for oral and three for topical use) were investigated as a model for the preparation of the microemulsion. Table 6.4 briefly summarises the application and components of these candidate microemulsions. These microemulsions were then prepared and evaluated in terms of appearance, including colour and odour, and whether or not they were appropriate for this study in terms of spreadability, transparency and oiliness.

Table 6.4. Microemulsions (ME) reported on in the literature.

ME	Application of ME in reference article	Main ingredients of ME	Appearance and Suitability	Ref.
1	Oral ME	Mygliol [®] 812, imwitor 308, crillet 3, water	Clear, transparent, very oily, liquid → Too oily and liquid (viscosity) – not suitable	179
2	Topical ME including 4-Methylbenzylidene camphor (MBC) and Ethylhexyl methoxycinnamate (EMC) as UV-filters	C ₁₂₋₁₅ alkylbenzoate, cyclomethicone, ethanol soyalecithin, 1,2-hexanediol, water	Clear, yellowish, liquid → Unpleasant colour and odour – not suitable	115
3	Topical ME including EMC as UV-filter	Mygliol [®] 812, oleth-20, glyceryl monostearate, water	White, liquid → ME not formed – not suitable	117
4	Topical ME including EMC as UV-filter	Mygliol [®] 812, oleth-20, glyceryl oleate, water	Clear, opaque, liquid (viscosity) → Suitable , requiring modification	117

Microemulsion number 4, which contained glyceryl oleate (2.2 %), oleth-20 (5.5 %), triglyceride caprylic/capric (mygliol[®] 812) (5.0 %) and water (87.3 %), was then chosen as appropriate for the study.¹¹⁷ Several combinations of surfactants and lipids were reported on in relation to their effect on the skin penetration of the chemical UV-filter Ethylhexyl methoxycinnamate,¹¹⁷ which is described in detail in Chapter 2.

However, the prepared microemulsion was not appropriately viscous to be used as topical sunscreen and therefore a suitable thickener was required to be added. Gelatine, carboxy methylcellulose, carbomer 940 NF, guar gum, methylcellulose and xanthan gum were all evaluated as possible thickeners. Only the addition of carboxy methylcellulose and xanthan gum resulted in a product with suitable spreadability on the skin, while maintaining the required transparency. Xanthan gum was selected over carboxy methylcellulose, because of its known stability at high temperatures.¹⁹¹ Phenoxyethanol was included, as it is commonly incorporated as a preservative in sunscreen products.

The amount of lipid from the original microemulsion was doubled to increase the oil component, in which the chemical UV-filters are dissolved. To accommodate this increased amount of lipid the amount of surfactant/co-surfactant was also doubled, but these amounts of surfactant/co-surfactant were still relatively low (15.4 %) compared to most microemulsions. These microemulsions often contain more than 40 % of surfactant, with the increased potential to be irritant to the skin.^{110,117}

6.3.2. Preliminary Stability Studies

Physical and chemical stability of a blank microemulsion, a microemulsion containing **BMDM** and **OC** and **BMDM**, **OC** and silica coated TiO₂ was evaluated. The silica coated TiO₂ microemulsion was chosen as candidate for the stability study due to the increased photoprotection of **BMDM** and **OC** in the microemulsion compared to that of micro- or nano-TiO₂.

Table 6.5 and 6.6 show the pH data, colour change and transparency of the microemulsion for those products stored at 25 °C and 40 °C/75 % RH, respectively. The pH stability of the microemulsions was evaluated, considering the natural skin surface pH. However, inconsistent pH ranges of the skin surface^{207,208} and as reviewed by Lambert et al.²⁰⁸ a wide overall range between 4.0 and 6.3 have been reported. An average skin surface pH of 4.7 was reported in this paper and that a pH of 4.0 - 4.5 is ideal in order to maintain the resident bacterial flora attached to the skin.²⁰⁸ In this study the reported overall pH range of 4.0 - 6.3 was regarded as acceptable for the pH values of the microemulsions.

Stored at 25 °C the pH decreased monthly for all three microemulsions (Table 6.5). The starting pH of the blank microemulsion and the microemulsion containing **BMDM** and **OC** was just under 4.7, the average skin surface pH, while the presence of silica coated TiO₂ increased this pH to 6.04, which is within the acceptable pH range. Although the pH remained over 4.0 over the six months period, the slight variation in pH indicates an advantage for the inclusion of a buffer into the microemulsion for long term stability. The pH in the microemulsion containing **BMDM**, **OC** and TiO₂, stored for six months at 25 °C the pH was 5.99 and therefore nearly the same as before storage.

No colour change occurred in any microemulsion over the six months time period and microemulsions without TiO₂ remained transparent when spread on the skin. The microemulsion was stable throughout the six month period (Table 6.5).

Table 6.5. Physical stability of microemulsions, stored at 25 °C.

Storage time	pH			Colour change			Transparent	
	blank	BMDM +OC	BMDM +OC +TiO ₂	blank	BMDM +OC	BMDM +OC +TiO ₂	blank	BMDM +OC
0 month	4.67	4.68	6.04	✓	✓	✓	✓	✓
1 month	4.62	4.60	5.84	✓	✓	✓	✓	✓
2 months	4.57	4.55	5.63	✓	✓	✓	✓	✓
3 months	4.50	4.52	5.57	✓	✓	✓	✓	✓
4 months	4.44	4.50	5.49	✓	✓	✓	✓	✓
5 months	4.42	4.50	4.92	✓	✓	✓	✓	✓
6 months	4.33	4.43	5.99	✓	✓	✓	✓	✓

✓: No colour change; remained transparent → stable

The pH declined more under the accelerated conditions than at 25 °C (Table 6.6). The pH for the blank microemulsion was maintained within an acceptable range (pH: 4.0 - 6.3) only for the first two months, while the pH for the other two microemulsions stayed stable for three months.

While microemulsions stored at 40 °C/75 % RH showed no colour change over the three months, the two microemulsions without TiO₂ showed a slightly white colouration on the skin (Table 6.6).

Table 6.6. Physical stability results of microemulsions, stored at 40 °C/75 % RH.

Storage time	pH			Colour change			Transparent	
	blank	BMDM +OC	BMDM +OC +TiO ₂	blank	BMDM +OC	BMDM +OC +TiO ₂	blank	BMDM +OC
	0 month	4.67	4.68	6.04	✓	✓	✓	✓
1 month	4.44	4.52	5.62	✓	✓	✓	✓	✓
2 months	4.09	4.51	5.37	✓	✓	✓	✓	✓
3 months	3.72	4.30	5.07	✓	✓	✓	✗	✗

✓: No colour change; remained transparent → stable

✗: Not transparent on skin → not stable

Chemical stability of **BMDM** and **OC** was determined and data each month were compared to the reference sample, which was analysed directly after preparation, taking into account weight loss due to evaporation. Table 6.7 and 6.8 show the % recovery of **BMDM** and **OC**, stored at 25 °C and 40 °C/75 % RH, respectively. According to the “Australian regulatory guidelines for sunscreens” a sunscreen product should contain between 90 and 120 % of the labelled amount of UV-filter, after stability studies.¹⁴ This range was adopted to determine whether the UV-filters are stable in the microemulsion over time. In both microemulsions both UV-filter concentrations were maintained within this range over the complete three/six months.

Table 6.7. Chemical stability of **BMDM** and **OC** in microemulsions, stored at 25 °C.

Storage time	BMDM % Recovery		OC % Recovery	
	BMDM+OC	BMDM+OC+TiO ₂	BMDM+OC	BMDM+OC+TiO ₂
0 month	100.00	100.00	100.00	100.00
1 month	95.78	95.56	99.76	99.19
2 months	101.65	98.48	106.38	102.77
3 months	104.72	103.45	101.08	100.08
4 months	97.63	96.40	98.94	98.18
5 months	100.11	101.21	99.19	99.85
6 months	102.28	102.27	103.04	103.06

Table 6.8. Chemical stability of **BMDM** and **OC** in microemulsions, stored at 40 °C/75 % RH.

Storage time	BMDM % Recovery		OC % Recovery	
	BMDM+OC	BMDM+OC+TiO ₂	BMDM+OC	BMDM+OC+TiO ₂
0 month	100.00	100.00	100.00	100.00
1 month	94.17	93.73	98.13	101.14
2 months	95.69	101.44	99.37	102.09
3 months	102.72	100.94	99.29	98.18

Although the pH of the microemulsion containing **BMDM** and **OC** decreased to below 4.0 after three months of storage at 40 °C/75 % RH, the amount of both UV-filters remained within the acceptable range. Stability of **BMDM** at low pH levels has been reported in the literature, where **BMDM** was stable between pH 2.0 and 5.0 during degradation studies in phosphate buffer at 60 °C.¹⁷⁶

6.3.3. Photostability Studies

The two UV-filters **BMDM** and **OC** were incorporated in the microemulsion and the cream, separately and in combination, in the absence and presence of silica coated, micro- and nano-TiO₂.

To determine the efficiency of the employed extraction method, the calculated UV-filter concentration was compared to the measured concentration of a non-irradiated sample. After extraction, the measured **BMDM** concentration in the microemulsion and cream was 104.94 and 98.13 % of the calculated value, respectively, while the **OC** concentration was 101.83 % in the microemulsion and 102.25 % in the cream. These results clearly demonstrate the efficiency of the employed extraction method.

Table 6.9 (page 163) shows the mean % recovery ± SD for both chemical UV-filters after irradiation. In general, the recovery of **BMDM** is lower than the recovery of **OC**, confirming literature reports, where **OC** is described as more photostable than **BMDM**.^{45,46,49} The presence of silica coated TiO₂ did not result in a significant reduction in UV-filter recovery and confirms therefore literature reports, that the coating of TiO₂ particles reduces ROS generation and thus UV-filter degradation.⁸⁶

Irradiation of **BMDM** separately from **OC** resulted in less than 4 % recovery in both, the microemulsion and the cream. Recovery of **BMDM** without TiO₂, with silica coated and micro-TiO₂ in the microemulsion were between 2 and 4 %, but not significantly different from each other. On the other hand, the presence of nano-TiO₂ resulted in a complete degradation of

BMDM ($F_{2,9} = 2.004$, $p = 0.191$). In the cream, the recovered concentration of **BMDM** irradiated without TiO_2 , with silica coated and micro- TiO_2 were all over the LOD, but under the LOQ, while no **BMDM** was detected in the presence of nano- TiO_2 .

In combination with **OC**, **BMDM** recovery from the microemulsion without TiO_2 , with silica coated and micro- TiO_2 was increased to more than 12 %, while with nano- TiO_2 less than 1 % of **BMDM** remained. No significant difference between **BMDM** recovery without TiO_2 , with silica coated and micro- TiO_2 was detected, while **BMDM** recovery in the presence of nano- TiO_2 was significantly lower and under the LOQ ($F_{3,15} = 38.777$, $p < 0.000$). In the cream, **BMDM** recovery without TiO_2 , with silica coated and micro- TiO_2 was between 14 and 23 %, with no significant difference, while in the presence of nano- TiO_2 **BMDM** recovery was only about 3 % and hence significantly lower ($F_{3,15} = 15.120$, $p < 0.000$).

Separate irradiation of **OC** in the microemulsion resulted in no significant difference in degradation without TiO_2 , with coated and micro- TiO_2 . On the other hand, the presence of nano- TiO_2 resulted in a significant degradation of nearly 12 % in the microemulsion ($F_{3,12} = 13.660$, $p < 0.000$). Although **OC** recovery in the presence of nano- TiO_2 was lower compared to the degradation without TiO_2 , with silica coated or micro- TiO_2 , irradiated in the cream, this difference was not significant ($F_{3,12} = 0.738$, $p < 0.549$).

In combination with **BMDM**, **OC** did not significantly degrade without TiO_2 or with silica coated TiO_2 in the microemulsion. The presence of both, micro- and nano- TiO_2 , resulted in a recovery rate of less than 95 %, which showed a significant degradation ($F_{3,14} = 4.386$, $p = 0.022$). Irradiated in the cream, **OC** showed no significant difference in degradation without TiO_2 , with silica coated or micro- TiO_2 , but the presence of nano- TiO_2 resulted in a significant degradation of nearly 12 % ($F_{3,16} = 3.475$, $p < 0.041$).

Table 6.9. % Recovery of **BMDM** and **OC** ($n \geq 3$) \pm SD in both formulations in the presence and absence of TiO₂.

UV-filter combination	BMDM % Recovery		OC % Recovery	
	ME	Cream	ME	Cream
BMDM	3.81 \pm 1.15	0.80 \pm 0.42*	-	-
BMDM + coated TiO ₂	3.43 \pm 0.83	0.42 \pm 0.16*	-	-
BMDM + micro-TiO ₂	2.05 \pm 0.73	0.45 \pm 0.20*	-	-
BMDM + nano-TiO ₂	0.00*	0.00*	-	-
OC	-	-	98.54 \pm 2.35	97.05 \pm 2.63
OC + coated TiO ₂	-	-	99.98 \pm 4.26	98.76 \pm 2.84
OC + micro-TiO ₂	-	-	96.71 \pm 2.78	98.30 \pm 4.18
OC + nano-TiO ₂	-	-	88.33 \pm 0.77	95.07 \pm 5.14
BMDM + OC	16.08 \pm 2.04	22.37 \pm 5.50	101.57 \pm 1.37	102.04 \pm 8.99
BMDM + OC + coated TiO ₂	16.00 \pm 1.32	14.83 \pm 2.82	98.23 \pm 5.97	99.98 \pm 2.48
BMDM + OC + micro-TiO ₂	12.59 \pm 3.13	14.46 \pm 1.79	94.98 \pm 1.96	97.64 \pm 3.46
BMDM + OC + nano-TiO ₂	0.64 \pm 0.52*	3.12 \pm 0.78	92.45 \pm 3.86	88.86 \pm 3.49

*measured concentrations under LOQ (**BMDM**: 0.15 μ g/mL)

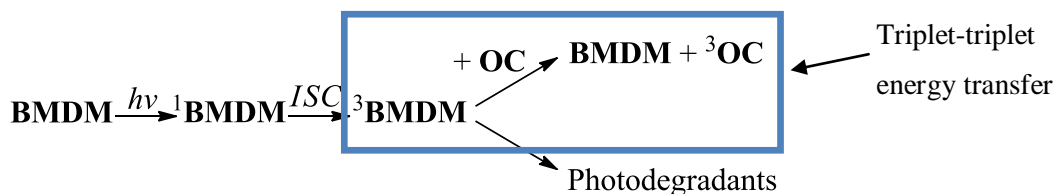
The important outcome from Chapter 5 was that TiO₂ particle size influences the photostability of **BMDM** and **OC** in methanol. In the presence of nano-TiO₂ photodegradation of both chemical UV-filters was higher compared to those solutions with the same amount of micro-TiO₂. These results were confirmed in this chapter, after irradiation in a solar simulator with UV-filters incorporated in two topical formulations. Differences in the results between the microemulsion and the cream were marginal and can be disregarded. The major outcome that the photodegradation of **BMDM** and **OC** is higher in the presence of nano-TiO₂ compared to micro-TiO₂ was observed in both formulations. Direct photolysis, as described in Chapter 5, was the pathway for the photodegradation of UV-filter **BMDM** in this chapter. As the photocatalyst TiO₂ generates ROS on the particle surface, which can induce the photodegradation of UV-filters, also described in detail in Chapter 5. The greater surface area of nano-TiO₂, due to its smaller particle size, thus results in the generation of more ROS compared to micro-TiO₂.

A high irradiation dose of 21 MJ/m² in the solar simulator was justified as it is comparable with the daily solar exposure in summer in Australia. Between October 2013 and March 2014 the average daily solar exposure was between 20 and 28 MJ/m² in about 90 % of Australia, while the summer before (October 2012 - March 2013) the daily solar exposure was between 20 and 30 MJ/m² in the whole country.²⁰¹

The higher **BMDM** recovery in combination with **OC** can be explained by the stabilising effect of **OC** on **BMDM** during UV-irradiation (Scheme 6.1). As described in Chapter 5, during direct photolysis, photodegradation of **BMDM** occurs *via* the triplet excited state, after migration from the ground state into the singlet excited state (¹**BMDM**), due to UV-irradiation, and further migration to the triplet excited state (³**BMDM**) *via* ISC.

OC can directly quench ³**BMDM** by triplet-triplet energy transfer. During this process the excited electrons from ³**BMDM** transfer to the ground state of **OC**. ³**BMDM** is regarded as the donor, which reverts back to the ground state after the exchange, while **OC**, the acceptor, is elevated to the triplet excited state ³**OC**. **OC** is more stable in the triplet state than **BMDM** and reverts back to the ground state before it degrades, forming photodegradants.⁵⁵ This described triplet-triplet energy transfer occurs because the triplet energy level of **OC** is lower than that of the enol-form of **BMDM**.²⁰⁹ While the triplet energy level of **BMDM** was reported in the literature ($T_{\text{BMDM}} = 247.65 \pm 3.18$ kJ/mol),^{150,210,211} the triplet energy level of **OC** could not directly be determined. The triplet energy level is measured by the phosphorescence of a molecule, but **OC** is non-phosphorescent or only weakly phosphorescent.²⁰⁹ Although the triplet energy level of **OC** remains unreported, very recently the experimental evidence for

triplet-triplet energy transfer from **BMDM** to **OC** was provided by measuring the phosphorescence decay of the energy donor, **BMDM**.²⁰⁹



Scheme 6.1. Photodegradation of **BMDM**, including stabilisation by **OC**.

6.3.4. Skin Penetration Studies

The skin penetration of **BMDM** and **OC** separately and in combination was studied using the developed microemulsion. Results were compared to the skin penetration of UV-filter **B3**. Table 6.10 (page 167) shows the UV-filter recovery in % from the applied dose. UV-filter concentrations in the microemulsion after preparation were determined and designated as 100 %.

The overall recoveries of UV-filters **BMDM** and **OC**, separately and in combination, were between 94 and 97 %, which were not significantly different from each other. UV-filter **B3**, on the other hand, showed a significant lower overall recovery of 89 % ($F_{4,25} = 7.633$, $p < 0.000$). According the Colipa “Guideline for percutaneous absorption/penetration” the overall recovery of the analysed substance should be at least 85 %. Only if the overall recovery is under the limit of 85 %, further investigations about the whereabouts of the substance have to be undertaken.¹⁰² The overall recoveries of the studied UV-filters during skin penetration studies remained over this limit and are therefore acceptable.

BMDM and **OC** were not detected in the receptor fluid over 24 hours and therefore steady state fluxes could not be calculated for these two UV-filters. **B3** was detected after six and 24 hours, but the concentration after six hours was less than 0.01 % and was regarded as negligible. A steady state flux of **B3** could thus also not be calculated, but the cumulative amount penetrated through the skin after 24 hours was $0.23 \mu\text{g}/\text{cm}^2$.

The low or absent UV-filter concentration in the receptor fluid confirms findings by Montenegro et al.,¹¹⁷ who reported no skin penetration for UV-filter EMC from a microemulsion containing mygliol® 812, oleth-20 and glyceryl oleate. The presence of mygliol® 812 was also described as key factor for low skin penetration of UV-filter EMC in a

microemulsion compared to a gel formulation without mygliol® 812.⁹⁹ Other studies have also reported that skin penetration and skin retention of UV-filters is formulation dependant.^{101,116}

Low or no penetration from formulations containing mygliol® 812 was explained by hydrophobic interactions between the lipid and surfactant/co-surfactant. Mygliol® 812 is a lipid with medium length acyl chains, which may result in a close packing of surfactants around lipid droplets imbedding the UV-filters. The closer the packing the slower is the UV-filter release from the formulation,¹¹⁷ highlighting the importance of both the lipophilicity and structure of surfactants and co-surfactants.

As mentioned above, in order to protect the skin from UV-radiation UV-filters should remain on the skin surface or in the stratum corneum and not penetrate the viable epidermis into the dermis with its blood vessels. It would therefore be problematic if the UV-filter content is significant in the viable epidermis and dermis. The UV-filter with the highest recovery in the viable epidermis/dermis was **B3** (1.09 ± 0.30 %) followed by **BMDM** (0.14 ± 0.02 %) and **OC** (0.02 ± 0.04 %). This order correlates with the increasing lipophilicity and lower molecular weight of the UV-filters: **B3** ($\text{Log } P_{\text{oct/wat}} = 3.6^{101}$, 228.3 g/mol) < **BMDM** ($\text{Log } P_{\text{oct/wat}} = 4.8^{116}$, 310.4 g/mol) < **OC** ($\text{Log } P_{\text{oct/wat}} = 6.9^{178}$, 361.5 g/mol). Lipophilic substances tend to remain on the surface of the skin or accumulate in the stratum corneum, because the viable epidermis is the more hydrophilic skin compartment.⁸¹ The Log P value for substances to penetrate the skin easily is usually between 2 and 3,¹⁹² and therefore the closest to the Log P of **B3**. Molecular weight plays an important role during skin penetration as well.¹⁹²

Table 6.10. UV-filter recovery in % after skin penetration studies.

	UV-filter recovery in % in microemulsion (n = 6) ± SD				
	BMDM	BMDM (+ OC)	OC	OC (+ BMDM)	B3
RF ^a : 0 hours	0.00	0.00	0.00	0.00	0.00
RF ^a : 1 hours	0.00	0.00	0.00	0.00	0.00
RF ^a : 6 hours	0.00	0.00	0.00	0.00	< 0.01
RF ^a : 24 hours	0.00	0.00	0.00	0.00	0.03 ± 0.03
Non-penetrated material ^b	93.21 ± 1.26	96.14 ± 2.60	94.12 ± 2.84	94.67 ± 2.53	87.65 ± 2.11
Stratum corneum ^c	0.79 ± 0.34	0.27 ± 0.21	0.26 ± 0.21	0.34 ± 0.22	0.52 ± 0.41
Viable epidermis/dermis ^d	0.14 ± 0.02	0.10 ± 0.09	0.02 ± 0.04	0.03 ± 0.04	1.09 ± 0.30
Overall	94.13 ± 1.07	96.50 ± 2.56	94.39 ± 3.26	95.04 ± 2.55	89.29 ± 2.06

^a samples drawn from receptor fluid (RF) directly after the start of the experiment (0h) and after certain time intervals

^b non-penetrated UV-filter material, recovered from the surface of the skin

^c stratum corneum, separated from viable epidermis/dermis by 25 adhesive tape strips

^d viable epidermis/dermis (as rest skin)

6.4. Summary

A microemulsion was prepared and preliminary stability studies were undertaken under normal and accelerated conditions. Photostability of **BMDM** and **OC** was determined in this microemulsion in the presence and absence of TiO_2 , while skin penetration was determined for the chemical UV-filters **BMDM**, **OC** and **B3**.

Preliminary stability was determined for three microemulsions, a blank, with **BMDM** and **OC** and a microemulsion containing **BMDM**, **OC** and silica coated TiO_2 . Stored at 25 °C all three microemulsions were stable in regards to pH, colour change, transparency and chemical stability of the component UV-filters. Stored at 40 °C/75 % RH the pH and transparency were only stable for two months, while chemical stability of **BMDM** and **OC** was confirmed for three months and no colour change occurred in the microemulsions.

Photostability of **BMDM** and **OC**, irradiated separately and in combination in a solar simulator, was determined without TiO_2 , with silica coated, micro- and nano- TiO_2 . Results of the microemulsion were compared to photostability results in a reference cream. In both, the microemulsion and the cream, the presence of nano- TiO_2 induced higher photodegradation of **BMDM** and **OC**, than in the absence or presence of silica coated and micro- TiO_2 . **BMDM** was more stable in the presence of **OC** than irradiated alone, highlighting the role for **OC** as UV-protection and stabilisation agent for **BMDM**. The improved stability of **BMDM** in the presence of **OC** can be explained by the stabilising effect of **OC** *via* triplet-triplet energy transfer.

Generally, skin penetration of **BMDM**, **OC** and **B3** was low. The concentration of **B3** was the highest in the receptor fluid and the skin (viable epidermis/dermis), because it was the least lipophilic UV-filter with the smallest molecular weight of the three studied chemical UV-filters.

Photostability studies confirmed the results from Chapter 5, that a smaller TiO_2 particle size clearly decreases the photostability of **BMDM** and **OC**.

Chapter 7

Conclusions and Recommendations

7.1. Conclusions

Sunscreen products, containing UV-filters, are used worldwide to protect from harmful effects of UV-irradiation, such as sunburn or skin cancer. The photostability and skin penetration of various chemical UV-filters have been reported on and are reviewed in Chapter 2. Photostability studies have been undertaken using a variety of test methods and this has included the use of different light sources, irradiation times, solvents and UV-filter concentrations, often resulting in controversial results in terms of their photostability for some UV-filters. While a UV-filter may be reported as photostable, that same UV-filter in another study is regarded as not photostable, which is largely attributed to the different conditions under which the UV-filter is irradiated.^{43-45,49} This highlights the limitations of the lack of standardised methods or guidelines to determine photostability of sunscreen products, with the potential outcome of sunscreen products on the market, which are not photostable. Sunscreen products often contain a number of active ingredients and excipients, such as chemical and physical UV-filters, resulting in a somewhat complex formulation. The chemical UV-filter may undergo direct photolysis on exposure to sunlight. Despite the ability of the physical UV-filter TiO₂ to cause photocatalysis it is often used in combination with chemical UV-filters in sunscreen products in order to afford broad spectrum protection. Although nano-TiO₂ is nowadays more often used in sunscreen products, there is a notable lack of studies investigating the effect of TiO₂ particle size on the photostability of chemical UV-filters. It is this lack of information on the photostability of these complex systems, which has informed the design of this study. Although the inclusion of nano-TiO₂ is aesthetically appealing and thus acceptable to customers, there has been some concern if these particles have the ability to penetrate the skin, but there is no evidence to support this concern and the TGA regards them as safe.^{15,18,80-82} Skin penetration of chemical UV-filters has however been reported, which may result in photosensitivity reactions.^{101,104,105} These reactions warrant the investigation of the skin penetration properties of chemical UV-filters, if they are included in sunscreen products.

The first objective of extensively reviewing the literature on the photostability and skin penetration of UV-filters has been met and resulted in the choice of the chemical UV-filters **BMDM** and **OC** for this study. The rationale for the choice of these two chemical UV-filters is attributed to their ability to provide broad spectrum protection in combination and the fact that they are widely used in sunscreen products, separately and also in combination. Since **B3** is

regarded as photostable and is also a good example of a UV-filter causing the most photoallergic skin reactions, it was included for comparison in the skin penetration studies.

The second objective was to characterise the three chemical UV-filters **BMDM**, **OC** and **B3** in order to confirm their purity and identity. While purity of **OC** and **B3** was confirmed by HPLC, DSC and melting range determinations, small impurities were detected on HPLC analysis of **BMDM**. Recrystallisation from methanol reduced the sum of impurities from 2.42 to 0.66 %, which was confirmed by a narrower melting range. Identity of all three UV-filters was confirmed by NMR-, IR- and UV-spectroscopy.

The third objective was to develop and validate an HPLC method for the simultaneous determination of the UV-filters **BMDM** and **OC** in the presence of their photodegradants. The method was developed to include mobile phase components, which are suitable to be used during LC-MS analysis, which was employed to identify major photodegradants, in addition determining UV-filter concentration of **B3** during skin penetration studies. Two major photodegradants (4-methoxy benzoic acid and 4-*t*-butyl benzoic acid) were identified for **BMDM**, which were confirmed by FTMS and by comparison to literature data. UV-irradiation of **OC** resulted in the generation of a major, novel photodegradant (methyl-2-cyano-3,3-diphenylacrylate), which was identified by LC-MS and the structure confirmed by FTMS. The developed HPLC method was valid with linearity, accuracy, precision, specificity, sensitivity and robustness and confirmed for the determination of all three chemical UV-filters. The separation of the two UV-filters in the presence of their photodegradants, confirmed the method to be selective and specific. This HPLC method developed and validated to analyse the combination of **BMDM** and **OC** in the presence of their photodegradants is not only simple and rapid but can also be applied to LC-MS.

Two further objectives of the study were to investigate the photostability of **BMDM** and **OC** in the presence of coated, micro- and nano-TiO₂, both in methanol and a stable microemulsion. Methanol was used as simple environment for photostability studies, while the microemulsion represented a typical formulation for sunscreen products.^{115-117,180-182} **BMDM** and **OC** alone and in combination degrade by direct photolysis. Extent of photocatalysis of these chemical UV-filters varies in the presence of coated, micro- and nano-TiO₂. Despite the known ability of silica coated TiO₂ reduce photocatalysis,^{84,86} it is often not used to replace other forms of TiO₂ in formulations, because it is not cost effective.

UV-irradiation without TiO₂ resulted in no degradation of **OC**, but a significant reduction in **BMDM** recovery, showing that **OC** is stable during direct photolysis, while confirming **BMDM**'s lack of photostability. Results in the presence of TiO₂ clearly showed that nano-TiO₂ reduced the photostability of **BMDM** and **OC**, compared to that of the micro-TiO₂. This is

explained by its smaller particle size and larger surface area, increasing the generation of ROS, which potentially may cause UV-filter degradation, by photocatalysis. This result is significant as the reduced amount of UV-filter, in addition to the presence of photodegradants, which often have different UV-absorbance spectra, can compromise the broad spectrum photoprotection of the sunscreen product. The reduced UV-filter photostability, due to nano-TiO₂, was observed in methanol and in two formulations, the developed microemulsion and a reference cream, showing that this phenomenon is not directly related to formulation ingredients. Therefore caution should be exercised during formulation of sunscreen products containing chemical UV-filters and nano-TiO₂ in combination.

The stabilising effect of **OC** on **BMDM** in the microemulsion occurs *via* triplet-triplet energy transfer. Micro-TiO₂ in both formulations had only a minor effect on the photodegradation of **BMDM** and **OC**, attributed to its larger particle size, resulting in less light-absorption, and more light-reflection. Therefore, it can be concluded that the photodegradation in the presence of micro-TiO₂ is dominated by the direct photolysis. Silica coated TiO₂ had no significant impact on the photostability of **BMDM** and **OC** in the formulations, showing that the coating is effective in limiting the photodegradation by photocatalysis, making this form of TiO₂ optimum for inclusion into sunscreen products.

Sunscreen products are usually formulated as creams and lotions, which are often coarse emulsions, microemulsions or aqueous-based systems such as gels.^{107,108} A microemulsion was chosen for this study, due to its transparent appearance on the skin, its stability and the dynamic microstructure of oily and aqueous components. Reports that the skin penetration of UV-filters included in microemulsion was reduced compared to that of other formulations has been attributed to the particular components of the microemulsion. A microemulsion with a low surfactant/co-surfactant content (15.4 %) was developed, from a reported formula,¹¹⁷ with the viscosity increased using xanthan gum to optimise spreadability on the skin. The microemulsion was stable in terms of pH, colour, transparency and chemical stability of the chemical UV-filters **BMDM** and **OC** at 25 °C for six months and under accelerated conditions for at least two months. It was thus considered appropriate for use in the photostability and skin penetration studies.

The final objective of this study was to investigate the skin penetration *in vitro* of **BMDM**, **OC** and **B3** in the developed microemulsion, using Franz diffusion cells. Skin penetration of chemical UV-filters is reported to be affected by their lipophilicity and molecular weight.^{81,192} The three chemical UV-filters are lipophilic and therefore were included in the lipid, which is imbedded by a close packing of surfactants and co-surfactants. The combination of **BMDM** and **OC** did not negatively impact the skin penetration of either UV-filter. The lowest skin

penetration was observed for **OC** followed by **BMDM** and **B3**, which was expected due to the lipophilicity (high) and molecular weight (high), while **B3** is the least lipophilic UV-filter with the smallest molecular weight. This confirms that lipophilicity and molecular weight of UV-filters are in fact factors, which affect the skin penetration of these chemical UV-filters.

The hypothesis of the study was that for chemical UV-filters in combination with TiO₂ in a sunscreen product the photostability decreases and that the skin penetration of a combination of chemical UV-filters increases. The first part of the hypothesis has been proven in this study, while the second part disproven. It can be concluded that TiO₂, in particular nano-TiO₂, decreases the photostability of the chemical UV-filters **BMDM** and **OC**, but that the combination of both chemical UV-filters does not affect their skin penetration, as there is no significant difference in skin penetration between **BMDM** and **OC** separately or in combination.

7.2. Recommendations

This study presents a broad perspective on the photostability of sunscreen products, with the extensive review of the literature confirming the non-standardised nature of the photostability testing and the lack of regulatory control of these products. The candidate sunscreen product ingredients were characterised, analysed and evaluated for photostability and for the first time the effect of particle size of TiO₂ on the photostability of the chemical UV-filters has been investigated. Although the skin penetration of the chemical UV-filters was investigated *in vitro* using Franz diffusion cells, a limitation of the study is that another technique e.g. *in vivo* blood analysis of chemical UV-filters was not used to verify these results. However, this was not within the scope of the project.

Results from photostability studies have highlighted the need for further investigations on the influence of nano-TiO₂ on the photostability of chemical UV-filters. Newer, broad spectrum UV-filters, such as Bemotrizinol or Bisotrizole, may be investigated, due to being increasingly used in sunscreen products, currently and in the future. There is also a need to improve regulatory control of these products by including mandatory photostability testing.

UVA-filter **BMDM** has been shown to be photounstable, even in combination with **OC**, acting as stabilising agent. If this UVA-filter is to be incorporated into sunscreen products, novel drug delivery systems, e.g. liposomes, will need to be investigated to optimise its photostability.

Further optimisation of the microemulsion formulation is also recommended to ensure its long term stability under accelerated conditions.

8. References

1. Australian Radiation Protection and Nuclear Safety Agency (ARPANSA). Monthly Average UV-Index, Townsville. Accessed 31. Jan. 2014, at: www.arpansa.gov.au/uvindex/models/index.cfm.
2. Marrot L, Meunier JR 2008. Skin DNA photodamage and its biological consequences. *J Am Acad Dermatol* 58(5):S139-S148.
3. Madronich S, McKenzie RL, Bjorn LO, Caldwell MM 1998. Changes in biologically active ultraviolet radiation reaching the earth's surface. *J Photochem Photobiol B Biol* 46(1-3):5-19.
4. Velasco MVR, Sarruf FD, Salgado-Santos IMN, Haroutiounian-Filho CA, Kaneko TM, Baby AR 2008. Broad spectrum bioactive sunscreens. *Int J Pharm* 363(1-2):50-57.
5. Kullavanijaya P, Lim HW 2005. Photoprotection. *J Am Acad Dermatol* 52(6):937-958.
6. Setlow RB, Grist E, Thompson K, Woodhead AD 1993. Wavelengths effective in induction of malignant-melanoma. *Proc Natl Acad Sci USA* 90(14):6666-6670.
7. De Fabo EC, Noonan FP, Fears T, Merlino G 2004. Ultraviolet B but not ultraviolet A radiation initiates melanoma. *Cancer Res* 64(18):6372-6376.
8. Cancer Council 2010. Sun protection media kit, Summer 2010-11. Accessed 29. Jan. 2014, at: www.cancer.org.au/content/pdf/CancerControlPolicy/Publications/MediaMaterials/2010_Sun_protection_media_kit.pdf.
9. Parkin DM, Bray F, Ferlay J, Pisani P 2005. Global cancer statistics, 2002. *CA-Cancer J Clin* 55(2):74-108.
10. Australian Institute of Health and Welfare 2013. Cancer in Australia, key facts. Accessed 29. Jan. 2014, at: www.aihw.gov.au/cancer/cancer-in-australia/.
11. Australian Institute of Health and Welfare 2013. Skin Cancer. Accessed 29. Jan. 2014, at: www.aihw.gov.au/cancer/skin/.
12. Cancer Council Australia 2013. Non-melanoma Cancer. Accessed 29. Jan. 2014, at: www.cancer.org.au/about-cancer/types-of-cancer/skin-cancer/non-melanoma.html.
13. Cancer Council Australia 2013. Skin Cancer. Accessed 10. Jan. 2014, at: www.cancer.org.au/about-cancer/types-of-cancer/skin-cancer.html.
14. Therapeutic Goods Administration 2012. Australian regulatory guidelines for sunscreens, Version 1.0, November 2012. Accessed 20. Jan. 2014, at: www.tga.gov.au/industry/sunscreens-args.htm#.Uu7SSj2SykN.
15. More BD 2007. Physical sunscreens: On the comeback trail. *Indian J Dermatol Venereol Leprol* 73(2):80-85.
16. Giacomoni PU, Teta L, Najdek L 2010. Sunscreens: The impervious path from theory to practice. *Photochem Photobiol Sci* 9(4):524-529.
17. Urbach F 2001. The historical aspects of sunscreens. *J Photochem Photobiol B Biol* 64(2-3):99-104.
18. Nash JF 2006. Human safety and efficacy of ultraviolet filters and sunscreen products. *Dermatol Clin* 24(1):35-50.
19. Australian/New Zealand Standard™. 2012. Sunscreen products - Evaluation and classification (AS/NZS 2604:2012). Standards Australia Limited/Standards New Zealand.
20. Wakefield G, Green M, Lipscomb S, Flutter B 2004. Modified titania nanomaterials for sunscreen applications - reducing free radical generation and DNA damage. *Mater Sci Technol* 20(8):985-988.
21. Moyal D 2010. UVA protection labeling and *in vitro* testing methods. *Photochem Photobiol Sci* 9(4):516-523.
22. Agar NS, Halliday GM, Barnetson RS, Ananthaswamy HN, Wheeler M, Jones AM 2004. The basal layer in human squamous tumors harbors more UVA than UVB fingerprint mutations: A role for UVA in human skin carcinogenesis. *Proc Natl Acad Sci USA* 101(14):4954-4959.

23. Fourtanier A, Bernerd F, Bouillon C, Marrot L, Moyal D, Seite S 2006. Protection of skin biological targets by different types of sunscreens. *Photodermatol Photoimmunol Photomed* 22(1):22-32.
24. European Commission 2006. Standardisation Mandate assigned to CEN concerning methods for testing efficacy of sunscreen products. Accessed 23. Jan. 2014, at: www.ec.europa.eu/consumers/sectors/cosmetics/files/doc/sunscreen_mandate_en.pdf.
25. European Commission 2006. Commission Recommendation of 22 September 2006 on the efficacy of sunscreen products and claims made relating thereto. Accessed 23. Jan. 2014, at: www.eur-lex.europa.eu/LexUriServ/LexUriServ.do?uri=OJ:L:2006:265:0039:0043:en:PDF.
26. ICH Harmonised Tripartite Guideline 1996. Stability testing: Photostability testing of new drug substances and products Q1B. Accessed 20. Jan. 2014, at: www.ich.org/fileadmin/Public_Web_Site/ICH_Products/Guidelines/Quality/Q1B/Step_4/Q1B_Guideline.pdf.
27. U. S. Department of Health and Human Services. Food and Drug Administration. 2011. Labeling and effectiveness testing; sunscreen drug products for over-the-counter human use; Final Rule. www.gpo.gov/fdsys/pkg/FR-2011-06-17/pdf/2011-14766.pdf.
28. National Industrial Chemicals Notification and Assessment Scheme 2007. Cosmetics Standard 2007, Industrial Chemicals (Notification and Assessment) Act 1989. Accessed 3. Feb. 2014, at: www.comlaw.gov.au/Details/F2013C00556.
29. International Standard ISO 24444:2010(E). Cosmetics - Sun protection test methods - *In vivo* determination of the sun protection factor (SPF). ISO 2010.
30. International Standard ISO 24443:2012(E). Determination of sunscreen UVA photoprotection *in vitro*. ISO 2012.
31. U. S. Department of Health and Human Services - Food and Drug Administration. 1999. Sunscreen drug products for over-the-counter human use; Final Monograph. www.accessdata.fda.gov/scripts/cdrh/cfdocs/cfcfr/CFRSearch.cfm?CFRPart=352&sho wFR=1.
32. European Commission 2009. Regulation (EC) No 1223/2009 of the European Parliament and the Council of 30 November 2009 on cosmetic products. Accessed 23. Jan. 2014, at: www.eur-lex.europa.eu/LexUriServ/LexUriServ.do?uri=OJ:L:2009:342:0059:0209:EN:PDF.
33. Colipa 2005. Guideline for evaluating sun product water resistance. Accessed 31. Jan 2014, at: www.cosmeticseurope.eu/publications-cosmetics-europe-association/guidelines.html?view=item&id=18.
34. Serpone N, Salinaro A, Emeline AV, Horikoshi S, Hidaka H, Zhao JC 2002. An *in vitro* systematic spectroscopic examination of the photostabilities of a random set of commercial sunscreen lotions and their chemical UVB/UVA active agents. *Photochem Photobiol Sci* 1(12):970-981.
35. Couteau C, Power M, Papisaris E, Coiffard LJM 2007. Study of the efficacy of 18 sun filters authorized in European Union tested *in vitro*. *Pharmazie* 62(6):449-452.
36. Vielhaber G, Grether-Beck S, Koch O, Johncock W, Krutmann J 2006. Sunscreens with an absorption maximum of ≥ 360 nm provide optimal protection against UVA1-induced expression of matrix metalloproteinase-1, interleukin-1, and interleukin-6 in human dermal fibroblasts. *Photochem Photobiol Sci* 5(3):275-282.
37. Schwack W, Rudolph T 1995. Photochemistry of dibenzoyl methane UVA filters. Part 1. *J Photochem Photobiol B Biol* 28(3):229-234.
38. The Merck Index. Medicines Complete Accessed 12. July 2011, at: www.proxy30.use.hcn.com.au/mc/merck/current/.
39. Shaath NA 2010. Ultraviolet filters. *Photochem Photobiol Sci* 9(4):464-469.
40. British Pharmacopoeia. 2011. Volume II. Monographs: Medicinal and pharmaceutical substances. Mexenone. London: British Pharmacopoeia Commission.
41. Osterwalder U, Luther H, Herzog B 2001. Leitthema: Sonnenschutz und Sonnenschutzmittel. *Bundesgesundheitsbl Gesundheitsforsch Gesundheitsschutz* 44:463-470.

42. Tarras-Wahlberg N, Stenhagen G, Larko O, Rosen A, Wennberg AM, Wennerstrom O 1999. Changes in ultraviolet absorption of sunscreens after ultraviolet irradiation. *J Invest Dermatol* 113(4):547-553.
43. Couteau C, Faure A, Fortin J, Papis E, Coiffard LJM 2007. Study of the photostability of 18 sunscreens in creams by measuring the SPF *in vitro*. *J Pharm Biomed Anal* 44(1):270-273.
44. Couteau C, El-Boury S, Papis E, Sebille-Rivain V, Coiffard LJM 2009. *In vitro* UVA protection factor (PF-UVA) of organic and inorganic sunscreens. *Pharm Dev Technol* 14(4):369-372.
45. Lhiaubet-Vallet V, Marin M, Jimenez O, Gorchs O, Trullas C, Miranda MA 2010. Filter-filter interactions. Photostabilization, triplet quenching and reactivity with singlet oxygen. *Photochem Photobiol Sci* 9(4):552-558.
46. Gaspar LR, Campos P 2006. Evaluation of the photostability of different UV-filter combinations in a sunscreen. *Int J Pharm* 307(2):123-128.
47. Allen JM, Gossett CJ, Allen SK 1996. Photochemical formation of singlet molecular oxygen ($^1\text{O}_2$) in illuminated aqueous solutions of p-aminobenzoic acid (PABA). *J Photochem Photobiol B Biol* 32(1-2):33-37.
48. Allen JM, Gossett CJ, Allen SK 1996. Photochemical formation of singlet molecular oxygen in illuminated aqueous solutions of several commercially available sunscreen active ingredients. *Chem Res Toxicol* 9(3):605-609.
49. Damiani E, Baschong W, Greci L 2007. UV-Filter combinations under UVA exposure: Concomitant quantification of over-all spectral stability and molecular integrity. *J Photochem Photobiol B Biol* 87(2):95-104.
50. Hanson KM, Gratton E, Bardeen CJ 2006. Sunscreen enhancement of UV-induced reactive oxygen species in the skin. *Free Radic Biol Med* 41(8):1205-1212.
51. Inbaraj JJ, Bilski P, Chignell CF 2002. Photophysical and photochemical studies of 2-phenylbenzimidazole and UVB sunscreen 2-phenylbenzimidazole-5-sulfonic acid. *Photochem Photobiol* 75(2):107-116.
52. Herzog B, Wehrle M, Quass K 2009. Photostability of UV absorber systems in sunscreens. *Photochem Photobiol* 85(4):869-878.
53. Ricci A, Chretien MN, Marette L, Scaiano JC 2003. TiO_2 -promoted mineralization of organic sunscreens in water suspension and sodium dodecyl sulfate micelles. *Photochem Photobiol Sci* 2(5):487-492.
54. Rodil R, Moeder M, Altenburger R, Schmitt-Jansen M 2009. Photostability and phytotoxicity of selected sunscreen agents and their degradation mixtures in water. *Anal Bioanal Chem* 395(5):1513-1524.
55. Bonda G 2008. Research pathways to photostable sunscreens. *Cosmet Toil* 123(2):49-60.
56. Kikuchi A, Yagi M 2011. Direct observation of the intermolecular triplet-triplet energy transfer from UVA absorber 4-*tert*-Butyl-4'-methoxydibenzoylmethane to UVB absorber Octyl methoxycinnamate. *Chem Phys Lett* 513(1-3):63-66.
57. Bonda CA. 2005. The photostability of organic sunscreen actives: A review. In Shaath N, editor. *Sunscreens Regulations and Commercial Development*, 3rd ed., New York, USA: Taylor and Francis Group. p 321-349.
58. Bonda CA, Pavlovic A, Hanson KM, Bardeen CJ 2010. Singlet quenching proves faster is better for photostability. *Cosmet Toil* 125(2):40-48.
59. Bonda C, Zhang J, Pavlovic A 2011. The photostability and photostabilization of *trans*-reseratrol. *Cosmet Toil* 126:652-660.
60. Bonda C, Zhang J 2011. Photostabilization of retinol and retinyl palmitate by ethylhexyl methoxycrylene. *Cosmet Toil* 126:40-48.
61. Roscher NM, Lindemann MKO, Kong SB, Cho CG, Jiang P 1994. Photodecomposition of several compounds commonly used as sunscreen agents. *J Photochem Photobiol A Chem* 80(1-3):417-421.

62. Karlsson I, Hillerstrom L, Stenfeldt AL, Martensson J, Borje A 2009. Photodegradation of dibenzoylmethanes: Potential cause of photocontact allergy to sunscreens. *Chem Res Toxicol* 22(11):1881-1892.
63. Huong SP, Rocher E, Fourneron JD, Charles L, Monnier V, Bun H, Andrieu V 2008. Photoreactivity of the sunscreen butylmethoxydibenzoylmethane (DBM) under various experimental conditions. *J Photochem Photobiol A Chem* 196(1):106-112.
64. Mturi GJ, Martincigh BS 2008. Photostability of the suncreening agent 4-*tert*-Butyl-4'-methoxydibenzoylmethane (Avobenzone) in solvents of different polarity and proticity. *J Photochem Photobiol A Chem* 200(2-3):410-420.
65. Pattanaargson S, Limphong P 2001. Stability of octyl methoxycinnamate and identification of its photodegradation product. *Int J Cosmet Sci* 23(3):153-160.
66. Pattanaargson S, Munhapol T, Hirunsupachot N, Luangthongaram P 2004. Photoisomerization of octyl methoxycinnamate. *J Photochem Photobiol A Chem* 161(2-3):269-274.
67. Huong SP, Andrieu V, Reynier JP, Rocher E, Fourneron JD 2007. The photoisomerization of the sunscreen ethylhexyl p-methoxy cinnamate and its influence on the sun protection factor. *J Photochem Photobiol A Chem* 186(1):65-70.
68. Dondi D, Albini A, Serpone N 2006. Interactions between different solar UVB/UVA filters contained in commercial suncreams and consequent loss of UV protection. *Photochem Photobiol Sci* 5(9):835-843.
69. The Merck Manual 2013. Merck Manual Online for Health Care Professionals – Photosensitivity. Accessed 21. Jan. 2014, at: www.merckmanuals.com/professional/dermatologic_disorders/reactions_to_sunlight/photosensitivity.html?qt=photosensitivity&alt=sh.
70. Lautenschlager S, Wulf HC, Pittelkow MR 2007. Photoprotection. *Lancet* 370(9586):528-537.
71. Gilbert E, Pirot F, Bertholle V, Roussel L, Falson F, Padois K 2013. Commonly used UV-filter toxicity on biological functions: Review of last decade studies. *Int J Cosmet Sci* 35(3):208-219.
72. Marrot L, Belaidi JP, Lejeune F, Meunier JR, Asselineau D, Bernerd F 2004. Photostability of sunscreen products influences the efficiency of protection with regard to UV-induced genotoxic or photoageing-related endpoints. *Br J Dermatol* 151(6):1234-1244.
73. Butt ST, Christensen T 2000. Toxicity and phototoxicity of chemical sun filters. *Radiat Prot Dosim* 91(1-3):283-286.
74. Wahie S, Lloyd JJ, Farr PM 2007. Sunscreen ingredients and labelling: A survey of products available in the UK. *Clin Exp Dermatol* 32(4):359-364.
75. Kerr AC 2011. A survey of the availability of sunscreen filters in the UK. *Clin Exp Dermatol* 36(5):541-543.
76. Achilleos A, Hapeshi E, Xekoukoulotakis NP, Mantzavinos D, Fatta-Kassinou D 2010. Factors affecting diclofenac decomposition in water by UV-A/TiO₂ photocatalysis. *Chem Eng J* 161(1-2):53-59.
77. Buchalska M, Kras G, Oszejca M, Lasocha W, Macyk W 2010. Singlet oxygen generation in the presence of titanium dioxide materials used as sunscreens in suntan lotions. *J Photochem Photobiol A Chem* 213(2-3):158-163.
78. Dalrymple OK, Yeh DH, Trotz MA 2007. Removing pharmaceuticals and endocrine-disrupting compounds from wastewater by photocatalysis. *J Chem Technol Biotechnol* 82(2):121-134.
79. Dunford R, Salinaro A, Cai LZ, Serpone N, Horikoshi S, Hidaka H, Knowland J 1997. Chemical oxidation and DNA damage catalysed by inorganic sunscreen ingredients. *FEBS Lett* 418(1-2):87-90.
80. Australian Government (DHATGA) 2013. Literature review on the safety of titanium dioxide and zinc oxide nanoparticles in sunscreens (Scientific review report), Version 1.0, August 2013. Accessed 15. Feb. 2014, at: www.tga.gov.au/pdf/sunscreens-nanoparticles-review-2013.pdf.

81. Gonzalez H 2010. Percutaneous absorption with emphasis on sunscreens. *Photochem Photobiol Sci* 9(4):482-488.
82. Schilling K, Bradford B, Castelli D, Dufour E, Nash JF, Pape W, Schulte S, Tooley I, van den Bosch J, Schellauf F 2010. Human safety review of "nano" titanium dioxide and zinc oxide. *Photochem Photobiol Sci* 9(4):495-509.
83. Lewicka ZA, Yu WW, Oliva BL, Contreras EQ, Colvin VL 2013. Photochemical behavior of nanoscale TiO₂ and ZnO sunscreen ingredients. *J Photoch Photobiol A Chem* 263:24-33.
84. Mitchnick MA, Fairhurst D, Pinnell SR 1999. Microfine zinc oxide (Z-Cote) as a photostable UVA/UVB sunblock agent. *J Am Acad Dermatol* 40(1):85-90.
85. El-Boury S, Couteau C, Boulande L, Paparis E, Coiffard LJM 2007. Effect of the combination of organic and inorganic filters on the Sun Protection Factor (SPF) determined by *in vitro* method. *Int J Pharm* 340(1-2):1-5.
86. Carlotti ME, Ugazio E, Sapino S, Fenoglio I, Greco G, Fubini B 2009. Role of particle coating in controlling skin damage photoinduced by titania nanoparticles. *Free Radic Res* 43(3):312-322.
87. Wakefield G, Lipscomb S, Holland E, Knowland J 2004. The effects of manganese doping on UVA absorption and free radical generation of micronised titanium dioxide and its consequences for the photostability of UVA absorbing organic sunscreen components. *Photochem Photobiol Sci* 3(7):648-652.
88. Park B, Martin PA, Harris C, Guest R, Whittingham A, Jenkinson P 2009. Preliminary *in vitro* investigation of the potential health effects of Optisol (TM), a nanoparticulate manganese modified titanium dioxide UV-filter used in certain sunscreen products. *Nanotoxicology* 3(2):73-90.
89. Casey PS, Rossouw CJ, Boskovic S, Lawrence KA, Turney TW 2006. Incorporation of dopants into the lattice of ZnO nanoparticles to control photoactivity. *Superlattice Microst* 39(1-4):97-106.
90. Wakefield G, Stott J 2006. Photostabilization of organic UV-absorbing and antioxidant cosmetic components in formulations containing micronized manganese doped titanium oxide. *J Cosmet Sci* 57:385-395.
91. Sun L, Rippon JA, Cookson PG, Koulaeva O, Wang XG 2009. Effects of undoped and manganese-doped zinc oxide nanoparticles on the colour fading of dyed polyester fabrics. *Chem Eng J* 147(2-3):391-398.
92. Pinnell SR, Fairhurst D, Gillies R, Mitchnick MA, Kollias N 2000. Microfine zinc oxide is a superior sunscreen ingredient to microfine titanium dioxide. *Dermatol Surg* 26(4):309-313.
93. Chen L, Hu JY, Wang SQ 2012. The role of antioxidants in photoprotection: A critical review. *J Am Acad Dermatol* 67(5):1013-1024.
94. Damiani E, Rosati L, Castagna R, Carloni P, Greci L 2006. Changes in ultraviolet absorbance and hence in protective efficacy against lipid peroxidation of organic sunscreens after UVA irradiation. *J Photochem Photobiol B Biol* 82(3):204-213.
95. Moison RMW, Beijersbergen van Henegouwen GMJ 2002. Topical antioxidant vitamins C and E prevent UVB-radiation-induced peroxidation of eicosapentaenoic acid in pig skin. *Radiat Res* 157(4):402-409.
96. Carlotti ME, Ugazio E, Gastaldi L, Sapino S, Vione D, Fenoglio I, Fubini B 2009. Specific effects of single antioxidants in the lipid peroxidation caused by nano-titania used in sunscreen lotions. *J Photochem Photobiol B Biol* 96(2):130-135.
97. Maier H, Schauburger G, Brunnhofer K, Honigsmann H 2001. Change of ultraviolet absorbance of sunscreens by exposure to solar-simulated radiation. *J Invest Dermatol* 117(2):256-262.
98. Niculae G, Badea N, Meghea A, Oprea O, Lacatusu I 2013. Coencapsulation of butyl methoxy dibenzoylmethane and octocrylene into lipid nanocarriers: UV performance, photostability and *in vitro* release. *Photochem Photobiol* 89(5):1085-1094.

99. Puglia C, Bonina F, Rizza L, Blasi P, Schoubben A, Perrotta R, Tarico MS, Damiani E 2012. Lipid nanoparticles as carrier for octylmethoxycinnamate: *In vitro* percutaneous absorption and photostability studies. *J Pharm Sci* 101(1):301-311.
100. Ambrogi V, Latterini L, Marmottini F, Pagano C, Ricci M 2013. Mesoporous silicate MCM-41 as a particulate carrier for octylmethoxycinnamate: Sunscreen release and photostability. *J Pharm Sci* 102(5):1468-1475.
101. Vilela FMP, Fonseca YM, Vicentini F, Fonseca MJV, do Amaral MDH 2011. Determination of three ultraviolet filters in sunscreen formulations and from skin penetration studies by high-performance liquid chromatography. *Quim Nova* 34(5):879-883.
102. Colipa 1997. Guidelines for percutaneous absorption/penetration. Accessed 31. Jan. 2014, at: www.cosmeticseurope.eu/publications-cosmetics-europe-association/guidelines.html?view=item&id=26.
103. Klang V, Haberfeld S, Hartl A, Valenta C 2012. Effect of gamma-cyclodextrin on the *in vitro* skin permeation of a steroidal drug from nanoemulsions: Impact of experimental setup. *Int J Pharm* 423(2):535-542.
104. Hayden CGJ, Cross SE, Anderson C, Saunders NA, Roberts MS 2005. Sunscreen penetration of human skin and related keratinocyte toxicity after topical application. *Skin Pharmacol Physiol* 18(4):170-174.
105. Durand L, Habran N, Henschel V, Amighi K 2009. *In vitro* evaluation of the cutaneous penetration of sprayable sunscreen emulsions with high concentrations of UV filters. *Int J Cosmet Sci* 31(4):279-292.
106. Chatelain E, Gabard B, Surber C 2003. Skin penetration and sun protection factor of five UV filters: Effect of the vehicle. *Skin Pharmacol Appl Skin Physiol* 16(1):28-35.
107. Maier H, Schmalwieser AW 2010. Sunscreens and occupation: The austrian experience. *Photochem Photobiol Sci* 9(4):510-515.
108. Neudahl GA, Zhang J 2010. Formulating sun protection products that people will use: Designing broad-spectrum, photostabilized sunscreens with favourable aesthetics. *H&PC Today* 3:18-20.
109. Azeem A, Rizwan M, Ahmad FJ, Khan ZI, Khar RK, Aqil M, Talegaonkar S 2008. Emerging role of microemulsions in cosmetics. *Recent Pat Drug Deliv Formul* 2(3):275-289.
110. Heuschkel S, Goebel A, Neubert RHH 2008. Microemulsions - Modern colloidal carrier for dermal and transdermal drug delivery. *J Pharm Sci* 97(2):603-631.
111. Grampurohit N, Ravikumar P, Mallya R 2011. Microemulsions for topical use - A review. *Ind J Pharm Edu Res* 45(1):100-107.
112. Shishu, Rajan S, Kamalpreet 2009. Development of novel microemulsion-based topical formulations of acyclovir for the treatment of cutaneous herpetic infections. *AAPS Pharm Sci Tech* 10(2):559-565.
113. Zhu W, Guo C, Yu A, Gao Y, Cao F, Zhai G 2009. Microemulsion-based hydrogel formulation of penciclovir for topical delivery. *Int J Pharm* 378(1-2):152-158.
114. Gasco MR, Gallarate M, Pattarino F 1991. *In vitro* permeation of azelaic acid from viscosized microemulsions. *Int J Pharm* 69:193-196.
115. Carlotti ME, Gallarate M, Rossatto V 2003. O/W microemulsions as a vehicle for sunscreens. *J Cosmet Sci* 54:451-462.
116. Montenegro L, Carbone C, Conclorelli G, Drago R, Puglisi G 2006. Effect of oil phase lipophilicity on *in vitro* drug release from O/W microemulsions with low surfactant content. *Drug Dev Ind Pharm* 32(5):539-548.
117. Montenegro L, Carbone C, Puglisi G 2011. Vehicle effects on *in vitro* release and skin permeation of octylmethoxycinnamate from microemulsions. *Int J Pharm* 405(1-2):162-168.
118. European Multicentre Photopatch Test Study (EMCPPTS) Taskforce 2012. A European multicentre photopatch test study. *Br J Dermatol* 166(5):1002-1009.
119. Bryden AM, Moseley H, Ibbotson SH, Chowdhury MMU, Beck MH, Bourke J, English J, Farr P, Foulds IS, Gawkrödger DJ, George S, Orton DI, Shaw S, McFadden

- J, Norris P, Podmore P, Powell S, Rhodes LE, Sansom J, Wilkinson M, van Weelden H, Ferguson J 2006. Photopatch testing of 1155 patients: Results of the UK multicentre photopatch study group. *Br J Dermatol* 155(4):737-747.
120. Victor FC, Cohen DE, Soter NA 2010. A 20-year analysis of previous and emerging allergens that elicit photoallergic contact dermatitis. *J Am Acad Dermatol* 62(4):605-610.
 121. Stiefel C, Schwack W 2013. Rapid screening method to study the reactivity of UV filter substances towards skin proteins by high-performance thin-layer chromatography. *Int J Cosmet Sci* 35(6):588-599.
 122. Gaspar LR, Tharmann J, Campos P, Liebsch M 2013. Skin phototoxicity of cosmetic formulations containing photounstable and photostable UV-filters and vitamin A palmitate. *Toxicol in Vitro* 27(1):418-425.
 123. United States Pharmacopeia 34. 2011. Volume I. General Chapters. Physical tests and determinations. Rockville: The United States Pharmacopeial Convention.
 124. Meyer VR. 2010. Detectors. In: *Practical high-performance liquid chromatography*, 5th ed., West Sussex, UK: John Wiley and Sons. p 91-109.
 125. Snyder LR, Kirkland JJ, Dolan JW. 2010. Introduction. In: *Introduction to Modern Liquid Chromatography*, 3rd ed., New Jersey, USA: John Wiley and Sons. p 1-15.
 126. Gabbott P. 2008. A Practical introduction to differential scanning calorimetry. In: *Principles and applications of thermal analysis*, 1st ed., Oxford, UK: Blackwell Publishing. p 1-50.
 127. Silverstein RM, Webster FX, Kiemle DJ. 2005. Proton NMR spectrometry. In: *Spectrometric identification of organic compounds*, 7th ed., New Jersey, USA: John Wiley and Sons. p 127-203.
 128. Silverstein RM, Webster FX, Kiemle DJ. 2005. Infrared spectrometry. In: *Spectrometric identification of organic compounds*, 7th ed., New Jersey, USA: John Wiley and Sons. p 72-126.
 129. Tong W-QT. 2007. Practical aspects of solubility determination in pharmaceutical preformulation. In Augustijns P, Brewster ME, editors. *Solvent systems and their selection in pharmaceuticals and biopharmaceuticals*, 1st ed., New York, USA: Springer-Verlag. p 137-149.
 130. Lam H. 2004. Performance verification of UV-VIS spectrophotometers. In Chan CC, Lam H, Lee YC, Zhang X-M, editors. *Analytical method validation and instrument performance verification*, 1st ed., New Jersey, USA: John Wiley and Sons. p 153-172.
 131. British Pharmacopeia. 2011. Volume IV. Appendices. Appendix V A. Determination of melting point. London: British Pharmacopoeia Commission.
 132. Safety data sheet - Merck - Eusolex® 9020. November 2010. Version 5.0. Accessed 15. Feb. 2014, at: www.merck-performance-materials.com/merck-ppf/detailRequest?unit=CHEM&owner=MDA&productNo=105844&docType=MSD&source=GDS&language=EN&country=EU&docId=/mda/chemicals/msds/en-EU/105844_SDS_EU_EN.PDF.
 133. United States Pharmacopeia 34. 2011. Avobenzone. Rockville: The United States Pharmacopeial Convention. p 1960.
 134. Yang J, Wiley CJ, Godwin DA, Felton LA 2008. Influence of Hydroxypropyl-beta-cyclodextrin on transdermal penetration and photostability of Avobenzone. *Eur J Pharm Biopharm* 69(2):605-612.
 135. Dubois M, Gilard P, Tiercet P, Deflandre A, Lefebvre MA 1998. Photoisomerisation of the sunscreen filter PARSOL® 1789. *J Chim Phys* 95(2):388-394.
 136. Zawadiak J, Mrzyczek M, Piotrowski T 2011. Synthesis and properties of aromatic 1,3-diketones and *bis*-(1,3-diketones) obtained from acetophenone and phthalic acids esters. *Eur J Chem* 2(3):289-294.
 137. Safety data sheet - Merck - Eusolex® OCR. January 2014. Version 8.0. Accessed 15. Feb. 2014, at: www.merck-performance-materials.com/merck-ppf/detailRequest?unit=CHEM&owner=MDA&productNo=105377&docType=MSD&

- [source=GDS&language=EN&country=EU&docId=/mda/chemicals/msds/en-EU/105377_SDS_EU_EN.PDF.](#)
138. Safety data sheet - Merck - Eusolex® 4360. May 2011. Version 2.4. Accessed 15. Feb. 2014, at: www.merck-performance-materials.com/merck-pmf/detailRequest?unit=CHEM&owner=MDA&productNo=105376&docType=MSD&source=GDS&language=EN&country=EU&docId=/mda/chemicals/msds/en-EU/105376_SDS_EU_EN.PDF.
 139. Safety data sheet - Sigma-Aldrich - Oxybenzone. April 2013. Version 5.1. Accessed 15. Feb. 2014, at: www.sigmaaldrich.com/MSDS/MSDS/DisplayMSDSPage.do?country=AU&language=en&productNumber=59647&brand=FLUKA&PageToGoToURL=http%3A%2F%2Fwww.sigmaaldrich.com%2Fcatalog%2Fproduct%2Ffluka%2F59647%3Fflang%3Den.
 140. Mori K, Itoh K, Suzuki S, Nakamura H 1996. Analysis of ultraviolet absorbers in cosmetics by two dimension NMR spectroscopy. *Jpn J Toxicol Environ Health* 42(1):60-66.
 141. Stamatakis G, Knuutinen U, Laitinen K, Spyros A 2010. Analysis and aging of unsaturated polyester resins in contemporary art installations by NMR spectroscopy. *Anal Bioanal Chem* 398(7-8):3203-3214.
 142. Gomaa AY, Darwish IA, Boraei NA, El-Khordagui LK 2010. Formulation of wax oxybenzone microparticles using a factorial approach. *J Microencapsul* 27(7):628-639.
 143. ICH Harmonised Tripartite Guideline 2005. Validation of analytical procedures: Text and methodology Q2(R1). Accessed 20. Jan. 2014, at: www.ich.org/fileadmin/Public_Web_Site/ICH_Products/Guidelines/Quality/Q2_R1/Step4/Q2_R1_Guideline.pdf.
 144. Gago-Ferrero P, Badia-Fabregat M, Olivares A, Pina B, Blanquez P, Vicent T, Caminal G, Silvia Diaz-Cruz M, Barcelo D 2012. Evaluation of fungal- and photo-degradation as potential treatments for the removal of sunscreens BP3 and BP1. *Sci Total Environ* 427:355-363.
 145. Chatelain E, Gabard B 2001. Photostabilization of butyl methoxydibenzoylmethane (Avobenzone) and ethylhexyl methoxycinnamate by *bis*-ethylhexyloxyphenol methoxyphenyl triazine (Tinosorb S), a new UV-broadband filter. *Photochem Photobiol* 74(3):401-406.
 146. De Orsi D, Giannini G, Gagliardi L, Porra R, Berri S, Bolasco A, Carpani I, Tonelli D 2006. Simple extraction and HPLC determination of UV-A and UV-B filters in sunscreen products. *Chromatographia* 64(9-10):509-515.
 147. Dencausse L, Galland A, Clamou JL, Basso J 2008. Validation of HPLC method for quantitative determination of Tinosorb S and three other sunscreens in a high protection cosmetic product. *Int J Cosmet Sci* 30(5):373-382.
 148. Moreta C, Teresa Tena M 2011. Determination of UV filters in packaging by focused ultrasonic solid-liquid extraction and liquid chromatography. *J Chromatogr A* 1218(21):3392-3399.
 149. Nyeborg M, Pissavini M, Lemasson Y, Doucet O 2010. Validation of HPLC method for the simultaneous and quantitative determination of 12 UV-filters in cosmetics. *Int J Cosmet Sci* 32:47-53.
 150. Sayre RM, Dowdy JC, Gerwig AJ, Shields WJ, Lloyd RV 2005. Unexpected photolysis of the sunscreen octinoxate in the presence of the sunscreen avobenzone. *Photochem Photobiol* 81(2):452-456.
 151. Scalia S, Simeoni S, Barbieri A, Sostero S 2002. Influence of Hydroxypropyl-beta-cyclodextrin on photoinduced free radical production by the sunscreen agent, Butyl-methoxydibenzoylmethane. *J Pharm Pharmacol* 54(11):1553-1558.
 152. Simeoni S, Tursilli R, Bianchi A, Scalia S 2005. Assay of common sunscreen agents in suncare products by high-performance liquid chromatography on a cyanopropyl-bonded silica column. *J Pharm Biomed Anal* 38(2):250-255.
 153. Smyrniotakis CG, Archontaki HA 2004. Development and validation of a non-aqueous reversed-phase high-performance liquid chromatographic method for the determination

- of four chemical UV-filters in sun care formulations. *J Chromatogr A* 1031(1-2):319-324.
154. Wharton M, Geary M, O'Connor N, Murphy B 2011. A rapid high performance liquid chromatographic (HPLC) method for the simultaneous determination of seven UV filters found in sunscreen and cosmetics. *Int J Cosmet Sci* 33(2):164-170.
 155. Dolan JW, Jupille TH. John Dolan's Masterclasses: HPLC troubleshooting and diagnostics-Seminar, Melbourne, Australia, 2011.
 156. Majors R. 2010. Sample Preparation. In Snyder LR, Kirkland JJ, Dolan JW, editors. *Introduction to Modern Liquid Chromatography*, 3rd ed., New Jersey, USA: John Wiley and Sons. p 757-805.
 157. Skoug JW, Halstead GW, Theis DL, Freeman JE, Fagan DT, Rohrs BR 1996. Strategy for the development and validation of dissolution tests for solid oral dosage forms. *Pharm Tech* 20(5):58-72.
 158. Swartz M. 2010. Method Validation. In Snyder LR, Kirkland JJ, Dolan JW, editors. *Introduction to Modern Liquid Chromatography*, 3rd ed., New Jersey, USA: John Wiley and Sons. p531-566
 159. British Pharmacopoeia. 2011. Volume IV. Appendices. Appendix III. Chromatographic separation techniques. London: British Pharmacopoeia Commission.
 160. Crowther JB. Validation of pharmaceutical test methods. In Ahuja S, Scypinski S, editors. *Handbook of modern pharmaceutical analysis*, San Diego, USA: Academic Press. p 435.
 161. Kockler J, Kanakaraju D, Glass BD, Oelgemöller M 2012. Photochemical and photocatalytic degradation of diclofenac and amoxicillin using natural and simulated sunlight. *J Sustain Sci Manage* 7(1):23-29.
 162. Imamović B, Šober M, Bečić E 2009. Identification and determination Butylmethoxydibenzoylmethane in the presence Benzophenone-3 and Ethylhexyl methoxycinnamate in sun care preparation. *Int J Cosmet Sci* 31:383-389.
 163. Irakli MN, Samanidou VF, Papadoyannis IN 2012. Optimization and validation of the reversed-phase high-performance liquid chromatography with fluorescence detection method for the separation of tocopherol and tocotrienol isomers in cereals, employing a novel sorbent material. *J Agric Food Chem* 60(9):2076-2082.
 164. Kong LY, Su BG, Bao ZB, Xing HB, Yang YW, Ren QL 2011. Direct quantification of mono- and di-D-alpha-tocopherol polyethylene glycol 1000 succinate by high performance liquid chromatography. *J Chromatogr A* 1218(48):8664-8671.
 165. Silverstein RM, Webster FX, Kiemle DJ. 2005. Mass spectrometry. In: *Spectrometric identification of organic compounds*, 7th ed., New Jersey, USA: John Wiley and Sons. 1-70.
 166. Frackowiak D 1988. The Jablonski diagram. *J Photochem Photobiol B Biol* 2:399-408.
 167. Zhao K, Lu Y, Lu N, Zhao YH, Yuan X, Zhang H, Teng LH, Li F 2013. Design of H3PW12O40/TiO₂ nano-photocatalyst for efficient photocatalysis under simulated sunlight irradiation. *Appl Surf Sci* 285:616-624.
 168. Konaka R, Kasahara E, Dunlap WC, Yamamoto Y, Chien KC, Inoue M 1999. Irradiation of titanium dioxide generates both singlet oxygen and superoxide anion. *Free Radic Biol Med* 27(3-4):294-300.
 169. Montalti M, Credi A, Prodi L, Gandolfi MT. 2006. *Handbook of Photochemistry*. 3rd ed., Boca, Raton, Florida, USA: CRC Press.
 170. Hazime R, Ferronato C, Fine L, Salvador A, Jaber F, Chovelon JM 2012. Photocatalytic degradation of imazalil in an aqueous suspension of TiO₂ and influence of alcohols on the degradation. *Appl Catal B* 126:90-99.
 171. Zhang ZB, Wang CC, Zakaria R, Ying JY 1998. Role of particle size in nanocrystalline TiO₂-based photocatalysts. *J Phys Chem B* 102(52):10871-10878.
 172. Wahi RK, Yu WW, Liu YP, Mejia ML, Falkner JC, Nolte W, Colvin VL 2005. Photodegradation of congo red catalyzed by nanosized TiO₂. *J Mol Catal A Chem* 242(1-2):48-56.

173. Kumar SG, Devi LG 2011. Review on modified TiO₂ photocatalysis under UV-Visible Light: Selected results and related mechanisms on interfacial charge carrier transfer dynamics. *J Phys Chem A* 115(46):13211-13241.
174. Thomas AG, Syres KL 2012. Adsorption of organic molecules on rutile TiO₂ and anatase TiO₂ single crystal surfaces. *Chem Soc Rev* 41(11):4207-4217.
175. Sabliov CM, Fronczek C, Astete CE, Khachatryan M, Khachatryan L, Leonardi C 2009. Effects of temperature and UV-light on degradation of alpha-tocopherol in free and dissolved form. *J Am Oil Chem Soc* 86(9):895-902.
176. Mbah CJ 2007. Degradation kinetics of butylmethoxydibenzoylmethane (Avobenzone) in aqueous solution. *Pharmazie* 62(10):747-749.
177. Givens RS, Levi N. 1979. The photochemistry of organic acids, esters, anhydrides, lactones and imides. In Patai S, editor. *The chemistry of acid derivatives Part 1*, New York, USA: John Wiley and Sons. p 642-753.
178. Karlsson I, Persson E, Martensson J, Borje A 2012. Investigation of the sunscreen octocrylene's interaction with amino acid analogs in the presence of UV-radiation. *Photochem Photobiol* 88(4):904-912.
179. Agatonovic-Kustrin S, Glass BD, Wisch MH 2004. Strategy for development of thermodynamically stable microemulsion for oral administration. *Curr Drug Discov Technol* 1(2):165-171.
180. Knueppel A, Grotelueschen B 2003. Sunscreen microemulsions with high UV-filter content and low amount of lipids. DE10134415. Beiersdorf AG, Germany.
181. Gers-Barlag H, Mueller A, Doerscher A, Knueppel A 2001. Cosmetic and dermatological photoprotective O/W-macroemulsions or O/W-microemulsions containing sulfonated sunscreen agents. DE19950059. Beiersdorf AG, Germany.
182. Sugiyama Y, Abe K, Yoshida S 2011. Sunblock composition having biocontinuous microemulsion phase. JP2011178769. Kokai Tokyo Koho, Japan.
183. KORRES S.A. NATURAL PRODUCTS. Accessed 21. Jan. 2014, at: www.korres.com/default.aspx?page_id=115.
184. Koop HS, Da-Lozzo EJ, de Freitas RA, Franco CRC, Mitchell DA, Silveira JLM 2012. Rheological characterization of a xanthan-galactomannan hydrogel loaded with lipophilic substances. *J Pharm Sci* 101(7):2457-2467.
185. Chudasama A, Patel V, Nivsarkar M, Vasu K, Shishoo C 2011. Investigation of microemulsion system for transdermal delivery of itraconazole. *J Adv Pharm Technol Res* 2(1):30-38.
186. Spiclin P, Homar M, Zupancic-Valant A, Gasperlin M 2003. Sodium ascorbyl phosphate in topical microemulsions. *Int J Pharm* 256(1-2):65-73.
187. Peira E, Scolari P, Gasco MR 2001. Transdermal permeation of apomorphine through hairless mouse skin from microemulsions. *Int J Pharm* 226(1-2):47-51.
188. Kantaria S, Rees GD, Lawrence MJ 1999. Gelatin-stabilised microemulsion-based organogels: Rheology and application in iontophoretic transdermal drug delivery. *J Control Release* 60(2-3):355-365.
189. United States Pharmacopeia 34, The National Formulary 29. 2011. Xanthan Gum. Rockville: The United States Pharmacopeial Convention. p 1711-1712.
190. Martindale - The complete drug reference 2013. Xanthan Gum. Accessed 27. Jan. 2014, at: www.micromedexsolutions.com.elibrary.jcu.edu.au/micromedex2/librarian/ND_T/evidencexpert/ND_PR/evidencexpert/CS/173311/ND_AppProduct/evidencexpert/DUPLICATIONSHIELDSYNC/7BAC20/ND_PG/evidencexpert/ND_B/evidencexpert/ND_P/evidencexpert/PFActionId/evidencexpert.IntermediateToDocumentLink?docId=5465-a&contentSetId=30&title=Xanthan+Gum&servicesTitle=Xanthan+Gum.
191. Sworn G. 2011. Xanthan gum - Functionality and application. In Norton IT, Spyropoulos F, Cox P, editors. *Practical food rheology - An interpretive approach*, Chichester, UK: Wiley-Blackwell. p 85-112.

192. Selzer D, Abdel-Mottaleb MMA, Hahn T, Schaefer UF, Neumann D 2013. Finite and infinite dosing: Difficulties in measurements, evaluations and predictions. *Adv Drug Deliv Rev* 65(2):278-294.
193. Mavon A, Miquel C, Lejeune O, Payre B, Moretto P 2007. *In vitro* percutaneous absorption and *in vivo* stratum corneum distribution of an organic and a mineral sunscreen. *Skin Pharmacol Physiol* 20(1):10-20.
194. Huong SP, Bun H, Fourneron JD, Reynier JP, Andrieu V 2009. Use of various models for *in vitro* percutaneous absorption studies of ultraviolet filters. *Skin Res Technol* 15(3):253-261.
195. Klang V, Schwarz JC, Lenobel B, Nadj M, Aubock J, Wolzt M, Valenta C 2012. *In vitro* vs. *in vivo* tape stripping: Validation of the porcine ear model and penetration assessment of novel sucrose stearate emulsions. *Eur J Pharm Biopharm* 80(3):604-614.
196. Reddy MB, Stinchcomb AL, Guy RH, Bunge AL 2002. Determining dermal absorption parameters *in vivo* from tape strip data. *Pharmaceut Res* 19(3):292-298.
197. Schwarz JC, Klang V, Hoppel M, Wolzt M, Valenta C 2012. Corneocyte quantification by NIR densitometry and UV/Vis spectroscopy for human and porcine skin and the role of skin cleaning procedures. *Skin Pharmacol Physiol* 25(3):142-149.
198. Simeoni S, Scalia S, Tursilli R, Benson H 2006. Influence of cyclodextrin complexation on the *in vitro* human skin penetration and retention of the sunscreen agent, Oxybenzone. *J Incl Phenom Macrocycl Chem* 54(3-4):275-282.
199. Pershing LK, Bakhtian S, Poncelet CE, Corlett JL, Shah VP 2002. Comparison of skin stripping, *in vitro* release, and skin blanching response methods to measure dose response and similarity of triamcinolone acetonide cream strengths from two manufactured sources. *J Pharm Sci* 91(5):1312-1323.
200. International Organization for Standardization (ISO). 2010. International Standard ISO 24444: Cosmetics - Sun protection test methods - *In vivo* determination of the sun protection factor (SPF). Annex C4: P7: Low SPF reference formula. p 29-31.
201. Australian Government—Bureau of Meteorology, Six-Monthly Solar Exposure for Australia. Accessed 31. April 2014, at: <http://www.bom.gov.au/jsp/awap/solar/archive.jsp?map=solarave&colour=colour&map=solarave&year=2014&month=3&period=6month&area=nat>
202. ICH Harmonised Tripartite Guideline 2003. Stability testing of new drug substances and products Q1A (R2). Accessed 20. Jan. 2014, at: www.ich.org/fileadmin/Public_Web_Site/ICH_Products/Guidelines/Quality/Q1A_R2/Step4/Q1A_R2_Guideline.pdf.
203. Karlsson I, Broecke KV, Martensson J, Goossens A, Borje A 2011. Clinical and experimental studies of Octocrylene's allergenic potency. *Contact Dermatitis* 64(6):343-352.
204. HallStar 24.04.2009. Product Information Sheet: HALLSTAR® GMO. Accessed 21. Jan. 2014, at: www.hallstar.com/pis.php?product=1H023.
205. Pescia AC, Astolfi P, Puglia C, Bonina F, Perrotta R, Herzog B, Damiani E 2012. On the assessment of photostability of sunscreens exposed to UVA irradiation: From glass plates to pig/human skin, which is best? *Int J Pharm* 427(2):217-223.
206. Cross SE, Anissimov YG, Magnusson BM, Roberts MS 2003. Bovine-serum-albumin-containing receptor phase better predicts transdermal absorption parameters for lipophilic compounds. *J Invest Dermatol* 120:589-591.
207. Schreml S, Zeller V, Meier RJ, Korting HC, Behm B, Landthaler M, Babilas P 2012. Impact of age and body site on adult female skin surface pH. *Dermatology* 224(1):66-71.
208. Lambers H, Piessens S, Bloem A, Pronk H, Finkel P 2006. Natural skin surface pH is on average below 5, which is beneficial for its resident flora. *Int J Cosmet Sci* 28(5):359-370.
209. Kikuchi A, Oguchi-Fujiyama N, Miyazawa K, Yagi M 2014. Triplet-triplet energy transfer from a UV-A absorber butylmethoxydibenzoylmethane to UV-B absorbers. *Photochem Photobiol.* 90:511-516.

210. Gonzenbach H, Hill TJ, Truscott TG 1992. The triplet energy levels of UVA and UVB sunscreens. *J Photochem Photobiol B Biol* 16(3-4):377-379.
211. Kikuchi A, Oguchi N, Yagi M 2009. Optical and electron paramagnetic resonance studies of the excited states of 4-*tert*-butyl-4'-methoxydibenzoylmethane and 4-*tert*-butyl-4'-methoxydibenzoylpropane. *J Phys Chem A* 113(48):13492-13497.

APPENDIX A: International Biosafety Committee (IBC) Approval

This administrative form
has been removed

This administrative form
has been removed